Electrospray-friendly ligands for the mass spectral analysis of transition-metal complexes

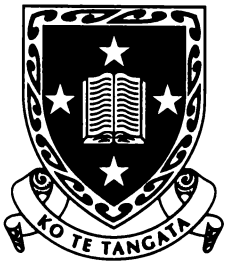

The University of Waikato

Te Whare Wānanga o Waikato

A thesis completed in partial fulfilment of the requirements for the Degree of Doctor of Philosophy at the University of Waikato by

Corry Decker

University of Waikato

2002

Abstract

The key aim of this project was to develop the concept of electrospray-friendly ligands as a new ionisation method for the analysis of neutral metal complexes by electrospray mass spectrometry (ESMS). This involved introducing active functional groups into traditional ligands which do not otherwise undergo chemical ionisation under ESMS conditions.

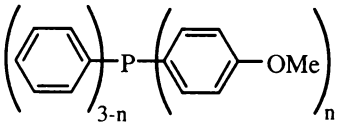

n = 1: P*
n = 2: P**
n = 3: P***

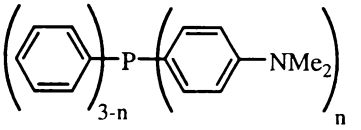

n = 1: P•
n = 2: P••
n = 3: P•••

Electrospray-friendly ligands (as illustrated above for PPh_3 derivatives) were incorporated into a series of metal carbonyl complexes of Mo, Fe and Ru, metal halide complexes of Pd, Pt and Au, and a number of zero-valent complexes of Pt and Pd. All carbonyl complexes with ES-friendly phosphine, arsine and stibine ligands ionised by protonation, yielding strong $[M + H]^+$ ions as the only signals in the spectrum. The metal halide complexes followed the known halide-loss mechanism. Pt(0) and Pd(0) complexes did not require functionalised ligands, as their PPh_3 derivatives already gave $[M + H]^+$ ions. Mo and W carbonyl complexes of the two 'naturally' electrospray-friendly ligands tpa (tpa = 1,3,5-triaza-7-phosphaadamantane) and tcep [tcep = tris(2-cyanoethyl)phosphine] could also be studied readily by ESMS. While all tpa complexes gave $[M + H]^+$ ions, complexes of tcep preferred ionisation by NH_4^+. The ionisation efficiencies of selected ligands and complexes are discussed.

Thiolate complexes of Ni, Pd, Pt, Au and Hg were prepared using the ligands SC_6H_4OMe-*p* (S*) and *p*-SC_5H_4N (S•), but only the S•-complexes reliably underwent the protonation-type mechanism. The Cd-thiolate complexes $[Cd_4(SPh)_{10}]^{2-}$, $[S_4Cd_{10}(SPh)_{16}]^{4-}$ and $[S_4Cd_{17}(SPh)_{28}]^{2-}$ underwent rapid ligand exchange with S*, but yielded insoluble products with S•. The complexes $[Pt_2(\mu\text{-}S)_2(L)_2]$ (L = PPh_3, P*, P**,

P***, P•, As*** [1]) were prepared, and by means of ESMS, aspects of ligand exchange as well as reactivity towards other metal centres were investigated.

Isonitrile derivatives of $[Fe_3(CO)_{12}]$ and $[Ru_3CO)_{12}]$ were prepared by ligand exchange with CNPh, CNC_6H_4OMe-*p* (CNPh*) and tosylmethylisocyanide. Substitution was observed for up to six CO ligands. Pyrolysis of $[Fe_3(CO)_{11}(L)]$ and $[Fe_3(CO)_{10}(L)_2]$ (L = CNPh, CNPh*) led to the products $[Fe_3(CO)_9(\mu_3\text{-}\eta^2\text{-L})]$ and $[Fe_3(CO)_8(\mu_3\text{-}\eta^2\text{-L})\ (L)]$, respectively. All complexes could be studied by ESMS as their $[M + H]^+$, $[M + MeO]^-$ or $[M - H]^-$ ions, depending on the exact nature of the analyte. $[Fe_3(CO)_{10}(CNPh)_2]$ was characterised structurally (below) and revealed an unprecedented substitution pattern, together with unexpected partial disorder in the metal framework.

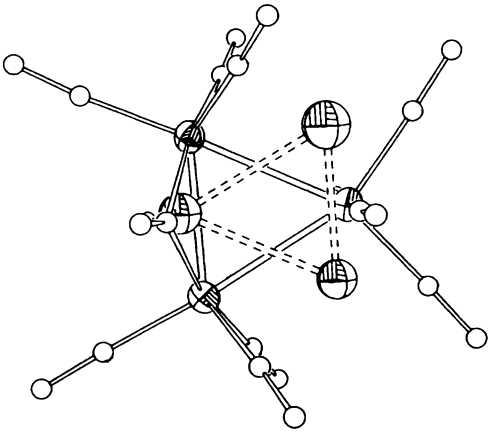

Detection by ESMS of products of the type $[Ru_4(CO)_{14-n}(L)_n]$ (L = CNPh, CNPh*; n = 2-4) in the reactions with ruthenium carbonyl led to the isolation and structural characterisation of $[Ru_4(CO)_{12}(CNPh)_4]$, which is the only fully characterised isonitrile derivative of $[Ru_3(CO)_{12}]$ with four metal atoms and exhibits an unusual imine-type bonding mode for the bridging isonitrile ligands.

[1] As*** = $As(C_6H_4OMe\text{-}p)_3$

Acknowledgements

First and foremost, I would like to thank both Bill Henderson and Brian Nicholson for being my supervisors over the last few years. Where I come from, supervisors are called 'Doktorvater' and, just like Dads in real life, are expected to continuously and patiently guide, encourage, listen, set examples, have all the answers, and eventually let go. They have exceeded all expectations.

Talking of Dads, I'd like to express my gratitude to my parents. Without their support and encouragement I would have never started this, let alone finish.

A special thank goes to all technical staff and the many student lab workers I have gone through over the years. This work could not have been completed without their help.

I would like to dedicate this thesis to the best parents in the world:

my Mum & Dad

Table of Contents

List of Figures

List of Tables and Schemes

List of Abbreviations and Symbols

a = anion

acac = acetylacetonate

amu = atomic mass units

API = atmospheric pressure ionisation

AS = aerospray

B = base

bipy = bipyridyl

b.p. = boiling point

br = broad (IR)

Bu^t = tertiary butyl

Bz = benzyl

c = cation

^{252}Cf-PD = ^{252}californium plasma desorption

CH_2Cl_2 = dichloromethane

$CHCl_3$ = chloroform

CID = collision-induced decomposition

COD = cyclooctadiene

cV = cone voltage

d = doublet (NMR)

Da = Dalton

dba = *trans, trans*-dibenzylidene acetone

d.c. = direct current

DCI = direct chemical ionisation

DEI = direct electron impact

dme = 1,2-dimethoxyethane

DMF = dimethylformamide

DMSO = dimethylsulfoxide

dppe = 1,2-bis(diphenylphosphino)ethane

dppm = bis(diphenylphosphino)methane

dppp = 1,3-bis(diphenylphosphino) propane

e = electron

E = group 15 element

E^+ = electrophilic reagent

EA = elemental analysis

EI = electron impact

ES = electrospray

ESMS = electrospray mass spectrometry/spectrometric

Et = ethyl

Et_2O = diethylether

EtOH = ethanol

eV = electron Volts

FAB = fast atom bombardment

FD = field desorption

FI = field ionisation

FIB = fast ion bombardment

GC/MS = gas chromatography mass spectrometry

Pr(i) = (iso-)propyl

IR = infrared

J = coupling constant (NMR)

L = ligand

LA-FTICR = Laser Ablation Fourier Transform Ion Cyclotron Resonance

Lit. = literature

m = medium (IR), multiplet (NMR)

M = molecular ion (MS), parent complex (ESMS), transition-metal atom

(MA)LDI = (matrix-assisted) laser

Me = methyl

desorption

MeCN = acetonitrile

MeOH = methanol

m.p. = melting point

MS = mass spectrometry/spectrum

m/z = mass-to-charge ratio

nm = nanometer

NMR = nuclear magnetic resonance

phen = 1,10-phenanthroline

PhI = photo ionisation

PeI = Penning ionisation

Ph = phenyl

pip = piperidine

pKa = acidity constant

py = pyridine

ppm = chemical shift (NMR)

r = radius

r.f. = radio-frequency

R = organic substitutent

s = strong (IR)

sh = shoulder (IR)

SIMS = secondary ion mass spectrometry

solv = solvent

t = triplet (NMR)

tcep = tris(2-cyanoethyl)phosphine

thd = 2,2,6,6-tetramethyl-3,5-heptanedione

THF = tetrahydrofuran

tlc = thin layer chromatography

TMS= tetramethylsilane

TOF = time-of-flight

tpa = 1,3,5-triaza-7-phosphaadamantane

TPPMS= triphenyl(mono *m*-sulfonated phenyl)phosphine

TS = thermospray

UV = ultra violet

vs = very strong (IR)

w = weak (IR)

xs = excess

Xy = xylyl

As*** = tris(*p*-methoxyphenyl)arsine

CNPh* = *p*-methoxyphenylisonitrile

dppe*** = 1,2-bis[di(*p*-methoxy phenyl)phosphino]ethane

HS* = *p*-methoxythiophenyl

$HS^{\bullet}$ = 4-mercaptopyridine

P* = diphenyl(*p*-methoxy phenyl)phosphine

P** = phenylbis(*p*-methoxy phenyl)phosphine

P*** = tris(*p*-methoxyphenyl)phosphine

$P^{\bullet}$ = diphenyl(*p*-dimethylamino phenyl)phosphine

$P^{\bullet\bullet}$ = phenylbis(*p*-dimethylamino phenyl)phosphine

$P^{\bullet\bullet\bullet}$ = tris(*p*-dimethylamino phenyl)phosphine

P^{9*} = tris(2,4,6-trimethoxy phenyl)phosphine

Sb*** = tris(*p*-methoxyphenyl)stibine

TosMIC = tosylmethylisocyanide

Chapter 1

Electrospray Mass Spectrometry

In 1913, the father of mass spectrometry, J. J. Thomson, wrote in the preface of his famous book, *Rays of Positive Electricity and Their Application to Chemical Analysis*[1]:

> **"One of the main reasons for writing this book was the hope that it might induce others, and especially chemists, to try this method of analysis. I feel sure that there are many problems in chemistry which could be solved with far greater ease by this than any other method."**

It is amazing how accurately Thomson was able to outline the potentialities of mass spectrometry back then. Not only is this tool now routinely used in almost all branches of pure science, but also in the applied sciences, such as technology, agriculture and medicine.

Although it is beyond the scope of this thesis to delve deeply into the theory of mass spectrometry, a brief introduction is necessary. In the next section, the basic instrumentation will be described, including the advantages and disadvantages of the different ionisation methods. This should provide enough background to appreciate the features that distinguish electrospray mass spectrometry (ESMS) from other methods of ionisation. ESMS will be discussed separately in the second part of this chapter. Within this subsection, which also includes aspects of ESMS history and instrumentation, the different methods available for generating ions in solution prior to their analysis are summarised. The use of electrospray-friendly ligands, the main concern of this thesis and one of the available options, is outlined in detail in the following chapter.

---

[1] J. J. Thomson, *Rays of Positive Electricity and their Application to Chemical Analysis*, Longmans, Green & Co., London, 1913.

1.1 Background

Mass spectrometry exhibits two main features which assured its immediate success and later rapid growth. They are:

1. Only the smallest amounts of sample are required in order to determine the relative molecular mass and even the elemental composition of a compound.

2. Important structural information may be drawn from the fragmentation pattern, induced by collision of the ions with electrons or other species.

However, the mass spectrometric determination of the relative molecular mass of analytes has also been limited in some respects. In order to transfer them into gas-phase ions (which is required for their detection by a mass analyser) they needed to be volatile and thermally robust. The polarity of a compound is, however, opposed to its volatility. Furthermore, the larger the molecular mass the more functional groups are generally present, leading to a higher probability of decomposition during the volatilisation process. This is why different methods of ionisation have been developed, allowing the mass spectrometric analysis of a larger number of compounds and there are continual efforts to further improve these methods. Today, fast and reliable instruments are available which are able to analyse an increasing number of compounds. These improvements have rendered the mass spectrometer a very powerful if not essential tool in chemistry and chemistry-related fields.

Mass spectrometry further distinguishes itself from other spectroscopic methods as it does not measure the energy necessary for the transition of energy levels. Besides determining the molecular weight, it rather analyses the products of a reaction process which is induced by ionising molecules. The way a mass spectrum looks is not only dependent on the structure and functional groups of a compound, but also on the conditions of analysis and choice of instrumentation. This implies that care should be taken when comparing spectra. It is also the reason why when giving an introduction into mass spectrometry, instrumentation should play a more important role than in UV, IR or NMR spectroscopy.

Many textbooks are available on mass spectrometry, which encompass various areas of the field, such as fundamental principles and instrumentation[2], coupling techniques[3], inorganic and complex chemistry[4], organic chemistry[5], as well as biochemistry and natural product chemistry[6,7]. A number of valuable journals appearing periodically also deserve a mention[8]. In comparison, the number of papers/reviews/textbooks on the principle of ESMS is rather limited, but growing constantly. For reviews and articles covering specific aspects of ESMS, the reader is referred to the second part of this chapter.

1.2 Instrumentation

A mass spectrometer is an instrument that produces ions, separates them according to their mass-to-charge (*m/z*) ratio, and detects them. In order to do this, every mass spectrometer requires four fundamental parts:

---

[2] H. Budzikiewicz, *Massenspectrometry: eine Einführung*, 4. Aufl. Wiley, Weinheim, 1998; J. T. Watson, *Introduction to Mass Spectrometry*, Lippincott-Raven Publishers, Philadelphia, 1997; M. E. Rose and D. H. Russell (eds.), *Experimental Mass Spectrometry*, Plenum Press, New York, 1994; A. M. Lawson (ed.), *Mass Spectrometry*, de Gruiter, Berlin, 1989; B. J. Millard, *Quantitative Mass Spectrometry*, Heyden & Son Ltd., London, 1978.

[3] H. J. Hübschmann, *Handbuch der GC/MS*, VCH, Weinheim, 1996; R. E. Ardey, *Liquid Chromatography-Mass Spectrometry*, VCH, Weinheim, 1993; K. L. Bush, G. L. Glish and S. A. McLuckey, *Mass Spectrometry/Mass Spectrometry*, VCH, New York, 1988.

[4] F. Adams, R. Gijbels and R, Van Grieken (eds.), *Inorganic Mass Spectrometry*, Wiley, New York, 1988; J. Charalambous (ed.), *Mass Spectrometry of Metal Compounds*, Butterworth, London, 1975.

[5] A. E. Ashcroft, *Ionisation Methods In Organic Mass Spectrometry*, The Royal Society of Chemistry, Cambridge, 1997; H. Budzikiewicz, C. Djerassi and D. H. Williams, *Mass Spectrometry of Organic Compounds*, Holden-Day, San Francisco, 1967.

[6] M. E. Rose and R. A. W. Johnstone, *Mass Spectrometry for Chemists and Biochemists*, 2nd ed., University Press, Cambridge, 1996.

[7] C. H. Suelter and J. T. Watson (eds.), *Biochemical Applications of Mass Spectrometry*, Wiley, New York, 1990; G. R. Waller (ed.), *Biochemical Applications of Mass Spectrometry*, Wiley, New York, 1972, supplementary volume 1980.

[8] *Advances in Mass Spectrometry* (since 1959): one to two volumes every three years, includes talks of the 'International Conference on Mass Spectrometry', which is held every three years on all areas of mass spectrometry; *European Mass Spectrometry* (since 1995): published every two months, includes works on inorganic, bioorganic and organic mass spectrometry; *International Journal of Mass Spectrometry and Ion Processes* (since 1968): several volumes per year, more theoretically and physically orientated (has been called: *...and ion Physics* until 1993); *Journal of Mass Spectrometry* (since 1995, through fusion of *Organic Mass Spectrometry* and *Biological Mass Spectrometry*): includes works according to the former titles; *Journal of the American Society of Mass Spectrometry* (since 1990): published monthly, includes work on all areas of mass spectrometry; *Mass Spectrometry Reviews* (since 1982): published every two months, includes review articles of all areas of mass spectrometry as well as lists of textbooks and other reviews; *Rapid Communications in Mass Spectrometry* (since 1987): published monthly, includes short communications of various areas of mass spectrometry.

1. An **inlet system** for the introduction of the sample,

2. an **ionisation source**, where the sample molecules are ionised (because only ions can be detected by the mass analyser),

3. a **mass analyser,** which separates the ions according to their *m/z* ratio,

4. and a **detector**, which makes the ions visible to the user by detecting them and feeding the signal to a data system where the results can be studied, processed and printed out.

The whole of the mass spectrometer [except for atmospheric pressure ionisation (API) sources] is maintained under vacuum to avoid involuntary collision between ions and other species. The various instruments are often interdependent, so that choice and combination of them are partly predetermined, but also depend on the requirements of the analytes and, last but not least, the budget available. Figure 1.1 shows the essential features in diagrammatic form, and the following sections describe each feature briefly.

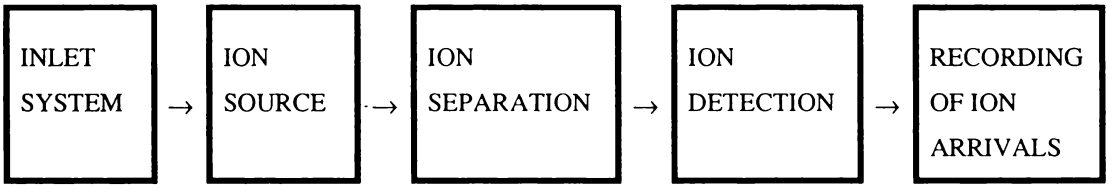

Fig. 1.1 The essential features of a mass spectrometer in diagrammatic form.

1.2.1 Inlet systems

The challenge with the inlet system, as may be derived from the above, is to transfer the analyte from atmospheric pressure to vacuum without interrupting the vacuum inside the instrument. There are many different ways of introducing samples into the ionisation source depending on the ionisation method being used and the type of sample under investigation. They can be divided into three classes:

1. The sample is evaporated before its ionisation. In this case, there are generally three types of inlet systems: The **gas inlet**, the **direct inlet** and the **coupling to a gas chromatograph (GC/MS)**. Many mass spectrometers are equipped with more than one inlet system. The gas inlet is used for gases and other very volatile analytes. Thus,

volatile liquids may be injected directly with a microsyringe through a septum into a previously evacuated reservoir. Gases enter through a container with a corresponding joint. Involatile and thermally unstable substances enter the instrument through the direct inlet. They are placed onto a heatable probe, which is passed into a lock chamber. After evacuation of the chamber, the cold probe is inserted directly into the ionisation source, where it is heated until the sample evaporates. The principle advantage of the direct inlet is that as a consequence of the low pressures in the source (~ 10^{-4} Pa), the sample needs a lower evaporation temperature (as opposed to the gas inlet). Moreover, the molecules have a shorter path to the ionisation region. Therefore, this inlet generally leads to less catalytic and thermal decomposition.

2. The ions are transferred into the gas phase from the condensed phase. This technique is described with the ion sources FD, FAB, SIMS, ^{252}Cf-PD and MALDI (refer to section 1.2.2).

3. The dissolved sample is nebulised into fine droplets from which gas-phase ions are formed. This technique is described with the spray techniques aerospray, thermospray and more detailed with electrospray (refer to sections 1.2.2 and 1.3.2).

1.2.2 Ion sources

Regardless of which inlet system is employed, a constant stream of vaporised sample enters the ion source, where it is ionised and fragmented[9]. The way in which the ions are produced determines the type of spectrometer. Each method exhibits its own special characteristics and requirements in terms of selectivity, preparation, speed of analysis, amount and type of analyte *etc.*

The first five methods of ionising the sample are for volatile and thermally robust samples (sections 1.2.2.1 – 1.2.2.4) whereas all following ones are able to deal with involatile and thermally instable compounds. Among them, the last six techniques (sections 1.2.2.8 – 1.2.2.12) involve rapid heating as part of the ionisation process.

[9] An exception is ESMS, where the ions are already formed in solution prior to their analysis. This process will be discussed in more detail in section 1.3.

1.2.2.1 Electron impact (EI)

Because of its wide distribution, extensive library of spectra and in particular its straightforward analysis of 'simple' organic compounds, EI remains the most common means of ionisation. In an EI ion source, the sample is bombarded with a beam of electrons, which normally operates at 70 eV because the maximum ion yield is obtained at this value. Since 20 eV is sufficient to ionise most sample molecules, an excess of energy is transferred to the molecular ion, causing it to fragment. Through interaction of the electrons with the neutral molecules, an electron is removed and positively charged ions (molecular ions) are formed according to:

$$M + e^- \rightarrow [M]^{\bullet+} + 2\,e^-$$

There are two major disadvantages of EI. They are the limitation to thermally robust and volatile compounds, such as neutral inorganic and organic compounds of low molecular mass. Secondly, a large number of fragment ions are produced in addition to the molecular ion $[M]^{\bullet+}$, leading to very complicated spectra. In some cases, the molecular ion is not observed at all. Hence, the highest *m/z* value does not necessarily correspond to the molecular ion. This is obviously a major disadvantage if working with unknown species, where the most important information in a mass spectrum is the molecular weight of the compound. On the other hand, the more fragmentation occurs the more structural information may be drawn from the spectrum. The spectrum of talbutal is shown as an example in Figure 1.2.

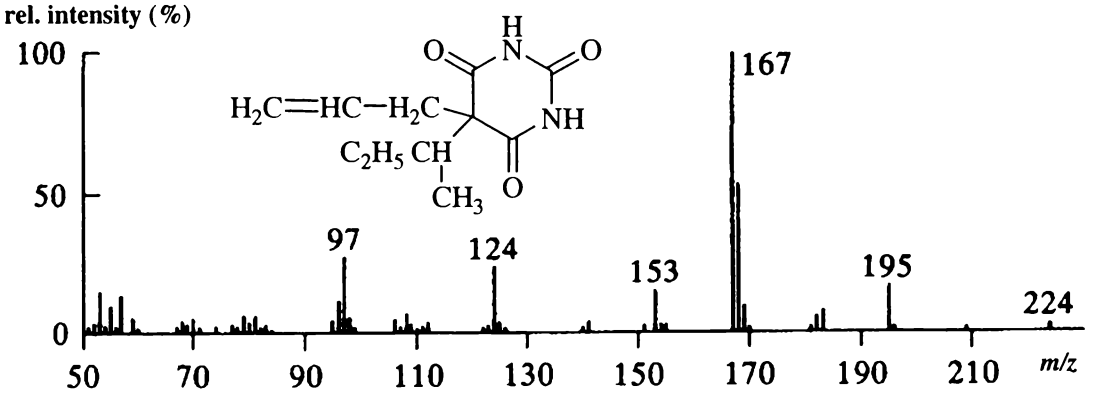

Fig. 1.2 The EI mass spectrum of talbutal (M_r = 224) [6].

1.2.2.2 Chemical ionisation (CI)

Chemical ionisation differs in that the sample is ionised by reaction with a set of reagent ions. These are produced by EI ionisation and ion-molecule collision of a reactant gas, mostly methane but also other hydrocarbons, noble gases, H_2 or NH_3, each having its own advantages and disadvantages. Depending on the type of reactant gas used, the reagent ions react with the sample forming $[M]^{\bullet+}$, $[M]^{\bullet-}$ or $[M + H]^+$ ions, the latter one is often described as quasimolecular ion.

Chemical ionisation can be applied to the same compound classes as EI, *i.e.* a range of volatile compounds up to 1000 Da. Formation of fragment ions can be controlled by the choice of reactant gas, making CI a softer alternative to EI (refer to Figure 1.3, which shows the same compound as above, but under CI conditions). CI is often used when EI leads to fragmentation to such an extent that $[M]^{\bullet+}$ is not observed or if the molecular weight of a sample is of sole importance. A disadvantage is that the spectra are extremely temperature dependent so that reproducibility is very poor. Moreover, there are cases where the quasimolecular ion is not the most intense ion. Alkyl transfer, *e.g.* M + $C_2H_5^+ \rightarrow [M + C_2H_5]^+$, may lead to ions with a higher *m/z* value than the quasimolecular ion, making ion assignment more complicated, in particular for unknown species.

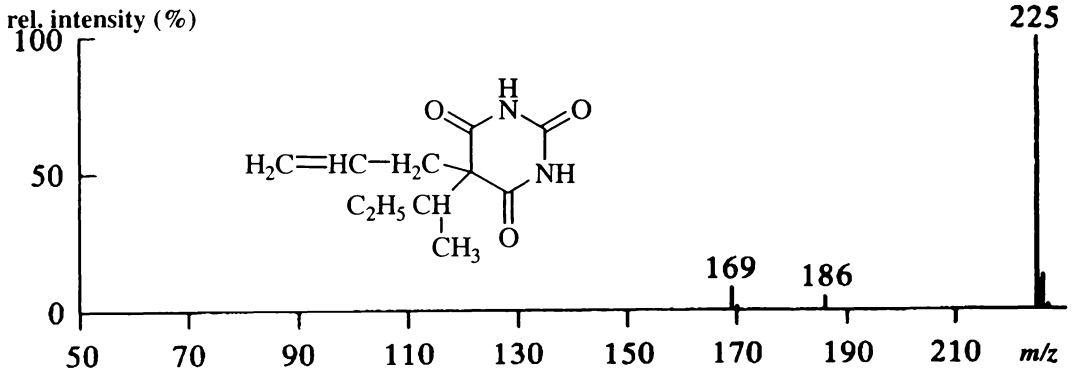

Fig. 1.3 The CI mass spectrum of talbutal (M_r = 224) [6].

1.2.2.3 Photo Ionisation (PhI) and Penning Ionisation (PeI)

For these methods, ionisation is achieved by bombarding the sample with either photons (PhI) or electronically excited neutral species (PeI). The concept is very similar to the EI and CI techniques described above. As they offer little or no advantage over EI and CI, their application is rather limited and will not be described in further detail.

1.2.2.4 Field Ionisation (FI)

In field ionisation, the molecules of interest are not ionised by collision with some kind of energetic particles. Rather, a number of microneedles on a tungsten wire (called the emitter) provide the ionisation sites. After the sample has been volatilised by heat, it condenses on the emitter needles. In positive-ion mode, a high positive electric potential is applied. The molecular orbitals (themselves an electric field) are distorted and an electron is removed from the molecule producing a molecular ion $[M]^{\bullet+}$, which is immediately repelled by the positive electrode and pulled into the mass spectrometer. In negative-ion mode, electron capture from the negatively charged needle tip leads to $[M]^{\bullet-}$ molecular ions. Depending on the sample (polar, non-polar, acidic, basic, ionic), proton abstraction, anion/cation attachment, or thermal emission of pre-formed ions are other possibilities of ion formation.

As there is only little excess energy, fragmentation is limited, as illustrated in Figure 1.4 (again for talbutal). However, like all the previous methods, FI is limited to volatile and therefore lower molecular weight compounds. There are also difficulties in focussing the ions into a beam because the time that the ions spend in the source is extremely short attributed to the repulsion by the positive electrode. Another drawback is the tedious and time-consuming preparation of the emitter electrode (they are very expensive to purchase), and the fact that magnetic sector mass analysers (see section 1.2.3) are required because of the high kinetic energy of the ions.

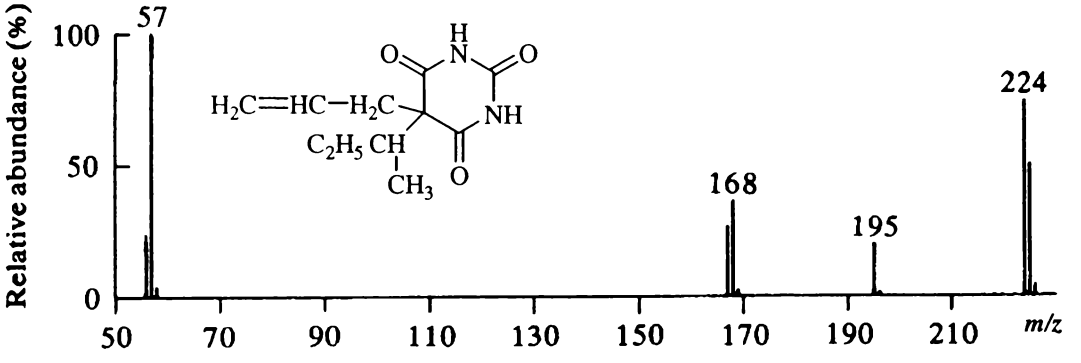

Fig. 1.4 The FI mass spectrum of talbutal (M_r = 224) [6].

1.2.2.5 Field Desorption (FD)

Since the beginning of mass spectrometry, the involatility and thermolability of many compounds has proven to be a significant obstacle for the determination of their molecular mass. The technique FD was developed for thermally unstable compounds that are of insufficient volatility for ionisation in the gas phase to be possible, as required for the methods discussed before. Examples of such compounds include polymers, peptides, sugars, inorganic and organometallic compounds *etc*. This technique is very similar to the FI method, as they both employ the same mode of ionisation.

In FI, the sample is introduced into the source in its vapour state by any means of inlet system and subsequently ionised through use of electric fields. FD differs from FI as the sample is coated onto the electrode/emitter prior to inserting the probe into the source. After the emitter has been inserted through a vacuum lock, the tip of the probe is very close to the counter electrode. Under the influence of high electric fields, positive ions are desorbed from the substrate and drawn into the mass analyser. Hence, ionisation occurs in the condensed phase on or near the emitter. This leads to a major advantage over FI, namely that it is suitable for analysing high molecular weight, thermally unstable compounds, because the volatilisation step is avoided. Moreover, since FD is a soft ionisation technique, it yields only the $[M]^+$ and/or $[M + H]^+$ ions (depending on the nature of the analyte). Figure 1.5 provides a good example of an FD spectrum, especially when comparing the spectrum with the previous ones. Both FI and FD (developed in the 1950s and 1960s) were pioneers of the development of ionisation techniques for thermally labile and high molecular weight samples. Their use declined, however, with the advent of FAB in the 1980s, and later ESMS.

FD suffers from the same drawbacks as FI, *i.e.* tedious preparation of the emitter plus the requirement for magnetic sector instruments. Moreover, the ion currents depend so heavily on the temperature of the emitter that heating control is crucial.

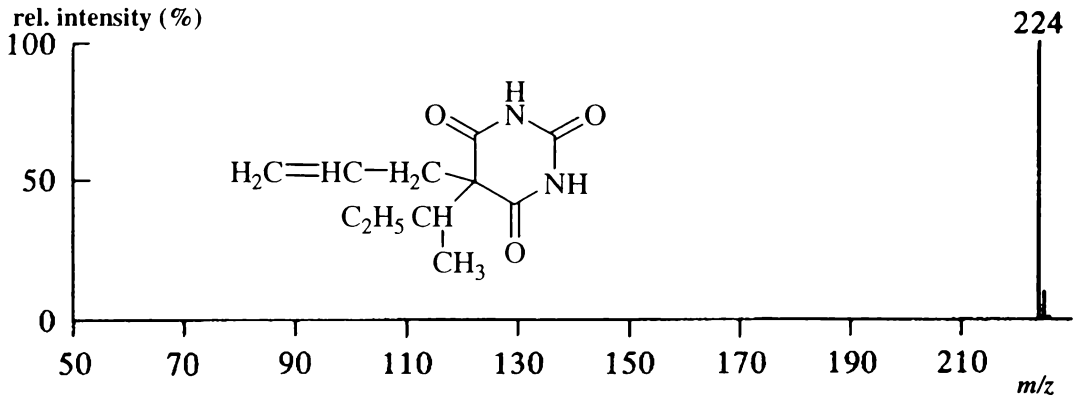

Fig. 1.5 The FD mass spectrum of talbutal (M_r = 224) [6].

1.2.2.6 Electrospray (ES), Thermospray (TS) and Aerospray (AS)

For ES, TS and AE, as for FD, strong electrostatic fields are used to desorb ions from the substrate, but rather than into vacuum, the ions are desorbed into a bath of gas. In all three cases, the analyte solution is dispersed as a spray of charged droplets from which the ions desorb. The three techniques differentiate in the way the charged droplets are produced, *i.e.* aerodynamically, thermally or electrically. Allegedly, TS was developed inadvertently when ions were still detected in a modified CI source although the filament was (unknowingly!) switched off[10]. In TS, the analyte solution is first passed through a hot capillary, where most of the solvent vaporises readily. The expansion of the solvent gas leads to acceleration forces on the remaining liquid, resulting in a dispersion of droplets, which emerge from the capillary as a supersonic jet. AS uses aerodynamic forces (as in a perfume atomiser) to vaporise most of the solvent, followed by the same kind of acceleration forces as in TS. Obviously, the ES technique uses an electric field to achieve the same results. The formation of charged droplets in ES is often described as 'atomisation by charging' *vs.* 'charging by atomisation' in AS and TS. This technique, being the main concern of this thesis, will be explained in detail in the next section (section 1.3). Common inlets for spray techniques are the direct infusion (conventional pumping through a solvent delivery pump), loop injection and the combination of loop injection with an on-line chromatograph. All three spray techniques are excellent for large biomolecules, such as polypeptides, sugars *etc.* ES distinguishes itself from the others by forming multiply-charged ions because it produces the smallest droplets with the highest charge-to-mass ratio. By generating these multiply-charged ions, which are

detected at *m/z* values much lower than the molecular weight of the large molecule, ESMS has removed the mass range limitations which traditionally restrict the analysis of singly-charged compounds.

1.2.2.7 Atmospheric pressure chemical ionisation (APCI)

The APCI source is a modified ES source. In both cases ionisation occurs at atmospheric pressure and the dissolved sample is converted into an aerosol by a combination of nebuliser gas and heat. With APCI, however, the high voltage is not applied at the probe tip, but at a corona discharge needle inside the heated source. Hence, the nebulising and ionisation steps are separated. A chemical ionisation reagent gas is produced in the area around the needle by collisions and charge transfer reactions. The sample molecules that pass through this region can be ionised in the same manner as described above for CI in section 1.2.2.2.

As opposed to ES ionisation, APCI does not generate multiply charged ions and is therefore not appropriate for very high mass samples. Structural information can be obtained (as in ES) by either in-source cone voltage fragmentation or MS/MS (provided a tandem mass spectrometer is available).

1.2.2.8 Fast atom bombardment (FAB)

For thermally labile substances, the rate of heating rather than the absolute temperature is the deciding factor in the competition between evaporation (breaking of intermolecular bonds) and decomposition (breaking of intramolecular bonds). According to Beuhler *et al.*[11], ionisation techniques that involve rapid heating (*i.e.* anywhere between 10 and 500°C s^{-1}) vaporise even complex molecules before decomposition can occur. There is less time for the molecules to transfer excess energy for dissociative processes and they also spend less time in the gas phase, where bimolecular interactions can lead to decomposition. The exact mechanism of ionisation is not fully understood. It could occur in the solid phase with subsequent ion desorption, in the solid/gas interface, or in the gas phase after intact neutral molecules have desorbed from the probe tip.

---

[10] C. R. Blakley and M. L. Vestal, *Anal. Chem.*, 1983, **55**, 750.
[11] R. J. Beuhler, E. Flanigan, L. J. Green and L. Friedmann, *J. Am. Chem. Soc.*, 1974, **96**, 3990.

In FAB, the analyte is first dissolved in a polar matrix, *i.e.* a relatively involatile solvent (since it must survive the high vacuum conditions) with good solvating properties. Glycerol, for example, is a commonly used matrix because it is a small, polar and viscous liquid. A matrix is necessary to keep the sample in position until a mass spectrum has been acquired and it also plays a role in the ion formation process. The mixture is placed onto the tip of a metal probe, which is then inserted into the ion source. The principle of this method is based on the surface of the probe being bombarded with high-energy (8-10 keV) atoms. The fast neutral atoms (usually argon) are produced in an enclosed unit, a so-called 'atom gun', close to the ionisation chamber. Abundant molecular ($[M]^{\bullet+}$ or $[M]^{\bullet-}$) or quasimolecular ions ($[M + H]^+$, $[M - H]^-$, $[M + me]^+$; me = metallic element) are observed together with fragment ions.

As the ions have excess energy, fragmentation and recombination processes yield complex spectra (refer to Figure 1.6). The presence of the matrix and traces of solvent can also complicate the spectra. The matrix can protonate, deprotonate or form cluster ions. Another limitation is that a precise quantitative analysis is very difficult with all ionisation techniques that use a direct insertion probe. The signal of the sample often dies away when the matrix, rather than the sample, is consumed.

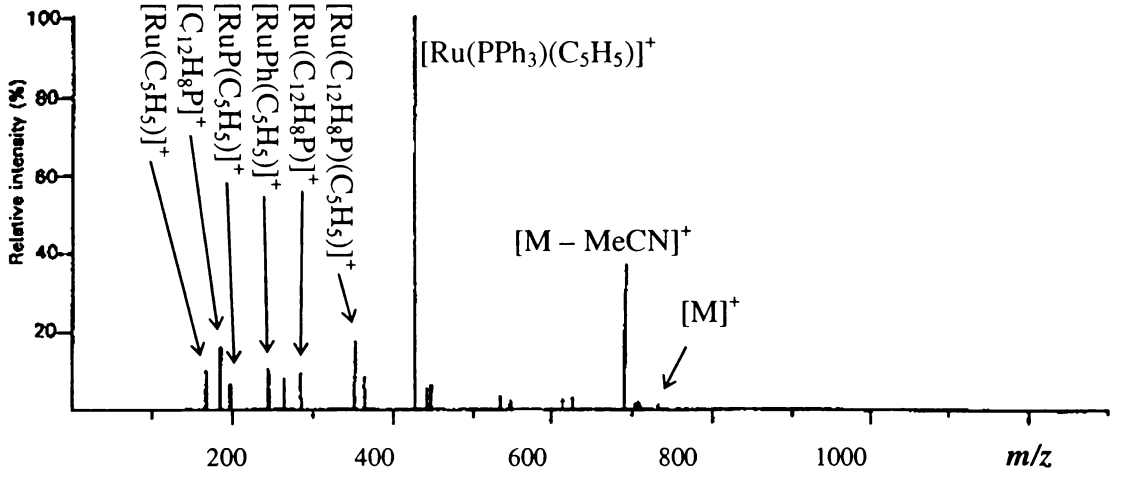

Fig. 1.6 The FAB mass spectrum of $[Ru(NCMe)(PPh_3)_2(\eta\text{-}C_5H_5)][PF_6]$ [12].

[12] M. I. Bruce and M. J. Liddell, *Appl. Organomet. Chem.*, 1987, **1**, 191.

1.2.2.9 Secondary-ion mass spectrometry (SIMS), also termed fast ion bombardment (FIB)

SIMS is closely related to FAB, with the difference that fast ions rather than fast atoms are used. A substance, coated on a metallic surface, is bombarded with primary ions (*e.g.* $Ar^{\bullet+}$) of high kinetic energy. Secondary ions (the ions of interest) are then produced through charge-exchange processes and ion/molecule reactions leading to either molecular or quasimolecular ions as well as fragment ions. SIMS is more convenient than FAB as the neutralisation step is avoided, but there are difficulties in its application associated with charging effects at the bombarded surface. In the 1980s, FAB and SIMS had become the method of choice for polar compounds and may be considered a milestone in the development of ionisation techniques for mass spectrometry, but they have declined in use with the advent of ES and laser desorption (refer to section 1.2.2.11).

1.2.2.10 Direct chemical ionisation (DCI), Direct electron impact (DEI)

Rapid heating can also be used in conjunction with electron impact or chemical ionisation, producing a modified EI or CI technique for involatile, thermally unstable substances. The sample is brought into the ion source with a direct insertion probe and is volatilised by rapid heating of the tip of the probe. The molecules then either travel to the region rich in reactant gas ions and are measured under CI conditions, or they travel to an electron beam of the ion source which is used for EI. When DCI is employed, the spectra resemble both those measured under FD conditions (more intense quasimolecular ions) as well as typical CI spectra (protonation of M with a significant fragmentation pattern). The same applies to the DEI spectra.

The techniques of DCI and DEI are also known as in-beam ionisation, desorption EI and CI, flash volatilisation and plasma desorption. The latter one is not to be confused with the ^{252}Cf-plasma desorption technique (see section 1.2.2.12).

1.2.2.11 Laser desorption (LD)

When a UV laser interacts with material, positive and negative ions are formed, which desorb from the surface. The energy can either be absorbed directly by the analyte (if a chromophore is present) or by the metal surface, from which it is subsequently

transferred to the analyte. The bombardment with intense pulses of laser light effects both desorption and ionisation of the sample. If the sample on the metal probe is subjected to a short but intense laser pulse it is termed a **high intensity pulse method**. Through such rapid heating, the molecules as well as alkali metal ions (present as impurities in the metallic probe or deliberately added) are flash-desorbed from the surface. The alkali metal ions attach to the molecules and form ions of the type $[M + Na]^+$, $[M + K]^+$ *etc*. The laser radiation does not add to the vibrational energy of the molecules, so that little fragmentation is observed in the spectra. Alternatively, a **low-intensity continuous laser beam** can be used to generate gaseous ions from thermally labile compounds.

MALDI (matrix-assisted laser desorption ionisation) follows the same ionisation mode as described above, the difference being that the sample is first dissolved or dispersed in a matrix before it is placed onto the metal probe. Because LD forms ions by means of a laser pulse, it is not compatible with scanning mass analysers, such as quadrupole or sector instruments. It is commonly interfaced with a time-of-flight (TOF) mass analyser (hence the name MALDI-TOF), which has the disadvantage of relatively poor resolution, but the advantage of no upper mass limit and the ability to cope with the short time scale of the pulsed laser. Scanning instruments require the uninterrupted presence of sample ions in order to scan continuously through the whole *m/z* range. In comparison, a TOF instrument can record all ions produced from one laser pulse simultaneously. Thus, very high molecular mass samples (> 9000 Da) can be ionised and detected in their intact form. By mixing the substrate with a highly absorbing matrix, the desorption and ionisation steps are separated. The matrix transforms the energy of the laser into excitation energy for the sample, and they sputter away from the surface. In this way, there is no excess energy imparted onto the sample, hence only limited decomposition. ESMS and MALDI are currently the two favoured techniques from the array of available ionisation techniques for large, polar and involatile samples. It is difficult to compare MALDI-TOF with ES, since they are usually equipped with different types of spectrometers, and hence some characteristics are attributable to the mass analyser used.

1.2.2.12 Californium-252 plasma desorption (^{252}Cf PD)

In ^{252}Cf PD, the radioactive ^{252}Cf is used to volatilise and ionise the solid sample in the ion source. ^{252}Cf decays into two highly energetic fission fragments of equal mass and energy that travel in opposite directions. When one of the fragments hits the sample, it creates a very high local temperature that causes volatilisation. The other fission fragment, which has been produced at the same time but has travelled into the opposite direction, is detected and used to provide a zero time. This method is very useful for high-molecular weight or thermally unstable compounds that produce poor mass spectra even with FD ionisation. As only a few ions are produced by each fission, results need to be accumulated over a long period of time. Thus, although very intense ions are obtained, the low ion yield and the many hours required for acquisition are a disadvantage. The radiation hazard also restricts the general application of this method.

In order for the ions to be attracted from the source into the mass analyser, the source is held at a high voltage (4-8 kV), which causes acceleration of the ions out of the source with a high velocity and towards the mass analyser.

1.2.3 Mass analysers

The separation of ions according to their mass-to-charge ratio occurs in the mass analyser. This is achieved using magnetic and/or electric fields. The basic differences between the various common types lie in the way in which the fields are used and combined. The better the analyser the better the resolution and, obviously, the higher the costs for the instrument. There is a variety of analysers, and the ones referred to in this review are those most frequently encountered: the magnetic sector, the quadrupole and the time-of-flight analyser. It should be noted that not every ionisation method is compatible with every analyser.

1.2.3.1 Sector mass analysers

A simple and therefore only low-resolution instrument is the **single-focussing analyser**. After the beam of ions has been accelerated through a high potential away from the ion source, it is divergent and therefore filtered through focussing slits in order to reduce the spread. The ions are subsequently separated in the field of an electric magnet. Among ions of the same charge, the lower mass fragments are deflected to a greater extent than

the heavier ones, *i.e.* the ions with different *m/z* values travel on mass-dependent curved trajectories. At a constant magnetic field strength, a number of detectors would be necessary in order to record the arrival of each ion *m/z* with its own radius curvature. It is, however, simpler to vary the magnetic field continuously (magnetic scanning), such that the radii of curvature are kept constant and each *m/z* species is brought to the detector at the corresponding field strength. Alternatively, the accelerating voltage may be varied (electric scanning) with a constant magnetic field. Resolution can be increased by improving the focus of the energy of the ion beam. This is achieved with a **double-focussing analyser** (illustrated in Figure 1.7). Most commercial magnetic sector instruments are of this type. The electric sector focuses the ion beam for translational energy and the magnetic sector for mass-to-charge ratio. All other analysers, the quadrupole, TOF and the single focussing magnetic sector instruments generally provide poorer resolution. However, magnetic sector mass spectrometers are often considered to be more difficult to operate than quadrupoles and TOFs, and the high voltage is certainly less forgiving to erroneous usage.

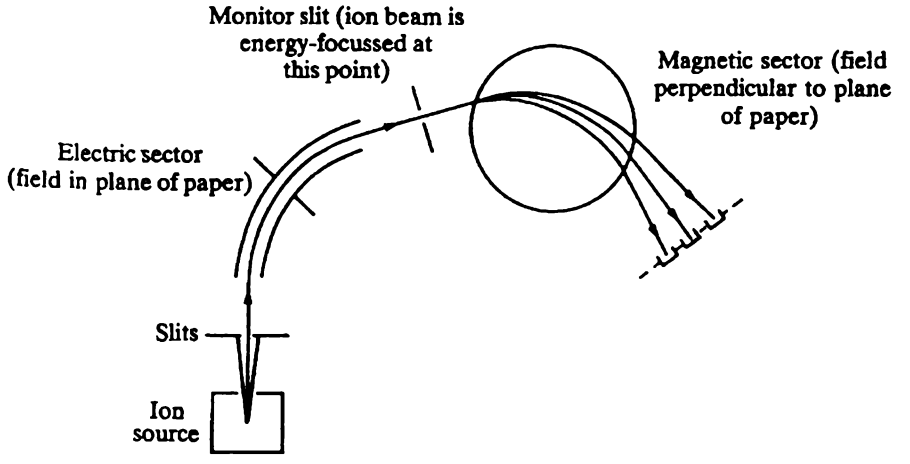

Fig. 1.7 The schematic diagram of a double-focussing mass analyser[6].

Reverse-geometry instruments are obtained when the magnetic sector precedes the electric sector and **triple analysers** have an additional electric sector following the magnetic sector of a double-focussing instrument. **Double-beam instruments** consist of any type of magnetic sector mass analyser only that two ion beams (sample and reference) pass through the same analyser, but arrive at two different detectors. Obviously, more accurate measurements can be made if a reference compound is analysed at the same time.

1.2.3.2 Quadrupole mass analysers

Unlike magnetic sector mass analysers, quadrupoles have no magnetic sector. Instead, the ion beam is directed through four parallel rods that are arranged symmetrically and are electrically connected, as illustrated in Figure 1.8. Between each pair of rods a direct current (d.c.) voltage and a superimposed radio-frequency (r.f.) are applied. Opposite rods have the same polarity while adjacent rods have opposite polarity. When the ions enter this combination of fields they follow complex trajectories. At a set d.c./r.f. ratio, ions of a certain *m/z* ratio follow a stable oscillation, they successfully traverse the quadrupole filter without colliding with the rods and proceed through the quadrupole assembly to the detector. All other masses are lost on the rods of the quadrupole. In this manner, mass separation is achieved. A mass spectrum is obtained by sweeping the voltage from low to high values at a constant r.f./d.c. ratio. Quadrupole mass analysers are faster, smaller, more robust and less costly as compared to magnetic sector instruments. They are also highly sensitive, easy to use and able to cope with large volumes of solvent (for LC coupling), but their capabilities are only equivalent to a single-focussing analyser. Because of their speed and toleration of high source pressures they are particularly suitable for GCMS work and CI.

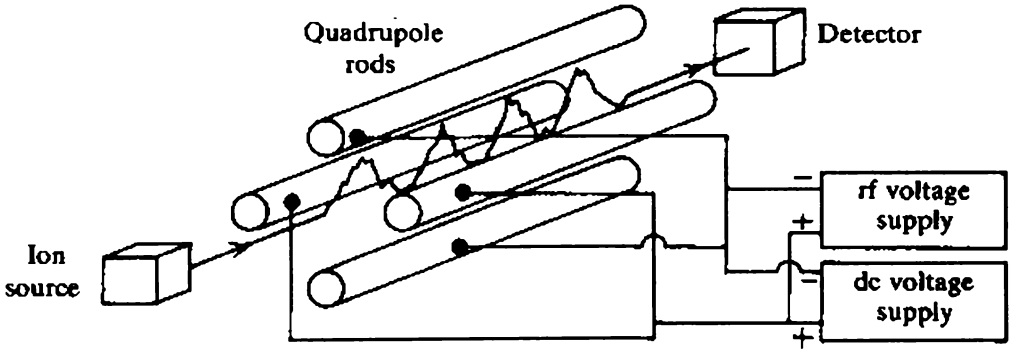

Fig. 1.8 The arrangement of a quadrupole mass analyser[6].

1.2.3.3 Time-of-flight mass analysers (TOF)

Ion velocity is mass dependent, and therefore ions can also be separated by their different velocities after they have been accelerated through a potential away from the ion source. The ions arrive at a detector at different time intervals, which are, however, very short and generally lead to low resolution. Since they have no upper mass range

limitation and are very fast in their response times, TOF analysers find their application in special cases such as fast reactions or detection of very high masses. They are therefore often coupled with ^{252}Cf-PD and are ideally suited for MALDI.

1.2.4 Detectors

After the beam of ions has been accelerated and focused, the ions require conversion to electrons, to allow the signal to be digitised and processed by a computer. Since some ionisation methods are less efficient than others and since the majority of the ions never reach the detector, the absolute number of ions that are actually detected is relatively small. Therefore, some form of amplifying system is required in order to enhance the weak ion streams.

There are several methods of detecting ions and amplifying the generated electric current. Each has its own points of excellence and shortcomings with respect to sensitivity, accuracy and response times. The use of a particular detector depends further on the type of mass analyser used. As an example, the electron-multiplier detector will be discussed. For a description of other detectors, the reader is referred to the literature[13].

The electron-multiplier (more accurately: the discrete dynode version, since there are several types of electron-multiplier detectors) consists of 10 or 20 electrodes (dynodes). The dynodes are of a certain surface material (*e.g.* a copper-beryllium alloy or a lead-doped glass) that is able to expel more than one electron when impacted by an ion. Thus, when an ion impinges on the first dynode, it releases a shower of secondary electrons. These electrons hit the second dynode producing a further shower of electrons. This cascading effect leads to gains in electrical current in the order of 10^6.

The amplified electric current is then sent to an external electric signal amplification circuit and finally to the computer, which acquires and processes the incoming data.

---

[13] S. Evans, Detectors. In J. A. McCloskey (ed.), *Methods in Enzymology*, Vol 193: Mass Spectrometry, Academic Press, San Diego, 1990; P. W. Geno, Ion detection in MS. In M. L. Gross (ed.), *Mass Spectrometry in the Biological Sciences: A Tutorial*, Kluwer Academic Publishers, The Netherlands, 1992.

1.3 ESMS

The advent of ESMS has revolutionised the biochemical and, more recently, the inorganic and organometallic applications of mass spectrometry. As a result, the body of literature has been growing exponentially since the 1990s. Some valuable information may be drawn from review articles on ESMS in general[14], its application to (bio-) organic[15], and to inorganic and organometallic chemistry[16]. The first book entirely devoted to ESMS has been published a few years ago[17]. It encompasses 15 chapters, which are all contributions from leading experts in the field.

1.3.1 Background

The actual process, *i.e.* creating a fine spray of charged droplets with assistance of an applied electric field, is not a new technique and its application is not restricted to mass spectrometry. In fact, as early as 1917 the first experimental study on the phenomenon of electrospray was reported by Zeleny[18]. Since then, it has been applied to various systems, *e.g.* electrostatic painting, fuel atomisation in combustion systems, rocket repulsion and drug delivery. The method is now of such an importance for the electrostatic dispersion of liquids and creation of aerosols that a special issue of the *Journal of Aerosol Science* has been devoted to this topic[19]. About 50 years after Zeleny first reported the ES process, Dole and co-workers coupled the ES source to a mass analyser[20] and carried out some early experiments. Thus, the first combination of electrospray and mass analysis is often credited to him. However, the first successful

---

[14] J. B. Fenn, M. Mann, C. K. Meng, S. F. Wong and C. M Whitehouse, *Mass Spectrom. Rev.*, 1990, **9**, 37; N. B. Cech and C. G. Enke, *Mass Spectrom. Rev.*, 2001, **20**, 362; P. Kebarle and L. Tang, *Anal. Chem.*, 1993, **65**, 972A; S. A. Hofstadler, R. Bakhtiar and R. D. Smith, *J. Chem. Ed.*, 1996, **73**, A82; I. I. Stewart, *Spectrochim. Acta*, 1999, **B54**, 1649.

[15] I. Jardine, *Nature*, 1990, **345**, 747; M. Mann, *Org. Mass Spectrom.*, 1990, **25**, 575; M. Mann and M. Wilm, *Trends in Biolog. Sciences*, 1995, **20**, 219; C. E. C. A. Hop and R. Bakhtiar, *J. Chem. Ed.*, 1996, **73**, A162; *J. Am. Soc. Mass Spectrom.*, 1993, **4**, whole issue devoted to ESMS of proteins.

[16] W. Henderson, B. K. Nicholson and L. J. McCaffrey, *Polyhedron*, 1998, **17**, 4291; R. Colton, A. D'Agostino and J. C. Traeger, *Mass Spectrom. Rev.*, 1995, **14**, 79; R. Colton and J. C. Traeger, *Inorg. Chim. Acta*, 1992, **201**, 153; J. C. Traeger and R. Colton, *Adv. Mass Spectrom.*, 1998, **14**, 637; I. I. Stewart and G. Horlick, *Trends in Anal. Chem.*, 1996, **15**, 80.

[17] R. B. Cole (ed.), *Electrospray Ionisation Mass Spectrometry: fundamentals, instrumentation and applications*, Wiley, New York, 1997.

[18] J. Zeleny, *Phys. Rev.*,1917, **10**, 1.

[19] Electrospray: Theory and Applications, Special issue, *J. Aerosol Sci.*, 1994, **25**.

[20] M. Dole, L. L. Mack, R. L. Hines, R. C. Mobley, L. D. Ferguson and M. Alice, *J. Chem. Phys.*, 1968, **49**, 2240.

experiment was actually performed by Iribarne and Thomson in the late 1970s[21]. In the mid-1980s, Yamashita and Fenn improved on the earlier work when they reported the successful interfacing of an electrospray source with a quadrupole mass analyser and published the first combined ESMS data[22]. At about the same time, the Russian Aleksandrov and co-workers coupled the ion source to another type of mass analyser, a magnetic sector instrument[23]. It was then when electrospray mass spectrometry, as we know it today, was born.

The advent of ESMS came with a large number of inherent advantages:

1. Being a very 'soft' ionisation technique, ESMS is able to produce intact ions even for very large and polar solute species. In fact, if the 'softness' of an ionisation technique is defined by the degree of fragmentation, *i.e.* the less fragmentation the softer the technique, then ESMS is the softest technique available.

2. Though no fragmentation of the parent ion usually occurs, fragmentation may be deliberately induced if required for the structural analysis of a compound. Thus, ESMS provides the chemist with the best of both methods.

3. Because of the unique feature of multiple charging, even molecules with a molecular weight of several hundred kDa are analysed at *m/z* values that are smaller than 3000 amu. This is not only a range where reproducible and clean spectra are easily obtained, it also enables the use of simple quadrupole mass analysers.

4. ESMS can be applied to not only large biomolecules, but also to several types of inorganic and organometallic compounds of various size provided they are soluble and stable in the mobile phase. Those compounds not amenable to ESMS (such as non-polar hydrocarbons) are ideally suited for conventional ionisation methods, allowing different techniques to perfectly complement one another.

5. The sample is introduced in solution. This makes ESMS compatible with various types of solution-based separation techniques, such as liquid chromatography or capillary electrophoresis. Furthermore, as most reactions take place in the liquid

---

[21] B. A. Thomson and J. V. Iribarne, *J. Chem. Phys.*, 1979, **71**, 4451.
[22] M. Yamashita and J. B. Fenn, *J. Phys. Chem.*, 1984, **88**, 4451.

phase, the crude reaction solution can be easily analysed or reactions may be monitored by ESMS. Hence, intermediates as well as rapidly exchanging species can be detected. Once the ions are transferred to the gas phase, ligand exchange stops immediately. Thus, reactions that are rapid on the NMR time scale at room temperature can be easily examined by ESMS with the detection of all exchanging species.

6. Only a minimal amount of sample is needed since all MS techniques are highly sensitive. This is of importance when analysing precious materials. It is possible to carry out reactions on a microscale in order to probe the reactivity of the analyte and, if required, reaction conditions can be altered with minimal waste of chemicals.

7. The sample can be analysed in a very short period of time.

8. Since no matrix is required to aid the ionisation process, the background ions or chemical noise are very low in intensity.

9. ESMS is an atmospheric pressure ionisation (API) technique, meaning that no vacuum lock is required to introduce the sample into the ion source.

1.3.2 Inside the ESMS

As discussed above, ESMS is an API technique. As with all API techniques, ion formation takes place outside the vacuum system of the instrument. The subsequent paragraphs will follow the analyte through the ESMS system according to Figure 1.9.

---

[23] M. L. Aleksandrov, L. N. Gall, N. V. Krasnov, V. I. Nikolaev and V. A. Shukurov, *Zhur. Anal. Khim.*, 1985, **40**, 1570.

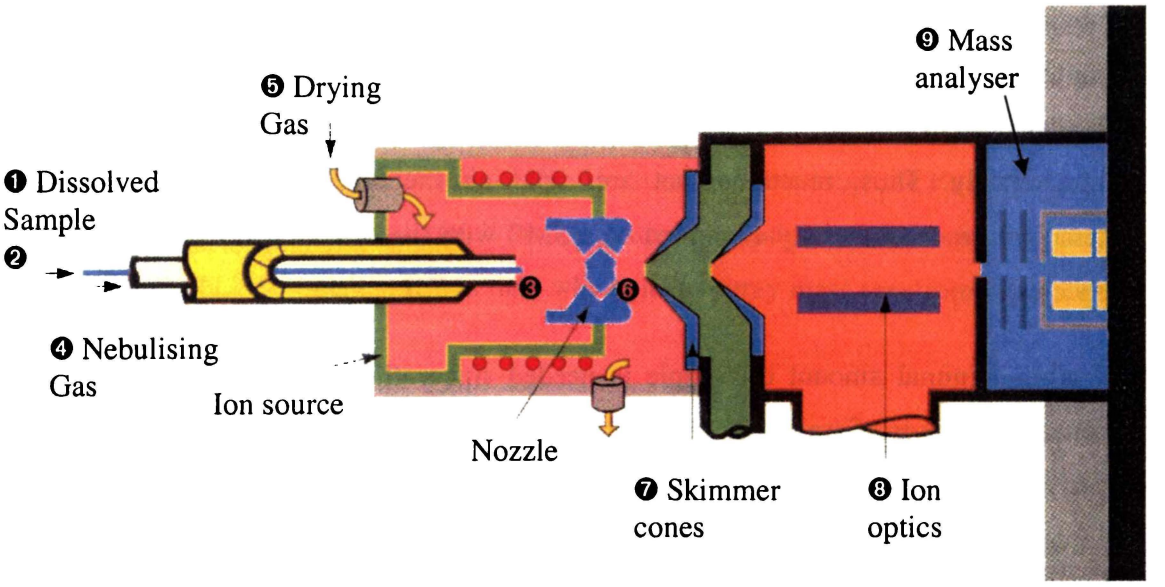

Fig. 1.9 The schematic diagram of an ESMS instrument[24].

❶ A small amount of **sample is dissolved** in an appropriate solvent. The concentration of the sample required to produce a good quality spectrum varies according to the sample's amenability to electrospray ionisation, but a typical region of concentration is 10-100 μg mL^{-1}. The solvent can range from 100% organic to 100% aqueous and is varied to suit the analyte. Neutral compounds are usually dissolved in a protic solvent such as MeCN/H_2O or MeOH. In these cases, protons provide the means of ion production through forming $[M + H]^+$ species. Other methods of ion production and solvent choices are discussed in more detail later (refer to section 1.3.5). In ESMS, it is already at this stage that ions are formed. Thus, the ions are not created within the spectrometer, rather pre-existing ions in solution are transferred into gas-phase ions, allowing detection.

❷ The sample is then **introduced *via* the injection loop**, where it is mainlined into the flow of the mobile phase. The mobile phase is usually the same electrolyte as the solvent. They are both pumped through a narrow tubing at a low flow rate (0.01 – 0.03 mL min^{-1}) into a stainless steel needle.

❸ The **tip of this needle** (or capillary) is the region where the actual spraying occurs. The capillary is held at a high voltage of approximately 3 – 3.5 kV (hence the term electrospray), which can be of either polarity depending on whether positive or negative

[24] VG Biotech, *VG Platform – putting API LC/MS on the Chromatographer's bench*, Altrincham, Cheshire, WA 14 5RZ, UK.

ions are analysed. For reasons of simplicity, only the positive ion mode will be considered in the following. Figure 1.10 displays a close-up of the capillary tip, where **the fine spray of charged droplets is created.**

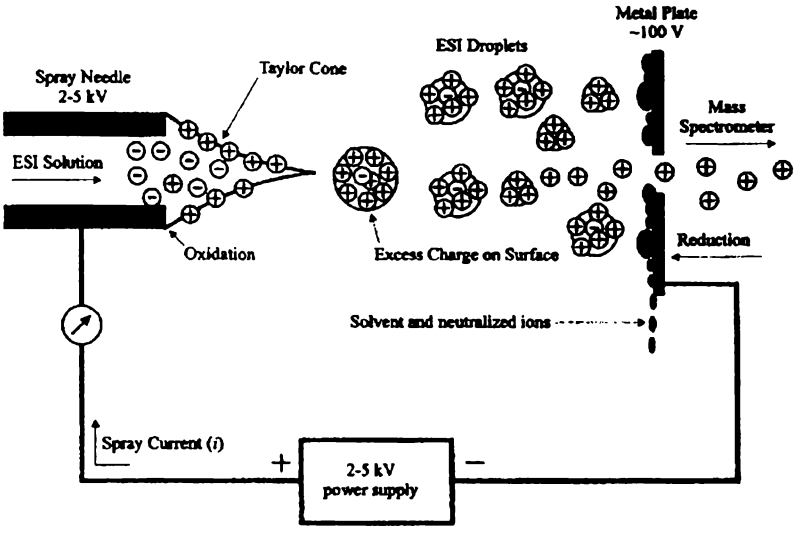

Fig. 1.10 The close-up of the tip of the capillary[25].

When an electric field is applied, positive ions migrate to the liquid surface and negative ions in the opposite direction into the capillary. This electrophoretic charge separation (*i.e.* separation of charge under the influence of an electric field) is responsible for the formation of charged droplets. The surface has an overall positive charge and is drawn toward low field. At the same time, it is still opposed by the forces of the surface tension. However, when increasing the field, the liquid surface is pulled toward the electrode, the surface tension is overcome and a bulk in form of a charged droplet is pulled free (toward the electrode). The surface relaxes and starts charging up again. At fast charging, *i.e.* at a high frequency, a steady state process is reached and a **Taylor cone** (named after G. I. Taylor[26]) at the tip of the capillary is formed. The spraying process has been examined microscopically[27] and it was found that the shape of the meniscus of the sprayed liquid and droplets change drastically with the electric field reaching its optimum. First, the liquid and droplet are drawn from the needle tip toward the ground plate. The liquid begins to expand and changes in shape from an elliptically-shaped fluid cone into the so-called Taylor cone. After a short flight path, the jet spreads

---

[25] N. B. Cech and C. G. Enke, *Mass Spectrom. Rev.*, 2001, **20**, 362.
[26] G. I. Taylor, *Proc. R. Soc. London A*, 1964, **280**, 383.
[27] M. S. Wilm and M. Mann, *Int. J. Mass Spectrom. Ion. Proc.*, 1994, **136**, 167.

into a plume of fine droplets, which soon become invisible to the observer because of the solvent evaporation.

The electrospray process is aided by a co-axial **nebulising gas ❹,** which also flows down the probe, but around the outside of the capillary. This gas is usually N_2 and assists in directing the spray emerging from the capillary tip. The charged droplets travel between the electrodes at atmospheric pressure while a warm (~ 60°C) counter-flow of nitrogen gas, **the drying gas ❺**, evaporates the bulk solvent, eventually resulting in **gas-phase ions**.

Another function of the imposed electric field is that it keeps the droplets from freezing during the endothermic solvent evaporation process by causing them to endure many collisions by which some translational energy is converted into internal energy, thereby warming the droplet. When the bulk solvent has evaporated to some extent, the overall radius of the charged droplet is reduced. Since the overall charge is maintained, repulsive electrostatic forces on the surface of the droplet increase. At a critical point (the Rayleigh limit, named after Lord Rayleigh, who first reported this phenomenon in 1882[28]), the repulsive forces between like charges in the electrolytic solution overcome the attractive surface tension, a rupture of the surface occurs leading to an explosion of mass and charge from the droplet (**'Coulomb explosion' or 'droplet fission'**). It has since then been studied by several other groups[29], who demonstrated that the Rayleigh limit does not actually have to be reached completely for the rupture of the droplet. The 'Coulomb explosion' produces many smaller charged droplets or offspring droplets (*ca.* 20), which subsequently repeat this sequence, *i.e.* are again reduced in radius by solvent evaporation followed by rupture at the surface. These evaporation and fissioning steps produce very small droplets ($r \approx 10$ nm), and it is at this point where two contentious mechanisms emerge. As shown in Scheme 1.1, two theories have been developed: either the ion is leaving the droplet (a) or the droplet is leaving the ion (b).

---

[28] Lord Rayleigh, *Philos. Mag.*, 1882, **14**, 184.
[29] D. C. Taflin, T. L. Ward and E. J. Davis, *Langmuir*, 1989, **5**, 376; A. Gomez and K. Tang, *Phys. Fluids*, 1994, 404.

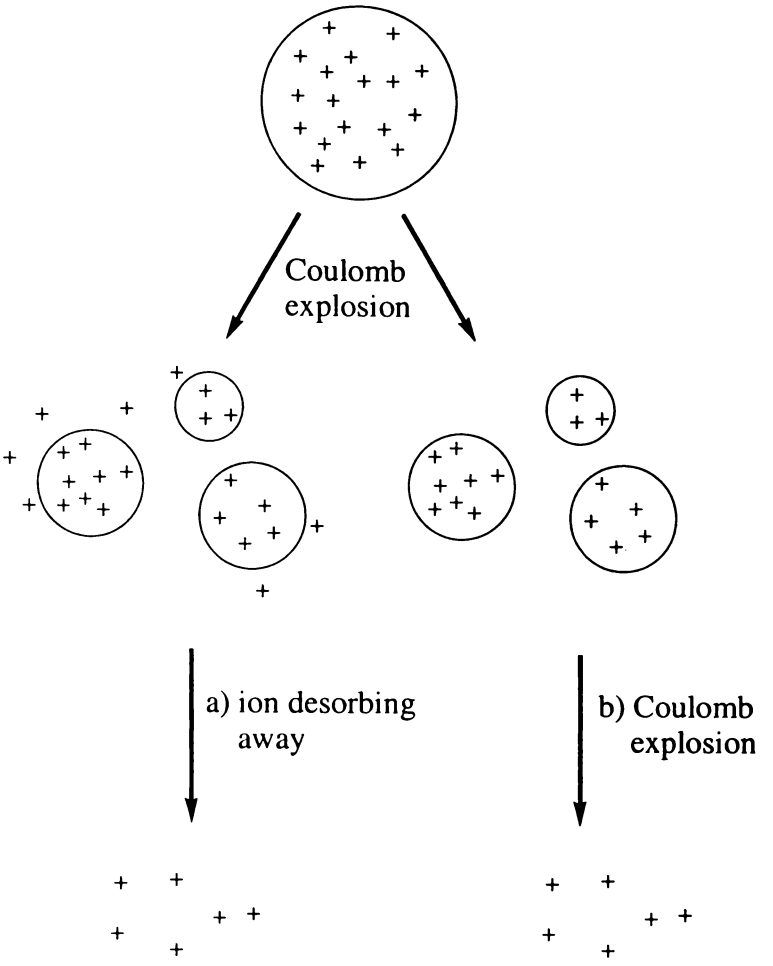

Scheme 1.1 The two mechanisms of creating gas-phase ions in ESMS.

In (a), an increase in droplet charge density leads to intact ions (gas-phase ions) desorbing from the surface of the droplet into the gas phase. This direct emission of gas-phase ions occurs when the droplet has reached a certain size ($r \leq 10$ nm) through several Coulomb fission processes. This **ion evaporation theory** was initially proposed by Iribarne and Thomson[21,30]. The rival model (b), known as the **charged residue theory** by Dole[20] and Roellgen[31], suggests that after sufficient evaporation/fission cycles, the droplet consists of a single charge (gas-phase ion) because some droplet charge remains after all solvent has been evaporated. Thus, according to (b), Coulomb fission continues below the size of 10 nm, while (a) claims that the Coulombic stress is released by ion emission when droplets have shrunk to a radius of $r \approx 10$ nm or smaller.

---

[30] J. V. Iribarne and B. A. Thomson, *J. Chem. Phys.*, 1976, **64**, 2287.
[31] R. Schemlzeisen-Redeker, L. Buttering and F. W. Roellgen, *Int. J. Mass Spectrom. Ion. Proc.*, 1989, **90**, 139.

Both theories predict the same result and an unequivocal decision has not been made for either mechanism. There is evidence[32] that the mechanism is different again for $r < 1$ nm (back to a) and is also different for macroions such as proteins (back to b)[17]. There are more theories around, but they are mostly based on or are extensions of these two models. Whatever the mechanism, the produced gas-phase ions migrate (driven by the magnetic field) into the vacuum region of the instrument.

Since the ES process occurs at atmospheric pressure and mass analysers require high vacuum (~10^{-6} torr), an atmospheric pressure interphase is needed to connect the ion source with the mass analyser. Most atmospheric pressure interfaces are based on a two- or multiple-stage pumping system, which eventually reduces the pressure from atmospheric to very low pressures.

1.3.2.1 Digression: Gaining structural information

In addition to analysing the molecular weight information, structural elucidation can be achieved. The nozzle-skimmer area ❻, where both ions and a bath gas are present, is crucial as it provides a collision region (collision being the second important role of the bath gas). Fragmentation is deliberately induced by either varying the skimmer cone voltage (to induce in-source fragmentation), or by using MS/MS techniques. The latter is only possible if the mass spectrometer incorporates more than one mass analyser, *i.e.* if it is a tandem mass spectrometer. The in-source collision-induced decomposition (CID) of a sample is occasionally referred to as 'cone voltage fragmentation'. The skimmer cone transmits the ions from the atmospheric pressure region to the intermediate vacuum region. From there, the ions accelerate towards the skimmer and into the high vacuum region of the mass analyser. By systematically increasing the skimmer cone voltage relative to the skimmer voltage, the ions are accelerated to a greater extent relative to the neutral solvent vapour/gas producing collisions between the two species. As a result of the collisions, simple solvated metal ions can lose their solvent ligands or more complex molecules can undergo fragmentation (Figure 1.11 and 1.12).

---

[32] J. B. Fenn, *J. Am. Soc. Mass Spectrom.*, 1993, **4**, 524.

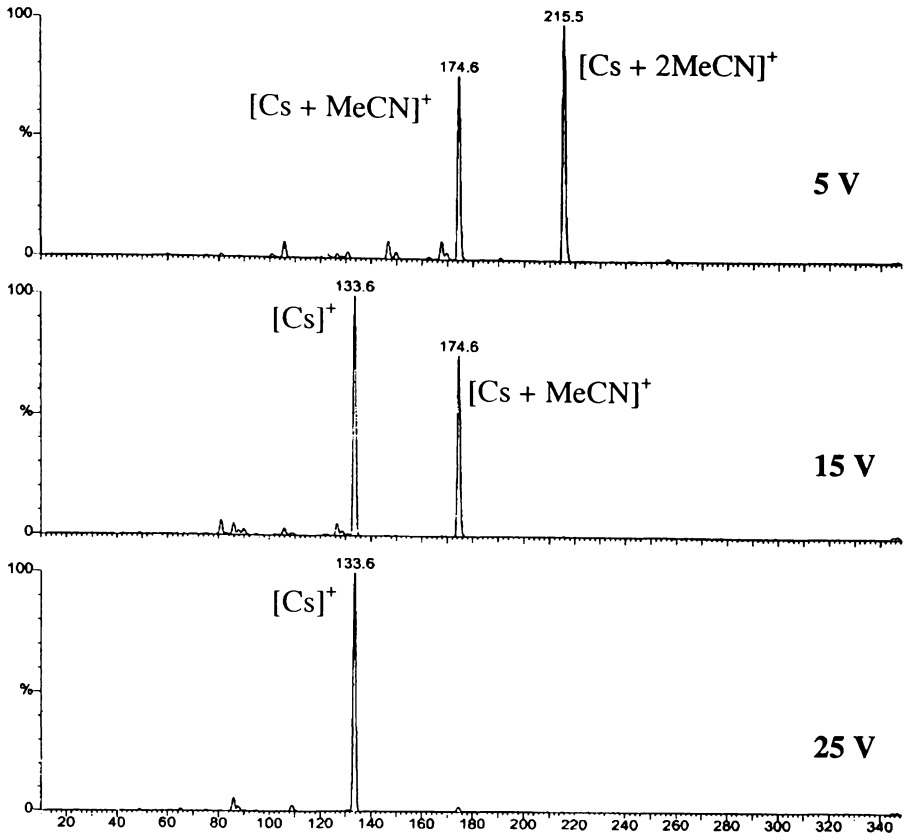

Fig. 1.11 The positive-ion ES mass spectra of CsBr, recorded in MeCN/H_2O at various cone voltages.

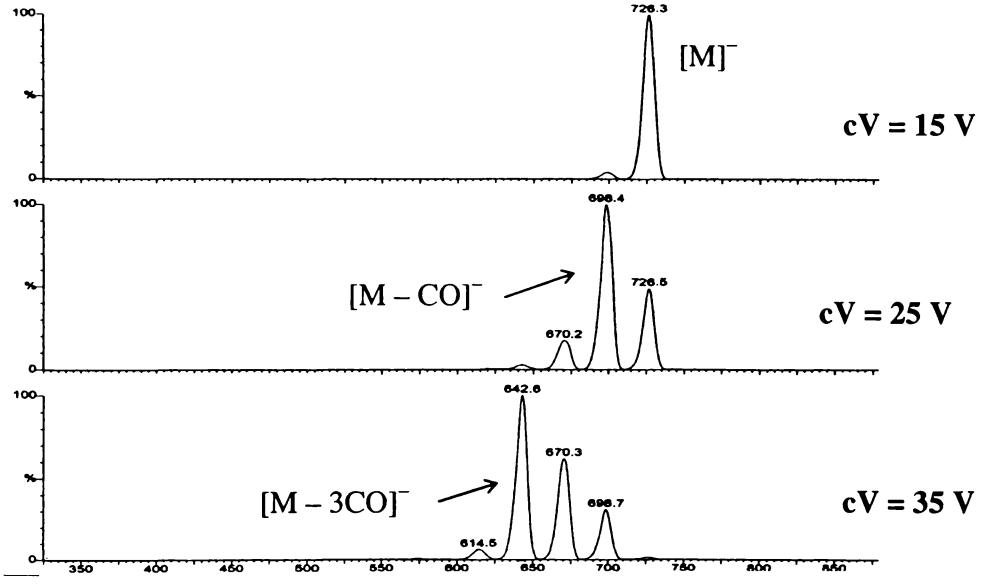

Fig. 1.12 The negative-ion ES mass spectra of $[CoRu_3(CO)_{13}]^-$, recorded in MeOH at various cone voltages[33].

[33] The sample, as a $[Et_4N]^+$ salt, was generously provided by C. Evans.

Information relative to the charge of particular ions is provided by their high-resolution isotope patterns. Thus, the peaks of a doubly-charged ion, for example, will be separated by 0.5 *m/z* units, of a triply-charged ion by 0.33 *m/z* units *etc.* The identification of multiply-charged ions by the corresponding isotope pattern can be achieved for up to four charges[34]. Anything beyond this is normally quite difficult because of resolution problems, unless the ES source is coupled to special mass analysers.

The masses and intensities of the isotope distribution patterns represent the 'fingerprint' of each ion and can be employed in assignment of the ion. This is achieved by comparing the observed isotope pattern with one simulated using the isotope abundance of the relevant elements. Programs to simulate such patterns are readily available (*e.g.* the ISOTOPE program developed by Arnold[35]). Inorganic compounds generally give distinctive isotope patterns since many inorganic elements possess several isotopes, *e.g.* Pd, Pt, Ru. Organic molecules traditionally contain the elements C, H, O, N, S and have rather simple isotope patterns, even relatively large compounds. Figure 1.13 illustrates this with an example from each field: the mercapto-containing tripeptide glutathione and $[Os_3(CO)_{12}]$.

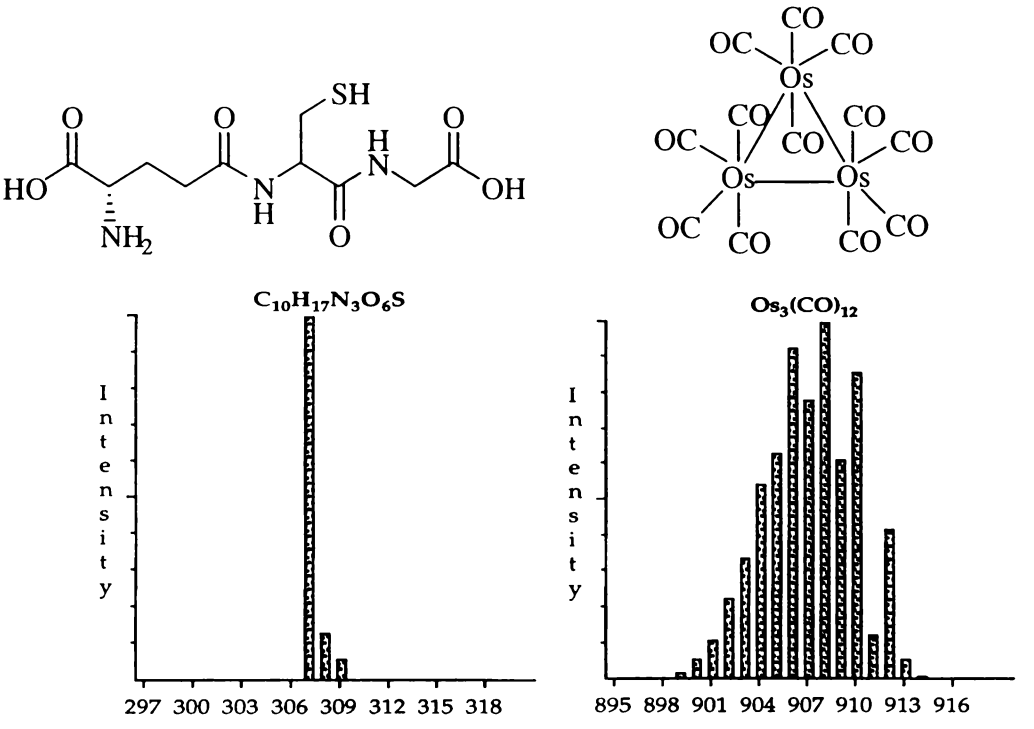

Fig. 1.13 The calculated isotope patterns of glutathione and $[Os_3(CO)_{12}]$.

[34] T. Løver, G. A. Bowmaker, W. Henderson, and R. P. Cooney, *Chem. Commun.*, 1996, 683.
[35] L. J. Arnold, *J. Chem. Ed.*, 1992, **69**, 811.

After the pumping stage in the nozzle-skimmer area, the ions pass through another small hole, **the skimmer ❼**. The skimmer acts as a momentum separator. It allows the heavier ions to proceed through the system while the light solvent and gas molecules are pumped away. The skimmer samples the central portion of the beam into the next vacuum stage, so that the ion optics receive a well-shaped ion beam. The **lensing system ❽** finally guides the ion beam into a **mass analyser ❾**, where they are separated and detected in a conventional manner.

Since the ES source has been coupled successfully with different types of mass analysers, the types of compounds amenable to ES as well as the application of ES in combination with other methods of separation has grown rapidly. Two major steps include the early interest of (bio-)organic chemists in the mid 1980s, followed by the application to inorganic and organometallic compounds during the 1990s. Both are outlined in the next two sections.

1.3.3 Application of ESMS to organic and (bio-)organic chemistry

In the mid 1980s, following the coupling of the ES source to a mass spectrometer by Fenn and co-workers (hence introducing ESMS as an analytical tool), the field of (bio-) analytical mass spectrometry experienced rapid growth. With conventional mass spectrometry, only small volatile compounds were amenable to mass spectrometry because higher-molecular weight species underwent substantial decomposition and fragmentation during ionisation. Alternative ionisation techniques such as FAB, SIMS or ^{252}Cf-PD had been successfully developed for larger compounds, but the upper mass limit of these techniques is comparatively low (< 3 – 5 kDa). MALDI is able to produce mainly singly-charged ions for analytes in excess of 100 kDa though drawbacks are the relatively poor resolution caused by the single charging. Furthermore, MALDI can only be connected to TOF mass analysers rather than to the superior scanning mass analysers (quadrupoles or sector instruments) because of its pulsed nature of the ion formation. With the ES technique, however, biochemical 'macromolecules' such as protein complexes, DNA adducts or organic polymers with molecular weights of several hundred kDa can be promoted into the gas phase as intact ions. Their analysis is possible because they are observed as multiply-charged ions within a relatively low *m/z* range. The analytes appear as a series of ions with different charges, each one differing from its adjacent members by one. As the mass spectrometer detects them according to their *m/z*

ratio, they appear in the range of 300 – 5000 amu. There is no need for extending the mass range and no loss of sensitivity. In general, the larger the molecule, the greater the extent of multiple charging. These higher-mass samples do not tend to fragment readily, as their lower-mass analogues do. This characteristic feature distinguishes ESMS from other ionisation techniques, since the majority of other available techniques produces singly-charged ions. Figure 1.14 illustrates this phenomenon with the ES mass spectrum of horse-heart myoglobin.

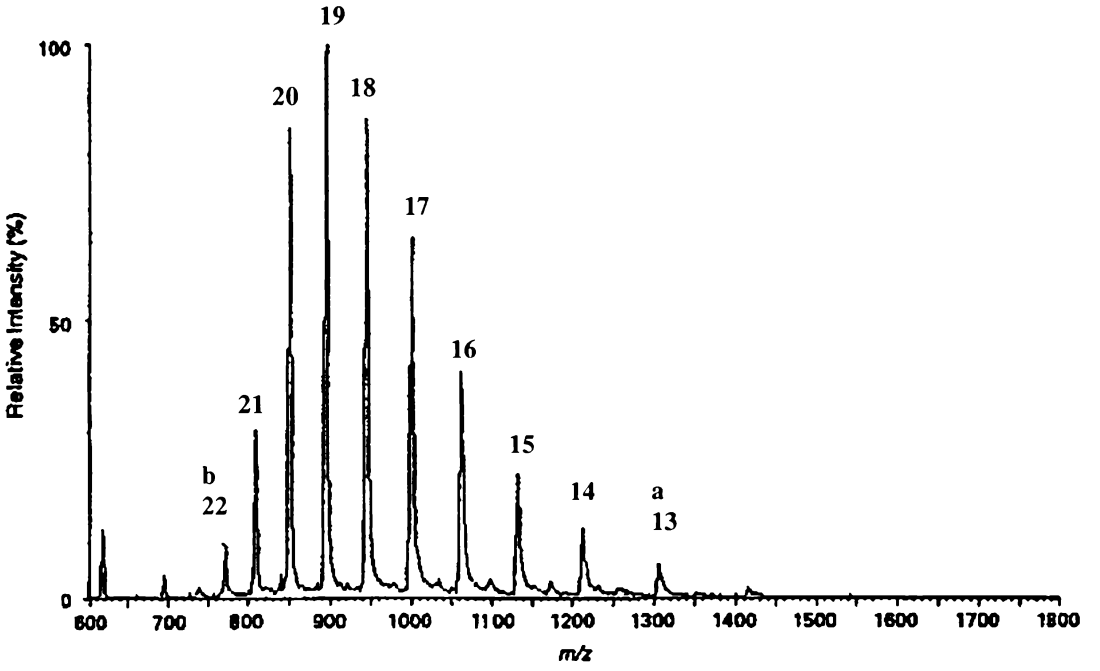

Fig. 1.14 The ES mass spectrum of horse-heart myoglobin (average M_r = 16951)[36].

In Figure 1.14, the ten observed peaks all differ by one charge, but represent a single species, a fact that may seem confusing to the untrained eye. In the example shown above, the charges range from a = 13 for $[M + 13H]^{13+}$ to b = 22 for $[M + 22H]^{22+}$. Computer software has been developed specifically to allow the calculation of the accurate mass of the parent molecule. The computer can present the result as a single peak corresponding to the parent molecule with one mass-less charge attached.

Peptides and proteins have multiple amino acid residues and are ionised *via* protonation to give ions of the type $[M + nH]^{n+}$, while oligonucleotides and fatty acids are charged by deprotonation of acidic groups and form $[M - nH]^{n-}$ ions.

1.3.4 Application of ESMS to inorganic and organometallic chemistry

Among the community of inorganic and organometallic chemists a similar rapid acceptance of ESMS appeared shortly after its adoption by biochemists. This is not surprising as, in principle, any ion or neutral molecule that can be ionised can be studied by ESMS, provided it is stable in the solution environment of the mass spectrometer for a few minutes. Simple cations such as tetraalkyl ammonium[22] and phosphonium[37] cations were among the first examples of ESMS examination of inorganic compounds, performed by Fenn and co-workers. The same group subsequently published results obtained from anionic samples[38]. The application to transition-metal coordination chemistry started in 1990 when Chait's group electrosprayed the ionic ruthenium complexes $[Ru(bipy)_3]Cl_2$ and $[Ru(phen)_3]Cl_2$ (bipy = bipyridyl; phen = 1,10-phenanthroline)[39]. The literature covering the application of ESMS to inorganic and organometallic chemistry has grown greatly since then. The reader is therefore referred to a number of review articles[16].

It has been demonstrated (mainly by NMR and electrochemistry[40,41]) that the ions detected by ESMS are representative of those originally present in solution. This is a very important point, in particular for solution chemistry. Thus, reactions can be monitored by ESMS, or ESMS can be used as a primary characterisation technique by injecting the crude reaction solution. The chemist is no longer solely dependent on NMR and IR data, or on growing suitable crystals for X-ray analysis.

Like the large biomolecules discussed earlier, a lot of inorganic and organometallic compounds are involatile and/or thermally unstable, making ESMS the tool of choice for their analysis. As opposed to large bio-organic molecules, multiple charging is not commonly observed. In fact, for small molecules (< 1000 amu) this is exceedingly rare because they favour an optimum charge density and multiple charging on a small molecule would lead to charge-charge repulsions. Although ESMS is a 'soft' ionisation

---

[36] D. S. Ashton C. R. Beddell, D. J. Cooper, B. N. Green and R. W. A. Oliver, *Org. Mass Spec.*, 1993, **28**, 721.
[37] C. M. Whitehouse, R. N. Dreyer, M. Yamashita and J. B. Fenn, *Anal. Chem.*, 1985, **57**, 675.
[38] M. Yamashita and J. B. Fenn, *J. Phys. Chem.*, 1984, **88**, 4671.
[39] V. Katta, S. K. Chowdhury and B. Chait, *J. Am. Chem. Soc.*, 1990, **112**, 5348.
[40] R. Colton, J. Harvey and J. C. Traeger, *Org. Mass Spectrom.*, 1992, **27**, 1030.
[41] A. M. Bond, R. Colton, D. A. Fiedler, J. E. Kevekordes, V. Tedesco and T. F. Mann, *Inorg. Chem.*, 1994, **33**, 5761.

technique (the analytes remain intact with no or minimal fragmentation), fragmentation may be induced by simply increasing the cone voltage. For coordination compounds, typically the loss of a complete ligand is observed rather than fragmentation of it. The assignment of each ion is normally achieved by recording the high-resolution isotope pattern and comparing it with one simulated from the elemental composition. Many transition metals (*e.g.* Mo, Pd, Pt) display significant isotopic variation yielding a distinctive isotope pattern for the particular complex. For the inorganic chemist, this is a major advantage over purely organic molecules. Compounds that contain only C, H, N, S or O show very simple isotope patterns even for large molecules because their elements contain only a single isotope. This has been discussed in detail previously (section 1.3.2.1).

1.3.5 Ionisation Pathways

The ES technique is an excellent tool for the mass spectrometric analysis of inorganic and organometallic compounds. It has expanded the range of analytes amenable to mass spectrometry to non-volatile compounds. By establishing different methods for ionisation, ESMS has become a routine technique in organometallic chemistry. However, not all compounds are amenable to ESMS. As outlined in Scheme 1.2, there are two major groups of compounds that are readily detectable by ESMS. The first group includes ionic species. Because they are already ionic in solution these species are directly transferred into gas-phase ions without the requirement of ionisation. The second group consists of neutral compounds that can be charged *via* one of various routes, the most common being protonation of a basic site. All other compounds may or may not be able to undergo chemical derivatisation prior to analysis, which makes them either ionic (and thus belong to the first group) or makes them chargeable (thus becoming a compound of group two).

The major ionisation pathways developed to date are described in more detail in the following sections. Examples are mainly given from organometallic chemistry, but the techniques are equally applicable to purely organic or inorganic compounds. The option of using 'electrospray-friendly' ligands is the most recent addition and appropriate to complexes that are not applicable to the previous methods.

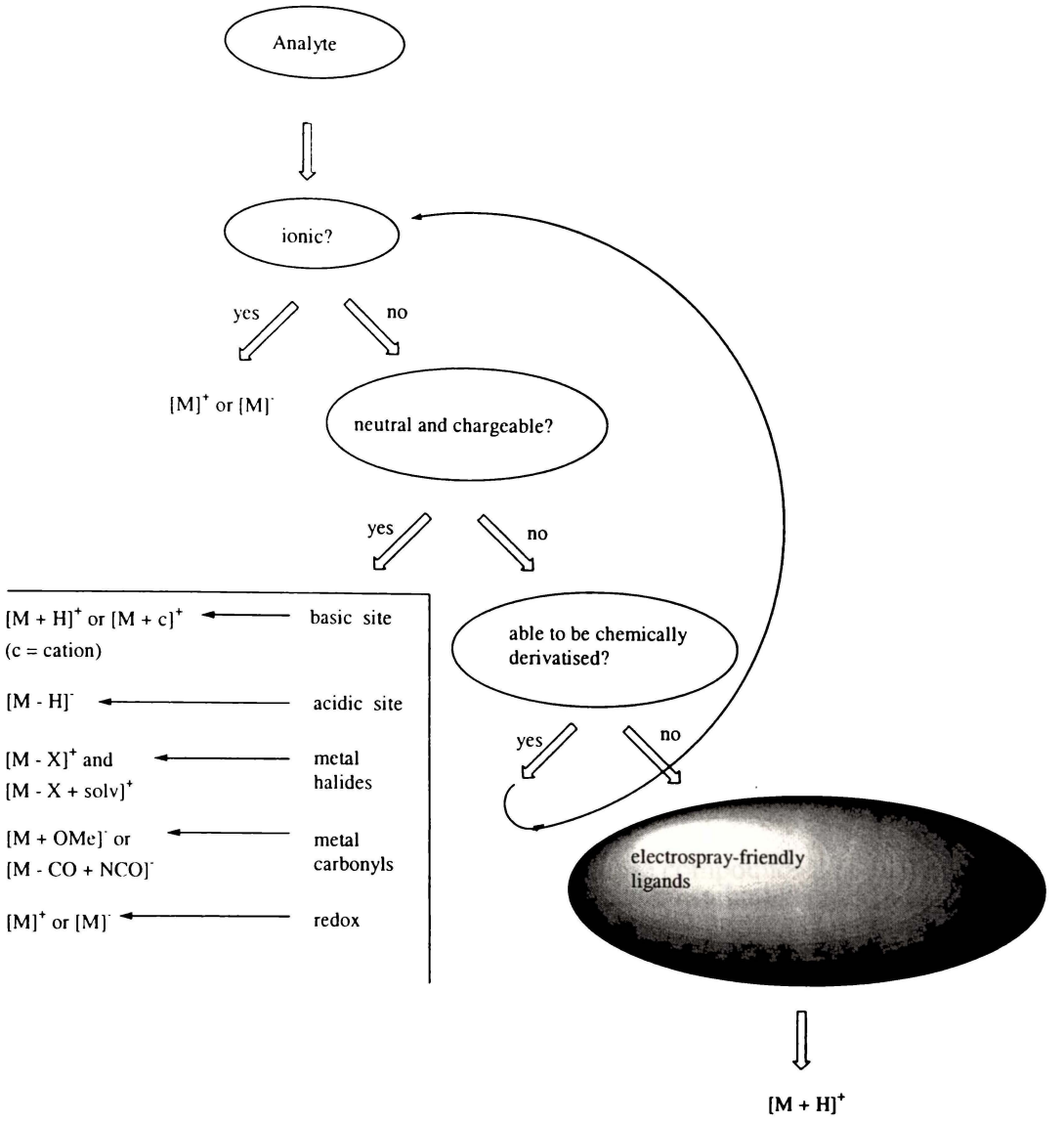

Scheme 1.2 The methods currently in use for ionising analytes in ESMS.

1.3.5.1 Ionic Compounds

ESMS is particularly useful for ionic compounds. Since ionic species are generally relatively involatile, they tend to decompose when examined by conventional mass spectrometric techniques, and so most mass spectrometric studies have been limited to non-ionic compounds. The ES technique distinguishes itself from other ionisation techniques in that it 'gently lifts' pre-existing ions from the solution into the gas phase. Obviously, this is most easily achieved for charged species, resulting in very intense signals and generally clean spectra. This is shown in Figure 1.15, illustrating the ES mass spectrum of $[CoRu_3(CO)_{13}]^-$. In principle, any ionic species should be visible in

the ESMS, provided it is soluble and stable in a solvent commonly used for ESMS. When analysing ions, either protic or aprotic solvents may be used. Positively charged ions are analysed in positive-ion mode whereas anions are analysed in negative-ion mode.

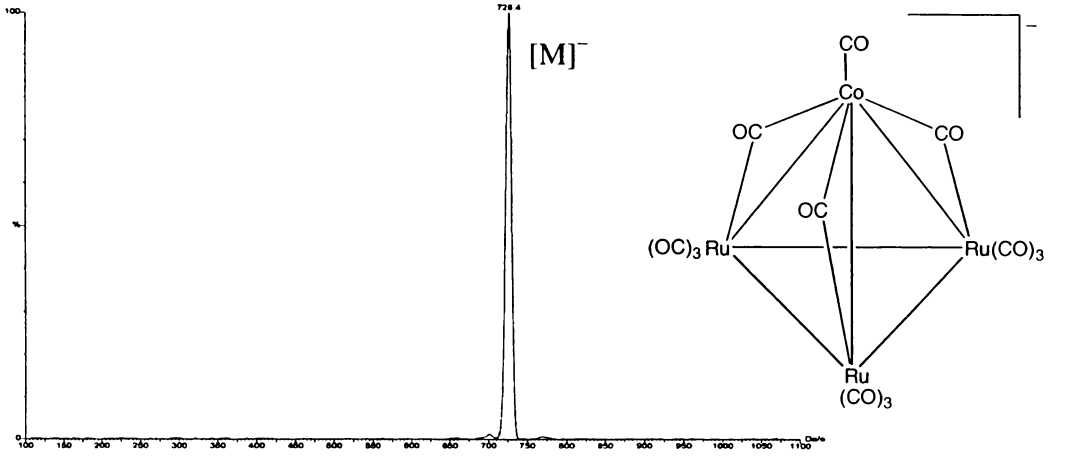

Fig. 1.15 The negative-ion ES mass spectrum of $[CoRu_3(CO)_{13}]^-$, recorded in MeOH at cV = 5 V [33].

The number of ESMS studies on ionic organometallic complexes is rapidly increasing. Some selected examples include phosphine complexes of gold(I)[42], metal carbonyls of Group 6 and 7 [43], detection of ionic rhenium reaction intermediates by ESMS[44] and comparison of ESMS with other soft ionisation techniques using cationic π-hydrocarbon complexes[45]. Fewer studies have been carried out on negative ions[46].

1.3.5.2 Protonation

Protonation is the original and most common pathway for ionising neutral molecules in the ESMS. Biochemists have been able to characterise large organic molecules, such as proteins or nucleic acids, by using this mechanism. The presence of protons is attributable to the self-dissociation of the solvent, *e.g.* water according to $H_2O \rightarrow H^+_{(aq)} + OH^-_{(aq)}$. Protic solvents commonly used include $MeCN/H_2O$, H_2O or MeOH. The

---

[42] R. Colton, K. L. Harrison, Y. A. Mah and J. C. Traeger, *Inorg. Chim. Acta*, 1995, **231**, 65.
[43] I. Ahmed, R. Colton, M. Jercevic, J. C. Traeger, and J. N. Walter, *J. Organomet. Chem.*, 1993, **447**, 59.
[44] H. Hori, O. Ishitani, K. Koike, K. Takeuchi and T. Ibusuki, *Anal. Sciences*, 1996, **12**, 587.
[45] L. A. P. Kane-Maguire, R. Kanitz and M. M. Sheil, *J. Organomet. Chem.*, 1995, **486**, 243.
[46] R. Colton, A. D'Agostino, J. C. Traeger and W. Kläui, *Inorg. Chim. Acta*, 1995, **233**, 51; M. J. Deery, O. W. Howarth and K. R. Jennings, *J. Chem. Soc. Dalton Trans.*, 1997, 4783.

analyte is generally dissolved in such a solvent, but can also be dissolved in an aprotic solvent provided a solvent with acidic H atoms is added to the solution. Molecules with a basic site (*i.e.* oxygen or nitrogen atoms with a lone pair of electrons) associate with protons forming cations of the type $[M + nH]^{n+}$. These ionic aggregates in solution are then transferred into the gas phase allowing detection by the mass spectrometer. Multiple protonation is of particular advantage for large molecules with masses > 3000 amu. Thus, large biomolecules typically give a family of peaks associated with *e.g.* 6+, 5+, 4+, *etc.* ions, respectively. If only single protonation occurs (normally the case for small inorganic and organometallic compounds), the spectra appear with a single peak, readily assigned to the parent ion $[M + H]^+$. In general, multiple charging is rather rare for smaller molecules because the addition of more than one proton leads to charge-charge repulsion, whereas large molecules require association with several protons to attain an optimum charge density. Occasionally more than one singly-protonated ion may be observed. This phenomenon occurs when the neutral molecule forms higher aggregates of the type $[2M + H]^+$, $[3M + H]^+$ *etc.* These aggregate ions are generally far less intense than the parent ion.

The protonation method is, however, limited to those compounds that contain basic groups. Thus, only ketone-, ether- or ester-type compounds, or metal complexes that contain a non-coordinated amine or imine N atom *etc.* are susceptible to protonation by the mobile phase. Three examples of ESMS studies on metal complexes with ligands that give strong $[M + H]^+$ ions are those of thd (thd = 2,2,6,6-tetramethyl-3,5-heptanedione)[47] due to its O atoms, tpa (tpa = 1,3,5-triaza-7-phosphaadamantane)[48] due to its N atoms, and thiosalicylate[49] due to the carboxylate O atom. The structures of the ligands are shown in Figure 1.16.

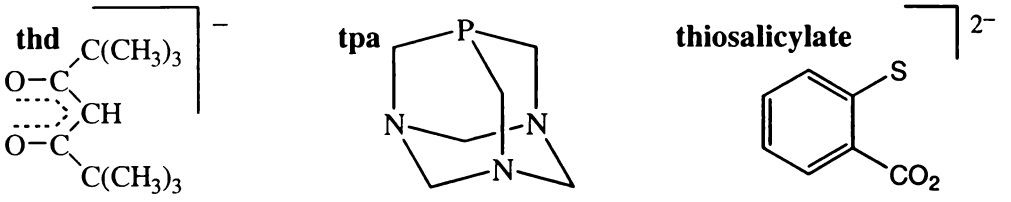

Fig. 1.16 The structures of thd, tpa and thiosalicylate.

---

[47] J. M. Curtis, P. J. Derrick, A. Schnell, E. Constantin, R. T. Gallagher, and J. R. Chapman, *Inorg. Chim. Acta*, 1992, **201**, 197.

[48] K. J. Fisher, I. G. Dance, G. D. Willett, R. Zhang, E. C. Alyea, *Eur. J. Mass Spectrom.*, 2000, **6**, 23.

Another example is the triphenylbiureto derivative [{$C_6H_3(CH_2NMe_2)$-2-(OMe)-5}Au{NPhC(O)NPhC(O)NPh}], produces a strong $[M + H]^+$ and a weaker $[2M + H]^+$ signal in its spectrum (illustrated in Figure 1.17).

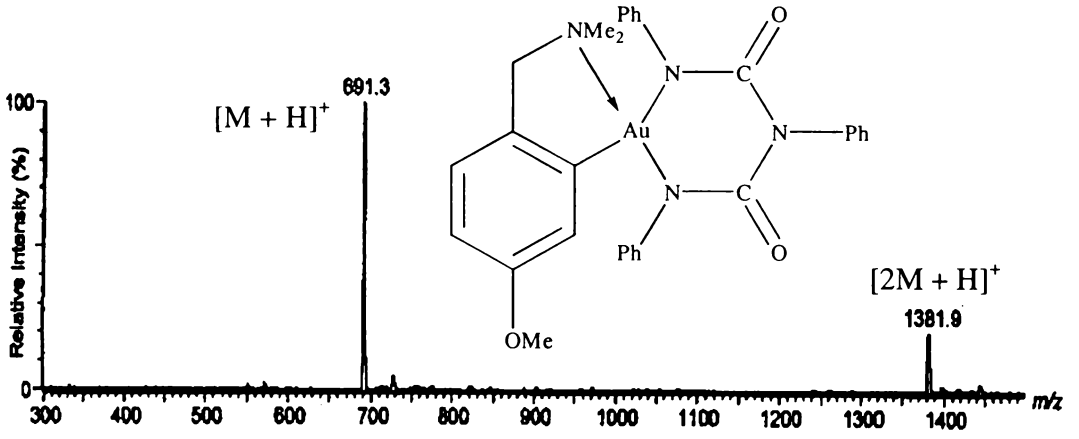

Fig. 1.17 The positive-ion ES mass spectrum of [{$C_6H_3(CH_2NMe_2)$-2-(OMe)-5}Au{NPhC(O)NPhC(O)NPh}] [50].

1.3.5.3 Adduct formation with metals (metallation) and non-metallic cations

Several neutral compounds show a higher affinity for cations than they do for protons. In that case, ions of the type $[M + c]^+$ (c = cation) are observed. These cations are typically of a metallic nature (such as alkali metal ions or silver(I) ions), which is why this ionisation pathway is often called metallation, but adduction of ammonium ions (NH_4^+) is also reported. Alkali metal adducts are commonly observed for polar organic compounds, such as carboxylic acid polyethers[51], but the numbers of examples from organometallic chemistry are constantly increasing. Among these are the nitrosyl compound $[Ru(NO)Cl_3(EPh_3)_2]$ (E = P, As or Sb)[52], *trans*-$[PtCl_2(NH_3)_2]$ [53] and some neutral rhenium bipyridyl complexes[54], all giving ES signals attributable to their $[M + Na]^+$ ions. These results are interesting as all of the complexes contain halide ligands, but do not undergo the alternative halide loss mechanism (described in section 1.3.5.5). Further examples include multiple phosphine-substituted metal carbonyl compounds, in

---

[49] L. J. McCaffrey, W. Henderson, B. K. Nicholson, J. E. Mackay and M. B. Dinger, *J. Chem. Soc. Dalton Trans.*, 1997, 2577.
[50] M. Dinger, D.Phil. Thesis, University of Waikato, 1998.
[51] R. P. Schneider, M. J. Lynch, J. F. Ericson and H. G. Fouda, *Anal. Chem.*, 1991, **63**, 1789.
[52] S. Chand, R. K. Coll, J. S. McIndoe, *Polyhedron*, 1998, **17**, 507.
[53] H. C. Ehrson, I. B. Wallin, A. S. Anderson and P. O. Edlund, *Anal. Chem.*, 1995, **67**, 3608.

which CO ligands were sufficiently electron-rich to coordinate to alkali metal cations[55,56] when trace amounts of LiBr, NaBr or KBr were added. The same study involved a range of neutral multinuclear metal carbonyls that gave rise to readily assignable ions attributable to their silver adducts. The silver cation is presumed to coordinate to the electron-rich metal-metal bond[57]. Silver adducts have also been reported for various phosphine ligands[58] and a number of alkene and arene ligands[59].

The association of the analyte with (metal) ions may be due to traces of Na^+, K^+, NH_4^+, *etc.* in the system. Corresponding salts are often deliberately added ('doping') in order to increase the intensity of the signals, and this generally leads to cleaner spectra if competition between protonation and metallation occurs.

An advantage of metallation over protonation is that it can be used with aprotic solvents such as DMF or THF[60]. This is important for compounds that are sensitive towards protons or when alternative solvent systems need to be used due to solubility problems.

1.3.5.4 Addition of alkoxide ions

The addition of negatively-charged species to a neutral molecule can give rise to ions of the type $[M + a]^-$ (a = anion), which are visible in the negative-ion mode of the ESMS. While the Ag^+ ion method described above is only applicable to certain multinuclear cluster carbonyls, the addition of the alkoxide ion in ROH solvents (*e.g.* NaOMe in MeOH) was found to be a more general alternative[56,61]. Neutral metal alkoxides have been observed as their $[M + OR]^-$ ions[62], formed by addition of a further anionic alkoxide ligand. In the case of metal carbonyls, nucleophilic addition of the alkoxide ion

---

[54] H. Hori, J. Ishiharo, K. Koike, K. Takeuchi, T. Ibusuki and O. Ishitani, *Chem. Lett.*, 1997, 273.
[55] W. Henderson and B. K. Nicholson, *J. Chem. Soc., Chem. Commun.*, 1995, 2531.
[56] W. Henderson, J. S. McIndoe, B. K. Nicholson and P. J. Dyson, *J. Chem. Soc. Dalton Trans.*, 1998, 519.
[57] G. N. Mott, N. J. Taylor and A. J. Carty, *Organometallics*, 1983, **2**, 447; R. Noyori, I. Tomino and Y. Tanimoto, *J. Am. Chem. Soc.*, 1979, **101**, 3131.
[58] W. Henderson and G. M. Olsen, *Polyhedron*, 1996, **15**, 2105; W. Henderson and G. M. Olsen, *Polyhedron*, 1998, **17**, 577.
[59] A. J. Canty and R. Colton, *Inorg. Chim. Acta*, 1994, **220**, 99.
[60] R. Saf, C. Mirtl and K. Hummel, *Tetrahedron Lett.*, 1994, **35**, 6653.
[61] W. Henderson, J. S. McIndoe, B. K. Nicholson and P. J. Dyson, *J. Chem. Soc., Chem. Commun.*, 1996, 1183.
[62] T. Løver, W. Henderson, G. A. Bowmaker, J. M. Seakins and R. P. Cooney, *J. Mater. Chem.*, 1997, **7**, 1553.

to the carbon atom of a CO ligand occurs, a reaction typical of metal carbonyls, according to:

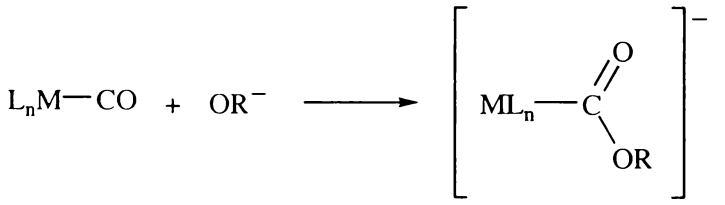

An example is shown in Figure 1.18 for $[Os_3(CO)_{12}]$.

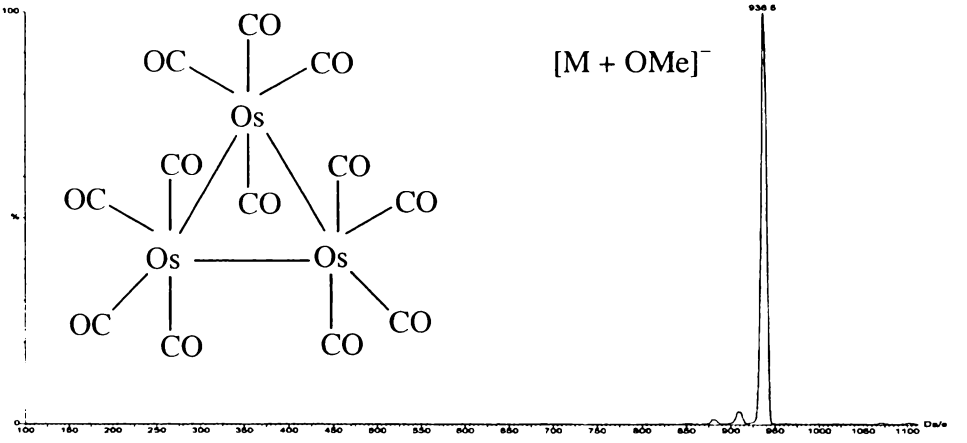

Fig. 1.18 The negative-ion ES mass spectrum of $[Os_3(CO)_{12}]$ with the addition of NaOMe, recorded in MeOH at cV = 5 V.

1.3.5.5 Addition of azide ions

The azide ion, N_3^- [56,63,64] was also found to ionise metal carbonyl complexes, though in a less specific manner. Analogous to the alkoxide addition, N_3^- attacks the carbon atom of the CO ligand. In the case of azide, however, subsequent conversion of CO to NCO^- under elimination of N_2 leads to isocyanate-containing anions according to the following equation:

$$M(CO)_x + N_3^- \rightarrow [M(CO)_{x-1}(NCO)]^- + N_2$$

The addition of N_3^- ions may also yield ions of the type $[M + N_3]^-$ or $[M - H]^-$, the latter being formed by proton abstraction, a competing process to the nucleophilic attack.

---

[63] J. S. McIndoe and B. K. Nicholson, *J. Organomet. Chem.*, 1999, **573**, 232.

1.3.5.6 Halide loss

The loss of a halide ligand is a reasonably general ionisation pathway for transition-metal halide complexes. At low cone voltages, the two principal ions observed are $[M - X]^+$ and $[M - X + solv]^+$. The latter one, $[M - X + solv]^+$, is formed by loss of the halide ligand followed by coordination of a solvent molecule (*e.g.* MeCN) or other neutral species (*e.g.* NH_3 or pyridine). In fact, pyridine was found to be highly successful for these systems[65] as a result of its strong donor ligand abilities. Figure 1.19 shows the spectrum of *cis*-$[PtCl_2(PPh_3)_2]$ at 20 V, run in $MeCN/H_2O$ (top) and with the addition of pyridine (bottom). The non-solvated ion $[M - X]^+$, produced by collisional activation, becomes dominant as the cone voltage is increased.

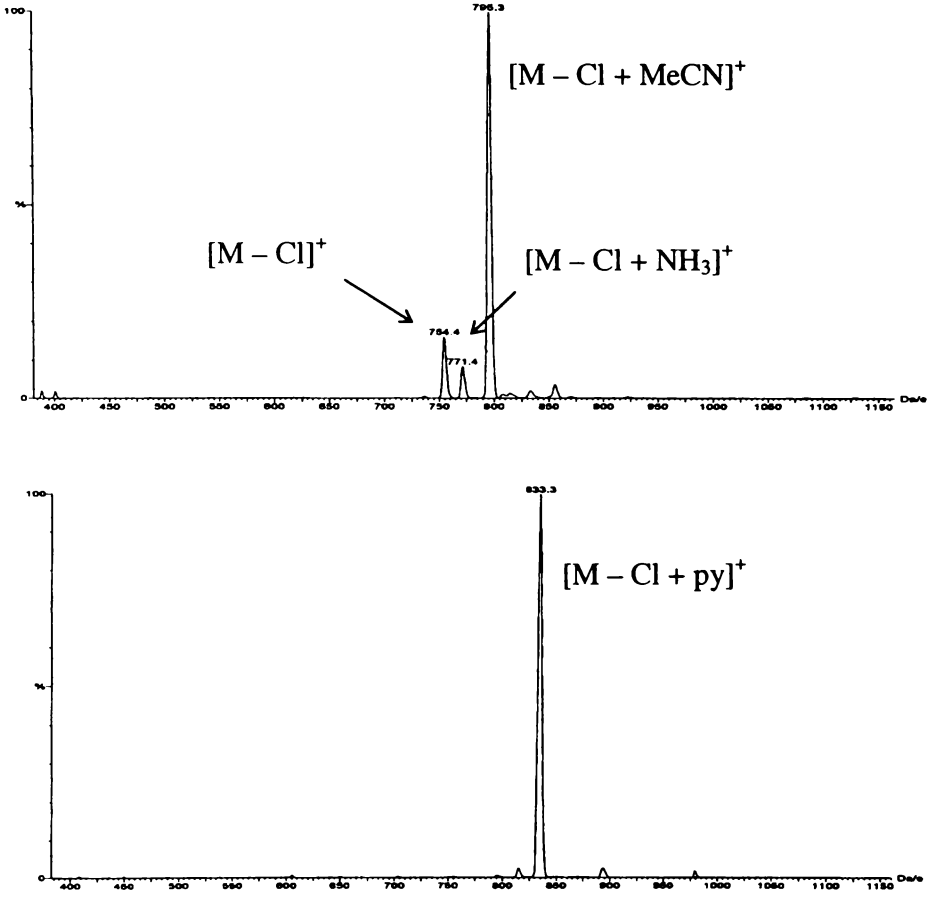

Fig. 1.19 The positive-ion ES mass spectrum of *cis*-$[PtCl_2(PPh_3)_2]$ (top) and with the addition of pyridine (bottom), recorded in $MeCN/H_2O$ at cV = 20 V.

---

[64] W. Beck, *J. Organomet. Chem.*, 1990, **383**, 143.

This halide-loss mechanism has been reported for a wide range of metal complexes, incorporating Hg(II)[66], Pt(II)[67], Ni(II)[68] or Au(III)[69]. An ESMS survey on a wide range of transition-metal halides has also been reported[65]. However, not every halide-containing metal complex reliably undergoes this mechanism. In the presence of a highly basic group, the formation of $[M + H]^+$ or $[M + Na]^+$ ions may be the preferred pathway of ionisation (for examples see section 1.3.5.3).

1.3.5.7 Proton abstraction

In organic chemistry, deprotonation of acidic groups is commonly observed for oligonucleotides or fatty acids. In organometallic chemistry, this ionisation pathway was found to compete with the alkoxide-ion addition (see section 1.3.5.4). Thus, ionisation by proton abstraction in the presence of MeO^- gives ions of the type $[M - H]^-$. This is attributable to the basic nature of the MeO^- ion and its ability to extract protons from compounds with acidic H atoms. This method was shown to be effective for complexes containing the ligand dppm [dppm = bis(diphenylphosphino)methane], as shown in Figure 1.20, but $[M - H]^-$ ions were also recorded for hydride complexes, complexes of methyl-aryl ketones and a cluster containing the toluene ligand[56].

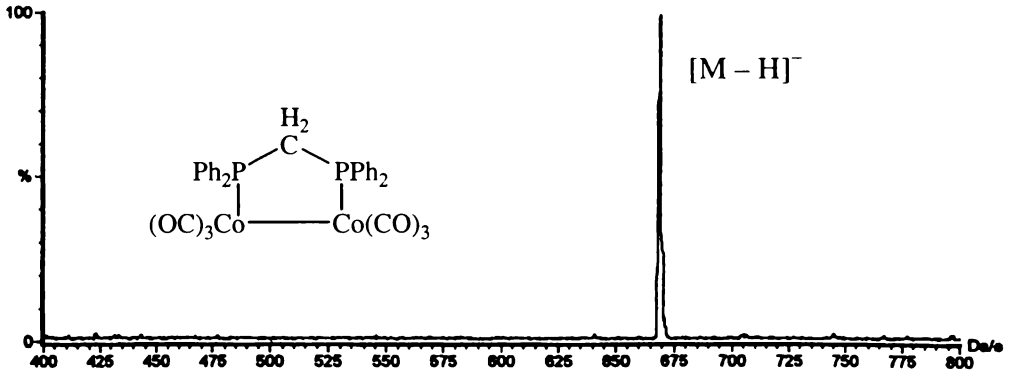

Fig. 1.20 The negative-ion ES mass spectrum of $[Co_2(CO)_6(dppm)]$ with the addition of NaOMe [70].

---

[65] W. Henderson and C. Evans, *Inorg. Chim. Acta*, 1999, **294**, 183.
[66] R. Colton and D. Dakternieks, *Inorg. Chim. Acta*, 1993, **208**, 173.
[67] P. Bergamini, O. Bortolini, O. Curcurutu and M. Hamdan, *J. Mass Spectrom.*, 1995, S77.; S. Favaro, L. Pandolfo and P. Traldi, *Rapid Commun. Mass Spectrom.*, 1997, **11**, 1859; J. Fawcett, W. Henderson, R. D. W. Kemmitt, D. R. Russell and A. Upreti, *J. Chem. Soc. Dalton Trans.*, 1996, 1897; W. Henderson, J. Fawcett, R. D. W. Kemmitt, P. McKenna, and D. R. Russell, *Polyhedron*, 1997, **16**, 2455; W. Henderson, B. K. Nicholson, and L. J. McCaffrey, *Inorg. Chim. Acta*, 1999, **285**, 145.
[68] S. R. Wilson and Y. Wu, *Organometallics*, 1993, **12**, 1478.
[69] M. B. Dinger and W. Henderson, *J. Organomet. Chem.*, 1998, **560**, 233.
[70] J. S. McIndoe, D.Phil. Thesis, University of Waikato, 1998.

1.3.5.8 Redox Processes

According to Kebarle and co-workers[71], the electrophoretic charging mechanism found in electrospray requires the conversion of ions to electrons at the metal-liquid interface of the capillary. If the buildup of opposite charge within the capillary was not neutralised the creation of an additional electric field would negate the externally applied one. This necessary requirement for charge balance is fulfilled by electrochemical oxidation/reduction processes (depending on the ion mode) at the metal capillary and/or other species in the electrolyte solution. The authors therefore claimed that "the ES device can be considered as an electrolytic cell of a somewhat special kind" as part of the ion transport occurs through the gas phase rather than through solution. Part of the evidence for such an electrochemical process was provided by observing additional ions in the spectrum associated with oxidation of the capillary, *e.g.* Zn^{2+} ions when using a zinc capillary or Fe^{2+} ions in the case of a stainless steel capillary. While one might consider this as a major drawback as it adds impurities, the concentrations of the electrode-produced ions are normally not noticeable. In fact, the reactions at the electrode can be exploited for analysing neutral species that easily undergo electrochemical oxidation (or reduction) to give radical cations (or anions). The conditions that determine whether or not a particular species will undergo redox reactions in the ES capillary have been studied in detail[72]. Thus, oxidation in the ES needle was observed for electron-rich species such as porphyrins, polycyclic aromatic hydrocarbons and heteroaromatics[73]. Ferrocene and other neutral metallocenes[74] were observed as their radical cations, while C_{60} and its derivatives were found to undergo both oxidation and reduction[75,76]. The spectra associated with C_{60} ionisation are shown in Figure 1.21.

---

[71] A. T. Blades, M. G. Ikonomou and P. Kebarle, *Anal. Chem.*, 1991, **63**, 2109.
[72] G. J. Van Berkel and F. Zhou, *Anal. Chem.*, 1995, **67**, 3958; G. J. Van Berkel and F. Zhou, *Anal. Chem.*, 1995, **67**, 2916.
[73] G. Van Berkel, S. A. McLuckey and G. L. Glish, *Anal. Chem.*, 1992, **64**, 1586.
[74] X. Xu, S. P. Nolan and R. B. Cole, *Anal. Chem.*, 1994, **66**, 119.
[75] T.-Y. Liu, L.-L. Shiu, T.-Y. Luh and G.-R. Her, *Rapid Commun. Mass Spectrom.*, 1995, **9**, 93.
[76] A. Dupont, J. P. Gisselbrecht, E. Leize, L. Wagner and A. Van Dorsselaer, *Tetrahedron Lett.*, 1994, **35**, 6083.

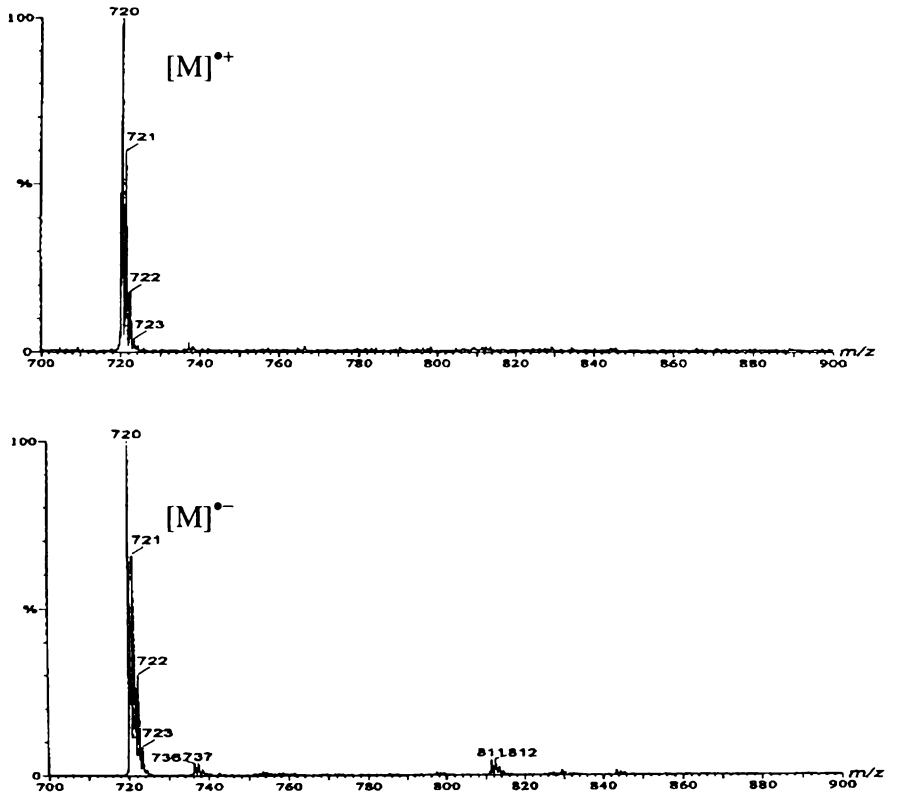

Fig. 1.21 The positive-ion (top) and negative-ion (bottom) ES mass spectra of C_{60} [74].

It should be noted that generating radical cations from neutral species can also be achieved by deliberate addition of an appropriate oxidising agent, such as nitrosonium salts (NO^+ acting as a one-electron oxidant)[77].

1.3.5.9 Chemical derivatisation

Neutral compounds that are not chargeable by adduct formation or electrochemical reactions may be derivatised prior to their analysis resulting in either ionic or chargeable species. These derivatives are often readily generated *in situ* by addition of a few drops of the derivatising agent to the solution of the analyte. For example, the conversion of uncharged phosphines into their corresponding phosphonium salts by reaction with methyl iodide (as shown in equation 1) has been reported by Colton *et al.*[78].

$$PR_3 + MeI \rightarrow [(R_3P)Me]I \qquad (1)$$

---

[77] A. M. Bond, R. Colton, A. D'Agostino, J. Harvey and J. C. Traeger, *Inorg. Chem.*, 1993, **32**, 3952.
[78] R. Colton, J. Harvey and J. C. Traeger, *Org. Mass Spectrom.*, 1992, **27**, 1030; R. Colton and J. C. Traeger, *Inorg. Chim. Acta*, 1992, **201**, 153.

Alternatively, tertiary phosphines may be converted into their hydroxymethylphosphonium salts with formaldehyde and HCl (equation 2)[79].

$$PR_3 + HCl + H_2CO \rightarrow [(R_3P)(CH_2OH)]Cl \qquad (2)$$

ESMS-active species can also be obtained by introduction of chargeable functional groups[80] (tagging of molecules with entire crown ethers has also been reported[81]) or electrochemically reactive functional groups[82]. An example of the latter approach is shown in Figure 1.22 where the ES-invisible cholesterol has been converted to its ferrocenecarbamate ester, which is ionised electrochemically by ES and can be observed as its radical cation.

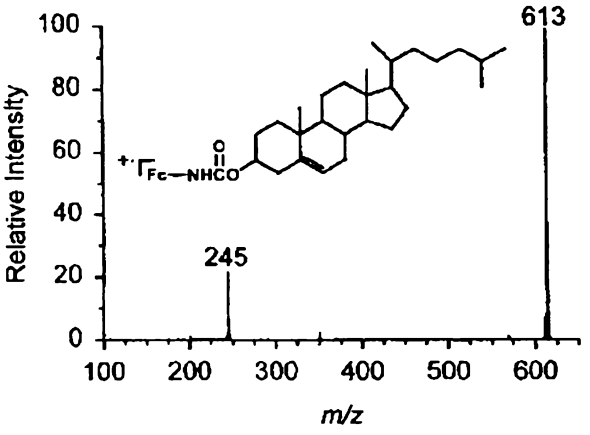

Fig. 1.22 The positive-ion ES mass spectrum of the ferrocenecarbamate ester of cholesterol (M_r = 613). The peak at *m/z* 245 is attributable to the ferrocenecarbamic acid fragment[82].

---

[79] W. Henderson and G. M. Olsen, *Polyhedron*, 1996, **15**, 2105.; W. Henderson and G. M. Olsen, *Polyhedron*, 1998, **17**, 577.

[80] G. J. VanBerkel, J. M. Quirke and C. L. Adams, *Rapid Commun. Mass Spectrom.*, 2000, **14**, 849; G. J. Van Berkel and K. G. Asano, *Anal. Chem.*, 1994, **66**, 2096; J. M. Quirke, C. L. Adams and G. J. Van Berkel, *Anal. Chem.*, 1994, **66**, 1302.

[81] S. R. Wilson and Q. Lu, *Tetrahedron Lett.*, 1993, **34**, 8043.

[82] G. J. Van Berkel, J. M. Quirke, R. A. Tigani and A. S. Dilley, *Anal. Chem.*, 1998, **70**, 1544.

1.4 Conclusion and thesis outline

Mass spectrometry provides an excellent means of characterising compounds. Electrospray mass spectrometry, in particular, has become the tool of choice for the analysis of not only (bio-)organic, but also inorganic and organometallic compounds. While conventional ionisation techniques (*e.g.* EI or CI) cannot be used for involatile and thermally instable compounds, ESMS is ideally suited to them.

Ionic species are observed most straightforwardly, as they only need to be lifted into the gas phase. The same applies to neutral compounds containing a basic site because they normally ionise in a protic solvent with formation of $[M + H]^+$ ions. All other neutral molecules require ionisation prior to analysis. Depending on their nature, many compounds can be converted from ES-inactive compounds to ES-active analytes. However, most of these techniques are suited to only a single class of compounds, *e.g.* transition-metal halide complexes may undergo the halide-loss mechanism, while metal carbonyls can form ions by coordination with methoxide ions. Hence, there is still a large number of organometallic compounds that are invisible in the ESMS. There appears to be a need for a technique that encompasses a wider range of complexes. This thesis presents such a technique: the use of electrospray-friendly ligands.

The strategy of using electrospray-friendly ligands for the electrospray mass spectrometric analysis of transition metal complexes will be outlined in detail in the next chapter, using phosphine ligands as examples. In theory, this method can be applied to almost every organic ligand. However, it is beyond the scope of this thesis to document them all. Therefore, each chapter will independently look at metal complexes incorporating different types of common ligands, investigate their applicability to electrospray-friendly derivatisation and discuss aspects of their chemistry. The ligand classes chosen are: phosphines (Chapter 2), arsines and stibines (Chapter 3), isocyanides (Chapter 4) and thiolates (Chapter 5).

Chapter 2

The concept of electrospray-friendly ligands

Electrospray-friendly ligands are ligands that are designed to be visible in the ESMS and are usually based on an invisible counterpart. The number of potential candidates in organometallic chemistry is endless. This chapter describes the concept and design of electrospray-friendly ligands with the examples based on PPh_3. To appreciate the important role of tertiary phosphine ligands in transition-metal chemistry this topic is reviewed first.

2.1 Tertiary phosphines in transition-metal chemistry

The area of transition-metal complexes of phosphines must be one of the most heavily studied in organometallic chemistry. It seems almost impossible to condense its chemistry, let alone summarise it to a satisfactory degree. The following review can only give a brief insight by emphasising the most important aspects and providing a few selected examples.

2.1.1 Background

Much pioneering work in organophosphorus chemistry has been done by P. E. Thénard and A. W. Hofmann, but especially by K. A. A. Michaelis of Rostock in Germany and the Russian A. E. Arbuzov during the second half of the 19th century. As a result, a lot of phosphorus-based chemistry has been done in these two countries. They were responsible for the preparation of a large number of organic phosphorus compounds and many of the synthetic routes are still used today. The area of organophosphorus chemistry has since become extensively broad resulting in numerous sub-areas, *e.g.* ^{31}P NMR spectroscopy[1], phosphorus natural product chemistry[2], the chemistry of ylides[3], and heterocyclic phosphorus chemistry[4] *etc.* There are numerous textbooks[5] and textbook series[6] that cover different parts of organophosphorus chemistry.

---

[1] J. Mason (ed.), *Multinuclear NMR*, Plenum Press, N.Y., 1987.
[2] S. C. Fields, *Tetrahedron*, 1999, **55**, 12237.
[3] W. C. Kaska, *Coord. Chem. Rev.*, 1983, **48**, 1.
[4] D. G. Holah, A. N. Hughes and K. Wright, *Coord. Chem. Rev.*, 1975, **15**, 239.

2.1.2 Properties of tertiary phosphines

Tertiary (and other) phosphines are ubiquitously used as ligands in transition-metal chemistry. This is not only due to their ability to manipulate the properties of the complex by slight changes in the steric and electronic properties of the ligand, but also because phosphorus itself is NMR active (^{31}P has a spin of ½). There is coupling of ^{31}P with ^{1}H and ^{13}C, and so structural information can be gained from the coupling constants. While the lower alkyl phosphine ligands are very volatile, extremely toxic and readily oxidise in air, tertiary aryl phosphines are air-stable, crystalline solids and therefore very easy to handle.

The key properties of tertiary phosphines are their steric demands, their σ-donor ability and their π-acidity. A range of techniques has been applied to investigate the relative contributions and their effects on the metal-phosphorus bond[7]. The relative steric, σ- and π-contributions depend strongly on the nature of the R groups in $PR_1R_2R_3$ as well as on the properties of the acceptor metal. Thus, it is extremely difficult to predict precisely the interaction between the metal and the ligand. At the same time, the relative steric, σ- and π-contributions are subject to deliberate control, and by varying the R groups, the course of reactions at the metal centre can be directed.

2.1.3 Synthesis of tertiary phosphines

PPh_3 is probably the archetypal phosphine ligand. It was first synthesised by Michaelis[8] in 1882. The synthesis of phosphines and other group 15-donor ligands is well described in the literature[5]. There are two major types of precursors: those containing a phosphorus halogen bond, R_nPX_{3-n}, and alkali metal derivatives, $M_{3-n}PR_n$. The alkali metal derivatives form tertiary phosphine ligands by reacting with RX, *e.g.*

---

[5] C. A. McAuliffe and W. Levason, *Phosphine, Arsine and Stibine complexes of the Transition Elements*, Elsevier, Amsterdam, 1979; C. A. McAuliffe, Phosphorus, Arsenic and Bismuth Ligands. In G. Wilkinson (ed.), *Comprehensive Coordination Chemistry*, Vol. 2, Pergamon Press, Oxford, 1987.
[6] G. M. Kosolapoff and L. Maier, *Organic Phosphorus Compounds*, 7 volumes, Wiley, N.Y., 1972; F. R. Hartley (ed.), *The chemistry of organophosphorus compounds*, 3 volumes, Wiley-Interscience, N.Y., 1994.
[7] H.-Y. Liu, K. Erics, A. Prock and W. P. Giering, *Organometallics*, 1990, **9**, 1758; M. N. Golovin, Md. M. Rahman, J. E. Belmonte and W. P. Giering, *Organometallics*, 1985, **4**, 1981 and refs. therein.
[8] A. Michaelis and L. Gleichmann, *Ber. d. deutsch. Chem. Ges.*, 1882, **15**, 802; A. Michaelis and H. V. Soden, *Annalen*, 1885, **229**, 295.

$$LiPPh_2 + RBr \rightarrow RPPh_2 + LiBr$$

The phosphorus halides react with either organolithium or Grignard reagents to produce (usually) only the tertiary ligand, *e.g.*

$$PhPCl_2 + 2\ RMgBr \rightarrow PhPR_2 + 2\ MgClBr$$

The Grignard method is probably the most convenient laboratory method. The starting materials are phosphorus trihalides, phosphonous dihalides, or phosphinous halides, which are all commercially available. Depending on the starting materials and the Grignard reagent, the reaction leads to the formation of tertiary phosphines with either identical or different R groups.

2.1.4 Applications of transition-metal phosphine complexes

In 1948, Reppe and Schweckendieck[9] reported that phosphine complexes of metal halides and carbonyls successfully catalyse the cyclisation of olefins and acetylenes. An undeniable explosion of interest occurred in the 1960s when complexes of the majority of transition metals were found to act as highly active catalysts. Complexes containing donor ligands of group 15 were particularly favoured, and among those, phosphines more than arsines or stibines. The catalytic activity of these compounds has been attributed to the dissociation of a ligand leading to a reactive intermediate with an empty coordination site, followed by the coordination of the substrate. Since the reactions are commonly carried out in one phase, this type of catalysis is known as homogeneous catalysis. The major advantage is that the ligand can be used as a controlling device to increase the selectivity of the desired product. On the other hand, it is difficult to separate the catalyst from the products after the reaction. Recovery of the catalyst has become increasingly significant due to both environmental and financial reasons. This can be achieved by fixation of the catalyst onto an insoluble polymeric support[10] or by working in an aqueous biphasic system where the catalyst is made water-soluble by appropriate ligands such as sulfonated PPh_3 [11]. The field of catalysis has grown greatly

---

[9] W. Reppe and W. J. Schweckendiek, *Ann. Chem.*, 1948, **560**, 104.
[10] C. Saluzzo, R. ter Halle, F. Touchard, F. Fache, E. Schulz and M. Lemaire, *J. Organomet. Chem.*, 2000, **603**, 30; E. Lindner, T. Schneller, F. Auer and H. A. Mayer, *Angew. Chem. Int. Ed.*, 1999, **38**, 2154.
[11] W. A. Herrmann and C. W. Kohlpaintner, *Angew. Chem. Int. Edn. Engl.*, 1993, **32**, 1524; H. Ding, B. E. Hanson, T. Bartik and B. Bartik, *Organometallics*, 1994, **13**, 3761.

and has been the topic of several reviews[12]. Wilkinson's catalyst[13], $[Rh(PPh_3)_3Cl]$, and its analogues are perhaps the most widely studied ones. This highly selective catalyst is used to hydrogenate unsaturated organic species and has become particularly important in synthetic natural product chemistry because it is able to reduce alkenes and alkynes in the presence of other reducible groups. Other examples are shown in Table 2.1.

Table 2.1 Examples of homogeneous catalysis by transition-metal phosphine complexes.

Catalyst	Reaction type	Example
$[Rh(PPh_3)_3Cl]$	Hydrogenation	$RCH{=}CH_2 \xrightarrow{H_2} RCH_2CH_3$
$[CoH(CO)_3(PR_3)]$	Hydro-formylation	$RCH{=}CH_2 \xrightarrow{H_2/CO} RCH_2CHO + RCH_2CH_2OH$ + branched products
$[Ni(PPh_3)_2Cl_2]$	Hydrosilation	$RCH{=}CH_2 \xrightarrow{HSiR_3} RCH(CH_3)SiR_3 + RCH_2CH_2SiR_3$
$[Pt(PPh_3)_4]$	Oxidation	$PPh_3 \xrightarrow{O_2} OPPh_3$

Added motivation for research in the area of transition-metal phosphine chemistry came when Chatt[14] discovered that phosphine ligands were able to stabilise platinum hydride complexes. Since then, a vast number of phosphine-stabilised transition-metal hydrides has been isolated and studied[15]. Tertiary phosphines were further found to stabilise transition-metal alkyls[16], aryls[17], cluster compounds[18], and transition metals in both high and low oxidation states[19].

---

[12] C. Boy and W. A. Herrmann (eds.), *Applied Homogeneous Catalysis with Organometallic Compounds*, 3 volumes, Wiley, Weinheim, 2002.
[13] J. A. Osborne, F. H. Jardine, J. F. Young and G. Wilkinson, *J. Chem. Soc. (A)*, 1966, 1711; S. Motelati, A. van der Ent, J. A. Osborn and G. Wilkinson, *J. Chem. Soc. (A)*, 1968, 1054.
[14] J. Chatt, L. A. Duncanson and B. L. Shaw, *Proc. Chem. Soc.*, 1957, 343.
[15] G. Jia and C. P. Lau, *J. Organomet. Chem.*, 1998, **565**, 37; A. M. Mueting, W. Bos, B. D. Alexander, P. D. Boyle, J. A. Casalnuovo, S. Balaban, N. Larry, S. M. Johnston and L. H. Pignolet, *New J. Chem.*, 1988, **12**, 505; A. P. Humphries and H. D. Kaesz, *Progr. Inorg. Chem.*, 1979, **25**, 145.
[16] W. J. Marshall, K. G. Moloy, A. Prock, W. P. Giering, C. M. Haar and S. P. Nolan, *Organometallics*, 1999, **18**, 474.
[17] M. R. Churchill, K. L. Kalra and M. V. Veidis, *Inorg. Chem.*, 1973, **12**, 1656; M. R. Churchill and M. V. Veidis, *J. Chem. Soc. Dalton Trans.*, 1972, 670.
[18] L. H. Pignolet, M. A. Aubart, K. L. Craighead, R. A. T. Gould, D. A. Krogstad and J. S. Wiley, *Coord. Chem. Rev.*, 1995, **143**, 219.
[19] R. Ugo, *Coord. Chem. Rev.*, 1968, **3**, 319; F. A. Cotton, G. Wilkinson, C. A. Murillo and M. Bochmann, *Advanced Inorganic Chemistry*, 6th ed., Wiley, N.Y., 1999.

A great deal of interest has been shown in the process of nitrogen fixation. This part of the nitrogen cycle has gained most attention partly due to the fascinating concept of converting the 'unreactive' atmospheric N_2 under mild conditions into NH_3. The enzyme nitrogenase is responsible for catalysing this process. Nitrogenase contains the metals molybdenum and iron, and so much research has been carried out on those two metals. Typical complexes are of the type $[M(N_2)(PR_3)_4]$, which have undergone kinetic, spectroscopic and structural studies in order to gain more insight into the reaction mechanism[20].

Metal complexes of tertiary phosphines have further found applications in medicine, not only in the treatment of certain diseases, but also for diagnostic purposes, for handling metabolic dysfunction or in the treatment of heavy-metal poisoning through formation of appropriate metal complexes[21]. Phosphine complexes of Cu(I), Ag(I), Au(I) as well as of the nickel triad[22] were all found to exhibit anticancer activity against several types of tumours. 'Auranofin'[23] is a gold-(triethyl)phosphine-based antiarthritic agent; its PPh_3 analogues have also received some attention[24]. Technetium complexes are commonly employed as radiopharmaceuticals[25], *e.g.* $[Tc(L–L)Cl_2]$ (L–L = diphosphine) as a heart-imaging agent.

---

[20] M. N. Huges, Coordination Compounds in Biology, In G. Wilkinson (ed.), *Comprehensive Coordination Chemistry*, Vol. 2, Pergamon Press, Oxford, 1987; H. Masanobu, *Coord. Chem. Rev.*, 1999, **185-186**, 99.

[21] H. E. Howard-Lock and C. J. Lock, Uses in Therapy. In G. Wilkinson, *Comprehensive Coordination Chemistry*, Vol. 6, Pergamon Press, Oxford, 1987.

[22] P. S. Jarrett, O. M. N. Dhubghail and P. J. Sadler, *J. Chem. Soc. Dalton Trans.*, 1993, 1863; P. S. Jarrett and P. J. Sadler, *Inorg. Chem.*, 1991, **30**, 2098; M. P. Hacker, E. B. Douple and I. H. Krakoff (eds.), *Platinum Coordination Complexes in Cancer Chemotherapy*, Martinus Nijhoff, Boston, 1984; M. T. Razi, G. Otiko, P. J. Sadler, Ligand Exchange Reactions of Gold Drugs in Model Systems and in Red Cells. In S. J. Lippard (ed.), *Platinum, Gold and other Metal Chemotherapeutic Agents*, ACS Symposium Series 209, American Chemical Society, Whashington, DC, 1983.

[23] B. M. Sutton, *Gold Bull.*, 1986, **19**, 15; J. D. Jessop, M. M. O'Sullivan, P. A. Lewis, L. A. Williams, J. P. Camilleri, M. J. Plant and E. C. Coles, *Br. J. Rheumatol.*, 1998, **37**, 992.

[24] L. S. Ahmed, W. Clegg, D. A. Davies, J. R. Dilworth, M. R. J. Elsegood, D. V. Griffiths, L. Horsburgh, R. J. Miller and N. Wheatley, *Polyhedron*, 1998 (volume date 1999), **18**, 593.

[25] E. Deutsch, K. Libson, S. Jurisson and L. F. Lindoy, *Progr. Inorg. Chem.*, 1983, **30**, 75.

2.2 The concept of electrospray-friendly ligands

Electrospray-friendly ligands are ligands that are designed to be visible in the ESMS. They are used instead of ligands that are not suitable for ESMS. In fact, this is the main feature distinguishing this concept from derivatisation methods[26]. The metal complexes are not submitted to a chemical reaction. Rather, new ligands are designed and employed in the synthesis of the complex. Thus, the term electrospray-friendly 'derivatives' only applies in the wider sense.

The new ligands need to be closely similar to the original one, so that the fundamental chemistry remains essentially unchanged. Furthermore, the protonation pathway, which is the most general one in ESMS (see Chapter one), should be employed for the detection of the ligands and their metal complexes.

This concept can be applied to neutral ligands that cannot be ionised by any of the methods discussed in Chapter one. As for PPh_3, once it is bonded to a metal centre, it does not have a basic site for protonation. As a result, metal complexes of PPh_3 usually cannot be detected in the ESMS unless they have other ionisable ligands.

When using ES-friendly ligands, all advantages that ESMS offers apply. Thus, the combination of the very rich chemistry of transition-metal phosphine complexes with the powerful tool of ESMS will ultimately lead to the following major advantages:

1. ESMS has already greatly increased the number of compounds amenable to mass spectrometry. With the concept of electrospray-friendly ligands the number of neutral organometallic compounds suitable to this technique increases even further.

2. Because the reaction solution itself can be injected into the mass spectrometer, ESMS has had a huge impact on solution chemistry. This feature is of particular use when monitoring reactions or in the detection of intermediates, *e.g.* in catalytic processes.

---

[26] A derivative is "a chemical compound derived from some other compound by a straightforward reaction, which usually retains the structure and some of the chemical properties of the original compound". In G. Waites and P. Harrison, *The Cassell Dictionary of Chemistry*, Cassell, 1998.

3. All species formed in a reaction can be detected. Pyrolysis reactions, for example, play a major role in the synthesis of multimetallic phosphine complexes and are known to lead to the formation of a large number of products. So far, the detection of phosphine clusters has depended on the compound that crystallised out for subsequent X-ray analysis.

4. Transition-metal phosphine chemistry often includes very expensive materials, *e.g.* complexes of rhodium, platinum, gold, *etc.* As compared to other methods, such as NMR, only a small amount of analyte is needed for an extensive ESMS study. Thus, reactions can be carried out on a very small scale and the reactivity of the phosphine ligand toward different metal centres may be investigated.

5. Phosphine complexes may also be characterised by ^{31}P NMR. The concept of electrospray-friendly ligands can, however, be extended to ligands other than phosphines, such as arsines or stibines (see following chapters). Analysis by mass spectrometry is of particular interest for complexes of those ligands as they do not have NMR-active nuclei and their ways of characterisation are therefore rather limited.

2.3 Ligand design

As mentioned above, the two key aims were to design ligands that are similar in most respects to the parent PPh_3 ligand and undergo the protonation-type mechanism for generating ions for their ESMS analysis.

To fulfil the latter requirement, the ligands need to exhibit a basic site. Molecules with a basic functional group generally associate readily in solution with H^+ ions to give the parent ion $[M + H]^+$, which can then be detected in the mass spectrometer. MeO and Me_2N groups are known to be readily protonated in solvents used to run ESMS spectra. The ligands in this study therefore contain the basic functional MeO and Me_2N groups.

The ligands are all derived from PPh_3, thus maintaining the original PPh_3 structure. The functionalised analogues further need to contain the basic group in the *para*-position because the *para*-isomer will be sterically and chemically most similar to the parent ligand.

It was decided to design ligands containing MeO and Me_2N groups on not only one, but also two and three phenyl rings. The structures and code names of the PPh_3 analogues are shown in Figure 2.1. The ligands with the greatest number of basic groups (P*** and P•••) as well as their metal complexes should be more soluble in organic solvents than PPh_3 or their PPh_3 analogues. Moreover, any electronic or steric differences (of the ligands as well as their complexes) are likely to be smaller with fewer substituents attached to the ligand. Thus, if very close similarity to the PPh_3 analogues is desired, then P* and P• should be the best ligands. On the other hand, the ligands with most MeO/Me_2N groups should be protonated most easily and hence should provide the best ES mass spectra.

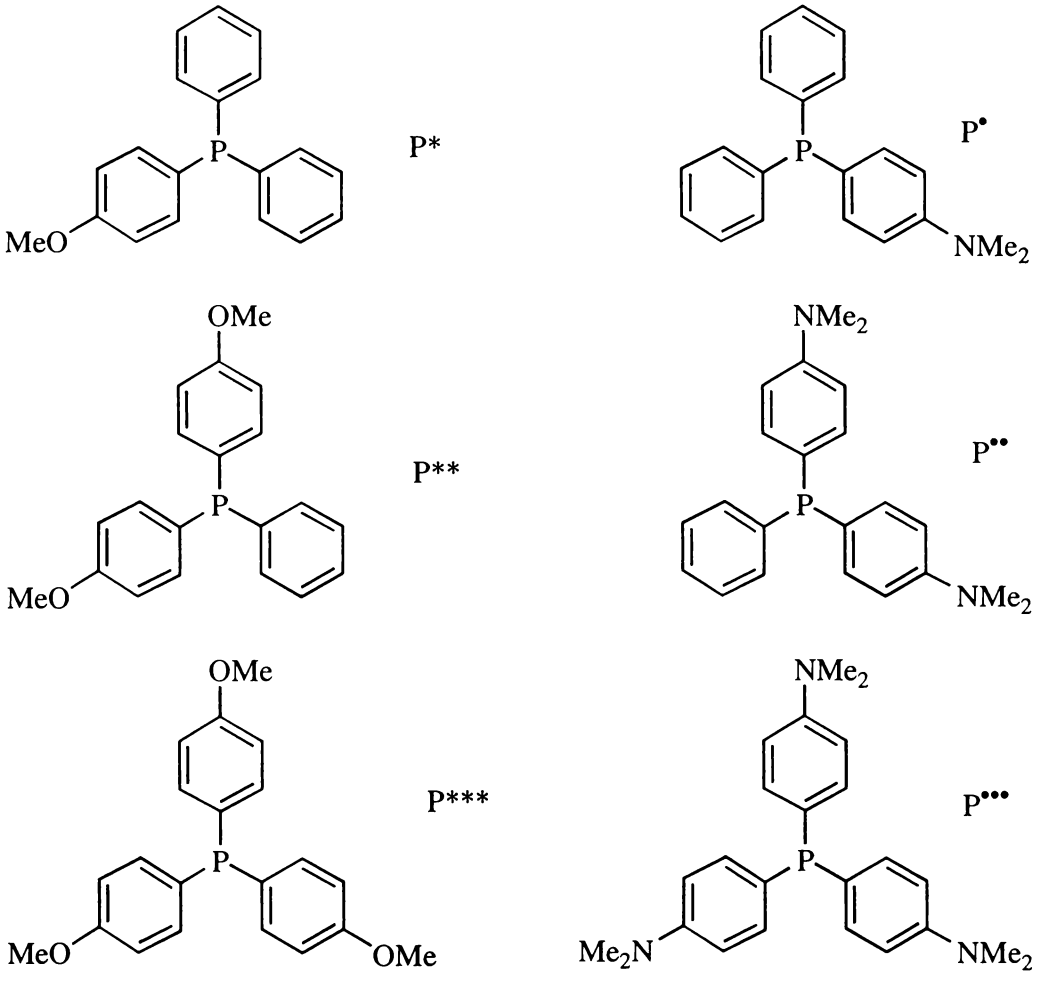

Fig. 2.1 The structures and code names of the electrospray-friendly derivatives of PPh_3.

2.4 Ligand synthesis and properties

All of the ligands shown in Figure 2.1 can be prepared readily from inexpensive starting materials and P*** may be also be obtained commercially. In this study, the ligands were synthesised from an appropriate Grignard reagent and the halo phosphine compounds Ph_nPCl_{3-n} (n = 0, 1, 2). Thus, the phenyl derivatives $PhPCl_2$, Ph_2PCl as well as PCl_3 were reacted with $MeOC_6H_4MgBr$ or $Me_2NC_6H_4MgBr$ to give the corresponding MeO- or Me_2N-functionalised analogues of the parent ligand PPh_3 (see Scheme 2.1).

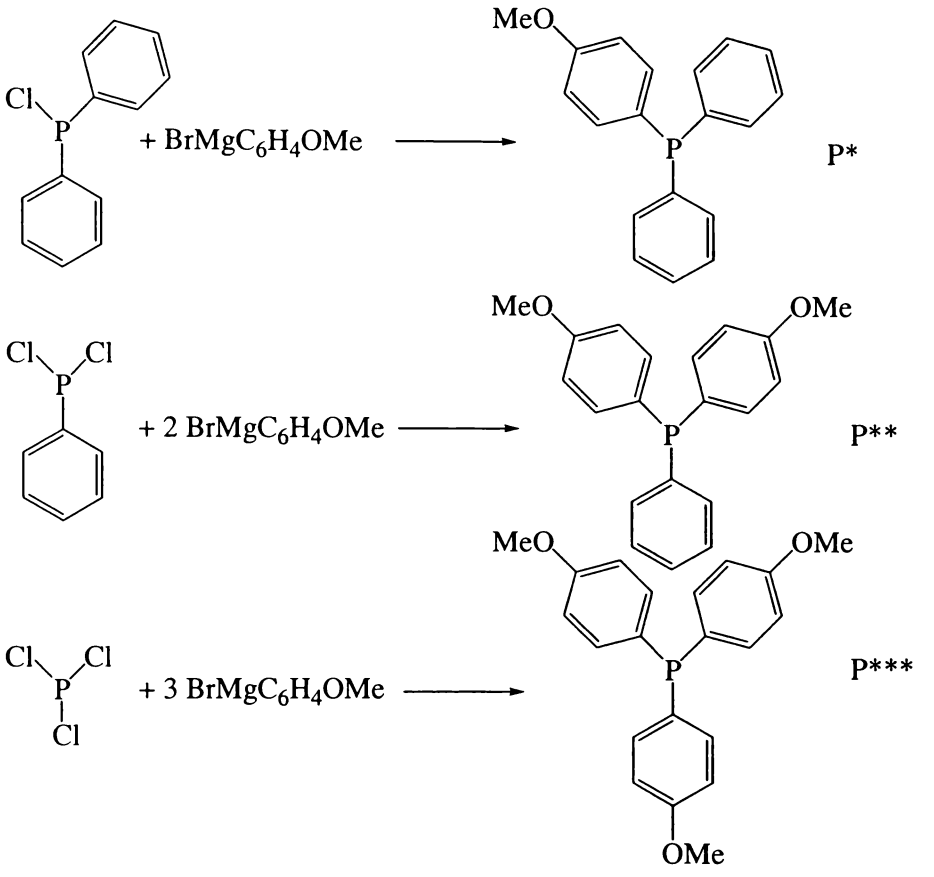

Scheme 2.1 The synthesis of the electrospray-friendly ligands P*, P** and P***. The Me_2N-based ligands were synthesised in an analogous manner from the appropriate Grignard reagent $Me_2NC_6H_4MgBr$.

The electrospray-friendly ligands are all air-stable crystalline solids, similar to the parent PPh_3. They are very soluble in organic solvents, which is good for ESMS analysis since they can be directly dissolved in the carrier solvent, usually MeOH or $MeCN/H_2O$. All of the derivatised phosphine ligands are known compounds. However, they have never been used to facilitate the mass spectrometric analysis of metal complexes.

2.5 ESMS of the ligands

Before the ligands were incorporated into metal complexes they were examined by mass spectrometry to see whether they give the expected $[M + H]^+$ ions in their ES mass spectra and how well they ionise compared to the PPh_3 ligand. The ES mass spectrum of P* is shown in Figure 2.2, and the data for the whole range of ligands are listed in Table 2.2. For all phosphines, the only ion observed was the $[M + H]^+$ ion. Other possible ions like $[M + NH_4]^+$ or $[M + Na]^+$ were never detected. Also, aggregation of parent ions such as $[2M + H]^+$ or $[3M + H]^+$ did not appear. The spectra are simple and the ions have a good signal to noise ratio. These results were very promising for the analysis of metal complexes of the substituted ligands.

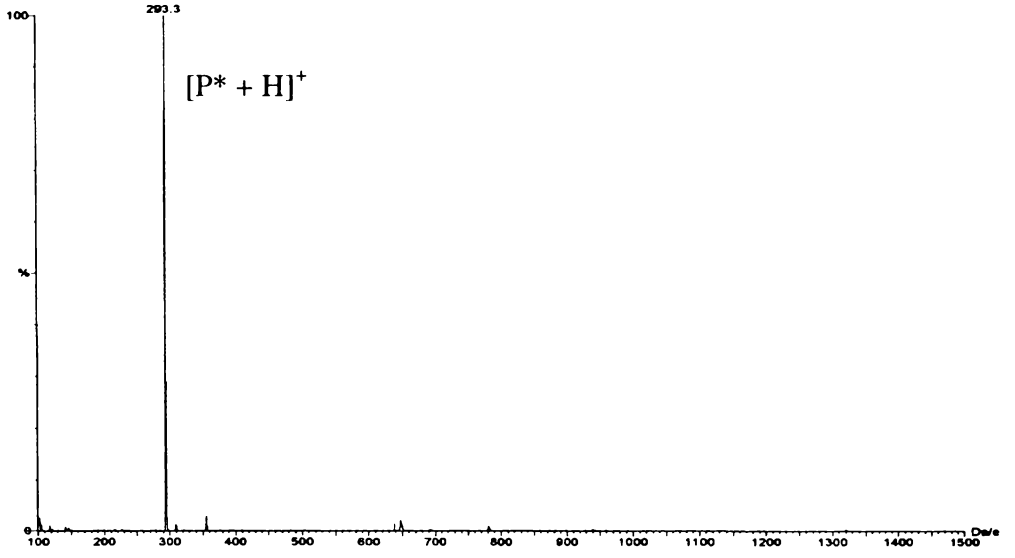

Fig. 2.2 The positive-ion ES mass spectrum of P* (M_r = 292), recorded in MeOH at cV = 20 V.

It should be noted that because of its lone pair of electrons the free ligand PPh_3 also gives an $[M + H]^+$ signal in the ES mass spectrometer. The lone electron pair on PPh_3 is, however, much less basic than the electron pairs on the methoxy or dimethylamino groups. Accordingly, the signal observed for PPh_3 is much lower in intensity compared to the signals of the derivatised ligands. In fact, in an equimolar mixture of PPh_3, P*, P** and P***, no signal was observed for PPh_3. The intensities of the $[M + H]^+$ ions of the functionalised ligands were greater with an increasing number of MeO groups (21:85:100% for P*:P**:P***). This result supports the assumption that the free ligands

mainly ionise at the functional groups rather than at the free electron pair at the P atom.

Table 2.2 The positive-ion ESMS data for the derivatised ligands, recorded in MeOH at cV = 20 V.

Ligand	Ions observed [*m/z*, relative peak height (%)]
P*	$[M + H]^+$ (293, 100)
P**	$[M + H]^+$ (323, 100)
P***	$[M + H]^+$ (353, 100)
P$^{\bullet}$	$[M + H]^+$ (306, 100)
P$^{\bullet\bullet}$	$[M + H]^+$ (349, 100)
P$^{\bullet\bullet\bullet}$	$[M + H]^+$ (392, 100)

2.6 Synthesis and properties of the metal complexes

A wide range of metal complexes with the methoxy- and amino-substituted ligands was prepared. In all cases, procedures for the previously published PPh_3 analogues were followed. In a straightforward one-pot reaction, ligand replacement occurred readily from either the metal carbonyl or an appropriate precursor. The prepared complexes are listed in Table 2.3. The examples were chosen to cover two main types of complexes: neutral metal phosphine carbonyl complexes and neutral metal phosphine halide complexes. Carbonyl complexes of molybdenum, iron and ruthenium were examined since the PPh_3 analogues do not give ESMS spectra[27]. Metal halide complexes are already known to undergo ionisation by halide loss[28,29] forming ions of the type $[M - X]^+$ and $[M - X + solv]^+$. Despite their visibility in the ESMS, they were chosen as a second group in order to evaluate the tendency (if any) of these complexes to undergo ionisation by protonation. The competition between the two possible ionisation

[27] Two exceptions are $[Ru_3(CO)_{11}(PPh_3)]$ and $[Ru_3(CO)_9(PPh_3)_3]$ which were found to form adducts when appropriate ionisation aids were added. See Ref 32.
[28] W. Henderson, J. Fawcett, R. D. W. Kemmitt, P. McKenna and D. R. Russell, *Polyhedron*, 1997, **16**, 2455; J. Fawcett, W. Henderson, R. D. W. Kemmitt, D. R. Russell and A. Upreti, *J. Chem. Soc. Dalton Trans.*, 1996, 1897.
[29] W. Henderson and C. Evans, *Inorg. Chim. Acta*, 1999, **294**, 183.

pathways could lead to the observation of ions due to halide loss only, ions due to both pathways, or only the $[M + H]^+$ ion due to protonation.

A small number of the complexes[30] incorporating electrospray-friendly ligands has been reported before, but most appeared to be new compounds. They have been fully characterised and their data can be found in the Experimental section. In addition to the complexes of electrospray-friendly ligands, all PPh_3 analogues were synthesised for comparative purposes.

For the free ligands, it has been shown[31] that the steric properties of PPh_3, P*** and P••• are identical, all three having cone angles of 145°. Their electronic properties are usually expressed by the pKa values and have also been studied[31]. With pKa values for the protonated phosphines of 2.73 for PPh_3, 4.59 for P*** and 8.65 for P•••, their electronic properties are only reasonably similar.

As ES-friendly analogues, close similarity to the parent PPh_3 complexes is important, but some differences in basicity as well as steric and electronic properties cannot be denied. In fact, it is those slight differences that have previously been made use of, because they may have an effect on reactivity, selectivity, product yields, *etc.*

An IR and NMR spectroscopic survey of the metal complexes was carried out in order to investigate the similarity of the complexes containing functionalised ligands compared to their PPh_3 analogues. The IR and ^{31}P NMR data are summarised in Table 2.3.

---

[30] *trans*-$[Fe(CO)_3P^{***}_2]$, *cis*-$[PtCl_2P^{•••}_2]$, $[PdCl_2P^{**}_2]$ and $[AuClP^{•••}]$.
[31] M. M. Rahman, H.-Y. Liu, K. Eriks, A. Prock and W. P. Giering, *Organometallics*, 1989, **8**, 1.

Table 2.3 The IR and ^{31}P NMR data for the prepared complexes.

Complex	IR ν_{CO} (cm^{-1})	^{31}P NMR (δ) [(a)]
cis-$[Mo(CO)_4(PPh_3)_2]$	2023(s), 1927(sh), 1908s, 1897(sh)	38.9
cis-$[Mo(CO)_4P^*_2]$	2021(s), 1919(sh), 1906s, 1879(sh)	37.1
cis-$[Mo(CO)_4P^{**}_2]$	2020(s), 1918(sh), 1905s, 1876(sh)	35.5
cis-$[Mo(CO)_4P^{***}_2]$	2018(s), 1917(sh), 1904s, 1874(sh)	34.0
cis-$[Mo(CO)_4P^{\bullet}_2]$	2019(s), 1920(sh), 1903s, 1875(sh)	36.0
cis-$[Mo(CO)_4P^{\bullet\bullet}_2]$	2016(s), 1913(sh), 1899s, 1872(sh)	33.3
cis-$[Mo(CO)_4P^{\bullet\bullet\bullet}_2]$	2013(s), 1907(sh), 1900s, 1873(sh)	30.8
trans-$[Fe(CO)_3(PPh_3)_2]$	1884	83.1
trans-$[Fe(CO)_3P^*_2]$	1882	81.3
trans-$[Fe(CO)_3P^{**}_2]$	1880	79.5
trans-$[Fe(CO)_3P^{***}_2]$	1874	77.8
$[Ru_3(CO)_9(PPh_3)_3]$	2044w, 1979(sh), 1967(br)	38.0
$[Ru_3(CO)_9P^*_3]$	2043w, 1979(sh), 1967s	36.7
$[Ru_3(CO)_9P^{**}_3]$	2047w, 1978(sh), 1967s	35.8
$[Ru_3(CO)_9P^{***}_3]$	2054w, 1977(sh), 1966s	34.6
$[Ru_3(CO)_9P^{\bullet}_3]$	2054w, 1977(sh), 1965s	36.0
$[Ru_3(CO)_9P^{\bullet\bullet}_3]$	2055w, 1972(sh), 1963s	34.3
$[Ru_3(CO)_9P^{\bullet\bullet\bullet}_3]$	2054w, 1970(sh), 1959s	32.7
cis-$[PtCl_2(PPh_3)_2]$		15.1 (3673)
cis-$[PtCl_2P^*_2]$		13.8 (3684)
cis-$[PtCl_2P^{**}_2]$		12.7 (3695)
cis-$[PtCl_2P^{***}_2]$		11.5 (3705)
cis-$[PtCl_2P^{\bullet\bullet\bullet}_2]$		9.7 (3758)
$[PdCl_2(PPh_3)_2]$		24.0

$[PdCl_2P^{**}_2]$		22.8
$[PdCl_2P^{**}_2]$		21.6
$[PdCl_2P^{***}_2]$		20.3
$[AuCl(PPh_3)]$		34.0
[AuClP*]		32.6
[AuClP**]		31.3
[AuClP***]		30.0
$[AuClP^{\bullet\bullet\bullet}]$		28.3

[a] The $^1J_{P,Pt}$ coupling constants (in Hz) are given in parentheses.

In the IR spectra, the general trend of a slight shift of CO stretching frequencies to lower wave numbers is observed with increasing numbers of MeO or Me_2N groups in the phosphine ligand. This is due to the increased back donation with a slightly more electron-rich phosphine ligand. However, the values are overall similar to those of the PPh_3 analogues. This is well illustrated by the series of $[Mo(CO)_4L_2]$ complexes, where there is a *ca.* 10 cm^{-1} decrease in CO stretching frequency going from $[Mo(CO)_4(PPh_3)_3]$ to $[Mo(CO)_4P^{\bullet\bullet\bullet}_2]$. Similar trends are observed for the iron carbonyl complexes and the stronger bands of the ruthenium carbonyl complexes. The observation of relatively small shifts is particularly interesting when comparing them to the respective pKa values listed earlier. Given the small changes in the IR stretching frequencies observed for the carbonyl complexes, the rather large difference in pKa values between PPh_3 and P*** is surprising. One might speculate that the pKa value for P*** involves protonation on the O and not only on the P atom. Hence, a comparison of the different CO stretching frequencies is a far better method of comparing the basicity and confirms the overall similarity for the prepared ligands.

The observations in the IR spectra are paralleled by the ^{31}P NMR chemical shifts. Here, shielding of the ^{31}P nucleus occurs upon incorporation of every MeO and Me_2N group. There is a small stepwise decrease in the δ (^{31}P) value from $[Mo(CO)_4(PPh_3)_3]$ (38.9) to $[Mo(CO)_4P^*_2]$ (37.1) to $[Mo(CO)_4P^{**}_2]$ (35.5) to $[Mo(CO)_4P^{***}_2]$ (34.0). Very approximately, the presence of two Me_2N groups {in $[Mo(CO)_4P^{\bullet}_2]$} has around the same effect on the ^{31}P NMR shift as four MeO groups {in $[Mo(CO)_4P^{**}_2]$}. Similar

trends in δ (^{31}P) were observed for the other series of complexes, with Me_2N-substituted complexes having lower values than the analogous complexes with MeO substituents.

In summary, the basic group in the *para*-position (instead of *ortho* or *meta*) ensures close similarity to PPh_3 with respect to its electronic and steric properties. The MeO and Me_2N groups can therefore be said to make the ligand derivatives 'chemically innocent' but electrospray-friendly.

2.7 ESMS of the metal complexes

In order to investigate whether the prepared ligands are also suitable for ESMS analysis when coordinated to a metal centre, all metal complexes were analysed by ESMS.

2.7.1 Metal carbonyl complexes

Table 2.4 lists the ions observed in the ES mass spectra of the prepared metal carbonyl complexes.

Table 2.4 The positive-ion ESMS data for the transition-metal carbonyl complexes, recorded in either MeCN/H_2O or MeOH solution.

Complex	Solvent	cV (V)	Ions observed [*m/z*, relative peak height (%)]
$[Mo(CO)_4P^*_2]$	MeCN/ H_2O	20	$[M + H]^+$ (795, 100), $[M + NH_4]^+$ (812, 20)
		60	$[M + H]^+$ (795, 69), $[M + H - CO]^+$ (767, 12), $[M + H - 2CO]^+$ (739, 100), $[M + H - 3CO]^+$ (711, 48), $[M + H - 4CO]^+$ (683, 49)
		80	$[M + H]^+$ (795, 90), $[M + H - CO]^+$ (767, 19), $[M + H - 2CO]^+$ (739, 20), $[M + H - 3CO]^+$ (711, 13), $[M + H - 4CO]^+$ (683, 100)
$[Mo(CO)_4P^{**}_2]$	MeCN/ H_2O	20	$[M + H]^+$ (855, 100), $[M + NH_4]^+$ (872, 4)
$[Mo(CO)_4P^{***}_2]$	MeOH	20	$[M + H]^+$ (915, 100)
		60	$[M + H]^+$ (915, 15), $[M + H - 2CO]^+$ (859, 100), $[M + H - 3CO]^+$ (831, 41), $[M + H - 4CO]^+$ (803, 18)

$[Mo(CO)_4P^{\bullet}{}_2]$	MeCN/ H_2O	20	$[M + H]^+$ (821, 100)
$[Mo(CO)_4P^{\bullet\bullet}{}_2]$	MeOH	20	$[M + H]^+$ (907, 100)
$[Mo(CO)_4P^{\bullet\bullet\bullet}{}_2]$	MeOH	20	$[M + H]^+$ (993, 100)
$[Fe(CO)_3P^*{}_2]$	MeOH	20	$[M + H]^+$ (725, 53), $[M + NH_4]^+$ (742, 100)
$[Fe(CO)_3P^{**}{}_2]$	MeCN/ H_2O	20	$[M + H]^+$ (785, 100)
		60	$[M + H]^+$ (785, 100), $[M + H - 3CO]^+$ (701, 60)
		80	$[M + H]^+$ (785, 32), $[M + H - 3CO]^+$ (701, 100)
$[Fe(CO)_3P^{***}{}_2]$	MeCN/ H_2O	20	$[M + H]^+$ (845, 100)
		60	$[M + H]^+$ (845, 28), $[M + H - 3CO]^+$ (761, 100)
		80	$[M + H]^+$ (845, 18), $[M + H - 3CO]^+$ (761, 100)
$[Ru_3(CO)_9P^*{}_3]$	MeOH	20	$[M + H]^+$ (1434, 100)
		60	$[M + H]^+$ (1434, 45), $[M + H - CO]^+$ (1406, 100), $[M + H - 2CO]^+$ (1378, 36), $[M + H - 3CO]^+$ (1350, 23), $[M + H - 4CO]^+$ (1322, 12), $[M + H - 5CO]^+$ (1294, 5),
		80	$[M + H]^+$ (1434, 88), $[M + H - CO]^+$ (1406, 69), $[M + H - 2CO]^+$ (1378, 99), $[M + H - 3CO]^+$ (1350, 77), $[M + H - 4CO]^+$ (1322, 100), $[M + H - 5CO]^+$ (1294, 93), $[M + H - 6CO]^+$ (1266, 47)
$[Ru_3(CO)_9P^{**}{}_3]$	MeOH	20	$[M + H]^+$ (1524, 100)
		60	$[M + H]^+$ (1524, 100), $[M + H - CO]^+$ (1496, 88), $[M + H - 2CO]^+$ (1468, 20), $[M + H - 3CO]^+$ (1440, 9), $[M + H - 4CO]^+$ (1412, 4)
$[Ru_3(CO)_9P^{***}{}_3]$	MeOH	20	$[M + H]^+$ (1614, 100)
		60	$[M + H]^+$ (1614, 100), $[M + H - CO]^+$ (1586, 90), $[M + H - 2CO]^+$ (1558, 28), $[M + H - 3CO]^+$ (1530, 11), $[M + H - 4CO]^+$ (1502, 4)

		80	$[M + H]^+$ (1614, 18), $[M + H - CO]^+$ (1586, 95), $[M + H - 2CO]^+$ (1558, 63), $[M + H - 3CO]^+$ (1530, 68), $[M + H - 4CO]^+$ (1502, 100), $[M + H - 5CO]^+$ (1474, 49), $[M + H - 6CO]^+$ (1446, 9)
$[Ru_3(CO)_9P^{\bullet}_3]$	MeCN/ H_2O	20	$[M + H]^+$ (1473, 100), $[M + Na]^+$ (1495, 10)
		60	$[M + H]^+$ (1473, 25), $[M + H - CO]^+$ (1445, 92), $[M + H - 2CO]^+$ (1417, 100), $[M + H - 3CO]^+$ (1389, 69), $[M + H - 4CO]^+$ (1361, 56), $[M + H - 5CO]^+$ (1333, 29)
		80	$[M + H]^+$ (1473, 18), $[M + H - CO]^+$ (1445, 29), $[M + H - 2CO]^+$ (1417, 50), $[M + H - 3CO]^+$ (1389, 14), $[M + H - 4CO]^+$ (1361, 40), $[M + H - 5CO]^+$ (1333, 79), $[M + H - 6CO]^+$ (1305, 100)
$[Ru_3(CO)_9P^{\bullet\bullet}_3]$	MeCN/ H_2O	20	$[M + H]^+$ (1602, 100), $[M + Na]^+$ (1624, 29)
		60	$[M + H]^+$ (1602, 70), $[M + Na]^+$ (1624, 20), $[M + H - CO]^+$ (1574, 100), $[M + H - 2CO]^+$ (1546, 65), $[M + H - 3CO]^+$ (1518, 30), $[M + H - 4CO]^+$ (1490, 27)
		80	$[M + H]^+$ (1602, 59), $[M + H - CO]^+$ (1574, 48), $[M + H - 2CO]^+$ (1546, 68), $[M + H - 3CO]^+$ (1518, 35), $[M + H - 4CO]^+$ (1490, 78), $[M + H - 5CO]^+$ (1362, 79), $[M + H - 6CO]^+$ (1434, 100)
$[Ru_3(CO)_9P^{\bullet\bullet\bullet}_3]$	MeCN/ H_2O	20	$[M + H]^+$ (1731, 100), $[M + Na]^+$ (1753, 30)
		60	$[M + H]^+$ (1731, 100), $[M + Na]^+$ (153, 16), $[M + H - CO]^+$ (1703, 65), $[M + H - 2CO]^+$ (1675, 20), $[M + H - 3CO]^+$ (1647, 8), $[M + H - 4CO]^+$ (1619, 8), $[M + H - 5CO]^+$ (1582, 8), $[M + H - 6CO]^+$ (1552, 10)

As expected, the neutral complexes $[Mo(CO)_4(PPh_3)_2]$ and $[Fe(CO)_3(PPh_3)_2]$ did not give ions in their ES mass spectra. With the absence of a basic site there is no means of protonation available. The CO ligands are not basic enough to associate with protons, and once PPh_3 is bonded to the metal centre it no longer has free electron pairs available for protonation. An exception was $[Ru_3(CO)_9(PPh_3)_3]$, which yielded an $[M + H]^+$ ion. This result was not entirely surprising, as the $[M + Na]^+$ ion has been observed before

for the same complex[32]. With the presence of three phosphine ligands, the CO ligands are probably sufficiently electron-rich to associate with protons or other cations.

All of the neutral metal complexes containing the amine-or methoxy-modified ligands ionised readily and gave good, simple ES mass spectra with strong $[M + H]^+$ signals. At low skimmer cone voltages (*i.e.* up to 20 V) there was generally no fragmentation. Two examples are shown in Figure 2.3 and Figure 2.4. In some cases, $[M + NH_4]^+$ ions were observed as well, but their intensities were generally low.

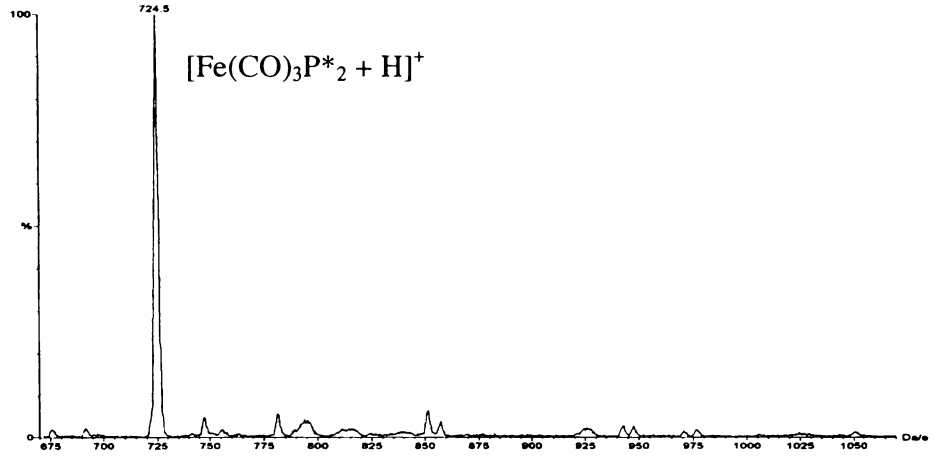

Fig. 2.3 The positive-ion ES mass spectrum of $[Fe(CO)_3P^*_2]$ (M_r = 724), recorded in MeOH at cV = 20 V.

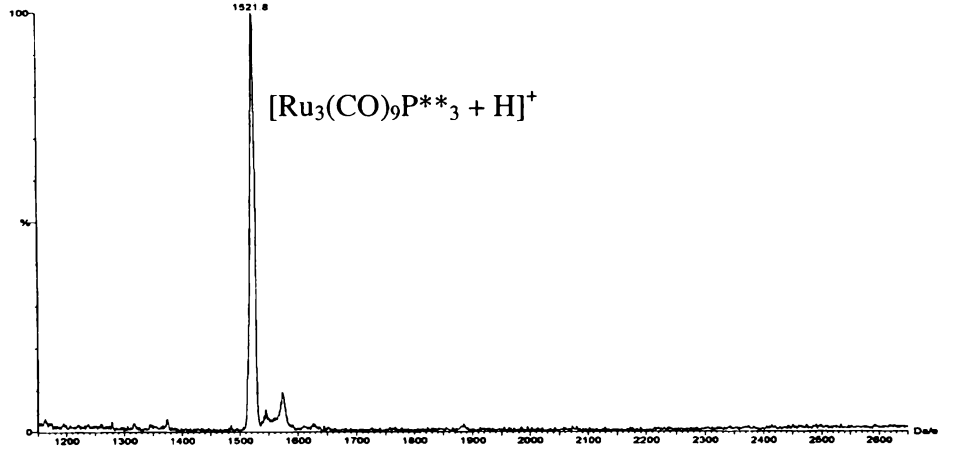

Fig. 2.4 The positive-ion ES mass spectrum of $[Ru_3(CO)_9P^{**}_3]$ (M_r = 1522), recorded in MeOH at cV = 20 V.

---

[32] W. Henderson, J. S. McIndoe, B. K. Nicholson and P. J. Dyson, *J. Chem. Soc. Dalton Trans.*, 1998, 519.

In each case, the parent $[M + H]^+$ could readily be assigned by comparison of experimental and calculated isotope patterns. This is demonstrated for the molybdenum complex $[Mo(CO)_4P^{***}{}_2]$ in Fig 2.5.

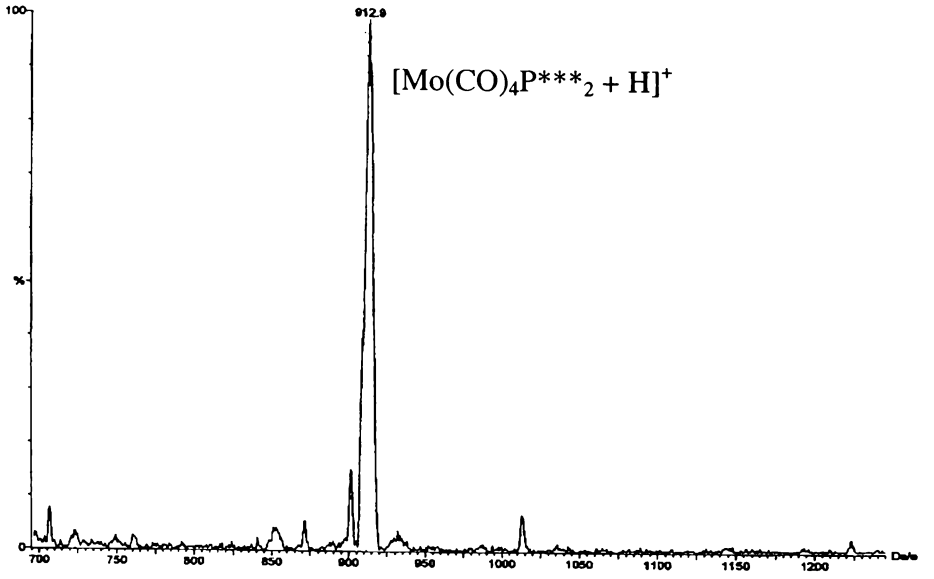

Fig. 2.5a The positive-ion ES mass spectrum of $[Mo(CO)_4P^{***}{}_2]$ (M_r = 912), recorded in MeOH at cV = 20 V.

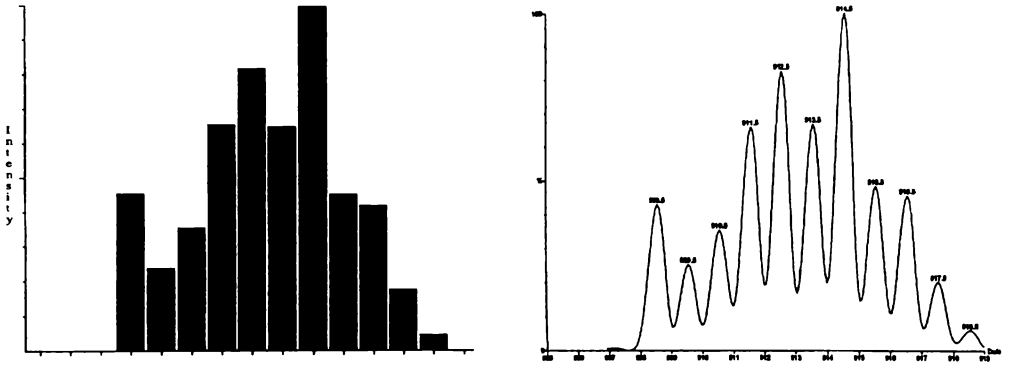

Fig. 2.5b The calculated (left) and observed (right) isotope patterns for $[Mo(CO)_4P^{***}{}_2 + H]^+$.

Such lack of fragmentation is typical for the electrospray process when low cone voltages are used. On increasing the cone voltage, carbonyl ligands are lost sequentially, as illustrated in Fig 2.6 for $[Ru_3(CO)_9P^*{}_3]$. Similar loss of carbonyl ligands has been observed previously in studies of neutral metal carbonyl complexes investigated using

alkoxide[32] or azide[33] ionisation. In this case, however, the neutral metal complexes can be analysed directly without addition of ionisation aids.

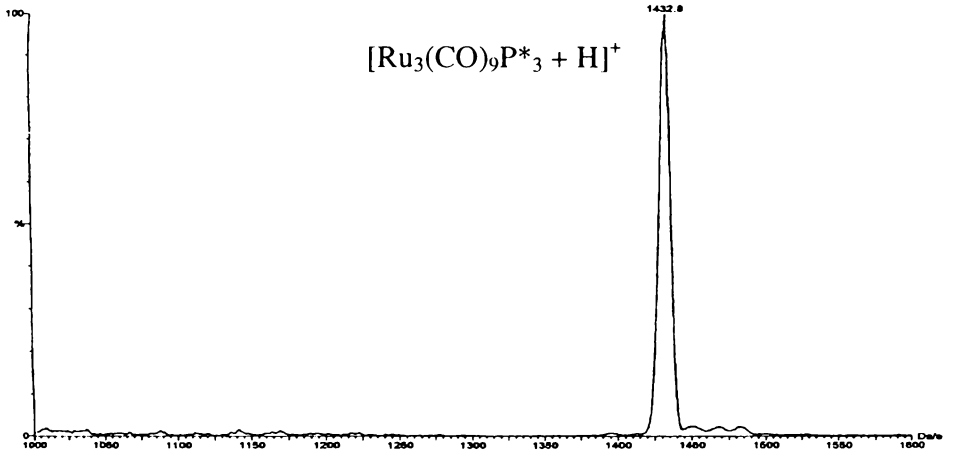

Fig. 2.6a The positive-ion ES mass spectrum of $[Ru_3(CO)_9P^*_3]$ (M_r = 1432) at cV = 20 V, recorded in MeOH.

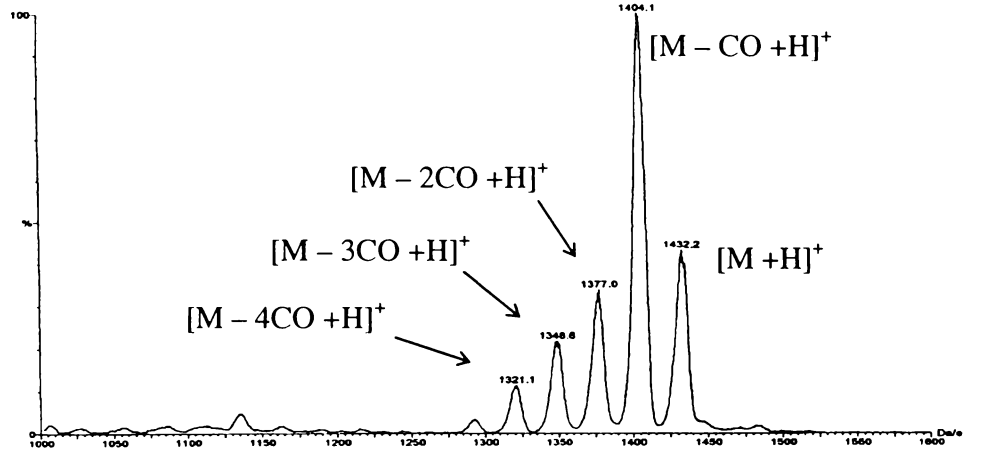

Fig. 2.6b The positive-ion ES mass spectrum of $[Ru_3(CO)_9P^*_3]$ at cV = 60 V, recorded in MeOH.

Having established the generality of the use of the derivatised phosphines, it was of interest to carry out a comparison of the ionisation efficiencies of the different ligands. Two separate ESMS experiments were carried out in order to compare the effect of MeO- *vs.* Me_2N-substitution, and of one substituent per ligand *vs.* two or three. Firstly, a

[33] J. S. McIndoe and B. K. Nicholson, *J. Organomet. Chem.*, 1999, **573**, 232.

1:1 mixture of $[Mo(CO)_4P^{**}{}_2]$ and $[Mo(CO)_4P^{\bullet\bullet}{}_2]$ was analysed. In this case, the Me_2N-substituted complex showed much greater ionisation efficiency than the MeO-substituted one. The methoxy analogue appeared at only 20% relative intensity to the base peak of $[Mo(CO)_4P^{\bullet\bullet}{}_2] + H]^+$. In a second experiment, an equimolar mixture of the complexes $[Mo(CO)_4P^{*}{}_2]$, $[Mo(CO)_4P^{**}{}_2]$ and $[Mo(CO)_4P^{***}{}_2]$ was prepared in MeOH solution and analysed by ESMS. The relative intensities of the $[M + H]^+$ ions increased (24 : 51 : 100) in proportion to the increasing number of MeO groups in the complex from 2 to 4 to 6, as shown in Fig 2.7. As expected, the more basic and the greater the number of substituents the easier the ligands protonate. It should be noted that the complexes containing the ligand with only one methoxy group (P*) already give strong signals in their ES spectra (see for example Fig. 2.6). Thus, one methoxy group has been sufficient for protonation in the examples provided.

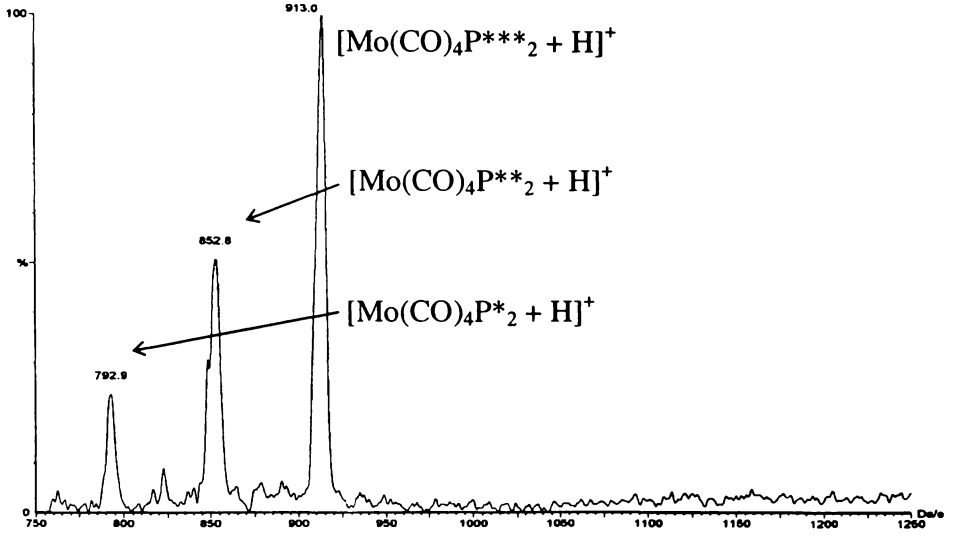

Fig. 2.7 The positive-ion ES mass spectrum of a 1:1:1 mixture of $[Mo(CO)_4P^{*}{}_2]$, $[Mo(CO)_4P^{**}{}_2]$ and $[Mo(CO)_4P^{***}{}_2]$, recorded in MeOH at cV = 20 V.

The ESMS analysis using the substituted ligands appeared to be very sensitive. Deliberate addition of extra acid such as formic acid or the use of very concentrated solutions was generally not necessary. Protic solvents like MeOH are sufficient to provide ions with a good signal to noise ratio. In order to examine the sensitivity of the ligands, the complex $[Ru_3(CO)_9P^{\bullet\bullet\bullet}{}_3]$ of a known concentration was diluted and electrosprayed several times until its signal disappeared in the noise. Without any special attempts to optimise signal intensity, the complex could be detected down to

concentrations of *ca.* 7 x 10^{-8} mol L^{-1}. For routine characterisations, however, more concentrated solutions are used (*ca.* 1 mg mL^{-1}).

As shown above, the ligands are basic enough to be analysed in protic solvents without the need of extra acid to encourage ion formation. However, some complexes are unstable in protic solvents and need to be analysed in aprotic ones, such as 1,2-dimethoxyethane (dme) or THF solutions. These types of complexes can still be made visible by using alkali metal salts as the ionisation source to give ions of the type $[M + c]^+$ (c = cation). Thus, the compounds $[Mo(CO)_4P^{\bullet\bullet}{}_2]$ and $[Mo(CO)_4P^{\bullet\bullet\bullet}{}_2]$ were analysed in THF solution with a small quantity of added $Na[BPh_4]$. With this sodium salt as an ionisation aid, the ions $[M + Na]^+$ were recorded as the base peaks for both compounds at *m/z* 982 and 1014, respectively. The use of a more strongly coordinating solvent such as dme is less preferred, since this will compete with the analyte for the Na^+ ions. In fact, analysis of complex $[Mo(CO)_4P^{***}{}_2]$ in dme gave the solvated species $[M + Na(dme)]^+$ at *m/z* 1026. These preliminary results suggest that the concept of electrospray-friendly ligands should be applicable to complexes with a wide range of solvents.

2.7.2 Metal halide complexes

Previously, a study was carried out on a wide range of transition metal complexes containing halide ligands in addition to other neutral donor ligands, such as phosphines[29]. In almost all cases, loss of a halide ligand, with solvation of the resulting cation by a solvent molecule at low cone voltages provided the dominant ionisation pathway. For the complexes in this study containing MeO- or Me_2N-substituted phosphine ligands, the protonation mechanism might become competitive with halide loss. However, no $[M + H]^+$ ions were detected for any of the complexes. All spectra were dominated by the ions $[M - Cl]^+$, $[M - Cl + solv]^+$ and $[M - Cl + NH_3]^+$. Not even the complexes *cis*-$[PtCl_2P^{\bullet\bullet\bullet}{}_2]$ and $[AuClP^{\bullet\bullet\bullet}]$, which contain the ligand with the greatest number of the very basic Me_2N group, gave any ions due to protonation. Table 2.5 summarises the ESMS data for the prepared metal halide complexes. The intensities of the ions appeared to depend on the number and type of basic groups present. The observed ions were $[M - Cl]^+$, $[M - Cl + solv]^+$ and $[M - Cl + NH_3]^+$, but the major ion could be any one of them. In the platinum series, for example, $[M - Cl + solv]^+$ was the most intense ion for *cis*-$[PtCl_2P^*{}_2]$, while $[M - Cl]^+$ was the most abundant signal for

cis-[$PtCl_2P^{**}_2$], and $[M - Cl + NH_3]^+$ for *cis*-[$PtCl_2P^{•••}_2$]. For all gold compounds, the bis(phosphine)gold cation $[AuL_2]^+$ dominated both the high and low cone voltage spectra, but smaller solvated $[M - Cl + MeCN]^+$ ions were observed. This behaviour is typical for gold(I) phosphine complexes that tend to be labile in solution[34]. For the complex [$AuClP^{•••}$] the base peak was the ammonia containing ion $[M - Cl + NH_3]^+$, as was also observed for the platinum complex *cis*-[$PtCl_2P^{•••}_2$], containing the same ligand.

Dilute HCl was added in order to suppress the loss of chloride from the metal centre and to promote protonation. However, the spectra were basically unchanged, with the exception that the $[M - Cl + NH_3]^+$ ions observed in $MeCN/H_2O$ solution had disappeared. No $[M + H]^+$ ions were observed. Addition of pyridine (py) to the analyte solution resulted in the observation of the expected $[M - Cl + py]^+$ ions. This phenomenon has been observed previously[29] and it shows again that the derivatised ligands behave the same way as their PPh_3 analogues.

Table 2.5 The positive-ion ESMS data for the transition-metal halide complexes, recorded in $MeCN/H_2O$ at cV = 20 V.

Complex	Ions observed [*m/z*, relative peak height (%)]
cis-[$PtCl_2P^*_2$]	$[M - Cl + MeCN]^+$ (856, 100), $[M - Cl + NH_3]^+$ (832, 9), $[M - Cl]^+$ (815, 52)
cis-[$PtCl_2P^{**}_2$]	$[M - Cl + MeCN]^+$ (916, 99, $[M - Cl]^+$ (875, 100)
cis-[$PtCl_2P^{***}_2$]	$[M - Cl + MeCN]^+$ (976, 30), $[M - Cl + NH_3]^+$ (952, 10), $[M - Cl]^+$ (935, 100)
cis-[$PtCl_2P^{•••}_2$]	$[M - Cl + NH_3]^+$ (1030, 100), $[M - Cl]^+$ (1013, 84)
[$PdCl_2P^*_2$]	$[M - Cl + MeCN]^+$ (768, 40), $[M - Cl + NH_3]^+$ (744, 18), $[M - Cl]^+$ (727, 100)
[$PdCl_2P^{**}_2$]	$[M - Cl + MeCN]^+$ (828, 26), $[M - Cl + NH_3]^+$ (804, 13), $[M - Cl]^+$ (787, 100)
[$PdCl_2P^{***}_2$]	$[M - Cl]^+$ (847, 100)
[AuClP*]	$[AuP^*_2]^+$ (781, 100), $[M - Cl + MeCN]^+$ (530, 7)

[34] R. Colton, K. L. Harrison, Y. A. Mah and J. C Traeger, *Inorg. Chim. Acta*, 1995, **231**, 65.

[AuClP**]	$[AuP^{**}_2]^+$ (841, 100), $[M - Cl + MeCN]^+$ (560, 8)
[AuClP***]	$[AuP^{***}_2]^+$ (901, 100), $[M - Cl + MeCN]^+$ (590, 18)
[AuClP$^{\bullet\bullet\bullet}$]	$[AuP^{\bullet\bullet\bullet}_2]^+$ (979, 15), $[M - Cl + MeCN]^+$ (629, 50), $[M - Cl + NH_3]^+$ (605, 100)

2.8 Summary and conclusions

The incorporation of MeO and NMe_2 groups into the PPh_3 ligand provides a general means of facilitating the ESMS characterisation of neutral transition metal complexes. The derivatised ligands and their carbonyl complexes give strong $[M + H]^+$ peaks in the ES mass spectrum. Observed ions can be readily assigned to the intact parent ions. Fragmentation may be induced if desired. All of the prepared halide complexes follow the previously known pathway of halide loss. Thus, the use of electrospray-friendly ligands appears to offer no advantages when the complexes contain halide ligands.

A single MeO group is sufficient to allow analysis by ESMS, but greater ionisation efficiency is achieved by higher numbers of MeO groups and particularly by the use of the more basic Me_2N group. The use of these ligands may play a very useful role in transition-metal chemistry, allowing the detection of products and intermediates not previously characterised. In this respect, the ability to sample directly from reaction solutions carried out on a very small scale is a major advantage of ESMS over other methods of monitoring.

2.9 Experimental

Unless otherwise stated, all reactions were performed under a dinitrogen atmosphere using standard Schlenk techniques. The solvents CH_2Cl_2 and pet. spirits (b.p. 60 - 80°C) were distilled from calcium hydride, while tetrahydrofuran and diethylether were distilled from sodium-benzophenone. Other reagent grade solvents were used without purification.

Melting points were recorded on a Reichert Thermopan apparatus and are uncorrected. Infrared spectra were obtained in solution on a BioRad FTS-40 instrument, and elemental analyses were carried out by the Campbell Microanalytical Laboratory, University of Otago. ^1H, ^{13}C-{^1H} and ^{31}P-{^1H} NMR spectra were obtained on a Bruker AC300P spectrometer at 300.13, 75.47 and 121.5 Hz, respectively. All NMR spectra were recorded in $CDCl_3$ solution, ^1H and ^{13}C referenced to residual $CHCl_3$ and ^{31}P to an external standard of 85% H_3PO_4. The atom-labelling scheme for the ligands PPh_3 P*, P** and P*** is given in Figure 2.8. The dimethylamino ligands ($P^•$, $P^{••}$, $P^{•••}$) were numbered accordingly.

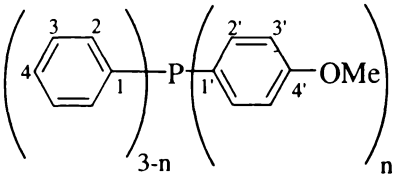

n = 1, 2, 3

Fig. 2.8 The atom-labelling scheme used in the assignment of NMR signals.

Electrospray mass spectra were obtained with a VG Platform II mass spectrometer. Samples were injected *via* a Rheodyne valve fitted with a 10 μL sample loop using a Thermo Separation products SpectraSystem P1000 LC pump at a flow rate of 0.02 mL min^{-1}. The mass spectrometer source was kept at 60°C and nitrogen was used both as a drying and nebulising gas. The skimmer cone voltage was usually 20 V and was varied up to 60 V to investigate fragmentation processes. Samples (typically 1 mg) were usually dissolved in the mobile phase (1 mL, either MeCN/H_2O or MeOH), but may also be dissolved in CH_2Cl_2 (1 drop), to which the mobile phase is added. When required, the ionisation aids pyridine (1 drop) and $Na[BPh_4]$ (1 mg) were added immediately before

sample injection. Peaks were assigned from the *m/z* values and from the isotope distribution patterns, which were simulated using the ISOTOPE program[35]. The *m/z* values given are for the most intense peak.

The compounds $PhPCl_2$, Ph_2PCl (Strem Chemicals), PCl_3 (BDH), *p* -bromoanisole and *p*-bromo-N, N-dimethylaniline (Aldrich) were used as supplied. $[Fe(CO)_5]$ and $[Ru_3(CO)_{12}]$ were purchased from Strem Chemicals, PPh_3 from BDH and $Na[BH_4]$ from Sigma.

The precursors $[Mo(CO)_4(pip)_2]$ (pip = piperidine)[36], $[PtCl_2(COD)]$ [37], $[PdCl_2(COD)]$ [38], (COD = cyclooctadiene), and $H[AuCl_4]$ [39] were prepared by literature procedures.

2.9.1 Syntheses of the phosphine ligands

The phosphine ligands P*, P** and P*** were prepared as reported by Schiemenz[40]. A general description is given for the preparation of P*. Procedures and work up were the same for all other ligands. Another method for the preparation of $P^{\bullet}$ and $P^{\bullet\bullet\bullet}$ has been reported[41].

2.9.1.1 Synthesis of $P(C_6H_5)_2(C_6H_4OCH_3)$, P*

A Grignard solution from Mg (0.61 g, 25.5 mmol) and *p*-bromoanisole (4.75 g, 3.15 mL, 25.5 mmol) in THF (40 mL) was prepared. A solution of chlorodiphenylphosphine (3.75 g, 3.13 mL, 17 mmol) in THF (40 mL) was added slowly at 0°C. The reaction mixture was refluxed for another hour, cooled to room temperature and hydrolysed with strong (*ca.* 10%) aqueous NH_4Cl solution at 0°C. The phosphine was extracted with toluene (3x100 mL) and evaporated to dryness under reduced pressure. Recrystallisation from MeOH gave P* as white crystals. Yield: 4.75 g (95%).

^{31}P NMR ($CDCl_3$): δ -6.1.

---

[35] L. J. Arnold, *J. Chem. Ed.*, 1992, **69**, 811.
[36] D. J. Darensbourg and R. L. Kump, *Inorg. Chem.*, 1978, **17**, 2680.
[37] J. X. McDermott, J. F. White and G. M. Whitesides, *J. Am. Chem. Soc.*, 1976, **98**, 6521.
[38] D. Drew and J. R. Doyle, *Inorg. Synth.*, 1972, **13**, 52.
[39] B. P. Block, *Inorg. Synth.*, 1953, **4**, 15.
[40] G. P. Schiemenz, *Liebigs Ann. Chem.*, 1971, **752**, 30.
[41] H. A. Brune, M. Falck, R. Hemmer, G. Schmidtberg, *Chem. Ber.*, 1984, **117**, 2791.

ESMS (MeOH, +ve ion, 20 V): $[M + H]^+$ *m/z* 293 (100%).

2.9.1.2 Synthesis of $P(C_6H_5)(C_6H_4OCH_3)_2$, P**

The Grignard from Mg (1.1 g, 46 mmol) and *p*-bromoanisole (8.6 g, 5.75 mL, 46 mmol) was treated with dichlorophenylphosphine (2.73 g, 2.1 mL, 15.5 mmol) and gave P** as white crystals. Yield: 4.82 g (96%).

^{31}P NMR ($CDCl_3$): δ -7.8.

ESMS (MeOH, +ve ion, 20 V): $[M + H]^+$ *m/z* 323 (100%).

2.9.1.3 Synthesis of $P(C_6H_4OCH_3)_3$, P***

The Grignard from Mg (1.55 g, 64 mmol) and *p*-bromoanisole (12 g, 8 mL, 64 mmol) was treated with freshly distilled PCl_3 (1.9 g, 2.1 mL, 14 mmol) and gave P*** as white crystals. Yield: 4.43 g (89%).

^{31}P NMR ($CDCl_3$): δ -9.3. [Lit. δ -10.1 [42]].

ESMS (MeOH, +ve ion, 20 V): $[M + H]^+$ *m/z* 353 (100%).

2.9.1.4 Synthesis of $P(C_6H_5)_2(C_6H_4N(CH_3)_2)$, P•

The Grignard from Mg (0.6 g, 24.75 mmol) and *p*-bromo-N, N-dimethylaniline (5 g, 24.75 mmol) was treated with chlorodiphenylphosphine (2.75 g, 2.3 mL, 16.5 mmol) and gave P• as white crystals. Yield: 4.2 g (84%).

^{31}P NMR ($CDCl_3$): δ -6.4.

ESMS (MeOH, +ve ion, 20 V): $[M + H]^+$ *m/z* 306 (100%).

2.9.1.5 Synthesis of $P(C_6H_5)(C_6H_4N(CH_3)_2)_2$, P••

The Grignard from Mg (1.04g, 43.2 mmol) and *p*-bromo-N, N-dimethylaniline (8.64 g, (43.2 mmol) was treated with dichlorophenylphosphine (1.95 mL, 2.53 g, 14.4 mmol) and gave P•• as white crystals. Yield: 4.4 g (80%).

^{31}P NMR ($CDCl_3$): δ -8.3.

ESMS (MeOH, +ve ion, 20 V): $[M + H]^+$ *m/z* 349 (100%).

2.9.1.6 Synthesis of $P(C_6H_4N(CH_3)_2)_3$, P•••

The Grignard from Mg (1.4 g, 57.6 mmol) and *p*-bromo-N, N-dimethylaniline (11.5 g, 57.6 mmol) was treated with freshly distilled PCl_3 (1.1 mL, 1.76 g, 12.8 mmol) and gave P••• as white crystals. Yield: 3.0 g (60%).

^{31}P NMR ($CDCl_3$): δ -10.4. [Lit. δ -11.1 [42]].

ESMS (MeOH, +ve ion, 20 V): $[M + H]^+$ *m/z* 392 (100%).

2.9.2 Syntheses of the phosphine metal complexes

Unless otherwise stated, all PPh_3 complexes were prepared by the published methods. The complexes incorporating electrospray-friendly ligands were prepared and worked up in analogous manners.

2.9.2.1 Synthesis of *cis*-$[Mo(CO)_4(PPh_3)_2]$

This complex was prepared according to the literature[36]. $[Mo(CO)_4(pip)_2]$ (0.102 g, 0.27 mmol) was partially dissolved in CH_2Cl_2 (10 mL) and PPh_3 (0.142 g, 0.54 mmol) was added as a solid. The reaction mixture was heated to reflux whereupon $[Mo(CO)_4(pip)_2]$ fully dissolved and reflux was maintained for 15 minutes. The reaction solution was allowed to cool to room temperature and the orange solution was filtered. The filtrate was reduced in volume to *ca.* 4 mL and MeOH (10 mL) was added. The solution was cooled at -20°C overnight whereupon the pale yellow product crystallised. The product was collected by filtration and dried under vacuum. Recrystallisation from CH_2Cl_2/MeOH gave *cis*-$[Mo(CO)_4(PPh_3)_2]$ as yellow crystals. Yield: 0.05 g (25%).

IR (CH_2Cl_2): ν (CO region) 2022 (s), 1926 (sh), 1908 (s), 1881 (sh) cm^{-1}. [Lit. 2023 (s), 1927 (sh), 1908 (s), 1897 (sh) cm^{-1} [36]].

^{31}P NMR ($CDCl_3$): δ 38.9.

---

[42] C. J. Cobley and P. G. Pringle, *Inorg. Chim. Acta*, 1997, **265**, 107.

^{1}H NMR ($CDCl_3$): δ 7.32 - 7.22 (30H, m, H2-4).

^{13} C-{^{1}H} NMR ($CDCl_3$): δ 136.3 (virtual t, $^{1}J_{C1,P}$ = 16.3 Hz, C1), δ 133.5 (virtual t, $^{3}J_{C3,P}$ = 6.4 Hz, C2), δ 129.5 (s, C4), δ 128.2 (virtual t, $^{2}J_{C2,P}$ = 4.5 Hz, C3).

2.9.2.2 Synthesis of *cis*-[$Mo(CO)_4P^*_2$]

[$Mo(CO)_4(pip)_2$] (0.095 g, 0.25 mmol) and P* (0.146 g, 0.5 mmol) gave *cis*-[$Mo(CO)_4P^*_2$] as yellow crystals. Yield: 0.202 g (81%).

m.p. 149 - 150°C.

Elemental analysis: C, 63.36; H, 4.25%. $C_{42}H_{34}MoO_6P_2$ requires C, 63.64; H, 4.33%.

IR (CH_2Cl_2): ν (CO region) 2021 (s), 1919 (sh), 1906 (s), 1879 (sh) cm^{-1}.

^{31}P NMR ($CDCl_3$): δ 37.1.

^{1}H NMR ($CDCl_3$): δ 7.30 - 7.22 (24H, m, H2-4, H2'), δ 6.73 (4H, d, $^{3}J_{H3',H2'}$ = 9 Hz, H3'), δ 3.8 (6H, s, $OC\underline{H}_3$).

^{13} C-{^{1}H} NMR ($CDCl_3$): δ 160.6 (s, C4'), δ 137.0 (virtual t, $^{1}J_{C1,P}$ = 16.6 Hz, C1), δ 135.4 (virtual t, $^{2}J_{C2',P}$ = 7.1 Hz, C2'), δ 133.2 (virtual t, $^{2}J_{C2,P}$ = 6.1 Hz, C2), δ 129.3 (s, C4), δ 128.4 (virtual t, $^{3}J_{C3,P}$ = 7.6 Hz, C3), δ 126.7 (virtual t, $^{1}J_{C1',P}$ = 17.7 Hz, C1'),δ 113.7 virtual t, $^{3}J_{C3',P}$ = 4.9 Hz, C3'), δ 55.2 (s, $O\underline{C}H_3$).

ESMS (MeOH, +ve ion, 20 V): $[M + H]^+$ *m/z* 795 (100%), $[M + NH_4]^+$ *m/z* 812 (20%).

2.9.2.3 Synthesis of *cis*-[$Mo(CO)_4P^{**}_2$]

[$Mo(CO)_4(pip)_2$] (0.132 g, 0.35 mmol) and P** (0.225 g, 0.7 mmol) gave *cis*-[$Mo(CO)_4P^{**}_2$] as yellow crystals. Yield: 0.261 g (87%).

m.p. 144 - 145°C.

Elemental analysis: C, 61.66; H, 4.46%. $C_{44}H_{38}MoO_8P_2$ requires C, 61.98; H, 4.50%.

IR (CH_2Cl_2): ν (CO region) 2020 (s), 1918 (sh), 1905 (s), 1876 (sh) cm^{-1}.

^{31}P NMR ($CDCl_3$): δ 35.5.

^{1}H NMR ($CDCl_3$): δ 7.26 - 7.17 (18H, m, H2-4, H2'), δ 6.73 (8H, d, $^{3}J_{H3',H2'}$ = 8.2 Hz, H3'), δ 3.78 (12H, s, OC<u>H</u>$_3$).

^{13} C-{^{1}H} NMR ($CDCl_3$): δ 215.5 (virtual t, $^{2}J_{C,P}$ = 4.6 Hz, <u>C</u>O), δ 210.6 (virtual t, $^{2}J_{C,P}$ = 4.7 Hz, <u>C</u>O), δ 160.9 (s, C4'), δ 137.6 (virtual t, $^{1}J_{C1,P}$ = 15.1 Hz, C1), δ 135.1 (virtual t, $^{2}J_{C2',P}$ = 7.2 Hz, C2'), δ 132.9 (virtual t, $^{2}J_{C2,P}$ = 6.4 Hz, C2), δ 129.1 (s, C4), δ 128.1 (virtual t, $^{3}J_{C3,P}$ = 4.6 Hz, C3), δ 127.4 (virtual t, $^{1}J_{C1',P}$ = 17.8 Hz, C1'), δ 113.7 (virtual t, $^{3}J_{C3',P}$ = 4.9 Hz, C3'), δ 55.2 (s, O<u>C</u>H$_3$).

ESMS (MeCN/H_2O, +ve ion, 20 V): $[M + H]^+$ *m/z* 855 (100%), $[M + NH_4]^+$ *m/z* 872 (4%).

2.9.2.4 Synthesis of *cis*-[Mo(CO)$_4$P***$_2$]

[Mo(CO)$_4$(pip)$_2$] (0.144 g, 0.38 mmol) and P*** (0.268 g, 0.76 mmol) gave *cis*-[Mo(CO)$_4$P***$_2$] as yellow crystals. Yield: 0.242 g (69%).

m.p. 142 - 143°C.

Elemental analysis: C, 60.08; H, 4.66%. $C_{46}H_{42}MoO_{10}P_2$ requires C, 60.53; H, 4.65%.

IR (CH_2Cl_2): ν (CO region) 2018 (s), 1917 (sh), 1904 (s), 1874 (sh) cm^{-1}.

^{31}P NMR ($CDCl_3$): δ 34.0.

^{1}H NMR ($CDCl_3$): δ 7.18 (12H, dd, $^{3}J_{H2',H3'}$ = 8.9 Hz, $^{3}J_{H2',P'}$ = 9.4 Hz, H2'), δ 6.73 (12H, d, $^{3}J_{H3',H2'}$ = 8.1 Hz, H3'), δ 3.78 (18H, s, OC<u>H</u>$_3$).

^{13} C-{^{1}H} NMR ($CDCl_3$): δ 160.4 (s, C4'), δ 134.8 (virtual t, $^{2}J_{C2',P}$ = 7.2 Hz, C2'), δ 113.6 (virtual t, $^{3}J_{C3',P}$ = 4.9 Hz, C3'), δ 55.2 (s, O<u>C</u>H$_3$).

ESMS (MeOH, +ve ion, 20 V): $[M + H]^+$ *m/z* 915 (100%).

2.9.2.5 ESMS of *cis*-[Mo(CO)$_4$P*$_2$], *cis*-[Mo(CO)$_4$P**$_2$] and *cis*-[Mo(CO)$_4$P***$_2$]

For a 1:1:1 ratio, *cis*-[Mo(CO)$_4$P*$_2$] (0.0016 g, 0.002 mmol), *cis*-[Mo(CO)$_4$P**$_2$] (0.0017

g, 0.002 mmol) and *cis*-[$Mo(CO)_4P^{***}_2$] (0.0018 g, 0.002 mmol) were dissolved in *ca.* 1 drop of CH_2Cl_2, to which MeOH (0.5 mL) was added. The mixture was subsequently analysed by ESMS.

ESMS (MeOH, +ve ion, 20 V): {*cis*-[$Mo(CO)_4P^*_2$] + H}$^+$ *m/z* 793 (24%), {*cis*-[$Mo(CO)_4P^{**}_2$] + H}$^+$ *m/z* 853 (51%), {*cis*-[$Mo(CO)_4P^{***}_2$] + H}$^+$ *m/z* 913 (100%).

2.9.2.6 Synthesis of *cis*-[$Mo(CO)_4P^{\bullet}_2$]

[$Mo(CO)_4(pip)_2$] (0.312 g, 0.825 mmol) and $P^{\bullet}$ (0.5 g, 1.65 mmol) gave *cis*-[$Mo(CO)_4P^{\bullet}_2$] as yellow crystals. Yield: 0.415 g (62%).

m.p. 142 - 148°C.

Elemental analysis: C, 64.37; H, 4.75; N, 3.37%. $C_{44}H_{40}MoN_2O_4P_2$ requires C, 64.56; H, 4.89; N, 3.42%.

IR (CH_2Cl_2): ν (CO region) 2019 (s), 1920 (sh), 1903 (s), 1875 (sh) cm^{-1}.

^{31}P NMR ($CDCl_3$): δ 36.0.

^1H NMR ($CDCl_3$): δ 7.30 - 7.18 (24H, m, H2-4, H2'), δ 6.50 (4H, d, $^3J_{H3',H2'}$ = 8.3 Hz, H3'), δ 2.94 (12H, s, $N(C\underline{H}_3)_2$).

^{13}C-{^1H} NMR ($CDCl_3$): δ 215.7 (virtual t, $^2J_{C,P}$ = 4.1 Hz, $\underline{C}O$), δ 210.7 (virtual, $^2J_{C,P}$ = 4.7 Hz, $\underline{C}O$), δ 150.9 (s, C4'), δ 137.9 (virtual t, $^1J_{C1,P}$ = 16.2 Hz, C1), δ 135.4 (virtual t, $^2J_{C2',P}$ = 7.2 Hz, C2'), δ 133.1 (virtual t, $^2J_{C2,P}$ = 6 Hz, C2), δ 128.9 (s, C4), δ 127.9 (virtual t, $^3J_{C3,P}$ = 4.2 Hz, C3), δ 120.0 (virtual t, $^1J_{C1',P}$ = 19.3 Hz, C1'),δ 111.4 (virtual t, $^3J_{C3',P}$ = 4.5 Hz, C3'), δ 40.0 (s, $N(\underline{C}H_3)_2$).

ESMS ($MeCN/H_2O$, +ve ion, 20 V): [M + H]$^+$ *m/z* 821 (100%).

2.9.2.7 Synthesis of *cis*-[$Mo(CO)_4P^{\bullet\bullet}_2$]

[$Mo(CO)_4(pip)_2$] (0.272 g, 0.72 mmol) and $P^{\bullet\bullet}$ (0.5 g, 1.44 mmol) gave *cis*-[$Mo(CO)_4P^{\bullet\bullet}_2$] as yellow crystals. Yield: 0.507 g (78%).

m.p. 166 - 167°C.

Elemental analysis: C, 62.92; H, 5.79; N, 6.20%. $C_{48}H_{50}MoN_4O_4P_2$ requires C, 63.72; H, 5.53; N, 6.20%.

IR (CH_2Cl_2): ν (CO region) 2016 (s), 1913 (sh), 1899 (s), 1872 (sh) cm^{-1}.

^{31}P NMR ($CDCl_3$): δ 33.3.

^{1}H NMR ($CDCl_3$): δ 7.26 - 7.14 (18H, m, H2-4, H2'), δ 6.51 (8H, d, $^{3}J_{H3',H2'}$ = 9 Hz, H3'), δ 2.93 (12H, s, $N(C\underline{H}_3)_2$).

^{13} C-{^{1}H} NMR ($CDCl_3$): δ 150.6 (s, C4'), δ 139.8 (s, C1), δ 135.0 (virtual t, $^{2}J_{C2',P}$ = 6.8 Hz, C2'), δ 132.8 (virtual t, $^{2}J_{C2,P}$ = 6 Hz, C2), δ 128.4 (s, C4), δ 127.7 (virtual t, $^{3}J_{C3,P}$ = 4.5 Hz, C3), δ 122.9 (s, C1'), δ 111.4 (s, C3'), δ 40.1 (s, $N(\underline{C}H_3)_2$).

ESMS (MeOH, +ve ion, 20 V): $[M + H]^+$ *m/z* 907 (100%).

2.9.2.8 Synthesis of *cis*-[$Mo(CO)_4P^{\bullet\bullet\bullet}_2$]

$[Mo(CO)_4(pip)_2]$ (0.242 g, 0.64 mmol) and $P^{\bullet\bullet\bullet}$ (0.5 g, 1.28 mmol) gave *cis*-$[Mo(CO)_4P^{\bullet\bullet\bullet}_2]$ as yellow crystals. Yield: 0.258 g (41%).

m.p. 155 - 160°C.

Elemental analysis: C, 62.93; H, 6.18; N, 8.59%. $C_{52}H_{60}MoN_6O_4P_2$ requires C, 63.04; H, 6.06; N, 8.49%.

IR (CH_2Cl_2): ν (CO region) 2013 (s), 1907 (sh), 1900 (s), 1873 (sh) cm^{-1}.

^{31}P NMR ($CDCl_3$): δ 30.8.

^{1}H NMR ($CDCl_3$): δ 7.16 (12H, dd, $^{3}J_{H2',H3'}$ = $^{3}J_{H2',P'}$ = 9.0 Hz, H2'), δ 6.52 (12H, d, $^{3}JH_{3',H2'}$ = 9 Hz, H3'), δ 2.91 (18H, s, $N(C\underline{H}_3)_2$).

^{13} C-{^{1}H} NMR ($CDCl_3$): δ 211.4 (s, $\underline{C}O$), δ 150.3 (s, C4'), δ 134.6 (virtual t, $^{2}J_{C2',P}$ = 6.8 Hz, C2'), δ 111.5 (s, C3'), δ 40.2 (s, $N(\underline{C}H_3)_2$).

ESMS (MeOH, +ve ion, 20 V): $[M + H]^+$ *m/z* 993 (100%).

2.9.2.9 ESMS of *cis*-[Mo(CO)$_4$P**$_2$] and *cis*-[Mo(CO)$_4$P••$_2$]

For a 1:1 ratio, *cis*-[Mo(CO)$_4$P**$_2$] (0.0017 g, 0.002 mmol) and *cis*-[Mo(CO)$_4$P••$_2$] (0.0018 g, 0.002 mmol) were dissolved in *ca.* 1 drop of CH_2Cl_2, to which MeOH (0.5 mL) was added. The mixture was subsequently analysed by ESMS.

ESMS (MeOH, +ve ion, 20 V): {*cis*-[Mo(CO)$_4$P**$_2$] + H}$^+$ *m/z* 854 (20%), {*cis*-[Mo(CO)$_4$P••$_2$] + H}$^+$ *m/z* 906 (100%).

2.9.2.10 Synthesis of *trans*-[Fe(CO)$_3$(PPh$_3$)$_2$]

This complex was prepared according to the literature[43]. Na[BH_4] (0.058 g, 1.53 mmol) was first paced in the reaction flask, followed by EtOH (20 mL). PPh_3 (0.42 g, 1.6 mmol) was added as a solid followed by [$Fe(CO)_5$] (0.1 ml, 0.15 g, 0.76 mmol), which was added dropwise by a syringe. The reaction was refluxed for 2 hours. After cooling to room temperature the solvent was evaporated, the complex was redissolved in CH_2Cl_2 (5 mL) and filtered into a flask containing ice-cold MeOH (10 mL). The precipitate and solution were cooled at -20°C overnight. The product was collected by filtration, washed with MeOH and dried under vacuum. Recrystallisation from CH_2Cl_2/MeOH gave *trans*-[Fe(CO)$_3$(PPh$_3$)$_2$] as yellow crystals. Yield: 0.098 g (49%).

IR (CH_2Cl_2): ν (CO region) 1884 cm^{-1}. [Lit. 1885, 1872 [43]].

^{31}P NMR ($CDCl_3$): δ 83.1. [Lit. 82.5 [43]].

^{1}H NMR ($CDCl_3$): δ 7.41 - 7.33 (30H, m, H2-4).

^{13}C-{^{1}H} NMR ($CDCl_3$): δ 136.60 (virtual t, $^1J_{C1,P}$ = 23.0 Hz, C1), δ 133.37 (virtual t, $^3J_{C3,P}$ = 4.9 Hz, C2), δ 129.92 (s, C4), δ 128.23 (virtual t, $^2J_{C2,P}$ = 4.5 Hz, C3).

2.9.2.11 Synthesis of *trans*-[Fe(CO)$_3$P*$_2$]

Na[BH_4] (0.059 g, 1.53 mmol) and [$Fe(CO)_5$] (0.1 mL, 0.149 g, 0.76 mmol) were treated with P* (0.467 g,1.6 mmol) and gave *trans*-[Fe(CO)$_3$P*$_2$] as yellow crystals. Yield: 0.078 g (39%).

---

[43] R. L. Keiter, E. A. Keiter, C. A. Boecker, D. R. Miller and K. H. Hecker, *Inorg. Synth.*, 1997, **31**, 210.

m.p. 220 - 221°C.

Elemental analysis: C, 67.16; H, 4.60%. $C_{41}H_{34}FeO_5P_2$ requires C, 67.97; H, 4.74%.

IR (CH_2Cl_2): ν (CO region) 1882 cm^{-1}.

^{31}P NMR ($CDCl_3$): δ 81.3.

^{1}H NMR ($CDCl_3$): δ 7.58 - 7.40 (24H, m, H2-4, H2'), δ 6.94 (4H, d, $^{4}J_{H3',H2'}$ = 9 Hz, H3'), δ 3.84 (6H, s, $OC\underline{H}_3$).

$^{13}C-\{^{1}H\}$ NMR ($CDCl_3$): δ 206.9 (s, $\underline{C}O$), δ 135.2 (virtual t, $^{2}J_{C2',P}$ = 6 Hz, C2'), δ 133.2 (virtual t, $^{2}J_{C2,P}$ = 5.3 Hz, C2), δ 129.7 (s, C4), δ 128.1 (virtual t, $^{3}J_{C3,P}$ = 5.3 Hz, C3), δ 113.8 (virtual t, $^{3}J_{C3',P}$ = 4.9 Hz, C3'), δ 55.2 (s, $O\underline{C}H_3$).

ESMS ($MeCN/H_2O$, +ve ion, 20 V): $[M + H]^+$ *m/z* 993 (100%).

2.9.2.12 Synthesis of *trans*-[$Fe(CO)_3P^{**}_2$]

$Na[BH_4]$ (0.058 g, 0.53 mmol) and $[Fe(CO)_5]$ (0.1 mL, 0.149 g, 0.76 mmol) were treated with P** (0.515 g, 1.6 mmol) and gave *trans*-$[Fe(CO)_3P^{**}_2]$ as yellow crystals. Yield: 0.092 g (46%).

m.p. 222 - 223°C.

Elemental analysis: C, 65.08; H, 4.82%. $C_{43}H_{38}FeO_7P_2$ requires C, 65.83; H, 4.89%.

IR (CH_2Cl_2): ν (CO region) 1880 cm^{-1}.

^{31}P NMR ($CDCl_3$): δ 79.5.

^{1}H NMR ($CDCl_3$): δ 7.56 - 7.53 and 7.39 - 7.36 (18H, m, H2', H2-4), δ 6.92 (8H, d, $^{3}J_{H3',H2'}$ = 8.3 Hz, H3'), δ 3.83 (12H, s, $OC\underline{H}_3$).

$^{13}C-\{^{1}H\}$ NMR ($CDCl_3$): δ 215.1 (virtual t, $^{2}J_{C,P}$ = 22 Hz, $\underline{C}O$), δ 160.8 (s, C4'), δ 138.1 (virtual t, $^{1}J_{C1,P}$ = 23 Hz, C1), δ 135.0 (virtual t, $^{2}J_{C2',P}$ = 6 Hz, C2'), δ 132.9 (virtual t, $^{2}J_{C2,P}$ = 5.3 Hz, C2), δ 129.6 (s, C4), δ 128.1 (virtual t, $^{3}J_{C3,P}$ = 4.6 Hz, C3), δ 113.7 (virtual t, $^{3}J_{C3',P}$ = 5.3 Hz, C3'), δ 55.3 (s, $O\underline{C}H_3$).

ESMS ($MeCN/H_2O$, +ve ion, 20 V): $[M + H]^+$ *m/z* 725 (53%), $[M + NH_4]^+$ *m/z* 742 (100%).

2.9.2.13 Synthesis of *trans*-$[Fe(CO)_3P^{***}_2]$

$Na[BH_4]$ (0.058 g, 0.53 mmol) and $[Fe(CO)_5]$ (0.1 mL, 0.149 g, 0.76 mmol) were treated with P*** (0.563 g (1.6 mmol) and gave *trans*-$[Fe(CO)_3P^{***}_2]$ as yellow crystals. Yield: 0.071 g (36%). This complex has been reported before, but was prepared by an alternative method[44].

IR (CH_2Cl_2): ν (CO region) 1874 cm^{-1}. [Lit. 1872 cm^{-1} [44]].

^{31}P NMR ($CDCl_3$): δ 77.8. [Lit. 77.5 [44]]

^1H NMR ($CDCl_3$): δ 7.51 (12H, dd, $^3J_{H2',H3'} = {}^3J_{H2',P'}$ = 9.0 Hz, H2'), δ 6.73 (12H, d, $^3JH_{3',H2'}$ = 9.0 Hz, H3'), δ 3.83 (18H, s, $OC\underline{H}_3$).

^{13}C-{^1H} NMR ($CDCl_3$): δ 160.1 (s, C4'), δ 134.9 (s, C2'), δ 129.1 (s, C1'), δ 114.2 (s, C3'), δ 55.3 (s, $O\underline{C}H_3$).

ESMS ($MeCN/H_2O$, +ve ion, 20 V): $[M + H]^+$ *m/z* 845 (100%).

2.9.2.14 Synthesis of $[Ru_3(CO)_9(PPh_3)_3]$

$[Ru_3(CO)_{12}]$ (0.083 g, 0.175 mmol) was dissolved in toluene (10 mL). PPh_3 (0.138 g, 0.525 mmol) was added as a solid. The reaction was refluxed in air for 30 minutes. Chromatography on silica plates (Merck, Silica gel 60G) with pet. spirits (b.p. 60 - 80°C)/CH_2Cl_2 (1:4) gave $[Ru_3(CO)_9(PPh_3)_3]$ as dark red crystals. Yield: 0.162 g (69%). This complex has been reported before, but was prepared by an alternative method[45].

IR (CH_2Cl_2): ν (CO region) 1979 (sh), 1970 (s) cm^{-1} [Lit. 2044 (w), 1979 (sh), 1967 (br) cm^{-1} [45]].

^{31}P NMR ($CDCl_3$): δ 38.0.

---

[44] H. Inoue, T. Takei, G. Heckmann and E. Fluck, *Z. Naturforsch., Teil B*, 1991, **46**, 682.
[45] M. I. Bruce, G. Shaw and F. G. A. Stone, *J. Chem. Soc. Dalton Trans.*, 1972, 2094; M. I. Bruce, J. G. Matison and B. K. Nicholson, *J. Organomet. Chem.*, 1983, **247**, 321.

^{1}H NMR ($CDCl_3$): δ 7.47 - 7.34 (45H, m, H2-4).

^{13} C-{^{1}H} NMR ($CDCl_3$): δ 136.1 (d, $^{1}J_{C1,P}$ = 43.0 Hz, C1), δ 133.2 (d, $^{3}J_{C3,P}$ = 11.3 Hz, C2), δ 129.6 (s, C4), δ 128.1 (d, $^{2}J_{C2,P}$ = 10.6 Hz, C3).

ESMS (MeOH, +ve ion, 20 V): $[M + H]^+$ *m/z* 1444 (100%).

2.9.2.15 Synthesis of $[Ru_3(CO)_9P^*_3]$

$[Ru_3(CO)_{12}]$ (0.061 g, 0.14 mmol) and P* (0.123 g, 0.42 mmol) gave $[Ru_3(CO)_9P^*_3]$ as dark red crystals. Yield: 0.16 g (80%).

m.p. 138 - 144°C.

Elemental analysis: C, 54.73; H, 4.03%. $C_{66}H_{51}O_{12}P_3Ru_3$ requires C, 55.35; H, 3.06%.

IR (CH_2Cl_2): ν (CO region) 2043 (w), 1979 (sh), 1967 (s) cm^{-1}.

^{31}P NMR ($CDCl_3$): δ 36.8.

^{1}H NMR ($CDCl_3$): δ 7.47 - 7.35 (36H, m, H2-4, H2'), δ 6.89 (6H, d, $^{3}J_{H3',H2'}$ = 9 Hz, H3'), δ 3.83 (9H, s, OC<u>H</u>$_3$).

^{13} C-{^{1}H} NMR ($CDCl_3$): δ 160.8 (s, C4'), δ 136.7 (d, $^{1}J_{C1,P}$ = 42.3 Hz, C1), δ 135.2 (d, $^{2}J_{C2',P}$ = 13.6 Hz, C2'), δ 133.1 (d, $^{2}J_{C2,P}$ = 11.3 Hz, C2), δ 129.5 (s, C4), δ 128.1 (d, $^{3}J_{C3,P}$ = 10.6 Hz, C3), δ 126.8 (d, $^{1}J_{C1',P}$ = 47.6 Hz, C1'),δ 113.7 (d, $^{3}J_{C3',P}$ = 11.3 Hz, C3'), δ 55.3 (s, O<u>C</u>H$_3$).

ESMS (MeOH, +ve ion, 20 V): $[M + H]^+$ *m/z* 1434 (100%).

2.9.2.16 Synthesis of $[Ru_3(CO)_9P^{**}_3]$

$[Ru_3(CO)_{12}]$ (0.086 g, 0.2 mmol) and P** (0.19 g, 0.6 mmol) gave $[Ru_3(CO)_9P^{**}_3]$ as dark red crystals. Yield: 0.218 g (73%).

m.p. 134 - 142°C.

Elemental analysis: C, 53.82; H, 3.89%. $C_{69}H_{57}O_{15}P_3Ru_3$ requires C, 54.44; H, 3.78%.

IR (CH_2Cl_2): ν (CO region) 2047 (w), 1978 (sh), 1967 (s) cm^{-1}.

^{31}P NMR ($CDCl_3$): δ 35.8.

^{1}H NMR ($CDCl_3$): δ 7.52 - 7.37 (27H, m, H2-4, H2'), δ 6.92 (8H, d, $^{3}J_{H3',H2'}$ = 8.7 Hz, H3'), δ 3.84 (18H, s, $OC\underline{H}_3$).

^{13} C-{^{1}H} NMR ($CDCl_3$): δ 160.8 (s, C4'), δ 137.3 (d, $^{1}J_{C1,P}$ = 43.0 Hz, C1), δ 135.0 (d, $^{2}J_{C2',P}$ = 12.8 Hz, C2'), δ 132.9 (d, $^{2}J_{C2,P}$ = 11.3 Hz, C2), δ 129.4 (s, C4), δ 128.1 (d, $^{3}J_{C3,P}$ = 10.6 Hz, C3), δ 127.5 (d, $^{1}J_{C1',P}$ = 47.6 Hz, C1'), δ 113.7 (d, $^{3}J_{C3',P}$ = 11.3 Hz, C3'), δ 55.3 (s, $O\underline{C}H_3$).

ESMS (MeOH, +ve ion, 20 V): $[M + H]^+$ *m/z* 1524.

2.9.2.17 Synthesis of $[Ru_3(CO)_9P^{***}_3]$

$[Ru_3(CO)_{12}]$ (0.054 g, 0.124 mmol) and P*** (0.131 g, 0.372 mmol) gave $[Ru_3(CO)_9P^{***}_3]$ as dark red crystals. Yield: 0.172 g (86%).

m.p. 118 - 120°C.

Elemental analysis: C, 53.62; H, 4.36%. $C_{72}H_{63}O_{18}P_3Ru_3$ requires C, 53.63; H, 3.95%.

IR (CH_2Cl_2): ν (CO region) 2054 (w), 1977 (sh), 1966 (s) cm^{-1}.

^{31}P NMR ($CDCl_3$): δ 34.6.

^{1}H NMR ($CDCl_3$): δ 7.36 (12H, dd, $^{3}J_{H2',H3'}$ = $^{3}J_{H2',P'}$ = 9 Hz, H2'), δ 6.87 (12H, d, $^{3}J_{H3',H2'}$ = 9.0 Hz, H3'), δ 3.82 (27H, s, $OC\underline{H}_3$).

^{13} C-{^{1}H} NMR ($CDCl_3$): δ 160.6 (s, C4'), δ 134.8 (d, $^{2}J_{C2',P}$ = 12.8 Hz, C2'), δ 128.0 (d, $^{1}J_{C1',P}$ = 12.1 Hz, C1'), δ 113.6 (d, $^{3}J_{C3',P}$ = 12.1 Hz, C3'), δ 55.3 (s, $O\underline{C}H_3$).

ESMS (MeOH, +ve ion, 20 V): $[M + H]^+$ *m/z* 1614 (100%).

2.9.2.18 Synthesis of $[Ru_3(CO)_9P^{\bullet}_2]$

$[Ru_3(CO)_{12}]$ (0.029 g, 0.066 mmol) and $P^{\bullet}$ (0.06 g, 0.2 mmol) gave $[Ru_3(CO)_9P^{\bullet}_3]$ as dark red crystals. Yield: 0.053 g (53%).

m.p. 140 - 142°C.

Elemental analysis: C, 55.65; H, 3.89%. $C_{69}H_{60}N_3O_9P_3Ru_3$ requires C, 56.32; H, 4.08%.

IR (CH_2Cl_2): ν (CO region) 2054 (w), 1977 (sh), 1965 (s) cm^{-1}.

^{31}P NMR ($CDCl_3$): δ 36.0.

^{1}H NMR ($CDCl_3$): δ 7.49 - 7.42 and 7.35 - 7.29 (36H, m, H2', H2-4), δ 6.64 (6H, dd, $^{3}J_{H3',H2'}$ = 9 Hz, $^{4}J_{H3',P'}$ = 1.5 Hz, H3'), δ 2.99 (18H, s, $N(C\underline{H}_3)_2$).

^{13} C-{^{1}H} NMR ($CDCl_3$): δ 150.1. (s, C4'), δ 137.6 (d, $^{1}J_{C1,P}$ = 43.0 Hz, C1), δ 135.1 (d, $^{2}J_{C2',P}$ = 12.8 Hz, C2'), δ 132.9 (d, $^{2}J_{C2,P}$ = 11.3 Hz, C2), δ 129.0 (s, C4), δ 127.6 (d, $^{3}J_{C3,P}$ = 9.8 Hz, C3), δ 120.2 (d, $^{1}J_{C1',P}$ = 52.1 Hz, C1'), δ 111.3 (d, $^{3}J_{C3',P}$ = 11.3 Hz, C3'), δ 40.0 (s, $N(\underline{C}H_3)_2$).

ESMS ($MeCN/H_2O$, +ve ion, 20 V): $[M + H]^+$ *m/z* 1473 (100%).

2.9.2.19 Synthesis of $[Ru_3(CO)_9P^{\bullet\bullet}_3]$

$[Ru_3(CO)_{12}]$ (0.022 g, 0.05 mmol) and $P^{\bullet\bullet}$ (0.05 g, 0.14 mmol) gave $[Ru_3(CO)_9P^{\bullet\bullet}_3]$ as dark red crystals. Yield: 0.039 g (49%).

m.p. 148 - 150°C.

Elemental analysis: C, 56.21; H, 4.86%. $C_{75}H_{75}N_6O_9P_3Ru_3$ requires C, 56.27; H, 4.69%.

IR (CH_2Cl_2): ν (CO region) 2055 (w), 1972 (sh), 1963 (s) cm^{-1}.

^{31}P NMR ($CDCl_3$): δ 34.3.

^{1}H NMR ($CDCl_3$): δ 7.49 - 7.43 and 7.36 - 7.26 (27H, m, H2-4, H2'), δ 6.63 (12H, d, $^{3}J_{H3',H2'}$ = 7.44 Hz, H3'), δ 2.97 (18H, s, $N(C\underline{H}_3)_2$).

^{13} C-{^{1}H} NMR ($CDCl_3$): δ 150.7 (s, C4'), δ 138.9 (d, $^{1}J_{C1,P}$ = 43.0 Hz, C1), δ 134.8 (d, $^{2}J_{C2',P}$ = 12.8 Hz, C2'), δ 132.8 (d, $^{2}J_{C2,P}$ = 11.3 Hz, C2), δ 128.5 (s, C4), δ 127.6 (d, $^{3}J_{C3,P}$ = 10 Hz, C3), δ 122.1 (d, $^{1}J_{C1',P}$ = 51.0 Hz, C1'), δ 111.2 (d, $^{3}J_{C3',P}$ = 11.0 Hz, C3'), δ 40.1 (s, $N(\underline{C}H_3)_2$).

ESMS ($MeCN/H_2O$, +ve ion, 20 V): $[M + H]^+$ *m/z* 1602 (100%), $[M + Na]^+$ *m/z* 1624 (29%).

2.9.2.20 Synthesis of $[Ru_3(CO)_9P^{\bullet\bullet\bullet}_3]$

$[Ru_3(CO)_{12}]$ (0.029 g, 0.066 mmol) and $P^{\bullet\bullet\bullet}$ (0.078 g, 0.2 mmol) gave $[Ru_3(CO)_9P^{\bullet\bullet\bullet}_3]$ as dark red crystals. Yield: 0.039 g (34%).

m.p. 160 - 165°C.

Elemental analysis: C, 54.71; H, 5.44%. $C_{81}H_{90}N_9O_9P_3Ru_3$ requires C, 56.24; H, 5.21%.

IR (CH_2Cl_2): ν (CO region) 2054 (w), 1970 (sh), 1959 (s) cm^{-1}.

^{31}P NMR ($CDCl_3$): δ 32.7.

^1H NMR ($CDCl_3$): δ 7.34 (18H, dd, $^3J_{H2',H3'} = {}^3J_{H2',P'} = 9.0$ Hz, H2'), δ 6.63 (18H, d, $^3J_{H3',H2'} = 7.9$ Hz, H3'), δ 2.95 (54H, s, $N(C\underline{H}_3)_2$).

$^{13}C-\{^1H\}$ NMR ($CDCl_3$): δ 150.5 (s, C4'), δ 134.5 (d, $^2J_{C2',P} = 12.4$ Hz, C2'), δ 123.8 (d, $^1J_{C1',P} = 52.6$ Hz, C1'), δ 111.2 (d, $^3J_{C3',P} = 10.9$ Hz, C3'), δ 40.2 (s, $N(\underline{C}H_3)_2$).

ESMS ($MeCN/H_2O$, +ve ion, 20 V): $[M + H]^+$ *m/z* 1731 (100%), $[M + Na]^+$ *m/z* 1753 (30%).

2.9.2.21 Synthesis of *cis*-$[PtCl_2(PPh_3)_2]$

This complex was prepared in a similar manner to the literature[42]. No efforts were made to exclude air in this reaction. PPh_3 (0.142 g, 0.54 mmol) was added to a CH_2Cl_2 solution of $[PtCl_2(COD)]$ (0.1 g, 0.27 mmol). The reaction mixture was stirred at room temperature for 10 minutes. Addition of pet. spirits (b.p. 60 - 80°C) induced precipitation. The white product was subsequently filtered and washed with Et_2O. Yield: 0.164 g (77%).

^{31}P NMR ($CDCl_3$): δ 15.1 (s, $^1J_{P,Pt} = 3673$ Hz). [Lit. δ 14.1 (s, $^1J_{P,Pt} = 3675$ Hz)[42]].

^1H NMR ($CDCl_3$): δ 7.52 - 7.45, 7.33 - 7.31 and 7.20 - 7.16 (30H, m, H2-4).

^{13}C-{^{1}H} NMR ($CDCl_3$): δ 134.9 (virtual t, $^{3}J_{C3,P}$ = 5.2 Hz, C2), δ 130.8 (s, C4), δ 127.9 (virtual t, $^{2}J_{C2,P}$ = 5.5 Hz, C3).

ESMS ($MeCN/H_2O$, +ve ion, 20 V): $[M - Cl + MeCN]^+$ *m/z* 795 (100%), $[M - Cl]^+$ *m/z* 754 (15%), $[M - Cl + NH_3]^+$ *m/z* 771 (10%).

2.9.2.22 Synthesis of *cis*-[$PtCl_2P^*_2$]

[$PtCl_2$(COD)] (0.1 g, 0.27 mmol) and P* (0.158 g, 0.54 mmol) gave *cis*-[$PtCl_2P^*_2$] as a white powder. Yield: 0.152 g (66%).

m.p. 258 - 259°C.

Elemental analysis: C, 51.52; H, 4.00%. $C_{38}H_{34}Cl_2O_2P_2Pt$ requires C, 53.65; H, 4.04%.

^{31}P NMR ($CDCl_3$): δ 13.8 (s, $^{1}J_{P,Pt}$ = 3684 Hz).

^{1}H NMR ($CDCl_3$): δ 7.49 - 7.42, 7.33 - 7.28 and 7.18 - 7.12 (24H, m, H2-4, H2'), δ 6.69 (4H, d, $^{3}J_{H3',H2'}$ = 7.2 Hz, $^{4}J_{H3',P}$ = 1.6 Hz, H3'), δ 3.79 (6H, s, $OC\underline{H}_3$).

^{13}C-{^{1}H} NMR ($CDCl_3$): δ 161.6 (s, C4'), δ 136.8 (virtual t, $^{2}J_{C2',P}$ = 5.8 Hz, C2'), δ 134.6 (virtual t, $^{2}J_{C2,P}$ = 5.2 Hz, C2), δ 130.7 (s, C4), δ 129.7 (s, C1), δ 127.9 (virtual t, $^{3}J_{C3,P}$ = 5.5 Hz, C3), δ 119.4 (s, C1'), δ 113.5 (virtual t, $^{3}J_{C3',P}$ = 6 Hz, C3'), δ 55.5 (s, $O\underline{C}H_3$).

ESMS ($MeCN/H_2O$, +ve ion, 20 V): $[M - Cl + MeCN]^+$ *m/z* 856 (100%), $[M - Cl]^+$ *m/z* 815 (52%), $[M - Cl + NH_3]^+$ *m/z* 832 (9%).

2.9.2.23 Synthesis of *cis*-[$PtCl_2P^{**}_2$]

[$PtCl_2$(COD)] (0.1 g, 0.27 mmol) and P** (0.174 g, 0.54 mmol) gave *cis*-[$PtCl_2P^{**}_2$] as a white powder. Yield: 0.198 g (81%).

m.p. 242 - 243°C.

Elemental analysis: C, 52.29; H, 4.16%. $C_{40}H_{38}Cl_2O_4P_2Pt$ requires C, 52.75; H, 4.21%.

^{31}P NMR ($CDCl_3$): δ 12.7 (s, $^{1}J_{P,Pt}$ = 3695 Hz).

^{1}H NMR ($CDCl_3$): δ 7.47 - 7.38, 7.31 - 7.25 and 7.18 - 7.12 (18H, m, H2-4, H2'), δ 6.67 (8H, d, $^3J_{H3',H2'}$ = 7.2 Hz, H3'), δ 3.78 (12H, s, OC$\underline{H}_3$).

^{13} C-{^{1}H} NMR ($CDCl_3$): δ 161.4 (s, C4'), δ 136.6 (virtual t, $^2J_{C2',P}$ = 6 Hz, C2'), δ 134.4 (virtual t, $^2J_{C2,P}$ = 5.2 Hz, C2), δ 131.3 (s, C1), δ 130.5 (s, C4), δ 127.7 (virtual t, $^3J_{C3,P}$ = 5.6 Hz, C3), δ 120.7 (virtual t, $^1J_{C1',P}$ = 35.5 Hz, C1'), δ 113.4 (virtual t, $^3J_{C3',P}$ = 6.1 Hz, C3'), δ 55.4 (s, O$\underline{C}H_3$).

ESMS (MeCN/H_2O, +ve ion, 20 V): $[M - Cl]^+$ *m/z* 875 (100%), $[M - Cl + MeCN]^+$ *m/z* 916 (99%).

2.9.2.24 Synthesis of *cis*-[$PtCl_2P^{***}_2$]

This complex was kindly supplied by W. Henderson and was prepared by the same method as the other platinum complexes. It has been reported before by a similar method[42].

^{31}P NMR ($CDCl_3$): δ 11.5 (s, $^1J_{P,Pt}$ = 3705 Hz). [Lit. δ 10.4 (s, $^1J_{P,Pt}$ = 3708 Hz)[42]].

^{1}H NMR ($CDCl_3$): δ 7.39 (12H, dd, $^3J_{H2',H3'}$ = 10.9 Hz, $^3J_{H2',P'}$ = 8.8 Hz, H2'), δ 6.67 (12H, d, $^3J_{H3',H2'}$ = 8.7 Hz, H3'), δ 3.78 (18H, s, OC$\underline{H}_3$).

^{13} C-{^{1}H} NMR ($CDCl_3$): δ 161.3 (s, C4'), δ 136.3 (virtual t, $^2J_{C2',P}$ = 6 Hz, C2'), δ 121.4 (d, $^1J_{C1',P}$ = 36.5 Hz, C1'), δ 113.3 (virtual t, $^3J_{C3',P}$ = 6.1 Hz, C3'), δ 55.3 (s, O$\underline{C}H_3$).

ESMS (MeCN/H_2O, +ve ion, 20 V): $[M - Cl]^+$ *m/z* 875 (100%), $[M - Cl + MeCN]^+$ *m/z* 916 (99%).

2.9.2.25 Synthesis of *cis*-[$PtCl_2P^{•••}_2$]

[$PtCl_2$(COD)] (0.1 g, 0.27 mmol) and $P^{•••}$ (0.211 g, 0.54 mmol) gave *cis*-[$PtCl_2P^{•••}_2$] as a white powder. Yield: 0.105 g (39%). The preparation of this complex has been reported previously[42].

^{31}P NMR ($CDCl_3$): δ 9.7 (s, $^1J_{P,Pt}$ = 3758 Hz). [Lit. δ 8.9 (s, $^1J_{P,Pt}$ = 3747 Hz)[42]].

^{1}H NMR ($CDCl_3$): δ 7.34 (18H, dd, $^{3}J_{H2',H3'}$ = 10.9 Hz, $^{3}J_{H2',P'}$ = 8.9 Hz, H2'), δ 6.40 (18H, d, $^{3}J_{H3',H2'}$ = 7.4 Hz, H3'), δ 2.92 (36H, s, $N(C\underline{H}_3)_2$).

^{13} C-{^{1}H} NMR ($CDCl_3$): δ 150.9 (s, C4'), δ 135.9 (virtual t, $^{2}J_{C2',P}$ = 5.8 Hz, C2'), δ 117.1 (d, $^{1}J_{C1',P}$ = 39 Hz, C1'), δ 110.7 (virtual t, $^{3}J_{C3',P}$ = 5.9 Hz, C3'), δ 40.1 (s, $N(\underline{C}H_3)_2$).

ESMS ($MeCN/H_2O$, 20 V): $[M - Cl + NH_3]^+$ *m/z* 1030 (100%), $[M - Cl]^+$ *m/z* 1013 (84%).

2.9.2.26 Synthesis of $[PdCl_2(PPh_3)_2]$

All palladium complexes were prepared in the same manner as their platinum analogues. $[PdCl_2(COD)]$ (0.1 g, 0.35 mmol) and PPh_3 (0.183 g, 0.7 mmol) gave $[PdCl_2(PPh_3)_2]$ as a yellow powder. Yield: 0.225 g (92%). This complex has been prepared previously[46].

^{31}P NMR ($CDCl_3$): δ 24.0. [Lit. δ 23.6 [46]].

^{1}H NMR ($CDCl_3$): δ 7.72 - 7.68 and 7.44 - 7.36 (30H, m, H2-4).

^{13} C-{^{1}H} NMR ($CDCl_3$): δ 135.1 (virtual t, $^{3}J_{C3,P}$ = 6.2 Hz, C2), δ 130.6 (s, C4), δ 128.1 (virtual t, $^{2}J_{C2,P}$ = 5.3 Hz, C3).

ESMS ($MeCN/H_2O$, +ve ion, 20 V): $[M - Cl]^+$ *m/z* 667 (100%), $[M - Cl + MeCN]^+$ *m/z* 708 (71%).

2.9.2.27 Synthesis of $[PdCl_2P^*_2]$

$[PdCl_2(COD)]$ (0.1 g, 0.35 mmol) and P* (0.204 g, 0.7 mmol) gave $[PdCl_2P^*_2]$ as a yellow powder. Yield: 0.106 g (40%).

m.p. 175 - 176°C.

Elemental analysis: C, 58.59; H, 4.50%. $C_{38}H_{34}Cl_2O_2P_2Pd$ requires C, 59.90; H, 4.51%.

^{31}P NMR ($CDCl_3$): δ 22.8.

---

[46] J. P. Farr, M. M. Olmstead and A. L. Balch, *Inorg. Chem.*, 1983, **22**, 1229.

^{1}H NMR ($CDCl_3$): δ 7.71 - 7.64 and 7.42 - 7.37 (24H, m, H2-4, H2'), δ 6.91 (4H, d, $^{3}J_{H3',H2'}$ = 6.9 Hz, H3'), δ 3.82 (6H, s, OC<u>H</u>$_3$).

^{13} C-{^{1}H} NMR ($CDCl_3$): δ 161.5 (s, C4'), δ 137.0 (virtual t, $^{2}J_{C2',P}$ = 6.9 Hz, C2'), δ 134.9 (virtual t, $^{2}J_{C2,P}$ = 6.1 Hz, C2), δ 130.4 (s, C4), δ 130.4 (virtual t, $^{1}J_{C1,P}$ = 24.6 Hz, C1), δ 128.0 (virtual t, $^{3}J_{C3,P}$ = 5.3 Hz, C3), δ 120.5 (s, C1'), δ 113.9 (virtual t, $^{3}J_{C3',P}$ = 5.9 Hz, C3'), δ 55.3 (s, O<u>C</u>H$_3$).

ESMS (MeCN/H_2O, +ve ion, 20 V): $[M - Cl]^+$ *m/z* 727 (100%), $[M - Cl + MeCN]^+$ *m/z* 768 (40%), $[M - Cl + NH_3]^+$ *m/z* 744 (18%).

2.9.2.28 Synthesis of [$PdCl_2P^{**}_2$]

[$PdCl_2$(COD)] (0.1 g, 0.35 mmol) and P** (0.225 g, 0.7 mmol) gave [$PdCl_2P^{**}_2$] as a yellow powder. Yield: 0.17 g (60%). This complex has been reported previously[47].

^{31}P NMR ($CDCl_3$): δ 21.6.

^{1}H NMR ($CDCl_3$): δ 7.68 - 7.62 and 7.44 - 7.34 (18H, m, H2-4, H2'), δ 6.90 (8H, d, $^{3}J_{H3',H2'}$ = 6.7 Hz, H3'), δ 3.82 (12H, s, OC<u>H</u>$_3$).

^{13} C-{^{1}H} NMR ($CDCl_3$): δ 161.4 (virtual t, C4'), δ 136.8 (virtual t, $^{2}J_{C2',P}$ = 5.2 Hz, C2'), δ 134.7 (virtual t, $^{2}J_{C2,P}$ = 4.5 Hz, C2), δ 131.0 (virtual t, C1), δ 130.2 (s, C4), δ 127.9 (virtual t, $^{3}J_{C3,P}$ = 3.7 Hz, C3), δ 120.9 (virtual t, $^{1}J_{C1',P}$ = 20.3 Hz, C1'), δ 113.8 (virtual t, $^{3}J_{C3',P}$ = 4.3 Hz, C3'), δ 55.3 (s, O<u>C</u>H$_3$).

ESMS (MeCN/H_2O, +ve ion, 20 V): $[M - Cl]^+$ *m/z* 787 (100%), $[M - Cl + MeCN]^+$ *m/z* 828 (99%), $[M - Cl + NH_3]^+$ *m/z* 804 (13%).

2.9.2.29 Synthesis of [$PdCl_2P^{***}_2$]

[$PdCl_2$(COD)] (0.1 g, 0.35 mmol) and P*** (0.246 g, 0.7 mmol) gave [$PdCl_2P^{***}_2$] as a yellow powder. Yield: 0.2 g (65%).

m.p. 196 - 200°C.

^{31}P NMR ($CDCl_3$): δ 20.3.

^{1}H NMR ($CDCl_3$): δ 7.64 - 7.58 (12H, m, H2'), δ 6.89 (12H, dd, $^{3}J_{H3',H2'}$ = 8.2 Hz, $^{4}J_{H3',P}$ = 0.9 Hz, H3'), δ 3.81 (27H, s, $OC\underline{H}_3$).

^{13} C-{^{1}H} NMR ($CDCl_3$): δ 161.2 (s, C4'), δ 136.4 (virtual t, $^{2}J_{C2',P}$ = 6.9 Hz, C2'), δ 121.6 (virtual t, C1'), δ 113.7 (virtual t, $^{3}J_{C3',P}$ = 5.7 Hz, C3'), δ 55.3 (s, $O\underline{C}H_3$).

ESMS ($MeCN/H_2O$, +ve ion, 20 V): $[M - Cl]^+$ *m/z* 847 (100%).

2.9.2.30 Synthesis of [AuCl(PPh_3)]

This complex was prepared in a similar manner to the literature[48]. PPh_3 (0.154 g, 0.59 mmol) was added to an EtOH solution of $H[AuCl_4]$ (0.1 g, 0.29 mmol). The reaction mixture was stirred at room temperature for 10 minutes. Addition of water induced precipitation. The solution was cooled in the fridge overnight and the white product was filtered. Yield: 0.13 g (90%).

^{31}P NMR ($CDCl_3$): δ 33.9. [Lit. 32.7 [49]].

^{1}H NMR ($CDCl_3$): δ 7.56 - 7.48 (15H, m, H2-4).

^{13} C-{^{1}H} NMR ($CDCl_3$): δ 134.2 (d, $^{3}J_{C3,P}$ = 13.5 Hz, C2), δ 132.0 (d, $^{4}J_{C4,P}$ = 1.9 Hz, C4), δ 129.3 (virtual t, $^{2}J_{C2,P}$ = 11.0 Hz, C3).

ESMS ($MeCN/H_2O$, +ve ion, 20 V): $[M - Cl + MeCN]^+$ *m/z* 500 (100%), $[M - Cl + NH_3]^+$ *m/z* 476 (15%), $[Au(PPh_2)]^+$ *m/z* 721 (12%).

2.9.2.31 Synthesis of [AuClP*]

$H[AuCl_4]$ (0.1 g, 0.29 mmol) and P* (0.172 g, 0.59 mmol) gave [AuClP*] as a white powder. Yield: 0.063 g (41%).

m.p. 153 - 154°C.

---

[47] V. K. Polonyak, V. S. Slobodina, V. V. Kormachev and N. S. Akhmetov, *Zh. Neorg. Khim.*, 1983, **28**, 168.
[48] C. A. McAuliffe, R. V. Parish and P. D. Randall, *J. Chem. Soc. Dalton Trans.*, 1979, 1730.
[49] S. Attar, W. H. Bearden, N. W. Alcock, E. C. Alyea and J. H. Nelson, *Inorg. Chem.*, 1990, **29**, 425.

Elemental analysis: C, 43.76; H, 3.10%. $C_{19}H_{17}AuClOP$ requires C, 43.49; H, 3.27%.

^{31}P NMR ($CDCl_3$): δ 32.6.

^{1}H NMR ($CDCl_3$): δ 7.53 - 7.44 (12H, m, H2-4, H2'), δ 6.97 (2H, dd, $^{3}J_{H3',H2'}$ = 8.6 Hz, $^{4}J_{H3',P}$ = 1.5 Hz, H3'), δ 3.84 (3H, s, $OC\underline{H}_3$).

$^{13}C-\{^{1}H\}$ NMR ($CDCl_3$): δ 162.7 (s, C4'), δ 136.1 (d, $^{2}J_{C2',P}$ = 15.4 Hz, C2'), δ 133.9 (d, $^{2}J_{C2,P}$ = 13.7 Hz, C2), δ 131.9 (d, $^{4}J_{C4,P}$ = 1.7 Hz, C4), δ 129.9 (s, C1), δ 129.2 (d, $^{3}J_{C3,P}$ = 11.9 Hz, C3), δ 118.9 (d, $^{1}J_{C1',P}$ = 15.4 Hz, C1'), δ 114.9 (d, $^{3}J_{C3',P}$ = 13.2 Hz, C3'), δ 55.6 (s, $O\underline{C}H_3$).

ESMS ($MeCN/H_2O$, +ve ion, 20 V): $[AuP^*_2]^+$ *m/z* 781 (100%), $[M - Cl + MeCN]^+$ *m/z* 530 (7%).

2.9.2.32 Synthesis of [AuClP]**

$H[AuCl_4]$ (0.1 g, 0.29 mmol) and P** (0.189 g, 0.59 mmol) gave [AuClP**] as a white powder. Yield: 0.074 g (45%).

m.p. 92 - 93°C.

Elemental analysis: C, 44.16; H, 3.43%. $C_{20}H_{19}AuClO_2P$ requires C, 43.43; H, 3.50%.

^{31}P NMR ($CDCl_3$): δ 31.3.

^{1}H NMR ($CDCl_3$): δ 7.49 - 7.42 (9H, m, H2-4, H2'), δ 6.96 (4H, dd, $^{3}J_{H3',H2'}$ = 8.8 Hz, $^{4}J_{H3',P}$ = 1.9 Hz, H3'), δ 3.84 (6H, s, $OC\underline{H}_3$).

$^{13}C-\{^{1}H\}$ NMR ($CDCl_3$): δ 162.5 (s, C4'), δ 135.9 (d, $^{2}J_{C2',P}$ = 15.4 Hz, C2'), δ 133.8 (d, $^{2}J_{C2,P}$ = 13.7 Hz, C2), δ 131.7 (d, $^{4}J_{C4,P}$ = 1.9 Hz, C4), δ 130.1 (d, $^{1}J_{C1,P}$ = 62.9 Hz, C1), δ 129.1 (d, $^{3}J_{C3,P}$ = 11.9 Hz, C3), δ 119.7 (d, $^{1}J_{C1',P}$ = 68.1 Hz, C1'), δ 114.9 (d, $^{3}J_{C3',P}$ = 13.1 Hz, C3'), δ 55.5 (s, $O\underline{C}H_3$).

ESMS ($MeCN/H_2O$, +ve ion, 20 V): $[AuP^{**}_2]^+$ *m/z* 841 (100%), $[M - Cl + MeCN]^+$ *m/z* 560 (8%).

2.9.2.33 Synthesis of [AuClP*]**

$H[AuCl_4]$ (0.1 g, 0.29 mmol) and P*** (0.207 g, 0.59 mmol) gave [AuClP***] as a white powder. Yield: 0.154 g (90%).

m.p. 155 - 156°C.

Elemental analysis: C, 43.59; H, 3.49%. $C_{21}H_{21}AuClO_3P$ requires C, 43.13; H, 3.63%.

^{31}P NMR ($CDCl_3$): δ 30.0.

^{1}H NMR ($CDCl_3$): δ 7.43 (6H, dd, $^{3}J_{H2',H3'}$ = 12.0 Hz, $^{3}J_{H2',P}$ = 8.3 Hz, H2'), δ 6.95 (6H, d, $^{3}J_{H3',H2'}$ = 8.2 Hz, H3'), δ 3.84 (9H, s, $OC\underline{H}_3$).

^{13} C-{^{1}H} NMR ($CDCl_3$): δ 162.4 (s, C4'), δ 135.6 (d, $^{2}J_{C2',P}$ = 15.3 Hz, C2'), δ 120.5 (d, $^{1}J_{C1',P}$ = 68.4 Hz, C1'), δ 114.8 (d, $^{3}J_{C3',P}$ = 13.1 Hz, C3'), δ 55.5 (s, $O\underline{C}H_3$).

ESMS ($MeCN/H_2O$, +ve ion, 20 V): $[AuP^{***}_2]^+$ *m/z* 901 (100%), $[M - Cl + MeCN]^+$ *m/z* 590 (18%).

2.9.2.34 Synthesis of [AuClP$^{•••}$]

$H[AuCl_4]$ (0.1 g, 0.29 mmol) and P$^{•••}$ (0.227 g, 0.58 mmol) gave [AuClP$^{•••}$] as a white powder. Yield: 0.095 g (53%). This complex has been reported previously by a different route[50].

^{31}P NMR ($CDCl_3$): δ 28.3. [Lit. δ 27.86 [50]].

^{1}H NMR ($CDCl_3$): δ 7.36 (6H, dd, $^{3}J_{H2',H3'}$ = 9.2 Hz, $^{3}J_{H2',P'}$ = 6.4 Hz, H2'), δ 6.72 (6H, d, $^{3}JH_{3',H2'}$ = 5.8 Hz, H3'), δ 2.99 (18H, s, $N(C\underline{H}_3)_2$).

^{13} C-{^{1}H} NMR ($CDCl_3$): δ 151.5 (s, C4'), δ 135.1 (d, $^{2}J_{C2',P}$ = 11.2 Hz, C2'), δ 112.3 (d, $^{3}J_{C3',P}$ = 9.4 Hz, C3'), δ 40.4 (s, $N(\underline{C}H_3)_2$).

ESMS ($MeCN/H_2O$, +ve ion, 20 V): $[M - Cl + NH_3]^+$ *m/z* 605 (100%), $[M - Cl + MeCN]^+$ *m/z* 629 (50%), $[AuP^{•••}_2]^+$ *m/z* 979 (15%).

---

[50] H. Schmidbaur, B. Brachthauser, S. Gamper, A. Schier and O. Steigelmann, *Z. Naturforsch.*, 1992, **47**, 1725.

Chapter 3
Electrospray-friendly ligands incorporating group 15 elements

The previous chapter concerned electrospray-friendly analogues of the PPh_3 ligand. There are, however, many more ligands that have the potential of being electrospray-friendly. In this chapter, ligands incorporating other group 15 elements (E) are investigated. Among them are ligands based on common phosphines, arsines and stibines. These ligands follow the concept illustrated in the previous chapter, being methoxy-functionalised analogues of well-known parent compounds. In addition, complexes of two small phosphine ligands that are 'naturally' electrospray-friendly, and which are attracting current interest in the literature, have been studied by ESMS. The third part investigates aspects of the chemistry of zerovalent platinum and palladium complexes using the mono-methoxy-functionalised ligand P*.

3.1 Ligands incorporating group 15 elements

The general chemistry of the group 15 compounds is constantly growing, however the main work has been concerned with phosphines and less with arsines, stibines and bismuthines. The same trend is observed for their coordination chemistry. Far fewer examples of transition-metal complexes with ligands of the heavier group 15 elements are known and the number of well-characterised examples drops drastically when descending the group. Several concepts have been offered to explain this phenomenon:

1. The main reason is probably that the lone pair of electrons becomes less basic when moving down the group, making the bismuthines the weakest Lewis bases (form the longest and weakest M–E bonds) and with that the poorest donor ligands. All of the ER_3 ligands are relatively soft Lewis bases. Soft Lewis bases are generally more reluctant to coordinate to metals in higher oxidation states (harder acid centres). Most of the relatively few examples of coordination compounds of the heavier group 15 ligands are therefore with larger and later transition elements.

2. The E–C bonds become weaker and are more readily cleaved for the heavier pnictogens[1]. This is also true when E is attached to the metal, sometimes resulting in C–E bond fission within the ligand[2]. As a result of 1. and 2., the stability of complexes decreases in the order $R_3P > R_3As > R_3Sb > R_3Bi$.

3. Although the three elements As, Sb and Bi possess NMR active nuclei of high abundance and relatively high sensitivity, they have the drawback of not having a spin ½ nucleus. Because of their high spin numbers and the associated quadrupole moments, the relaxation times are short and the NMR signal line-widths are broad. In contrast, ^{31}P has a spin ½ nucleus, is 100% abundant and is highly sensitive. ^{31}P NMR is a quick, routine and well-established method. The vast amount of work carried out on phosphorus chemistry is therefore not surprising.

4. Access to elements of group 15 or compounds thereof becomes more limited when descending the group. Their abundance on earth in weight-% is 0.1 (P), 1.7×10^{-4} (As), 2×10^{-5} (Sb) and 2×10^{-5} (Bi), which corresponds to a weight ratio of 5000:10:1:1 [3].

5. Arsenic compounds have found a place in the treatment of disease. After arsenicals were announced to be effective drugs for the treatment of syphilis in 1910, this research area experienced rapid growth. Although the volume of research decreased again in 1943 (arsenic-based drugs were superseded by penicillin) the overall trend was never paralleled by antimony compounds, resulting in less impetus for research.

The heavier group 15-donor ligands are prepared in a similar manner to their phosphine analogues, the preparation of which has been described in the previous chapter. There

---

[1] H.-F. Grützmacher and D. Kirchhoff, *Organometallics*, 2001, **20**, 3738.
[2] A. Mentes, R. D. W. Kemmitt, J. Fawcett and D. R. Russell, *J. Organomet. Chem.*, 1997, **528**, 59; C. T. Tay and W. K. Leong, *J. Organomet. Chem.*, 2001, **625**, 231; O. bin Shawkataly, K. Puvanesvary, H. K. Fun and K. Sivakumar, *J. Organomet. Chem.*, 1998, **565**, 267.
[3] A. F. Holleman and E. Wiberg, *Lehrbuch der Anorganischen Chemie*, 101th ed., Berlin, 1995, p.637.

are a number of textbooks available about the synthesis and chemistry of the whole group 15 ligands[4], including some specific to the heavier elements[5].

Similar to phosphines, transition-metal compounds of the heavier group 15 elements find their applications mainly as catalysts for organic reactions[6], to stabilise transition metals in high and low oxidation states[7], and can be used for the treatment of diseases[8].

3.2 Ligand design

For the same reasons as already outlined for functionalised PPh_3 analogues in the previous chapter, methoxy groups were incorporated into other ligands containing group 15 elements. Their structures are shown in Figure 3.1. Thus, *p*-MeO-substituted versions of $AsPh_3$ and $SbPh_3$ gave the ligands As*** and Sb***. P^{9*} is the ligand obtained when MeO groups are incorporated in both *meta*-and *para*-positions. This ligand differs from PPh_3 in that it is highly basic (pKa 11.02 *vs.* 2.73 for PPh_3)[9], has a larger cone angle (184° *vs.* 145° for PPh_3)[10] and (because of the presence of both O- and P-donor atoms) shows a wider range of geometries and hapticities when coordinated in metal complexes [11]. However, the nine methoxy groups should make this ligand very interesting with respect to ESMS analysis. Another widely employed phosphine ligand is dppe [bis(diphenylphosphino)ethane]. For a dppe analogue, the ligand (*p*-

---

[4] C. A. McAuliffe and W. Levason, *Phosphine, Arsine and Stibine Complexes of the Transition Elements*, Elsevier, Amsterdam, 1979; C. A. McAuliffe, Phosphorus, Arsenic and Bismuth Ligands. In G. Wilkinson (ed.), *Comprehensive Coordination Chemistry*, Vol. 2, Pergamon Press, Oxford, 1987.

[5] N. C. Norman (ed.), *Chemistry of Arsenic, Antimony and Bismuth*, Thomson Science, London, 1998; S. Patai and Z. Rappoport (eds.), *The Chemistry of Organic Arsenic, Antimony and Bismuth Compounds*, Wiley, Chichester, Sussex, 1994; G. O. Doak and L. D. Freedman, *Organometallic Compounds of Arsenic, Antimony and Bismuth*, Wiley, New York, 1970.

[6] J. C. Bailar, Jr. and H. Itatani, *J. Am. Chem. Soc.*, 1967, **89**, 1592; K. Seyferth, R. Taube, L. Bencze and L. Markó, *J. Organomet. Chem.*, 1977, **137**, 275; R. Tang, F. Mares, N. Neary and D. E. Smith, *J. Chem. Soc., Chem. Commun.*, 1979, 274.

[7] A. Downard, L. R. Hanton, D. A. McMorran and R. L. Paul, *Inorg. Chem.*, 1993, **32**, 6028; N. Bricklebank, S. M. Godfrey, C. A. McAuliffe and R. G. Pritchard, *J. Chem. Soc. Dalton Trans*, 1996, 157; D. J. Gulliver, W. Levason and K. G. Smith, *J. Chem. Soc. Dalton Trans.*, 1981, 2153.

[8] P. S. Jarrett, O. M. Ni Dhubhghaill and P. J. Sadler, *J. Chem. Soc. Dalton Trans.*, 1993, 1863; O. M. Ni Dhubhghaill and P. J. Sadler, *J. Chem. Soc. Dalton Trans.*, 1990, 2913.

[9] M. Wada and S. Higashizaki, *J. Chem. Soc., Chem. Commun.*, 1984, 482.

[10] Y. Yamamoto, R. Sato, F. Matsuo, C. Sudoh and T. Igoshi, *Inorg. Chem.*, 1996, **35**, 2329 and refs. therein.

[11] L.-J. Baker, G. A. Bowmaker, D. Camp, Effendy, P. C. Healy, H. Schmidbaur, O. Steigelmann and A. H. White, *Inorg. Chem.*, 1992, **31**, 3656; K. R. Dunbar, J.-S. Sun, S. C. Haefner and J. H. Matonic, *Organometallics*, 1994, **13**, 2713; K. R. Dunbar, J. H. Matonic and V. P. Saharan, *Inorg. Chem.*, 1994, **33**, 25; K. R. Dunbar, S. C. Haefner and D. J. Burzynski, *Organometallics*, 1990, **9**, 1347.

$MeOC_6H_4)_2PCH_2CH_2P(C_6H_4OMe\text{-}p)_2$, dppe****, was considered. Derivatised ligands with one, two or three *p*-$MeOC_6H_4$ groups would not have the same symmetry as dppe itself, and would lead to mixtures of isomers when metal complexes are prepared. Except for P^{9*}, only the *para*-isomers were desired, as the derivatised ligands should to be chemically and sterically most similar to the parent ligands.

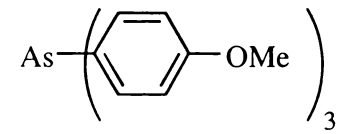

As***

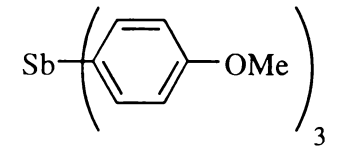

Sb***

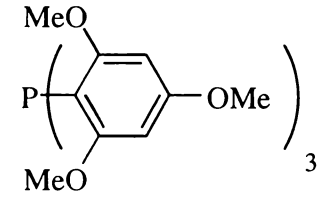

P^{9*}

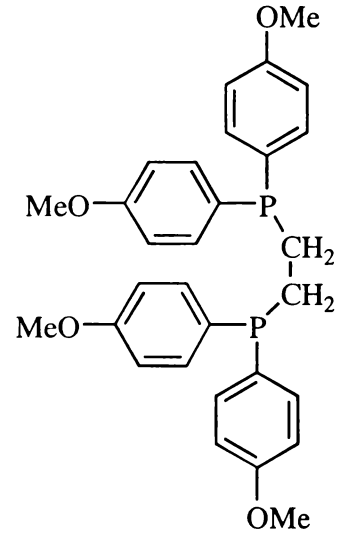

dppe****

Fig. 3.1 The structures of some electrospray-friendly ligands of group 15.

When utilising these electrospray-friendly ligands in the mass spectral analysis of transition-metal complexes, the same advantages as for the ligand derivatives of PPh_3 arise. Moreover, since the chemistry of the heavier group 15 elements has not been

studied to the same extent as that of phosphorus, the technique of electrospray will be valued even more as it provides more insight into their chemistry. Furthermore, because arsenic and antimony, unlike phosphorus, do not have a nucleus readily accessible by NMR spectroscopy, a new technique that allows the characterisation of arsine and stibine complexes will be very welcome.

3.3 Ligand synthesis

As*** and Sb*** were prepared in a similar manner to the phosphine analogues, *i.e.* from the Grignard reagent $MeOC_6H_4MgBr$ with $AsCl_3$ and $SbCl_3$, respectively. P[9*] was kindly provided by Prof. G. A. Bowmaker, University of Auckland. Several attempts to prepare dppe**** were unsuccessful and further attempts were stopped when a Dutch research group kindly supplied a number of methoxy-substituted diphosphines. Dppe**** could not be synthesised by following the same route as for dppe[12]. Dppe itself can be prepared from lithium and dichloroethane, according to:

$$PPh_3 + 2\ Li \rightarrow Ph_2PLi + PhLi$$

$$Ph_2PLi + ClCH_2CH_2Cl \rightarrow Ph_2PCH_2CH_2PPh_2$$

However, when using P*** instead of PPh_3, the intermediate $(MeOC_6H_4)_2PLi$ did not form (detection by red colouration). Possibly, cleavage at the methoxy group instead of at the P–Ph bond occurs. Another option was to prepare dppe**** analogous to the synthesis of P***, namely by the reaction of a Grignard reagent ($MeOC_6H_4MgBr$) and the appropriate phosphine halide ($Cl_2PCH_2CH_2PCl_2$). The halide can either be purchased (though relatively expensive) or prepared from dppe, $AlCl_3$ and PCl_3[13]. However, the preparation was found to be relatively tedious and (according to the literature) only yields very small amounts of the halide compared to the amount of starting material used[14]. In a study by Bouwman *et al.*[15], nickel complexes of various derivatives of dppe and $Ph_2P(CH_2)_3PPh_2$ (dppp) and various methoxy derivatives thereof had been used to

---

[12] P. Veya, *Organometallics,* 1993, **12**, 4365.
[13] K. Sommer, *Zeitschr. Anorg. Allg. Chem.*, 1970, **370**, 37.
[14] 1 g of dppe gives 0.3 mL of $Cl_2PCH_2CH_2PCl_2$, which still has to be distilled.
[15] I. M. Angulo, A. M. Kluwer and E. Bouwman, *Chem. Commun.*, 1998, 2689; I. M. Angulo, E. Bouwman, M. Lutz, W. P. Mul and A. L. Spek, *Inorg. Chem.*, 2001, **40**, 2073.

investigate their influence as catalysts in the hydrogenation reaction of oct-1-ene to *n*-octane. Interestingly, most methoxy-derivatives proved to have a very high catalytic activity, while their dppe and dppp analogues did not have any influence on the reaction. Table 3.1 shows the ligands that were used in this study and small amounts thereof were made available for an ESMS study.

Table 3.1 The structures of the methoxy-derivatised diphosphine ligands $R_2P(CH_2)_nPR_2$.

ligand	R	n
o-MeO-dppe	*o*-$MeOC_6H_4$	2
o-MeO-dppp	*o*-$MeOC_6H_4$	3
m-MeO-dppe	*m*-$MeOC_6H_4$	2
m-MeO-dppp	*m*-$MeOC_6H_4$	3
p-MeO-dppp	*p*-$MeOC_6H_4$	3

3.4 ESMS of the ligands

The relative basicity of the group 15 ligands can easily be studied by ESMS by comparing their relative signal intensities for the $[M + H]^+$ ions. Because of their lone pair of electrons, this experiment could be carried out on the free ligands PPh_3, $AsPh_3$ and $SbPh_3$. In fact, when using the ligands P***, As*** and Sb***, the site for protonation is not limited to the lone pair and the signal intensity will therefore not represent the basicity of the ligand. The spectrum of an equimolar mixture of the three ligands PPh_3, $AsPh_3$ and $SbPh_3$ is shown in Figure 3.2.

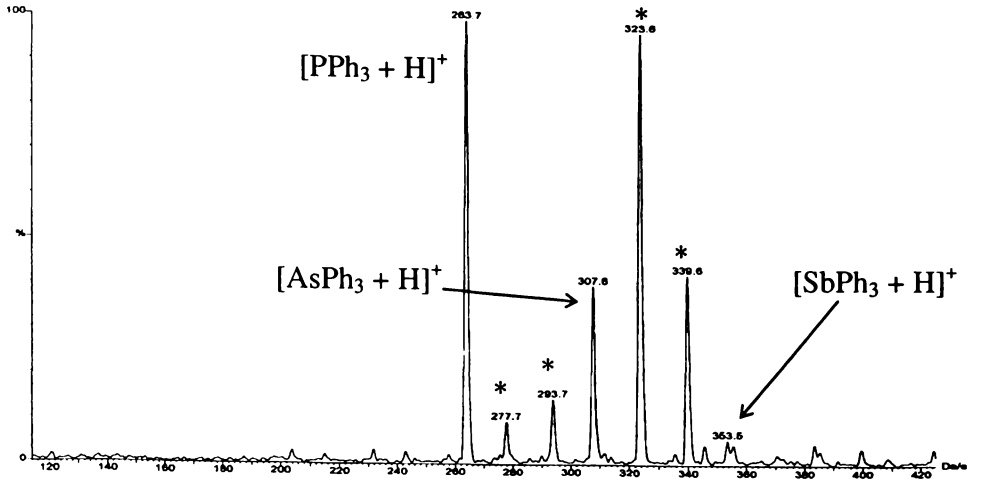

Fig. 3.2 The positive-ion ES mass spectrum of an equimolar mixture of PPh_3, $AsPh_3$ and $SbPh_3$, recorded in MeOH at cV = 20 V (signals arising from impurities are indicated by an asterisk).

The basicity of the ligands decreases in the order $PPh_3 > AsPh_3 > SbPh_3$. Accordingly, their signal intensities decreased in the ratio 100:40:5. A similar trend of decreasing basicity has been reported before towards silver(I) ions[16]. These values should however only be taken as an overall trend, since the phosphine and arsine seemed to generate other ions as well. Both PPh_3 and $AsPh_3$ signals were accompanied by $[M + 16 + H]^+$ and $[M + 32 + H]^+$ peaks. Decomposition through oxidation processes clearly leads to triphenylphosphine oxide (and similarly to triphenylarsine oxide), which will be significantly more susceptible to protonation than PPh_3 and will therefore give a strong signal even if it is only present in trace amounts. The second peak might be associated with either the corresponding sulfide or a peroxide species, which is believed to be formed as an intermediate in the oxidation reaction[17].

Antimony, unlike phosphorus and arsenic, has the two isotopes ^{121}Sb and ^{123}Sb with 57.3 and 42.7% abundance, respectively. The high-resolution isotope pattern of $SbPh_3$ therefore differs from that of PPh_3 and $AsPh_3$. Figure 3.3 shows the calculated isotope patterns of the three ligands as their $[M + H]^+$ ions. This is a major advantage when analysing mixtures of different ligands, as stibine fragments can readily be detected even

[16] L. S. Bonnington, R. K. Coll, E. J. Gray, J. I. Flett and W. Henderson, *Inorg. Chim. Acta*, 1999, **290**, 213.

at a resolution used to acquire large parts of the spectrum[18]. This is shown in the spectrum displayed in Figure 3.2, where the ion assigned to $[SbPh_3 + H]^+$ gave rise to two peaks being two mass units apart.

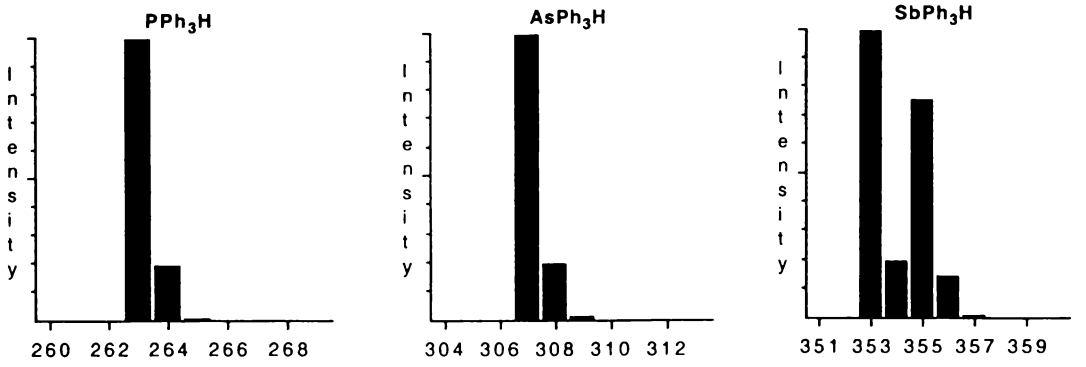

Fig. 3.3 The calculated isotope patterns of PPh_3, $AsPh_3$ and $SbPh_3$ as their $[M + H]^+$ ions.

While the electrospray-friendly ligands based on PPh_3 had all given strong $[M + H]^+$ signals (refer to previous chapter), the methoxy-substituted arsine, As***, and stibine, Sb***, did not show the $[M + H]^+$ ion as the dominating species in their spectra. This was surprising as they both have three MeO groups. In the case of the arsine, although the ^1H NMR showed only traces of the oxide as an impurity, the $[M + H]^+$ ion of the oxide, $[OAs*** + H]^+$, clearly dominated the spectrum, with the $[As*** + H]^+$ peak at only 9% with respect to the oxide at 100%. This phenomenon was even more obvious with the stibine, where no $[Sb*** + H]^+$ ion could be detected. Identical results were obtained when adding a small amount of acid, which normally enhances protonation. The only ions present were $[OSb*** + H]^+$, $[OSb*** + NH_4]^+$ and an $[Sb*** + 44]^+$ {or $[OSb*** + 28]^+$} ion, which was unable to be assigned. Other methods of characterisation (elemental analysis, NMR) suggested high purity for both ligands. If oxides are present, they generally protonate very easily and their peaks in the ESMS are therefore very intense. However, it was still surprising that the $[Sb*** + H]^+$ was not observed at all, because even with the presence of impurities, the MeO groups of the ligand should still give rise to its $[M + H]^+$ ion. A method of ionising arsines for their

[17] Z. B. Alfassi, P. Neta and B. Beaver, *J. Phys. Chem. A*, 1997, **101**, 2153.
[18] The resolution generally used for acquiring large parts of the spectrum is between 12-13, while a typical resolution for recording isotope patterns is 17 (arbitrary units).

ESMS analysis has been developed[19] and is based on the addition of Ag^+ ions. When employing this method to the derivatised ligands, signals attributable to the solvated [M + Ag + MeCN]$^+$ ions as well as [2M + Ag]$^+$, [3M + Ag]$^+$ and [4M + Ag]$^+$ (M = As***, Sb***) were identified. No [M + Ag]$^+$ ions were detected. These results are consistent with previous reports[16] and reflect the weak donor-ligand abilities and long metal–E bonds for arsines and stibines as compared to phosphines[20]. The observed ions are summarised in Table 3.2.

Table 3.2 The positive-ion ESMS data for As*** and Sb***, recorded in MeCN/H_2O, at cV = 20 V.

Ligand	Ions observed [*m/z*, relative peak height (%)]
As***	[M + H]$^+$ (397, 9), [OM + H]$^+$ (413, 100)
Sb***	[OM + H]$^+$ (459, 100), [OM + NH_4]$^+$ (478, 28), unidentified (487, 88)
As***/Ag[BF_4]	[M + Ag + MeCN]$^+$ (544, 100), [2M + Ag]$^+$ (899, 8), [3M + Ag]$^+$ (1296, 2), [4M + Ag]$^+$ (1693, 10)
Sb***/Ag[BF_4]	[M + Ag + MeCN]$^+$ (592, 100), [2M + Ag]$^+$ (993, 8), [3M + Ag]$^+$ (1437, 8), [4M + Ag]$^+$ (1880, 20)

The ligand P^{9*} gave a very strong [M + H]$^+$ signal at low cone voltages as one would expect with the large number of basic sites available. Multiple protonation to give ions of the type [M + nH]$^+$ was not observed and neither was aggregation to give [nM + H]$^+$ ions. A weak signal at *m/z* 1173 was detected, possibly corresponding to the formation of [2M + Ag]$^+$ [from silver(I) ions lingering in the system]. This was confirmed by addition of a drop of $AgNO_3$ solution, whereupon the signal increased in intensity. The fact that [2M + Ag]$^+$ formed but not [2M + H]$^+$ might be caused by the steric bulk of the ligand leading to a preference for larger cations. The same explanation applies for the absence of any [3M + Ag]$^+$ or [4M + Ag]$^+$ ions. When adding an excess of $AgNO_3$, several further peaks appeared. Among them were the [M + Ag]$^+$ ion, and the oxidation products [OM + H]$^+$ and [O_2M + H]$^+$. Analogous species had been observed when

[19] M. G. Fitzpatrick, L. R. Hanton, W. Henderson, P. E. Kneebone, E. G. Levy, L. J. McCaffrey and D. A. McMorran, *Inorg. Chim. Acta*, 1998, **281**, 101.
[20] PPh_3 gave an [M + Ag]$^+$, [2M + Ag]$^+$, a very weak [3M + Ag]$^+$ and no [4M + Ag]$^+$ ion.

analysing the ligands PPh_3, $AsPh_3$ and $SbPh_3$. Because of the addition of NO_3^- ions, oxidation seems more likely than sulfide formation. The intermediate peroxide species could be trapped by the steric bulk of the ligand allowing detection by ESMS.

When increasing the cone voltage to 60 V, no fragmentation occurred. Successive loss of methyl groups as well as loss of entire phenyl rings was observed at 100V. The need for a voltage this high is surprising as elimination of a methyl group is often observed in the reaction with transition-metal complexes, giving rise to dihapto (η^2-P,O) [21] and trihapto (η^3-P,O,O) [22] bonding modes. A summary of all observed ions is given in Table 3.3.

Table 3.3 The positive-ion ESMS data for P^{9*}, recorded in $MeCN/H_2O$ at cV = 20 V.

Salts added	cV (V)	Ions observed [*m/z*, relative peak height (%)]
–	20	$[M + H]^+$ (533, 100), $[2M + Ag]^+$ (1272, 2)
1 drop $AgNO_3$	20	$[M + H]^+$ (533, 100), $[2M + Ag]^+$ (1273, 12)
xs $AgNO_3$	20	$[M + H]^+$ (533, 100), $[2M + Ag]^+$ (1272, 100), $[OM + H]^+$ (549, 4), $[O_2M + H]^+$ (565, 10)
–	60	$[M + H]^+$ (533, 100), $[2M + Ag]^+$ (1272, 2)
–	100	$[M + H]^+$ (533, 100), $[2M + Ag]^+$ (1272, 8), $[M - CH_3 + H]^+$ (517, 2), $[M - 2CH_3 + H]^+$ (501, 2), $[M - 3CH_3 + H]^+$ (487, 5), $[M - 4CH_3 + H]^+$ (472, 2), $[M - 5CH_3 + H]^+$ (457, 2), $[M - C_6H_2(OCH_3)_3 + H]^+$ (365, 10), $[M - C_6H_2(OCH_3)_3 - CH_3 + H]^+$ (350, 4), $[M - C_6H_2(OCH_3)_3 - 2\ CH_3 + H]^+$ (335, 4), $[M - C_6H_2(OCH_3)_3 - 3\ CH_3 + H]^+$ (319, 5), $[M - C_6H_2(OCH_3)_3 - 4\ CH_3 + H]^+$ (306, 4), $[M - 2C_6H_2(OCH_3)_3 + H]^+$ (197, 10), $[M - 2C_6H_2(OCH_3)_3 - CH_3 + H]^+$ (181, 22), $[M - 2C_6H_2(OCH_3)_3 - 3\ CH_3 + H]^+$ (167, 4)

The diphosphines (listed in Table 3.1) all yielded the expected $[M + H]^+$ ions. Furthermore, aggregation of ions, such as $[2M + H]^+$, $[2M + Ag]^+$ and $[2M + Au]^+$ was observed attributed to trace amounts of the metals in the system. The high affinity of

[21] K. R. Dunbar and A. Quillevéré, *Organometallics*, 1993, **12**, 618.
[22] K. R. Dunbar, S. C. Haefner and L. E. Pence, *J. Am. Chem. Soc.*, 1989, **111**, 5504.

phosphine ligands to silver(I) and gold(I) ions in ESMS analysis has been reported[23], and aggregation readily occurs with bidentate ligands as they are better coordinating than analogous monodentate ligands. Another observed ion was $[P^{***} + H]^+$, presumably from traces of impurity caused by either the decomposition of P^{9*} or remaining starting material. Overall, the ions were very intense and the spectra clean with the exception of *m*-MeO-dppe and *m*-MeO-dppp, which failed to give readily assignable spectra. Unlike the other diphosphines, they were found to be almost insoluble in organic solvents. Table 3.4 gives the ESMS data for the derivatised ligands.

Table 3.4 The positive-ion ESMS data for the diphosphine ligands, recorded in MeOH at cV = 20 V.

Ligand	Ions observed [*m/z*, relative peak height (%)]
o-MeO-dppe	$[M + H]^+$ (519, 100), $[2M + H]^+$ (1037, 8), $[2M + Ag]^+$ (1144, 38), $[2M + Au]^+$ (1233, 6),
o-MeO-dppp	$[P^{***} + H]^+$ (353, 24), $[M + H]^+$ (533, 90), $[2M + Ag]^+$ (1172, 100), $[2M + Au]^+$ (1261, 8),
p-MeO-dppp	$[P^{***} + H]^+$ (353, 22), $[M + H]^+$ (533, 100), $[2M + Ag]^+$ (1172, 7), $[2M + Au]^+$ (1261, 19),

3.5 Synthesis and characterisation of the metal complexes

Several metal complexes were prepared in order to investigate whether the electrospray-friendly versions of the ligands discussed above protonate when coordinated. The metal complexes were prepared following similar procedures as for the phosphine analogues described in the previous chapter. In an attempt to prepare $[Fe(CO)_3As^{***}_2]$, the mono-substituted complex $[Fe(CO)_4As^{***}]$ was obtained upon recrystallisation, so its triphenylarsine analogue $[Fe(CO)_4(AsPh_3)]$ was prepared as well and the characterisation data are reported for these complexes only. For the stibines, the syntheses were carried out in higher boiling point solvents because no reaction took place when using CH_2Cl_2. This stands in agreement with the fact that ligands of the heavier group 15 elements are generally poorer ligands. Since it had been determined

[23] A. J. Canty and R. Colton, *Inorg. Chim. Acta*, 1994, **220**, 99; W. Henderson and G. M. Olsen, *Polyhedron*, 1998, **17**, 577; W. Henderson and G. M. Olsen, *Polyhedron*, 1996, **15**, 2105.

that transition-metal halides do not follow the protonation-type ionisation pathway (refer to Chapter two), only metal carbonyl complexes were prepared.

The metal complexes synthesised with the standard as well as derivatised ligands are listed in Table 3.5, together with their IR data. Regarding the CO stretching bands, there was a general shift towards lower wave numbers with incorporation of MeO groups. This trend has been observed before for phosphine complexes in the previous chapter. The incorporation of the electron-donating MeO group yields a slightly more electron-rich ligand, resulting in increased back donation toward the CO ligands and therefore weaker C≡O bonds. However, the shifts to lower wave numbers were only small, indicating an overall similarity of electronic properties of the complexes with derivatised ligands.

Table 3.5 The IR data for the prepared complexes.

Complex	IR ν_{CO} (cm^{-1})
$[Mo(CO)_4(AsPh_3)_2]$	2025(s), 1921(sh), 1913s, 1881(sh)
$[Mo(CO)_4As^{***}{}_2]$	2022(s), 1919(sh), 1909s, 1876(sh)
$[Mo(CO)_4(SbPh_3)_2]$	2024(s), 1952(sh), 1931s, 1917s, 1894(sh)
$[Mo(CO)_4Sb^{***}{}_2]$	2022(s), 1948(sh), 1928s, 1913s, 1891(sh)
$[Fe(CO)_4(AsPh_3)]$	2049(s), 1972(sh), 1940s
$[Fe(CO)_4As^{***}]$	2047(s), 1970(sh), 1938s
$[Fe(CO)_4(SbPh_3)]$	2046(s), 1972(sh), 1940s
$[Fe(CO)_4Sb^{***}]$	2045(s), 1970(sh), 1934s
$[Mo(CO)_4(o\text{-MeO-dppe})]$	
$[Mo(CO)_4(p\text{-MeO-dppp})]$	

The complexes $[Mo(CO)_4(o\text{-MeO-dppe})]$ and $[Mo(CO)_4(p\text{-MeO-dppp})]$ were only prepared on a very small scale for ESMS analyses. They were not isolated and therefore no characterisation data other than ESMS were obtained.

As opposed to the phosphine complexes discussed in Chapter two, NMR data for the arsine and stibine complexes were limited to ^{1}H and ^{13}C signals. Figures 3.5 and 3.6 show the ^{1}H and ^{13}C NMR of the complex $[Fe(CO)_4(AsPh_3)]$ and its methoxy analogue [Fe(CO)$_4$As***]. The NMR data are listed in Table 3.6 according to the NMR numbering scheme given in Figure 3.4. When comparing the ^{1}H NMR spectrum of the $[Fe(CO)_4(AsPh_3)]$ with its methoxy derivative, the latter is more informative and can be more readily assigned, as the signals attributed to the protons on the phenyl rings are resolved. While the $AsPh_3$ complex only shows a broad multiplet for all protons at the phenyl rings, the As*** complex gives two doublets assigned to the protons at C2' and C3' plus a further singlet for the protons of the methoxy group. Compared to complexes of P***, which showed additional coupling of the protons of C2' to the phosphorus nucleus, there is no further coupling in the arsines and stibines and so clean doublets are observed.

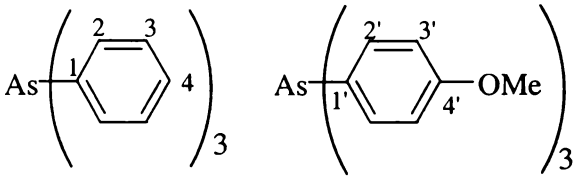

Fig. 3.4 The NMR numbering scheme for the ligands $AsPh_3$ and As***.

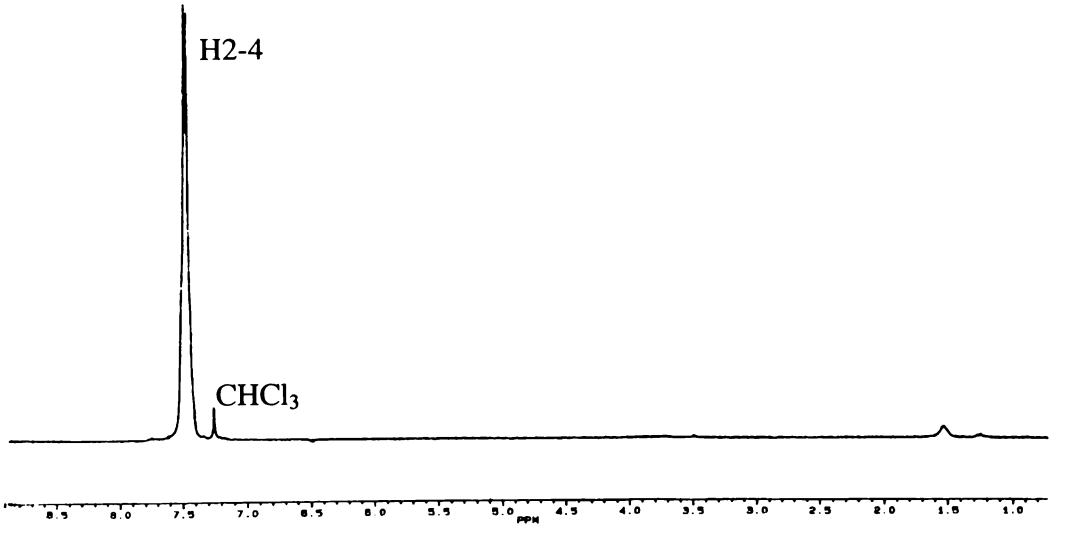

Fig. 3.5a The ^{1}H NMR spectrum of $[Fe(CO)_4(AsPh_3)]$, recorded in $CDCl_3$.

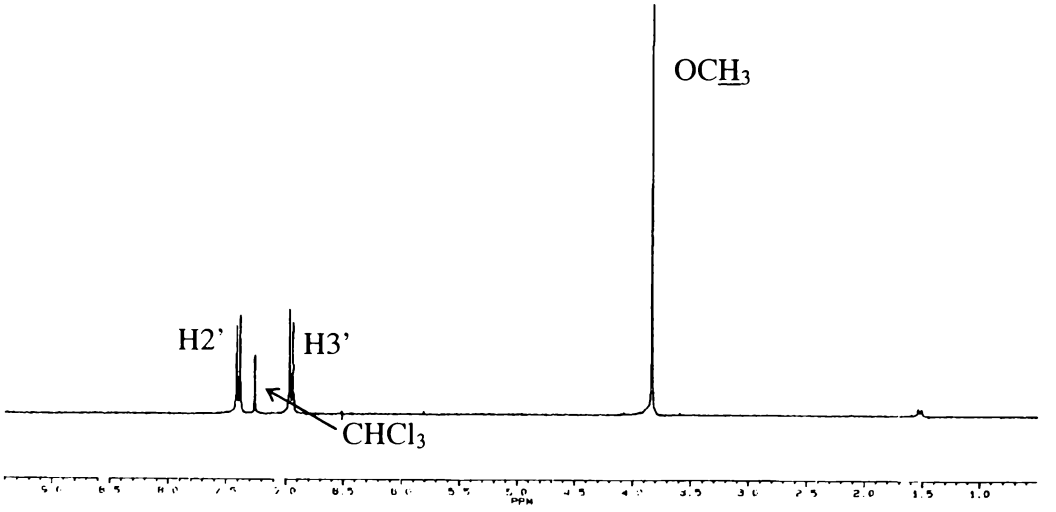

Fig. 3.5b The ^{1}H NMR spectrum of [$Fe(CO)_4As^{***}$], recorded in $CDCl_3$.

Although the arsine and stibine complexes are not amenable to ^{31}P NMR, the effects of incorporating methoxy groups into the ligands can be deduced from their carbon NMR spectra. The ^{13}C NMR spectrum of the methoxy derivative indicated that the environments of the carbon atoms of the phenyl rings were not as similar as they are for the $AsPh_3$ complex. The signals covered a wider chemical shift ranging from 161.4 ppm for C4' to 114.6 ppm for C3', whereas all 4 signals for the $AsPh_3$ carbons were between 134.7 and 129.2 ppm. The carbon atom with the greatest shift was at the site where the methoxy group is attached and showed a shift of 30.7 ppm when going from C4 to C4'. There seemed to be little difference in the environments of the CO ligands with signals occurring at 213.3 ppm for [$Fe(CO)_4(AsPh_3)$] and at 213.5 ppm for [$Fe(CO)_4As^{***}$]. This stands in agreement with the small shift in wave numbers for the CO stretches observed in the IR spectrum.

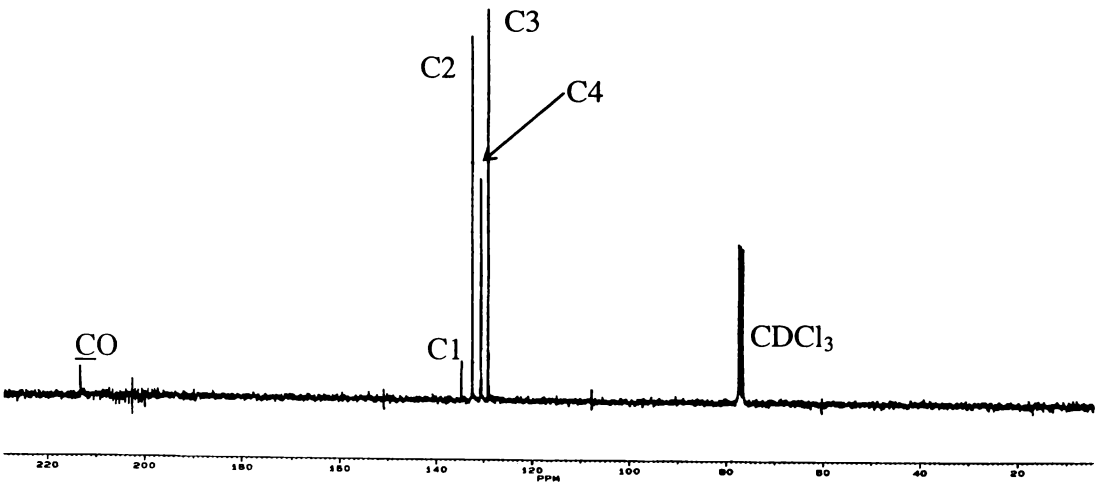

Fig. 3.6a The ^{13}C NMR spectrum of $[Fe(CO)_4(AsPh_3)]$, recorded in $CDCl_3$.

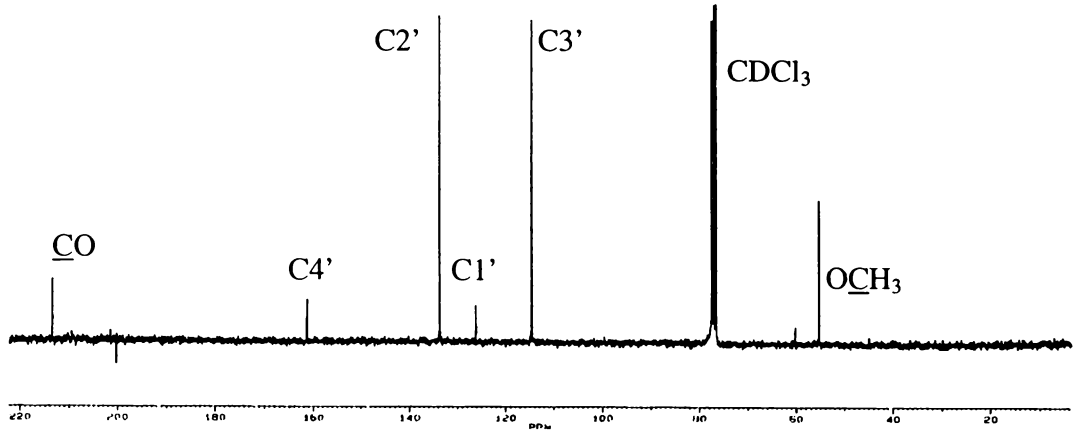

Fig. 3.6b The ^{13}C NMR spectrum of $[Fe(CO)_4As^{***}]$, recorded in $CDCl_3$.

Table 3.6 The NMR data for $[Fe(CO)_4(AsPh_3)]$ and $[Fe(CO)_4As^{***}]$, recorded in $CDCl_3$.

	$Fe(CO)_4(AsPh_3)$	$Fe(CO)_4As^{***}$
^1H NMR	δ 7.55 – 7.35 (15H, m, H2,3,4)	δ 7.40 (6H, d, H2', $^3J_{H2',H3'}$ = 9 Hz) δ 6.96 (6H, d, H3', $^3J_{H3',H2'}$ = 9 Hz) δ 3.83 (9H, s, $OC\underline{H}_3$)
^{13}C NMR	δ 213.3 (s, CO) δ 130.7 (s, C4) δ 129.2 (s, C3) δ 134.7 (s, C1) δ 132.5 (s, C2)	δ 213.5 (s, CO) δ 161.4 (s, C4') δ 133.8 (s, C2') δ 126.2 (s, C1') δ 114.6 (s, C3') δ 55.4 (s, $O\underline{C}H_3$)

3.6 ESMS of the metal complexes

Unlike the methoxy-functionalised arsine and stibine ligands above, the metal complexes provided intense $[M + H]^+$ signals. The complexes incorporating ligands without a methoxy group were not observed in the ESMS. The loss of the CO ligand may be deliberately induced by increasing the cone voltage. This can be seen for the compounds $[Mo(CO)_4As***_2]$ and $[Fe(CO)_4As***]$, as listed in Table 3.7.

Table 3.7 The positive-ion ESMS data for the transition-metal complexes incorporating electrospray-friendly ligands, recorded in either $MeCN/H_2O$ [(a)] or MeOH [(b)] solution.

Complex	cV	Ions observed [*m/z*, relative peak height (%)]
$[Mo(CO)_4As***_2]$ [(a)]	20	$[M + H]^+$ (1002, 100)
	60	$[M + H]^+$ (1002, 15), $[M + H - CO]^+$ (975, 10), $[M + H - 3CO]^+$ (915, 100)
$[Fe(CO)_4As***]$ [(a)]	20	$[M + H]^+$ (565,100)
	40	$[M + H]^+$ (565, 135), $[M + H - CO]^+$ (538, 100), $[M + H - 4CO]^+$ (453, 11)
$[Mo(CO)_4Sb***_2]$ [(b)]	20	$[M + H]^+$ (1096, 100), $[M + NH_4]^+$ (1114, 12), $[M + pip + H]^+$ (1180, 98) [24], $[2M + NH_4]^+$ (2208, 32)
$[Fe(CO)_4Sb***]$ [(b)]	20	$[M + H]^+$ (611, 100)
$[Mo(CO)_4(o\text{-MeO-dppe})]$ [(b)]	20	$[M + H]^+$ (727, 100)
$[Mo(CO)_4(p\text{-MeO-dppp})]$ [(b)]	20	$[M + H]^+$ (741, 100)

The crude product from the attempted synthesis of $[Fe(CO)_3As***_2]$ was found by ESMS to be a mixture of this complex together with the mono-substituted complex $[Fe(CO)_4As***]$, demonstrating the usefulness of the technique in determining product formation in such ligand substitution reactions. Figure 3.7a shows the ES spectrum of the crude reaction solution. The dominating ion was clearly the mono-substituted complex at *m/z* 565. Other ions present in the crude reaction mixture were the unreacted

[24] pip = piperidine {the complex was prepared from $[Mo(CO)_4(pip)_2]$}.

ligand As*** and its oxide. The di-substituted complex had only an intensity of 5%, but when expanding this region (refer to Figure 3.7b), this peak could readily be assigned to $[Fe(CO)_3As^{***}_2 + H]^+$ at *m/z* 932.

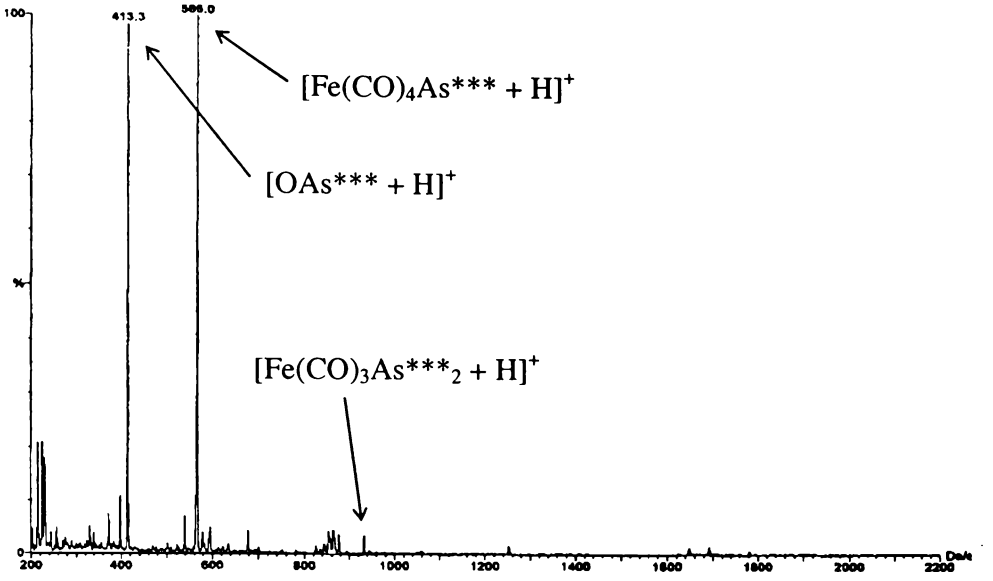

Fig. 3.7a The positive-ion ES mass spectrum of the crude products in the reaction between $[Fe(CO)_5]$ and As***, recorded in MeOH at cV = 20 V.

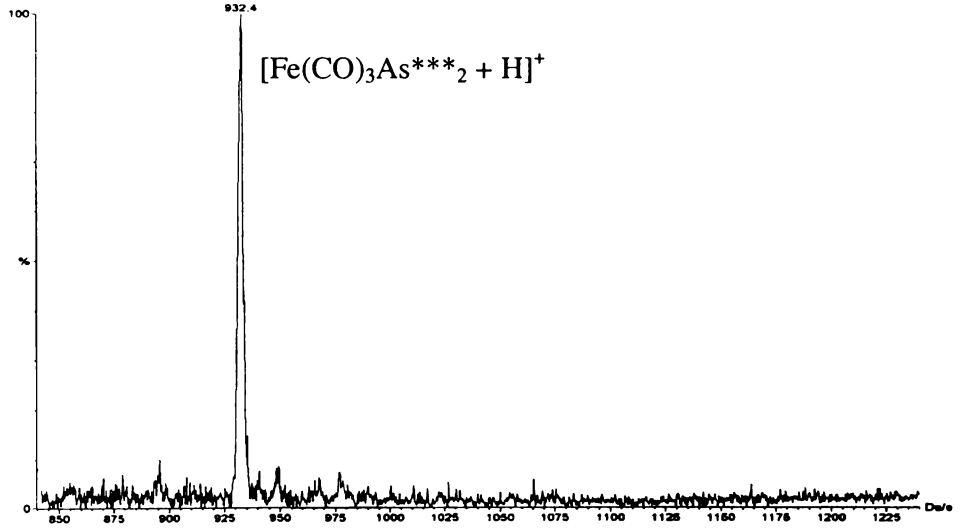

Fig. 3.7b The expanded region of the positive-ion ES mass spectrum of the reaction between $[Fe(CO)_5]$ and As***, showing the $[Fe(CO)_3As^{***}_2 + H]^+$ ion, recorded in MeOH at cV = 20 V.

The bidentate phosphines *o*-MeO-dppe and *p*-MeO-dppp (L–L), when treated with $[Mo(CO)_4(pip)_2]$ (pip = piperidine), yielded $[Mo(CO)_4(L–L)]$. Due to the microscopic scale they were not isolated, but the crude reaction solutions gave the expected $[M + H]^+$ ions at *m/z* 727 and *m/z* 741, respectively. The incorporation of basic groups into different types of ligands provides a general means of facilitating mass spectrometric characterisation of their complexes. Hence, even crude reaction products may be injected to check if the desired product has been formed and to what extent. This is particularly important if dealing with very small amounts of sample where purification of the product is difficult. Figure 3.8 shows the crude reaction solution of $[Mo(CO)_4(pip)_2]$ with *o*-MeO-dppe. The spectrum is quite 'messy', which is sometimes the case when many by-products are formed. However, the dominating peak was clearly from the product $[Mo(CO)_4(o\text{-MeO-dppe})]$.

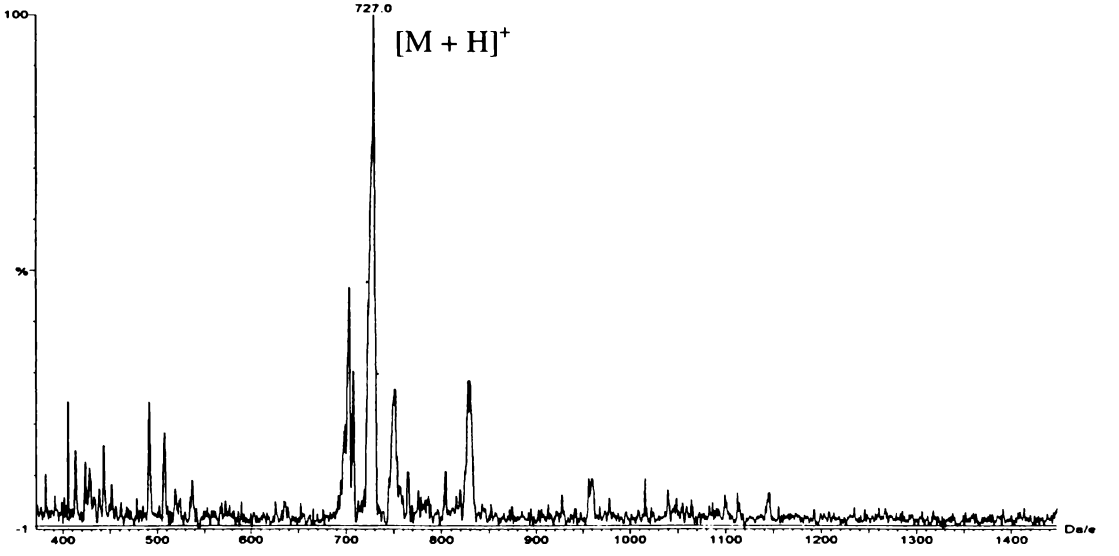

Fig. 3.8 The positive-ion ES mass spectrum of $[Mo(CO)_4(o\text{-MeO-dppe})]$ (injected as the crude reaction solution), recorded in MeOH at cV = 20 V.

3.7 Naturally electrospray-friendly phosphine ligands

Ligands that contain a basic oxygen or nitrogen do not need to be functionalised in order to be ionised by the protonation mechanism. In the next section, an ESMS analysis will be carried out on two of these ligands with different functional groups, and also some of their metal complexes.

3.7.1 Triazaphosphaadamantane (tpa)

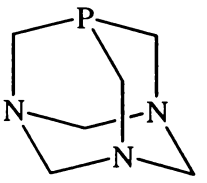

Fig 3.9 The structure of tpa.

1,3,5-Triaza-7-phosphaadamantane (tpa) is a small, crystalline, air-stable and water-soluble phosphine ligand. It is actually the smallest known phosphine (other than PH_3) with a cone angle of 102° [25]. This tertiary phosphine ligand is readily prepared from the reaction of tris(hydroxymethyl)phosphine, formaldehyde, and hexamethylenetetraamine[26], and was first synthesised by Daigle *et al.* in 1974[27]. The area in which tpa has probably gained its most fame is in biphasic catalysis. The non-ionic nature of tpa plus its small steric size and greater basicity make it an attractive alternative to the commonly employed sulfonated phosphines. The tpa analogue of $[RuCl_2(TPPMS)_2]$ [TPPMS = $Ph_2P(m\text{-}C_6H_4SO_3Na)$], $[RuCl_2(tpa)_4]$, has for example been found to be an active catalyst for the regioselective reduction of aldehydes to alcohols[28]. Furthermore, tpa is not a pronounced surfactant, as are the sulfonated phosphines, thus providing better phase separation during catalysis.

Because of its ability to form hydrogen bonds with both counterions and water molecules, tpa is not only an interesting ligand for structural analyses but also the three basic sites at the nitrogen atoms make it an excellent molecule for ESMS studies. The free ligand as well as neutral complexes of tpa should readily protonate at the nitrogen atoms to give $[M + H]^+$ ions in the ES mass spectrum. To date, there are only two reports on ESMS of tpa complexes[29], with all observed signals attributable to ionic metal complexes, rather than protonation of neutral pta complexes.

---

[25] C. A. Tolman, *Chem. Rev.*, 1977, **77**, 313.
[26] D. J. Daigle, *Inorg. Synth.*, 1998, **32**, 41.
[27] D. J. Daigle, A. B. Pepperman, Jr. and S. L. Vail, *J. Heterocycl. Chem.*, 1974, **11**, 407.
[28] D. J. Darensbourg, F. Joo, M. Kannisto, A. Katho, J. H. Reibenspies and D. J. Daigle, *Inorg. Chem.*, 1994, **33**, 200.
[29] D. J. Darensbourg, T. J. Decuir, N. W. Stafford, J. B. Robertson, J. D. Draper and J. H. Reibenspies, *Inorg. Chem.*, 1997, **36**, 4218; K. J. Fisher, I. G. Dance, G. D. Willett, R. Zhang and E. C. Alyea, *Eur. J. Mass Spectrom.*, 2000, **6**, 23.

3.7.1.1 Metal complexes of tpa

Because of the availability of starting materials, a number of carbonyl complexes of molybdenum and tungsten were prepared (listed in Table 3.8). The complexes have all been reported in the literature previously and studies have been done on their ^{31}P NMR, ^{95}Mo NMR [30], and IR [31] spectroscopic properties, their reactivity towards ligand dissociation[32], and on the crystal structure of $[Mo(CO)_5(tpa)]$ [33].

It should be mentioned that although the tpa ligand is very water-soluble, its complexes were not found to be at all. This was surprising as tpa is known to be a possible alternative to small phosphine ligands such as PMe_3 with the two advantages of being air-stable and water-soluble. However, upon closer inspection, all preparations of the complexes in the literature were carried out in solvents such as CH_2Cl_2, THF, heptane or MeCN, and IR or NMR data were recorded in solutions of hexane, acetone or chloroform, which are solvents not commonly employed for water-soluble compounds. Further, while the water-solubility of the ligand is often pointed out, a mention of the solubility of its complexes is commonly omitted.

3.7.1.2 ESMS of tpa and its metal complexes

When analysing the ligand at low cone voltages, it gave the expected parent ion $[M + H]^+$, but also associated with the solvent to form $[M + H + MeCN]^+$. At higher cone voltages only one fragment ion, either $[M - 43 + H]^+$ or $[M - 42]^{\bullet+}$, appeared. These two trends, initially observed for the free ligand, were also present when analysing the neutral metal complexes. ESMS data of the ligands as well as the metal complexes are summarised in Table 3.8.

---

[30] E. C. Alyea, K. J. Fisher, S. Foo and B. Philip, *Polyhedron*, 1993, **12**, 489.
[31] M. Y. Darensbourg and D. J. Daigle, *Inorg. Chem.*, 1975, **14**, 1217.
[32] D. J. Darensbourg and R. L. Kump, *Inorg. Chem.*, 1978, **17**, 2680.
[33] J. R. DeLerno, L. M. Trefonas, M. Y. Darensbourg and R. J. Majeste, *Inorg. Chem.*, 1976, **15**, 816.

Table 3.8 The positive-ion ESMS data for the tpa ligand and its metal complexes, recorded in $MeCN/H_2O$ solution.

Compound	cV (V)	Ions observed [*m/z*, relative peak height (%)]
tpa	20	$[M + H]^+$ (158, 100), $[M + H + MeCN]^+$ (199, 6)
	60	$[M + H]^+$ (158, 100), $[M + H + MeCN]^+$ (199, 15), $[M - 42]^{\bullet+}$ (115, 26)
$[Mo(CO)_4(tpa)_2]$	20	$[M + H]^+$ (524, 100), $[M + MeCN]^+$ (564, 5)
	60	$[M + H]^+$ (524, 100), $[M - CO + H]^+$ (495, 21), $[M - 42]^{\bullet+}$ (480, 28), $[M - 2CO + H]^+$ (467, 32), $[M - CO - 42]^{\bullet+}$ (455, 13), $[M - 3CO + H]^+$ (439, 39), $[M - 2CO - 42]^{\bullet+}$ (423, 23), $[M - 4CO + H]^+$ (411, 8), $[M - 3CO - 42]^{\bullet+}$ (396, 15)
$[Mo(CO)_5(tpa)]$	20	$[M + H]^+$ (395, 100), $[M + H + MeCN]^+$ (436, 25)
	60	$[M + H]^+$ (395, 100), $[M + H + MeCN]^+$ (436, 12), $[M - CO + H]^+$ (367, 43), $[M - 42]^{\bullet+}$ (352, 31), $[M - 2CO + H]^+$ (338, 74), $[M - CO - 42]^{\bullet+}$ (324, 52), $[M - 3CO + H]^+$ (311, 98), $[M - 2CO - 42]^{\bullet+}$ (295, 39), $[M - 4CO + H]^+$ (284, 40), $[M - 5CO + H]^+$ (256, 43)
$[W(CO)_4(tpa)_2]$	20	$[M + H]^+$ (611, 100)
	60	$[M + H]^+$ (611, 100), $[M - CO + H]^+$ (583, 12), $[M - 42]^{\bullet+}$ (568, 50), $[M - 2CO + H]^+$ (555, 5), $[M - CO - 42]^{\bullet+}$ (540, 28), $[M - 2CO - 42]^{\bullet+}$ (512, 28)
$[W(CO)_5(tpa)]$	20	$[M + H]^+$ (482, 100), $[M + H + MeCN]^+$ (523, 16)
	60	$[M + H]^+$ (482, 100), $[M + H + MeCN]^+$ (523, 10), $[M - CO + H]^+$ (454, 27), $[M - 42]^{\bullet+}$ (437, 68), $[M - 2CO + H]^+$ (424, 22), $[M - 3CO + H]^+$ (398, 23), $[M - 2CO - 42]^{\bullet+}$ (382, 30)

All tpa complexes showed $[M + H]^+$ ions as their major ions at low cone voltages, and {except for $[W(CO)_4(tpa)_2]$} they were all accompanied by an $[M + H + MeCN]^+$ ion at a lower intensity. Figure 3.10 shows the spectrum of $[Mo(CO)_4(tpa)_2]$ together with its calculated and observed isotope patterns.

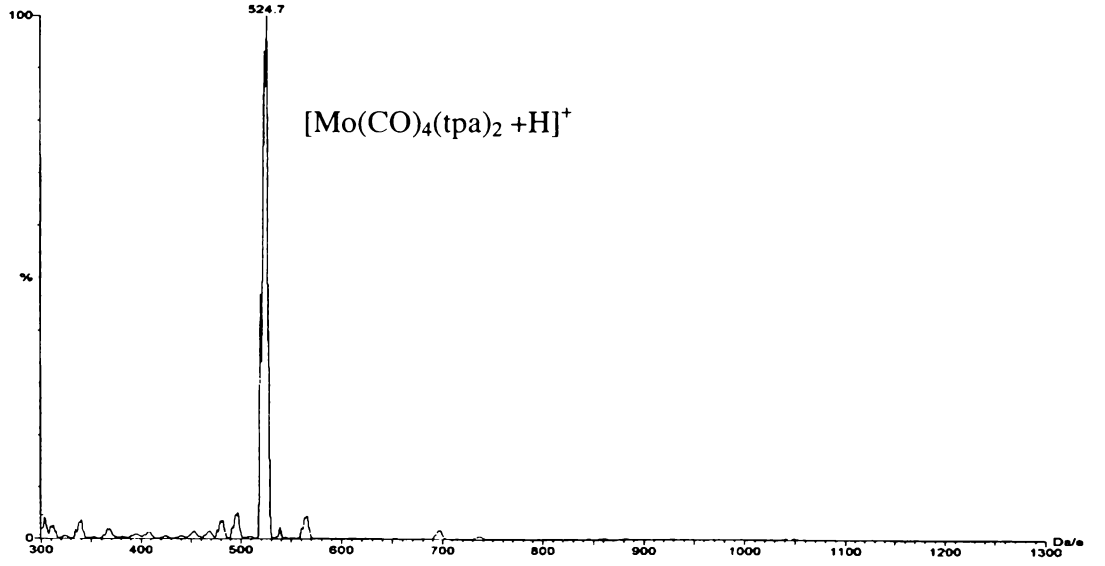

Fig 3.10a The positive-ion ES mass spectrum of $[Mo(CO)_4(tpa)_2]$, recorded in $MeCN/H_2O$.

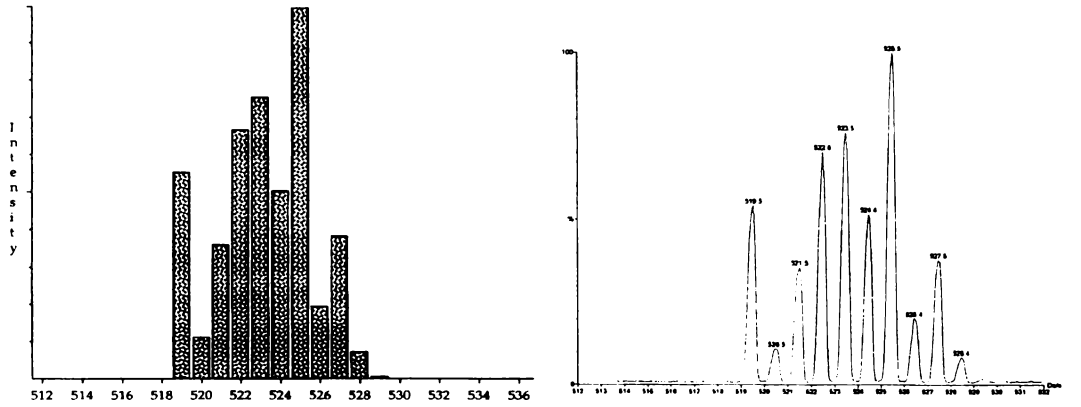

Fig 3.10b The calculated (left) and observed (right) isotope patterns for $[Mo(CO)_4(tpa)_2 + H]^+$.

When increasing the cone voltage, the complexes of tpa consecutively lost their CO ligands, but also lost an additional fragment of 43 amu {provided the formed species is also an $[M + H]^+$ ion}. The ES mass spectrum of $[W(CO)_4(tpa)_2]$, shown in Figure 3.11, illustrates this phenomenon. This fragmentation pattern has already been observed with the free ligand, indicating that the fragmentation occurs within the tpa ligand, rather than somewhere else in the complex. A mass difference of 43 is, however, one amu more than one would expect after the loss of three 14 fragments (which can be a combination

of CH_2 and N, as they have the same mass). The EI mass spectrum of the free ligand confirmed the expected fragmentation pathway, showing the parent ion at *m/z* 157, followed by two daughter ions at *m/z* 129 and 115. These peaks matched perfectly with the loss of two and three 14 units. In the ESMS, however, an overall positive charge has to be achieved. With the loss of three 14 units, the only way that the exact *m/z* values of the formed fragments could be explained was *via* formation of radical cations, rather than protonation, and so all ions of this type were assigned as radical cations. In the case of $[W(CO)_4(tpa)_2]$, MS/MS experiments of the $[M - 42]^{\bullet+}$ signal at *m/z* 583 showed that the peaks at *m/z* 540 and *m/z* 512 were daughter ions thereof. They most likely resulted from CO loss although the loss of two more 14 fragments could not be ruled out.

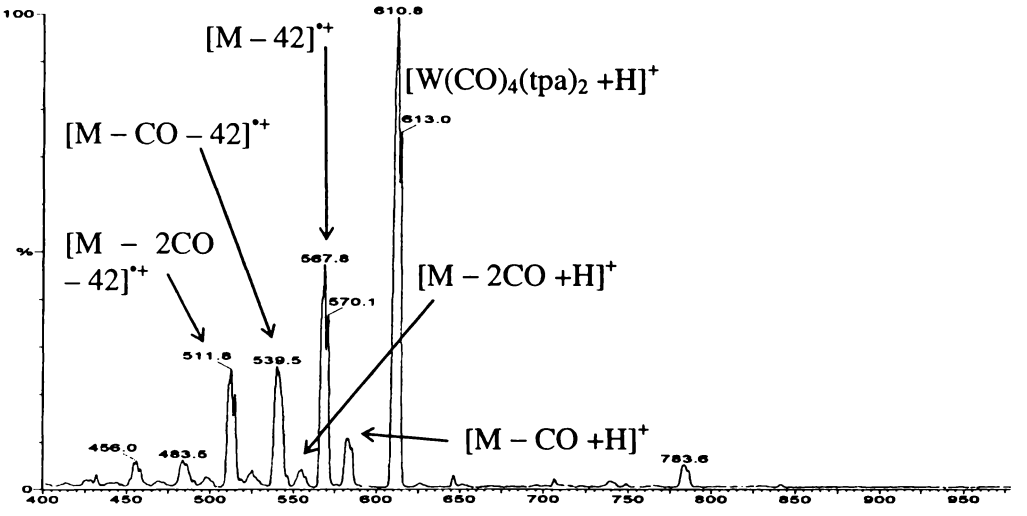

Fig. 3.11 The positive-ion ES mass spectrum of $[W(CO)_4(tpa)_2]$, recorded in $MeCN/H_2O$ at cV = 60 V.

3.7.2 Tris(2-cyanoethyl)phosphine (tcep)

Tris(2-cyanoethyl)phosphine, $P(CH_2CH_2CN)_3$, is also a very small, air-stable, crystalline and unique phosphine ligand. The presence of the β-cyano groups makes tcep very different from other small trialkylphosphines. Trialkylphosphines, in general, are easily oxidised by air[34] and have a pronounced basic character[35]. Tcep, however, is not oxidised by air, even at elevated temperatures. Moreover, tcep is only weakly basic (K_b

[34] W. C. Davies, P. L. Pearse and W. J. Jones, *J. Chem. Soc.*, 1929, 1262.

= 10^{-13}). In fact, it is the least basic trialkylphosphine known[36]. Its π-acceptor capacity is similar to that of $P(OPh)_3$. The reason for its low basicity is a decreased electron density around the phosphorus atom, which results from the inductive effect of the β-cyano groups. With respect to its low basicity and its resistance to oxidation, it more resembles triphenylphosphine than trialkylphosphines [37]. The presence of the hybrid soft (phosphorus) and the harder (nitrile) donor groups make tcep a potential multidentate ligand. It is capable of coordinating through the cyano groups[38], through the phosphorus atom [39], or both [40]. Many tcep complexes have been studied as catalysts, *e.g.* $[Co_2(CO)_6(tcep)_2]$ was found to catalyse the hydroformylation of hex-1-ene and propene[41], and $[Pt(tcep)_3]$ is known to catalyse the hydrophosphination of acrylonitrile[42].

The presence of the cyano group allows tcep and its complexes to be easily studied by IR spectroscopy (as opposed to PPh_3). However, since the complexes are not soluble in non-interacting solvents such as saturated hydrocarbons where the ν(CN) as well as the ν(CO) band widths are narrow, IR investigations have to be carried out in solvents such as CH_2Cl_2. The IR peak widths will be broader, making it more difficult to delineate the various vibrational modes. For this reason, ESMS appears to be a superior method for characterising complexes of tcep. As a neutral molecule with a basic site (N atom), tcep should be able to readily form $[M + H]^+$ ions. In connection with a study of metal-tcep complexes by Laser Ablation Fourier Transform Ion Cyclotron Resonance (LA-FTICR), the behaviour of the tcep ligand towards some alkali and transition-metal cations by means of ESMS has been investigated[43]. This appears to be the only ESMS study to date on tcep or its complexes.

---

[35] H. C. Brown, *J. Am. Chem. Soc.*, 1945, 503.
[36] C. A. Streuli, *Anal. Chem.*, 1960, **32**, 985; W. A. Henderson and C. A. Streuli, *J. Am. Chem. Soc.*, 1960, 5791.
[37] M. M. Rauhut, I. Heckenbleikner, H. A. Currier, F. C. Schaefer and V. P Wystrach, *J. Am. Chem. Soc.*, 1959, **81**, 1103.
[38] R. A. Walton and R. Whyman, *J. Chem. Soc. (A)*, 1968, 1394.
[39] F. A. Cotton, D. J. Darensbourg and W. H. Ilsley, *Inorg. Chem.*, 1981, **20**, 578.
[40] M. G. B. Drew, D. F. Lewis and R. A. Walton, *Chem. Commun.*, 1969, 326; K. Chent and B. M. Foxman, *J. Am. Chem. Soc.*, 1977, **99**, 8102.
[41] L. Rosi, A. Bini, P. Frediani, M. Bianchi and A. Salvini, *J. Mol. Catal. A: Chem.*, 1996, **112**, 367.
[42] P. G. Pringle and M. B. Smith, *J. Chem. Soc., Chem. Commun.*, 1990, 1701.
[43] K. J. Fisher, W. Henderson, I. G. Dance and G. D. Willett, *J. Chem. Soc. Dalton Trans.*, 1996, 4101.

3.7.2.1 Metal complexes of tcep

Complexes analogous to the tpa compounds described in section 3.7.1.1 were prepared and are listed in Table 3.9. The tcep complexes $[W(CO)_4(tcep)_2]$ and $[W(CO)_5(tcep)]$ were novel compounds whereas the Mo analogues have been mentioned in the literature before, mainly in ^{95}Mo NMR studies[44], but also in a study about the electronic effects on the ^{13}C NMR signals of various phosphorus, arsenic and antimony ligands in transition-metal carbonyl complexes[45]. The crystal structure of $[Mo(CO)_5(tcep)]$ has been reported[46].

3.7.2.2 ESMS of tcep and its metal complexes

As can be seen in Table 3.9, the ligand tcep had a high affinity for NH_4^+ ions present in the instrument. Similarly, all complexes of tcep showed an affinity for NH_4^+. In fact, they associated only with NH_4^+ to give ions of the type $[M + NH_4]^+$ while no $[M + H]^+$ ions were observed at all. When deliberately adding NH_4^+ ions to the analyte, the $[M + NH_4]^+$ signals increased in intensity confirming the trend to associate with NH_4^+ over protons and giving overall more intense spectra.

For the ligand alone, the intensity of the $[M + H]^+$ ion increased over $[M + NH_4]^+$ at higher cone voltages, but the intensity of the ions remained unchanged for the metal complexes of tpa. Furthermore, they successively lost their CO ligands, which has been observed several times before with other carbonyl compounds.

---

[44] E. C. Alyea and A. Somogyvari, *Trans. Met. Chem.*, 1987, **12**, 310; S. Song and E. C. Alyea, *Can. J. Chem.*, 1996, **74**, 2304; E. C. Alyea and A. Somogyvari, *Can. J. Chem.*, 1988, **66**, 397.
[45] G. M. Bodner, M. P. May and L. E. McKinney, *Inorg. Chem.*, 1980, **19**, 1951.
[46] F. A. Cotton, D. J. Darensbourg and W. H. Ilsley, *Inorg. Chem.*, 1981, **20**, 578.

Table 3.9 The positive-ion ESMS data for the tcep ligand and its metal complexes, recorded in $MeCN/H_2O$.

Compound	cV (V)	Ions observed [*m/z*, relative peak height (%)]
tcep	20	$[M + H]^+$ (194, 81), $[M + NH_4]^+$ (211, 100), $[OM + NH_4]^+$ (227, 35)
	60	$[M + H]^+$(194, 100) $[M + NH_4]^+$ (211, 15), $[OM + NH_4]^+$ (227, 5)
$[Mo(CO)_4(tcep)_2]$ [(a)]	20	$[M + NH_4]^+$ (613, 100), $[2M + NH_4]^+$ (1205, 5), $[M - CO + NH_4]^+$ (583, 18)
	60	$[M + NH_4]^+$ (613, 100), $[2M + NH_4]^+$ (1207, 9), $[M - CO + NH_4]^+$ (583, 13), $[M - CO + H]^+$ (567, 10), $[M - 2CO + H]^+$ (539, 66), $[M - 3CO + H]^+$ (513, 3), $[M - 4CO + H]^+$ (486, 31)
$[Mo(CO)_5(tcep)]$ [(a)]	20	$[M + NH_4]^+$ (488, 100), $[2M + NH_4]^+$ (877, 13), $[M - CO + NH_4]^+$ (419, 19)
	60	$[M + NH_4]^+$ (448, 14), $[2M + NH_4]^+$ (876, 7), $[M - CO + H]^+$ (402, 6), $[M - 2CO + H]^+$ (376, 17), $[M - 4CO + H]^+$ (324, 24), $[M - 5CO + H]^+$ (292, 100)
$[W(CO)_4(tcep)_2]$ [(a)]	20	$[M + NH_4]^+$ (699, 100), $[2M + NH_4]^+$ (1382, 19), $[3M + NH_4]^+$ (2063, 7), $[4M + NH_4]^+$ (2745, 2)
	60	$[M + NH_4]^+$ (699, 100), $[2M + NH_4]^+$ (1382, 17), $[3M + NH_4]^+$ (2062, 5), $[4M + NH_4]^+$ (2744, 3), $[M - 2CO + H]^+$ (626, 21), $[M - 4CO + H]^+$ (571, 6)
$[W(CO)_5(tcep)]$ [(a)]	20	$[M + NH_4]^+$ (535, 100), $[2M + NH_4]^+$ (1052, 4), $[M - CO + NH_4]^+$ (507, 24), $[M - CO + H]^+$ (488, 7),
	60	$[M + NH_4]^+$ (535, 42), $[M - CO + NH_4]^+$ (507, 10), $[M - CO + H]^+$ (490, 22), $[M - 2CO + H]^+$ (462, 31), $[M - 3CO + NH_4]^+$ (451, 33), $[M - 4CO + H]^+$ (409, 100), $[M - 5CO + H]^+$ (377, 72)

[(a)] deliberate addition of NH_4^+

In order to investigate why tcep and its complexes exhibit this strong affinity for the ammonium ion in the ESMS, a molecular modelling study was carried out. The state of lowest energy (Figure 3.12) shows that two of the ligand alkane chains are orientated toward two H atoms of the NH_4^+ ion. The calculated bond distances (1.715 and 1.749 Å) suggest strong hydrogen-bonding (typical H-bonding lies in the range of 1.73 – 2.23 Å for N–H•••N systems[47]). While the alkane chains of tcep are probably long enough for bonding through all three CN groups to the same NH_4^+ ion, the fact that only two of them exhibit H-bonding to NH_4^+ leaves two coordination sites for further H-bonding to another complex molecule. This stands in correlation with the additionally observed [2M + NH_4]$^+$ ions for all tcep complexes. In conclusion, tcep is a good ESMS ligand with NH_4^+ activation.

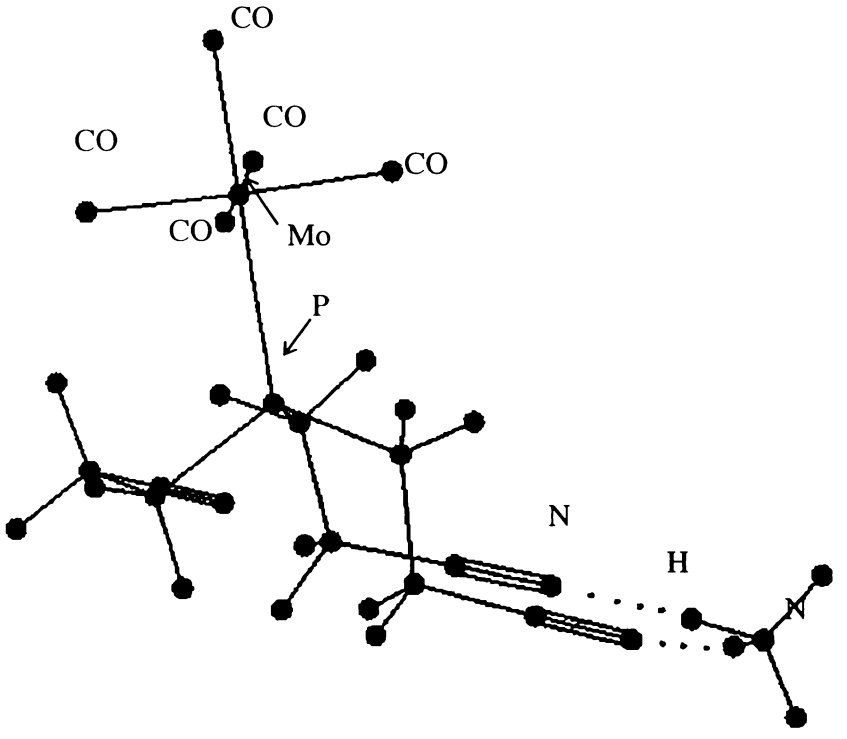

Fig. 3.12 The result of the molecular modelling of [$Mo(CO)_5$(tcep)] and NH_4^+.

[47] J. Bernstein, M. C. Etter and L Leiserowitz, The Role of Hydrogen Bonding in Molecular Assemblies, In H.-B. Bürgi and J. D. Dunitz (eds.), *Structure Correlation*, VCH, Weinheim, Germany, 1994.

3.8 ESMS of zerovalent complexes of platinum and palladium

3.8.1 Background

While the chemistry of most transition metals in the zerovalent oxidation state is dominated by carbonyl ligands, the most common ligands to allow the isolation of zerovalent complexes of the nickel triad are phosphines [48]. Similar to carbonyl complexes, where the oxidation state of zero was not taken into serious consideration for some decades after the isolation of the first complex in 1890[49], there was some early controversy whether the complexes $[Pt(PPh_3)_3]$ and $[Pd(PPh_3)_3]$ were true zerovalent compounds or merely hydride complexes of Pt(II) or Pd(II). Not only has their oxidation state been proven[50], it is now generally agreed that these type of compounds represent a model for metal surfaces as a single centre. Their coordinative reactivity reflects the chemi-adsorption of small molecules to the active centres of transition-metal surfaces and is therefore of great interest. Pioneering work in this area was carried out with Ir(I) complexes (d^8 configuration) by Vaska and co-workers[51]. Malatesta[52] extended this work to d^{10} zerovalent complexes such as $[Pt(PPh_3)_4]$ and $[Pd(PPh_3)_4]$. In fact, it makes more sense to use these d^{10} complexes as models for transition-metal surfaces than the (formally) positively charged d^8 complexes. The reactivity of this type of compounds can be attributed to two factors:

1. They are coordinatively unsaturated or dissociate in solution into unsaturated species, *e.g.*

$$[Pt(PPh_3)_4] \rightleftharpoons [Pt(PPh_3)_3] \rightleftharpoons [Pt(PPh_3)_2] \rightleftharpoons [Pt(PPh_3)]_n\ *$$

*cluster tetrameric molecule

2. 'Soft' ligands such as phosphines increase the 'softness' of the metal atom by creating a very polarisable electron density on the non-bonding metal orbitals. This

---

[48] L. Malatesta and S. Cenini, Zerovalent Compounds of Metals, In P. M. Maitlis, F. G. A. Stone and R. West (eds.), *Organometallic Chemistry. A series of monographs.*, Academic Press, London, 1974.
[49] L. Mond, C. Langer and F. Quinke, *J. Chem. Soc.*, 1890, **57**, 749.
[50] L. Malatesta and R. Ugo, *J. Chem. Soc.*, 1963, 2080.
[51] L. Vaska and J. W. DiLuzio, *J. Am. Chem. Soc.*, 1962, **84**, 679.

electron density can then become available for charge-transfer to a coordinated molecule, thus increasing the coordinative reactivity of the metal complex.

While a lot of work has been carried out on zerovalent complexes of platinum and palladium, they have never been studied by ESMS. Zerovalent platinum and palladium complexes of the type $[Pt(PPh_3)_n]$ and $[Pd(PPh_3)_n]$ are neutral and do not have a basic O or N atom for protonation in the ESMS. Electrospray-friendly phosphine ligands should enable the study of these types of complexes by ESMS. In this study, the zerovalent d^{10} complexes $[Pd(PPh_3)_4]$, $[Pt(PhCH=CHPh)(PPh_3)_2]$ and $[Pd_2(dba)_3]$ (dba = dibenzylideneacetone, PhHC=CHCOCH=CHPh) were used as precursors. $[Pd(PPh_3)_4]$ should readily undergo exchange reactions with *e.g.* P*, according to:

$$[Pd(PPh_3)_4] + n\ P^* \rightarrow [Pt(PPh_3)_{4-n}P^*_n] + n\ PPh_3$$

Similarly, $[Pt(PhCH=CHPh)(PPh_3)_2]$ and $[Pd_2(dba)_3]$ may yield complexes of the type $[ML_3]$ (M = Pt, Pd), by adding the appropriate amount of phosphine ligand, according to:

$$[Pt(PhCH=CHPh)(PPh_3)_2] + P^* \rightarrow [Pt(PPh_3)_2P^*] + PhCH=CHPh$$

$$[Pd_2(dba)_3] + 6n\ P^* \rightarrow 2\ [PdP^*_3] + 3\ dba$$

The products all contain electrospray-friendly ligands, enabling the formation of $[M + H]^+$ ions and with that analysis by ESMS.

3.8.2 ESMS of Pt(0) complexes

On a microscopic scale, equimolar amounts of $[Pt(PhCH=CHPh)(PPh_3)_2]$ and P* were added and subsequently analysed by ESMS. An envelope of peaks according to $[Pt(PPh_3)_nP^*_{3-n} + H]^+$ appeared and is shown in Figure 3.13. Thus, ligand exchange takes place readily at room temperature within seconds yielding products that are visible in the ESMS.

---

[52] L. Malatesta and C. Cariello, *J. Chem. Soc.*, 1958, 2323; L. Malatesta and M. Angoletta, *J. Chem. Soc.*, 1957, 1186.

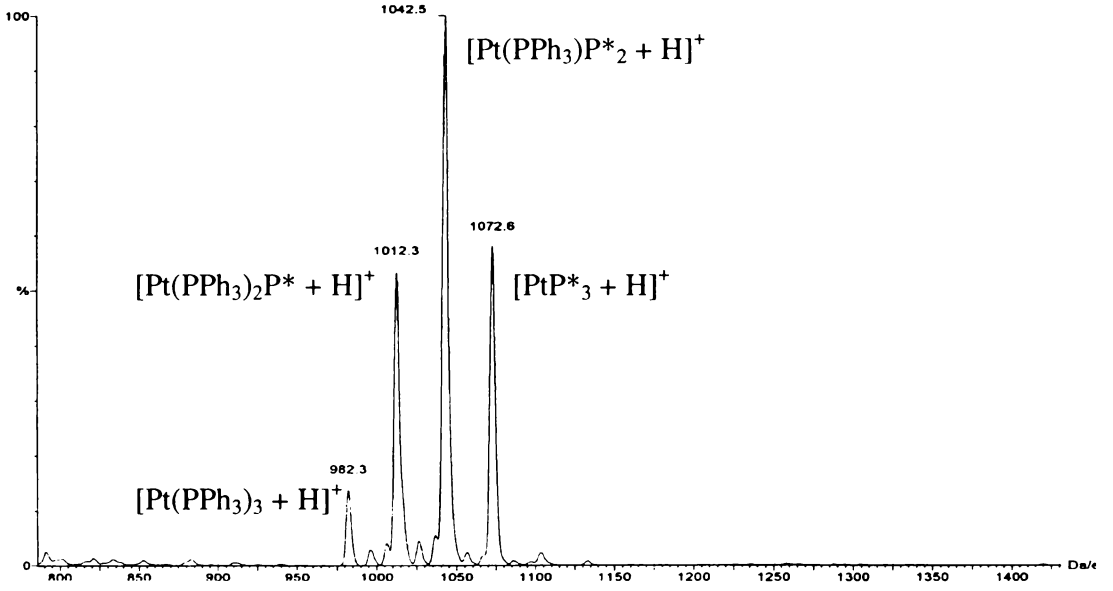

Fig. 3.13 The positive-ions ES mass spectrum of [Pt(PhCH=CHPh)(PPh_3)$_2$] and P* (1:1 ratio), recorded in MeOH at cV = 20 V.

Surprisingly, the complex [Pt(PPh_3)$_3$] without any electrospray-friendly ligands also gave an $[M + H]^+$ ion. The complex [Pt(PPh_3)$_3$] probably forms from [Pt(PhCH=CHPh)(PPh_3)$_2$] when free PPh_3 is present, possibly from dissociation processes. In fact, when mixing [Pt(PhCH=CHPh)(PPh_3)$_2$] with an equimolar amount of PPh_3, $[Pt(PPh_3)_3 + H]^+$ was observed as the only ion in the spectrum. It is known[53] that Pt(0) complexes interact with protonic acids to form hydride complexes *via* initial protonation at platinum giving a cationic hydride complex, according to:

$$[Pt(PR_3)_3] + HX \rightleftharpoons [PtH(PR_3)_3]^+ [X^-] \rightleftharpoons [PtHX(PR_3)_2 + PR_3]$$

The metal centre of [Pt(PPh_3)$_3$] appeared be basic enough to associate with protons from the solvent. Presumably, the P* complexes also protonated at the Pt centre rather than at the MeO group, although protonation at both sites cannot be excluded. Protonation on Pt, rather than on the basic O has been observed for the catalyst precursor [Pt(PCH_2OH)$_3$] [54]. In another experiment, a drop of formic acid was added to an equimolar solution of [Pt(PhCH=CHPh)(PPh_3)$_2$] and PPh_3. The two signals observed were $[Pt(PPh_3)_3 + H]^+$ (as

[53] D. M. Roundhill, Platinum, In G. Wilkinson (ed.), *Comprehensive Coordination Chemistry*, Vol. 5, Pergamon Press, Oxford, 1987, p. 355.

before) and $[Pt(PPh_3)_3 + 44]^+$ as the most intense peak. Addition of HCOOH would yield an ion with the mass of $[Pt(PPh_3)_3 + 46 + H]^+$, so that the observed signal is presumably formed by addition of the formate anion. Since the observed ion $[Pt(PPh_3)_3 + HCOO]^+$ is positively charged, the metal needs to be regarded as a formally Pt(II) centre, being the result of an oxidation reaction.

When adding more phosphine ligand to the system, the same products were obtained as before, but with an intensity shift to higher-substituted products. At higher cone voltages, ions of the type $[Pt(PPh_3)_{2-n}P^*_n + H]^+$ appeared. $[PtL_3]$ is known to dissociate into $[PtL_2]$ + L, which is enhanced at higher cone voltages. All observed ions are summarised in Table 3.10.

Table 3.10 The positive-ion ESMS data for the reaction between $[Pt(PhCH{=}CHPh)(PPh_3)_2]$ (M) and P* or PPh_3, recorded in MeOH.

Analytes (ratio)	cV (V)	Ions observed (*m/z*, relative peak height, %)
M + P* (1:1)	20	$[Pt(PPh_3)_3 + H]^+$ (982, 45), $[Pt(PPh_3)_2P^* + H]^+$ (1012, 100), $[Pt(PPh_3)P^*_2 + H]^+$ (1042, 70), $[PtP^*_3 + H]^+$ (1072, 20)
	60	$[Pt(PPh_3)_2 + H]^+$ (719, 62), $[Pt(PPh_3)P^* + H]^+$ (750, 65), $[PtP^*_2 + H]^+$ (781, 48), $[Pt(PPh_3)_3 + H]^+$ (982, 42), $[Pt(PPh_3)_2P^* + H]^+$ (1012, 100), $[Pt(PPh_3)P^*_2 + H]^+$ (1042, 72), $[PtP^*_3 + H]^+$ (1072, 17)
M + P* (1:2)	20	$[Pt(PPh_3)_3 + H]^+$ (982, 14), $[Pt(PPh_3)_2P^* + H]^+$ (1012, 52), $[Pt(PPh_3)P^*_2 + H]^+$ (1042, 100), $[PtP^*_3 + H]^+$ (1072, 57)
M + P* (1:3)	20	$[Pt(PPh_3)_2P^* + H]^+$ (1012, 28), $[Pt(PPh_3)_2P^* + H]^+$ (1042, 100), $[PtP^*_3 + H]^+$ (1072, 88)
M + P* (1:10)	20	$[Pt(PPh_3)_2P^* + H]^+$ (1012, 7), $[Pt(PPh_3)P^*_2 + H]^+$ (1042, 43), $[PtP^*_3 + H]^+$ (1072, 100)
M + PPh_3 (1:1)	20	$[Pt(PPh_3)_3 + H]^+$ (982, 100)
M + PPh_3 (1:1) + HCOOH	20	$[Pt(PPh_3)_3 + H]^+$ (982, 30), $[Pt(PPh_3)_3 + HCOO]^+$ (1026, 100)

[54] P. A. T. Hoye, P. G. Pringle, M. B. Smith and K. Worboys, *J. Chem. Soc. Dalton Trans.*, 1993, 269.

3.8.3 ESMS of Pd(0) complexes

The zerovalent palladium complexes $[Pd_2(dba)_3]$ and $[Pd(PPh_3)_4]$ were analysed in a similar manner to the platinum complex described above. Electrospray-friendly derivatives were obtained by ligand exchange with P*. As $[Pd(PPh_3)_4]$ is very air-sensitive, appropriate amounts were not weighed out. Instead, an excess (xs) of P* was added to the complex. Furthermore, $[Pd(PPh_3)_4]$ was analysed alone, while $[Pd_2(dba)_3]$ was also treated with PPh_3. The results are summarised in Table 3.11.

Table 3.11 The positive-ion ESMS data for the reactions between $[Pd_2(dba)_3]$ or $[Pd(PPh_3)_4]$ and P* or PPh_3, recorded in MeOH, at cV = 20V.

Analytes (ratio)	Ions observed [*m/z*, relative peak height (%)]
$[Pd(PPh_3)_4]$ + xs P*	$[PdP^*_2 + HCOO]^+$ (734, 9), $[PdP^*_3 + H]^+$ (984, 7), $[Pd(PPh_3)P^*_2 + HCOO]^+$ (996, 8), $[PdP^*_3Cl]^+$ (1017, 29), $[PdP^*_3 + HCOO]^+$ (1027, 100)
$[Pd(PPh_3)_4]$	$[Pd(PPh_3)_2 + HCOO]^+$ (674, 25), $[Pd(PPh_3)_3 + H]^+$ (892, 42), $[Pd(PPh_3)_3 + Cl]^+$ (927, 49), $[Pd(PPh_3)_3 + HCOO]^+$ (937, 100)
$[Pd_2(dba)_3]$ + P* (1:6)	$[Pd(PPh_3)_2 + H]^+$ (894, 17), $[Pd(PPh_3)_2P^*]^+$ (924, 70), $[Pd(PPh_3)P^*_2]^+$ (954, 100), $[PdP^*_3]^+$ (984, 55)
$[Pd_2(dba)_3]$ + PPh_3 (1:6)	$[Pd(PPh_3)_3 + H]^+$ (894, 100), $[Pd(PPh_3)_2]^+$ (633, 5)

In both cases, the complex $[PdP^*_3]$ formed readily when adding P* to either $[Pd_2(dba)_3]$ or $[Pd(PPh_3)_4]$, and gave the expected $[M + H]^+$ ions in the ESMS. At the time of recording, formic acid and chloride ions were present in the system, and ions associated with addition of formate and chloride [to a formally oxidised Pd(II) centre] dominated all spectra. This can be seen clearly in the case of $[Pd(PPh_3)_4]$ (with or without addition of P*), where $[Pd(PPh_3)_3 + HCOO]^+$ appeared at 100%, while ions attributed to protonation were much lower in intensity. The experiment was repeated at a later stage with $[Pd_2(dba)_3]$, where addition of P* or PPh_3 (1:6 ratio) gave $[M + H]^+$ signals only for various $[PdL_n]$ complexes. Thus, similar to the platinum system discussed earlier, it is possible to study zerovalent complexes of palladium with the common ligand PPh_3. Ligand exchange can however be achieved easily, leading to the formation of $[Pd(PPh_3)_{3-n}P^*_n + H]^+$.

3.9 Summary and conclusions

The concept of methoxy-fuctionalised and therefore electrospray-friendly ligands has been applied to a wider range of ligands. All of the metal complexes incorporating ES-friendly arsines, stibines and bidentate phosphines ionised as desired by protonation and could be readily studied by ESMS. Theoretically, any ligand for which a methoxy derivative can be prepared is potentially electrospray-friendly. This is of particular use for systems that have not been studied to a great extent or are limited in the methods for characterising them.

Spectra of very good quality were also obtained for neutral metal complexes containing the two ligands tpa and tcep. While tpa complexes gave parent signals corresponding to $[M + H]^+$, $[M + NH_4]^+$ ions were observed for all tcep complexes, which could be enhanced with addition of NH_4^+ ions.

Zerovalent phosphine complexes of platinum and palladium do not require functionalisation for their analysis in the ESMS, as the PPh_3 complexes already form the desired $[M + H]^+$ ions. This enables the study of reactions, such as oxidative addition or ligand exchange, which were shown to occur rapidly with the distribution of the products being readily detected by ESMS.

3.10 Experimental

General experimental procedures were as described in Chapter two. The NMR atom-labelling scheme for the ligands EPh_3 and E*** (E = group 15 element) is given in Figure 3.14. $AsCl_3$ (Riedel-de-Haën), $SbCl_3$ (Hopkin & Williams Ltd.), $SbPh_3$ (BDH), *trans*-stilbene (BDH), $[W(CO)_6]$ and $[Mo(CO)_6]$ (Pressure Chemical Company), were used as supplied. P^{9*} was kindly provided by Prof. G. A. Bowmaker, University of Auckland and initial ESMS analyses of P^{9*} were carried out by W. Henderson, but were repeated in order to confirm the reproducibility of the obtained data. The methoxy-fuctionalised diphosphines were received as a gift from E. Bouwman of Leiden University, The Netherlands. B. K. Nicholson generously provided $AsPh_3$ and $[Pd(PPh_3)_4]$, and $[Pd_2(dba)_3]$ (dba = *trans*, *trans*-dibenzylidene acetone) was kindly supplied by W. Henderson. Tpa [55], tcep [56], $[Pt(PhCH{=}CHPh)(PPh_3)_2]$ [57] and $[W(CO)_4(pip)_2]$ [58] (pip = piperidine), were prepared by the literature methods. Other materials and precursors were used or prepared as described in Chapter two. Molecular modelling studies were carried out by R. Thomson, using Spartan SGI version 5.1.3, Wavefunction Inc. Geometry optimisation was done with semi-empirical methods, using the AM1 model.

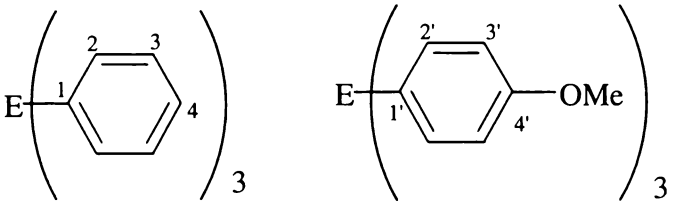

Fig. 3.14 The NMR numbering scheme for the ligands EPh_3 and E*** (E = group 15 element).

---

[55] D. J. Daigle, *Inorg. Synth.*, 1974, **11**, 407.
[56] W. J. Vullo, *Ind. Eng. Chem., Prod. Res. Div.*, 1966, **5**, 346.
[57] J. Chatt, B. L. Shaw and A. A. Williams, *J. Chem. Soc. A*, 1962, 3269.
[58] D. J. Darensbourg and R. L. Kump, *Inorg. Chem.*, 1978, **17**, 2680.

3.10.1 Syntheses of the ligands

An old literature preparation is available for As*** [59], but this ligand as well as Sb*** were prepared in an analogous manner to the methoxy-functionalised phosphines described in Chapter two.

3.10.1.1 Synthesis of $As(C_6H_4OCH_3)_3$, As***

The Grignard prepared from Mg (0.907 g, 37.8 mmol) and *p*-bromoanisole (7.07 g, 4.7 mL, 37.8 mmol) was treated with $AsCl_3$ (2.27 g, 1.1 mL, 12.6 mmol) and gave As*** as white crystals (3.2 g, 64%).

Elemental analysis: C, 63.60; H, 5.32%. $C_{21}H_{21}AsO_3$ requires C, 63.65; H, 5.32%.

^1H NMR ($CDCl_3$): δ 7.24 (6H, d, $^3J_{H2',H3'}$ = 9 Hz, H2'), δ 6.87 (6H, d, $^3J_{H3',H2'}$ = 9 Hz, H3'), δ 3.80 (9H, s, $OC\underline{H}_3$).

$^{13}C\{^1H\}$ NMR ($CDCl_3$): δ 159.9 (s, C4'), δ 134.8 (s, C2'), δ 131. 1 (s, C1'), δ 114. 3 (s, C3'), δ 55.2 (s, $O\underline{C}H_3$).

ESMS (MeOH, +ve ion, 20 V): $[M + H]^+$ *m/z* 397 (9%), $[OM + H]^+$ *m/z* 413 (100%).

ESMS ($MeCN/H_2O$, +ve ion, 20 V, addition of $Ag[BF_4]$): $[M + Ag + MeCN]^+$ *m/z* 544 (100%), $[2M + Ag]^+$ *m/z* 899 (8%), $[3M + Ag]^+$ *m/z* 1296 (12%), $[4M + Ag]^+$ *m/z* 1693 (10%).

3.10.1.2 Synthesis of $Sb(C_6H_4OCH_3)_3$, Sb***

$SbCl_3$ was dried under vacuum overnight before use. The Grignard prepared from Mg (0.907 g, 37.8 mmol) and *p*-bromoanisole (0.0071 g, 4.7 mL, 37.8 mmol) was treated with $SbCl_3$ (2.88 g, 0.92 mL, 12.6 mmol) and gave Sb*** as white crystals (1.13 g, 23.2%).

Elemental analysis: C, 56.91; H, 4.74%. $C_{21}H_{21}SbO_3$ requires C, 56.97; H, 4.79%.

---

[59] A. Michaelis and L. Weitz, *Chem. Ber.*, 1887, **20**, 49.

^{1}H NMR ($CDCl_3$): δ 7.33 (6H, d, $^3J_{H2',H3'}$ = 9 Hz, H2'), δ 6.88 (6H, d, $^3J_{H3',H2'}$ = 9 Hz, H3'), δ 3.79 (9H, s, $OC\underline{H}_3$).

^{13} C-{^{1}H} NMR ($CDCl_3$): δ 160.1 (s, C4'), δ 137.4 (s, C2'), δ 129.1 (s, C1'), δ 114. 7 (s, C3'), δ 55.1 (s, $O\underline{C}H_3$).

ESMS ($MeCN/H_2O$, +ve ion, 20 V): $[OM + H]^+$ *m/z* 459 (100%), $[OM + NH_4]^+$ *m/z* 478 (28%).

ESMS ($MeCN/H_2O$, +ve ion, 20 V, addition of $Ag[BF_4]$): $[M + Ag + MeCN]^+$ *m/z* 592 (100%), $[2M + Ag]^+$ *m/z* 993 (8%), $[3M + Ag]^+$ *m/z* 1437 (8%), $[4M + Ag]^+$ *m/z* 1880 (20%).

3.10.1.3 ESMS of PPh_3, $AsPh_3$ and $SbPh_3$

PPh_3 (0.0297 g, 0.11 mmol), $AsPh_3$ (0.0347 g, 0.11 mmol) and $SbPh_3$ (0.04 g, 0.11 mmol) were dissolved in a few drops of CH_2Cl_2, to which MeOH (*ca.* 0.5 mL) was added. For ESMS data, see section 3.4.

3.10.2 Syntheses of the metal complexes

Unless otherwise stated, the metal complexes were all prepared and worked up in the same manner as their phosphine analogues described in Chapter two.

3.10.2.1 Synthesis of *cis*-$[Mo(CO)_4(AsPh_3)_2]$

$[Mo(CO)_4(pip)_2]$ (0.15 g, 0.4 mmol) and $AsPh_3$ (0.245 g, 0.8 mmol) gave *cis*-$[Mo(CO)_4(AsPh_3)_2]$ as yellow crystals (0.19 g, 58%). This complex has been reported before, but was prepared by an alternative method[60].

IR (CH_2Cl_2): ν (CO region) 2025 (s), 1921 (sh), 1913 (s), 1881 (sh) cm^{-1}. [Lit. 2023 (m), 1927 (s), 1908 (vs), 1897 (s) [60]].

^{1}H NMR ($CDCl_3$): δ 7.33 – 7.22 (30H, m, H2-4).

---

[60] M. Graziani, F. Zingales and U. Belluco, *Inorg. Chem.*, 1967, **6**, 1582.

^{13} C-{^{1}H} NMR ($CDCl_3$): δ 202.4 (s, CO), δ 137.4 (s, C1), δ 132.9 (s, C2), δ 129.4 (s, C4), δ 128.6 (s, C3).

3.10.2.2 Synthesis of *cis*-[$Mo(CO)_4As^{***}_2$]

[$Mo(CO)_4(pip)_2$] (0.15 g, 0.4 mmol) and As*** (0.317 g, 0.8 mmol) gave *cis*-[$Mo(CO)_4As^{***}_2$] as yellow crystals (0.114 g, 29%).

m.p. 147 - 148°C.

Elemental analysis: C, 55.12; H, 4.23%. $C_{46}H_{42}As_2MoO_{10}$ requires C, 55.22; H, 4.20%.

IR (CH_2Cl_2): ν (CO region) 2022 (s), 1919 (sh), 1909 (s), 1876 (sh) cm^{-1}.

^{1}H NMR ($CDCl_3$): δ 7.13 (12H, d, $^{3}J_{H2',H3'}$ = 9 Hz, H2'), δ 6.74 (12H, d, $^{3}J_{H3',H2'}$ = 9 Hz, H3'), δ 3.78 (18H, s, OCH_3).

^{13} C-{^{1}H} NMR ($CDCl_3$): δ 160.3 (s, C4'), δ 134.1 (s, C2'), δ 129.0 (s, C1'), δ 114. 1 (s, C3'), δ 55.2 (s, OCH_3).

ESMS ($MeCN/H_2O$, +ve ion, 20 V): $[M + H]^+$ *m/z* 1002 (100%).

3.10.2.3 Synthesis of [$Fe(CO)_4(AsPh_3)$]

[$Fe(CO)_5$] (0.05 mL, 0.078 g, 0.4 mmol), Na[BH_4] (0.015 g, 0.4 mmol) and $AsPh_3$ (0.122 g, 0.4 mmol) gave [$Fe(CO)_4(AsPh_3)$] as yellow crystals (0.15 g, 80%). This complex has been reported before, but was prepared by an alternative method[61].

IR (CH_2Cl_2): ν (CO region) 2049 (s), 1972 (sh), 1940 (s) cm^{-1}. [Lit. 2048, 1972, 1942 [61]].

^{1}H NMR ($CDCl_3$): δ 7.49 - 7.47 (30H, m, H2-4).

^{13} C-{^{1}H} NMR ($CDCl_3$): δ 213.3 (s, CO), δ 134.7 (s, C1), δ 132.5 (s, C2), δ 130.7 (s, C4), δ 129.2 (s, C3).

---

[61] M. O. Albers, E. Singleton and N. J. Coville, *Inorg. Synth.*, 1990, **28**, 168.

3.10.2.4 Synthesis of [$Fe(CO)_4As^{***}$]

In an attempt to prepare [$Fe(CO)_3(As^{***})_2$], [$Fe(CO)_5$] (0.05 mL, 0.078 g, 0.4 mmol) and Na[BH_4] (0.03 g, 0.8 mmol) were treated with As*** (0.317 g, 0.8 mmol). Upon recrystallisation, the complex [$Fe(CO)_4As^{***}$] was obtained as yellow crystals (0.11 g, 49%).

m.p. 148 - 149°C.

Elemental analysis: C, 53.13; H, 3.45%. $C_{25}H_{21}AsFeO_3$ requires C, 53.19; H, 3.72%.

IR ($CHCl_3$): ν (CO region) 2047 (s), 1971 (sh), 1939 (s) cm^{-1}.

^1H NMR ($CDCl_3$): δ 7.40 (6H, d, $^3J_{H2',H3'}$ = 9 Hz, H2'), δ 6.96 (6H, d, $^3J_{H3',H2'}$ = 9 Hz, H3'), δ 3.83 (9H, s, O$\underline{C}H_3$).

^{13} C-{^1H} NMR ($CDCl_3$): δ 213.5 (s, $\underline{C}O$), δ 161.4 (s, C4'), δ 133.8 (s, C2'), δ 126.2 (s, C1'), δ 114. 6 (s, C3'), δ 55.3 (s, O$\underline{C}H_3$).

ESMS (MeCN/H_2O, +ve ion, 20 V): $[M + H]^+$ *m/z* 565 (100%).

3.10.2.5 Synthesis of *cis*-[$Mo(CO)_4(SbPh_3)_2$]

[$Mo(CO)_4(pip)_2$] (0.125 g, 0.33 mmol) was dissolved in THF (15 mL). $SbPh_3$ (0.235 g, 0.66 mmol) was added as a solid and the reaction mixture was refluxed for 1 hour. The solution was allowed to cool to room temperature and the solvent was evaporated. Recrystallisation from CH_2Cl_2/MeOH gave *cis*-[$Mo(CO)_4(SbPh_3)_2$] as yellow crystals (0.125 g, 42%). This complex has been reported before, but was prepared by an alternative method[60].

IR ($CHCl_3$): ν (CO region) 2024 (s), 1952 (sh), 1931 (s), 1917 (s), 1894 (sh) cm^{-1}. [Lit: 2024 (m), 1926 (s), 1912 (vs), 1896 (s) [60]].

^1H NMR ($CDCl_3$): δ 7.36 - 7.05 (30H, m, H2-4).

^{13} C-{^1H} NMR ($CDCl_3$): δ 214.9 (s, $\underline{C}O$), δ 210.3 (s, $\underline{C}O$), δ 135.5 (s, C1), δ 135.2 (s, C2), δ 129.6 (s, C4), δ 129.1 (s, C3).

3.10.2.6 Synthesis of *cis*-[$Mo(CO)_4Sb^{***}_2$]

[$Mo(CO)_4Sb^{***}_2$] was prepared and worked up in a similar manner to [$Mo(CO)_4(SbPh_3)_2$]. [$Mo(CO)_4(pip)_2$] (0.104 g, 0.27 mmol) and Sb*** (0.25 g, 0.56 mmol) gave *cis*-[$Mo(CO)_4Sb^{***}_2$] as yellow crystals (0.105 g, 35%).

m.p. 158 - 160°C.

Elemental analysis: C,51.52; H, 4.15%. $C_{46}H_{42}MoO_{10}Sb_2$ requires C, 50.46; H, 3.84%.

IR ($CHCl_3$): ν (CO region) 2022 (s), 1948 (sh), 1928 (s), 1913 (s), 1891 (sh) cm^{-1}.

^1H NMR ($CDCl_3$): δ 7.17 (6H, d, $^3J_{H2',H3'}$ = 9 Hz, H2'), δ 6.76 (6H, d, $^3J_{H3',H2'}$ = 9 Hz, H3'), δ 3.77 (s, $OC\underline{H}_3$).

^{13}C-{^1H} NMR ($CDCl_3$): δ 160.7 (s, C4'), δ 136.4 (s, C2'), δ 125.0 (s, C1'), δ 114. 7 (s, C3'), δ 55.1 (s, $O\underline{C}H_3$).

ESMS (MeOH, +ve ion, 20 V): $[M + H]^+$ *m/z* 1096 (100%), $[M + NH_4]^+$ *m/z* 1114 (12%), $[M + pip + H]^+$ *m/z* 1180 (98%), $[2M + NH_4]^+$ *m/z* 2208 (32%).

3.10.2.7 Synthesis of [$Fe(CO)_4(SbPh_3)$]

This complex was prepared similar to the literature[61]. $CoCl_2 \cdot 4H_2O$ was dried under vacuum for three hours before use during which time the colour changed from pink to blue. $SbPh_3$ (0.125 g, 0.35 mmol) was first placed in the reaction flask, followed by benzene (10 mL), and $CoCl_2$ (0.013 g, 0.1 mmol). The solution was brought to reflux and [$Fe(CO)_5$] (0.1 mL, 0.140 g, 0.7 mmol) was added. The reaction mixture was refluxed for another two hours. The solution was filtered and the solvent was removed. This complex was not isolated.

IR (benzene): ν (CO region) 2046s, 1972(sh), 1940s cm^{-1}. [Lit. 2045, 1970, 1938 [61]].

3.10.2.8 Synthesis of [$Fe(CO)_4Sb^{***}$]

This complex was obtained in an attempt to prepare [$Fe(CO)_3Sb^{***}_2$], following the procedure for [$Fe(CO)_3(PPh_3)_2$] described in Chapter two. $Na[BH_4]$ (0.029 g, 0.76

mmol), Sb*** (0.34 g, 0.76 mmol) and [$Fe(CO)_5$] (0.05 mL, 0.075 g, 0.38 mmol) gave [$Fe(CO)_4$Sb***] as yellow crystals (0.06 g, 26%).

m.p. 112 - 115°C.

Elemental analysis: C, 49.26; H, 3.54%. $C_{25}H_{21}SbFeO_3$ requires C, 49.10; H, 3.44%.

IR ($CHCl_3$): ν (CO region) 2045 (s), 1970 (sh), 1934 (s) cm^{-1}.

^{1}H NMR: δ 7.46 (6H, d, $^3J_{H2',H3'}$ = 8.7 Hz, H2'), δ 6.98 (6H, d, $^3J_{H3',H2'}$ = 8.7 Hz, H3'), δ 3.83 (9H, s, $OC\underline{H}_3$).

^{13} C-{^{1}H} NMR ($CDCl_3$): δ 212.9 (s, $\underline{C}O$), δ 161.7 (s, C4'), δ 136.1 (s, C2'), δ 121.1 (s, C1'), δ 115.3 (s, C3'), δ 55.3 (s, $O\underline{C}H_3$).

ESMS (MeOH, +ve ion, 20 V): $[M + H]^+$ *m/z* 611 (100%).

3.10.2.9 Synthesis of [Mo(CO)$_4$(*o*-MeO-dppe)]

[$Mo(CO)_4(pip)_2$] (0.0051 g, 0.0135 mmol) and *o*-MeO-dppe (0.007 g, 0.0135 mmol) were refluxed in CH_2Cl_2 (5 mL) for one hour. The crude reaction solution was injected directly into the ESMS without purification.

ESMS (MeOH, +ve ion, 20 V): $[M + H]^+$ *m/z* 727 (100%).

3.10.2.10 Synthesis of [Mo(CO)$_4$(*p*-MeO-dppp)]

In a similar manner to [$Mo(CO)_4$(*o*-MeO-dppe)], [$Mo(CO)_4(pip)_2$] (0.0051 g, 0.135 mmol) was treated with *p*-MeO-dppp (0.0071 g, 0.0135 mmol).

ESMS (MeOH, +ve ion, 20 V): $[M + H]^+$ *m/z* 741 (100%).

3.10.2.11 Synthesis of *cis*-[Mo(CO)$_4$(tpa)$_2$]

This complex was prepared according to the literature[62]. A solution of tpa (0.83 g, 5.3 mmol) in MeOH (20 mL) was added to a solution of [$Mo(CO)_4(pip)_2$] (1 g, 2.6 mmol) in

---

[62] E. C. Alyea, K. J. Fischer, S. Foo and B. Philip, *Polyhedron*, 1993, **12**, 489.

CH_2Cl_2 (20 mL). The solution was stirred for 30 minutes. The solvent was removed *in vacuo* and the resulting solid was recrystallised from MeCN to give *cis*-$[Mo(CO)_4(tpa)_2]$ as yellow crystals (0.712 g, 52%).

IR (CH_2Cl_2): ν (CO region) 2022 (s), 1926 (sh), 1909 (s), 1890 (sh) cm^{-1}. [Lit. 2012, 1932, 1910 [62]].

^{31}P NMR ($CDCl_3$): δ -52.30. [Lit. δ -54.9, in MeCN [62]].

ESMS ($MeCN/H_2O$, +ve ion, 20 V): $[M + H]^+$ *m/z* 524 (100%), $[M + H + MeCN]^+$ *m/z* 564 (5%).

3.10.2.12 Synthesis of $[Mo(CO)_5(tpa)]$

This complex was prepared according to the literature[62]. $Me_3NO{\bullet}2H_2O$ (0.444 g, 4 mmol) was added to a solution of $[Mo(CO)_6]$ (1.06 g, 4 mmol) in MeCN (20 mL). After 30 minutes stirring at room temperature a solution of tpa (0.644 g, 4.1 mmol) in MeOH (20 mL) was added to the yellow MeCN solution. The resulting solution was refluxed for 30 minutes. The solvent was removed *in vacuo*, the solid filtered, washed with cold pet. spirits (60 - 80°C) and water, and recrystallised from pet. spirits to give $[Mo(CO)_5(tpa)]$ as yellow crystals (0.502 g, 32%).

IR (CH_2Cl_2): ν (CO region) 2073 (s), 1986 (sh), 1944 (s) cm^{-1}.

^{31}P NMR ($CDCl_3$): δ -53.22. [Lit: δ -55.9, in MeCN [62]].

ESMS ($MeCN/H_2O$, +ve ion, 20 V): $[M + H]^+$ *m/z* 395 (100%), $[M + H + MeCN]^+$ *m/z* 436 (25%).

3.10.2.13 Synthesis of *cis*-$[W(CO)_4(tpa)_2]$

This complex was prepared according to the literature[62] in a similar manner to *cis*-$[Mo(CO)_4(tpa)_2]$. $[W(CO)_4(pip)_2]$ (1.21 g, 2.6 mmol) and tpa (0.83 g, 5.3 mmol) gave *cis*-$[W(CO)_4(tpa)_2]$ as yellow crystals (0.39 g, 25%).

IR (CH_2Cl_2): ν (CO region) 2018 (s), 1920 (sh), 1900 (s) cm^{-1}. [Lit. 2016, 1928, 1904, 1848 [62]].

^{31}P NMR ($CDCl_3$): δ -76.18 (s, $^1J_{P,W}$ = 226 Hz). [Lit. δ -75.0, in MeCN [62]].

ESMS (MeOH, +ve ion, 20 V): $[M + H]^+$ *m/z* 611 (100%).

3.10.2.14 Synthesis of $[W(CO)_5(tpa)]$

This complex was prepared according to the literature[62] in a similar manner to $[Mo(CO)_5(tpa)]$, except that the solution of $Me_3NO•2H_2O$ with $[W(CO)_6]$ was stirred for two hours. $[W(CO)_6]$ (1.41 g, 4 mmol) and $Me_3NO•2H_2O$ (0.444 g, 4 mmol) were treated with tpa (0.644 g, 4.1 mmol) to give $[W(CO)_5(tpa)]$ as yellow crystals (0.558 g, 29%).

IR (CH_2Cl_2): ν (CO region) 2072 (s), 1980 (sh), 1940 (s) cm^{-1}.

^{31}P NMR ($CDCl_3$): δ -76.7 (s, $^1J_{P,W}$ = 222.3 Hz). [Lit. δ -78.4, in MeCN].

ESMS ($MeCN/H_2O$, +ve ion, 20 V): $[M + H]^+$ *m/z* 482 (100%), $[M + NH_4]^+$ *m/z* 523 (16%).

3.10.2.15 Synthesis of *cis*-$[Mo(CO)_4(tcep)_2]$

cis-$[Mo(CO)_4(tcep)_2]$ was prepared and worked up in a similar manner to *cis*-$[Mo(CO)_4(tpa)_2]$. $[Mo(CO)_4(pip)_2]$ (1 g, 2.6 mmol) and tcep (1.02 g, 5.3 mmol) gave *cis*-$[Mo(CO)_4(tcep)_2]$ as yellow crystals (0.862 g, 56%). This complex has been reported before, but only ^{95}Mo NMR data are available[63].

IR (MeCN): ν (CO region) 2027 (m), 1929 (sh), 1902 (s), 1858 (m) cm^{-1}.

^{31}P NMR (DMSO): δ 34.2.

^1H NMR (DMSO): δ 2.84 (12H, m, P-C$\underline{H}_2$), δ 2.33 (12H, m, C$\underline{H}_2$-CN).

^{13} C-{^1H} NMR (DMSO): δ 211.5 (m, $\underline{C}O$), δ 121.9 (t, $^3J_{C,P}$ = 7.6 Hz, $\underline{C}N$), δ 26.6 (t, $^2J_{C,P}$ = 9.6 Hz, P-$\underline{C}H_2$), δ 13.7 (t, $^1J_{C,P}$ = 12.1 Hz, $\underline{C}H_2$-CN).

---

[63] E. C. Alyea and A. Somogyvari, *Can. J. Chem.*, 1988, **66**, 397; S. Song and E. C. Alyea, *Can. J. Chem.*, 1996, **74**, 2304.

ESMS ($MeCN/H_2O$, +ve ion, 20 V): $[M + NH_4]^+$ *m/z* 613 (100%), $[2M + NH_4]^+$ *m/z* 1205 (5%), $[M - CO + NH_4]^+$ *m/z* 583 (18%).

3.10.2.16 Synthesis of $[Mo(CO)_5(tcep)]$

$[Mo(CO)_5(tcep)]$ was prepared in a similar manner to $[Mo(CO)_5(tpa)]$. $[Mo(CO)_6]$ (1.06 g, 4 mmol), $Me_3NO{\bullet}2H_2O$ (0.444 g, 4 mmol) and tcep (0.791 g, 4.1 mmol) gave $[Mo(CO)_5(tcep)]$ as yellow crystals (0.775 g, 33%). This complex has been reported before, but was prepared by an alternative method[64].

IR (MeCN): ν (CO region) 2078 (s), 2027 (m), 1959 (sh), 1952 (vs), 1904 (sh), 1860 (m) cm^{-1}. [Lit. 2077(s), 1965 (sh), 1952 (vs) [64]].

^{31}P NMR (DMSO): δ 22.75.

^1H NMR (DMSO): δ 2.82 (6H, m, P-C$\underline{H}_2$), δ 2.40 (6H, m, C$\underline{H}_2$-CN).

^{13}C-{^1H} NMR (DMSO): δ 206.6 (m, $\underline{C}O$), δ 121.5 (m, $\underline{C}N$), δ 24.8 (m, P-$\underline{C}H_2$), δ 13.8 (m, $\underline{C}H_2$-CN) [65].

ESMS ($MeCN/H_2O$, +ve ion, 20 V): $[M + NH_4]^+$ *m/z* 488 (100%), $[2M + NH_4]^+$ *m/z* 877 (13%), $[M - CO + NH_4]^+$ *m/z* 419 (19%).

3.10.2.17 Synthesis of *cis*-$[W(CO)_4(tcep)_2]$

$[W(CO)_4(tcep)_2]$ was prepared in a similar manner to that described above for *cis*-$[Mo(CO)_4(tcep)_2]$. $[W(CO)_4(pip)_2]$ (1.21 g, 2.6 mmol) and tcep (1.02 g, 5.3 mmol) gave *cis*-$[W(CO)_4(tcep)_2]$ as yellow crystals (0.565 g, 32%).

m.p. 108 - 110°C.

Elemental analysis: C, 38.73; H, 3.68; N, 12.43%. $C_{22}H_{24}N_6O_4P_2W$ requires C, 38.71; H, 3.52; N, 12.32%.

IR (MeCN): ν (CO region) 2014 (m), 1948 (sh), 1892 (s), 1840 (m) cm^{-1}.

---

[64] F. A. Cotton, D. J. Darensbourg and W. H. Ilsley, *Inorg. Chem.*, 1981, **20**, 578.
[65] This spectrum was of low intensity, therefore no coupling constants were obtained.

^{31}P NMR (DMSO): δ 8.7 (s, $^{1}J_{P,W}$ = 275 Hz).

^{1}H NMR (DMSO): δ 2.83 (12H, m, P-C$\underline{H}_2$), δ 2.44 (12H, m, C$\underline{H}_2$-CN).

^{13} C-{^{1}H} NMR (DMSO): δ 202.8 (m, $\underline{C}$O), δ 121.7 (t, $^{3}J_{C,P}$ = 7.9 Hz, $\underline{C}$N), δ 27.3 (t, $^{2}J_{C,P}$ = 11.69 Hz, P-$\underline{C}H_2$), δ 14.3 (t, $^{1}J_{C,P}$ = 12.7 Hz, $\underline{C}H_2$-CN).

ESMS (MeCN/H_2O, +ve ion, 20 V): $[M + NH_4]^+$ *m/z* 699 (100%), $[2M + NH_4]^+$ *m/z* 1382 (19%), $[3M + NH_4]^+$ *m/z* 2063 (7%), $[4M + NH_4]^+$ *m/z* 2745 (2%).

3.10.2.18 Synthesis of [W(CO)$_5$(tcep)]

[W(CO)$_5$(tcep)] was prepared in a similar manner to [Mo(CO)$_5$(tcep)], except that the solution of $Me_3NO•2H_2O$ and [W(CO)$_6$] was stirred for two hours. [W(CO)$_6$] (1.41 g, 4 mmol), $Me_3NO•2H_2O$ (0.444 g, 4 mmol) and tcep (0.791 g, 4.1 mmol) gave [W(CO)$_5$(tcep)] as yellow crystals (0.085 g, 33%). A satisfactory elemental analysis was not obtained.

m.p. 208 - 210°C.

IR (MeCN): ν (CO region) 2076 (m), 2045 (m), 1941 (s), 1894 (vs), 1850 (sh), 1827 (sh) cm^{-1}.

^{31}P NMR (DMSO): δ 8.1 (s, $^{1}J_{P,W}$ = 275.2 Hz).

^{1}H NMR (DMSO): δ 2.73 (6H, m, P-C$\underline{H}_2$), δ 2.36 (6H, m, C$\underline{H}_2$-CN).

^{13} C-{^{1}H} NMR (DMSO): δ 201.6 (s, $\underline{C}$O), δ 120.5 ($^{3}J_{C,P}$ = 7.5 Hz, $\underline{C}$N), δ 26.0 (t, $^{2}J_{C,P}$ = 11.7 Hz, P-$\underline{C}H_2$), δ 13.0 (s, $\underline{C}H_2$-CN).

ESMS (MeCN/H_2O, +ve ion, 20 V): $[M + NH_4]^+$ *m/z* 535 (100%), $[2M + NH_4]^+$ *m/z* 1052 (4%), $[M - CO + NH_4]^+$ *m/z* 507 (24%), $[M - CO + NH_4]^+$ *m/z* 488 (7%).

3.10.3 Reactions of zerovalent complexes of platinum and palladium

All ESMS experiments were carried out on a microscopic scale. For the reactions with [Pt(PhCH=CHPh)(PPh_3)$_2$] and [Pd_2(dba)$_3$], accurate amounts of reagents were weighed

out, whereas for the reactions involving $[Pd(PPh_3)_4]$, a tiny speck of the complex and a larger speck of P* were dissolved in a few drops of CH_2Cl_2, to which MeOH (*ca.* 0.5 mL) was added. All solutions were freshly prepared and were subsequently injected into the ESMS. All spectra were obtained at a low cone voltage (20 V), using a mobile phase of MeOH.

3.10.3.1 ESMS experiments with $[Pt(PhCH=CHPh)(PPh_3)_2]$

A 1:1 ratio required $[Pt(PhCH=CHPh)(PPh_3)_2]$ (0.009 g, 0.01 mmol) and P* (0.0029 g, 0.01 mmol) or PPh_3 (0.0026 g, 0.01 mmol). Both reagents were dissolved in a few drops of CH_2Cl_2, to which MeOH (*ca.* 0.5 mL) was added. For ESMS data, see section 3.8.2.

3.10.3.2 ESMS experiments with $[Pd_2(dba)_3]$

A 1:6 ratio required $[Pd_2(dba)_3]\bullet CHCl_3$ (0.0045 g, 4.35×10^{-3} mmol) and P* (0.0076 g, 0.026 mmol) or PPh_3 (0.0068 g, 0.026 mmol). Both reagents were dissolved in a few drops of CH_2Cl_2, to which MeOH (*ca.* 0.5 mL) was added. For ESMS data, see section 3.8.3.

Chapter 4

Electrospray-friendly isonitrile derivatives of $[Fe_3(CO)_{12}]$ and $[Ru_3(CO)_{12}]$

In this chapter, the concept of electrospray-friendly ligands is extended to the field of transition-metal isonitrile chemistry. Reactions of various isonitrile ligands with $[Fe_3(CO)_{12}]$ and the heavier congener $[Ru_3(CO)_{12}]$ were investigated by ESMS. It was found that all isonitrile derivatives of $[Fe_3(CO)_{12}]$ and $[Ru_3(CO)_{12}]$ (*i.e.* even those without electrospray-friendly ligands) give signals in the ESMS, so these systems were investigated as well.

4.1 Isonitriles in transition-metal chemistry

Isonitriles are ubiquitously used as ligands in transition-metal chemistry, and this topic has been subject of a number of reviews[1]. Isonitriles are also known as isocyanides, but the former nomenclature is used in *Chemical Abstracts* and is used in this thesis.

The isonitrile molecule is isolobal with the carbon monoxide molecule, according to:

:C≡O :C≡N–R (R = H or organic group)

Consequently, because of their similar electronic and steric properties, isonitriles are often used to mimic CO reactivity. However, as the R group can be altered, the isonitrile ligand is generally known as a more versatile ligand than CO. Considering the importance of transition-metal carbonyls in catalysis or as precursors, the reasons for synthesising and studying the analogous isonitrile compounds become apparent. In certain cases, modification of the catalyst through substitution of CO by CNR has been shown to improve its efficiency by 35 times[2].

---

[1] E. Singleton and H. E. Oosthuizen, *Adv. Organomet. Chem.*,1983, **22**, 209; F. Bonati and G. Minghetti, *Inorg. Chim. Acta*, 1974, **9**, 95.
[2] M. O. Albers, N. J. Coville and E. Singleton, *J. Organomet. Chem.*, 1987, **326**, 229.

Isonitriles are very toxic, and the volatile ones are also extremely malodorous. Allegedly[3], some of the early synthetic routes were only discovered by the odour of the reaction products. The first synthesis of isonitriles may be attributed to Lieke[4], although he wrongly assumed he had prepared nitriles. Isonitriles were first specifically synthesised by Gautier in 1867[5], by alkylation of AgCN and, at about the same time, by Hofmann[6] from the reactions of primary amines with chloroform under alkaline conditions. Although these two methods only gave very limited yields, they remained the only preparative way to isonitriles until 1960, when Ugi and Meyr[7] reported the dehydration of formamides as a general method for isonitriles. This method is still one of the most commonly employed.

Although isonitriles closely mimic the steric and electronic properties of carbonyls, they exhibit a number of differences, often of advantage, over CO:

1. Probably the most important feature of isonitriles is that they contain an organic group that can be altered in order to fine-tune the metal complex electronically and sterically, and thereby influence its chemical and physical properties.

2. While the CO ligand can be considered as the prototype of π-acid ligands, requiring the synergic interaction of both σ-donation and π-acceptance in order to form stable metal complexes, isonitriles are good Lewis bases, but still have a π-acceptor ability as great as CO. Thus, they are also able to form bonds to metal atoms where only σ-donation is involved or where π-bonding is of little significance. The range of possible oxidation states (and with that the number of stable metal complexes) increases significantly. In $[Cr(CNPh)_6]^{n+}$ (n = 0, 1, 2, 3), for example, the metal can attain four different oxidation states while maintaining identical ligation[8].

---

[3] S. R. Sandler and W. Karo, *Organic Functional Group Preparations,* Vol. 12, Chapter 5, Academic Press, San Diego, 1989.
[4] W. Lieke, *Ann. Chem.*, 1859, **112**, 316.
[5] A. Gautier, *Ann. Chem.*, 1867, **142**, 289; 1868, **146**, 124; 1869, **151**, 239.
[6] A. W. Hofmann, *Ann. Chem.*, 1867, **144**, 114.
[7] I. Ugi and R. Meyr, *Chem. Ber.*, 1960, **93**, 239.
[8] D. A. Bohling and K. R. Mann, *Inorg. Chem.*, 1984, **23**, 1426.

3. Like carbon monoxide, isonitriles can occur as terminal or bridging ligands. The range of bonding modes is, however, greater for isonitriles, as they can incorporate heteroatoms on the R group or, in the case of diisonitriles, can act as chelating ligands.

4. Another consequence of the presence of the R group is the larger number of ligands available and with that a greater range of reactivity. Diisonitriles, for example, can link metal centres together to produce oligomers and polymers. These covalently-bridged polymers are useful in the design of supramolecular clusters exhibiting desirable chemical and physical properties[9].

4.2 Ligand design

Most work in transition-metal isonitrile chemistry has been carried out with the $CNBu^t$ ligand. Presumably, the fact that it is an air-stable liquid and can be prepared in very good yields makes it a popular ligand. Initially, an electrospray-friendly analogue was considered, but an appropriate counterpart for the $CNBu^t$ ligand did not seem straightforward to prepare. Thus, it appeared more reasonable to carry out work with different (but still electrospray-friendly) isonitriles. Figure 4.1 shows two potential candidates.

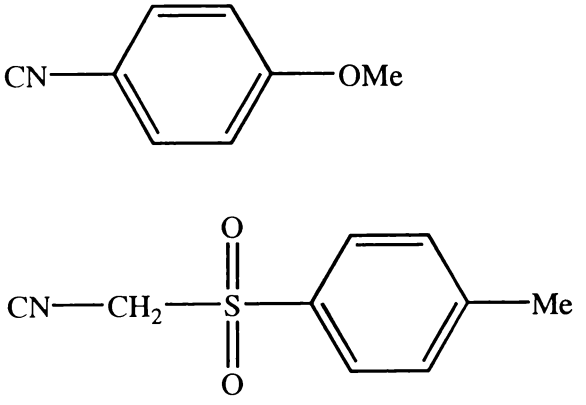

Fig. 4.1 The structures of two electrospray-friendly isonitriles.

---

[9] A. Efraty, I. Feinstein, F. and L. Wackerle, *J. Am. Chem. Soc.*, 1980, **102**, 6341; A. Efraty, I. Feinstein, F. Frolow and A. Goldman, *J. Chem. Soc., Chem. Commun.*, 1980, 864; M. J. Irwin, L. Manojlovic-Muir, K. W. Muir, R. J. Puddephatt and D. S. Yufit, *Chem. Commun.*, 1997, 219; M. J. Irwin, G. Jia, J. J. Vittal and R. J. Puddephatt, *Organometallics*, 1996, **15**, 5321.

The ligand CNPh* is the methoxy-functionalised version of the most simplest aromatic isonitrile ligand, CNPh. For the same reasons as illustrated in Chapter two, a methoxy group was incorporated into the ligand at the *para*-position. Hence, complexes of CNPh* should ionise by protonation in the ESMS. Tosylmethylisocyanide (TosMIC) should be electrospray-friendly because of its SO_2 group. A very small number of studies concerning the coordination chemistry of TosMIC has been published[10]. TosMIC can potentially coordinate through both the isonitrile carbon as well as the SO_2 function. However, to this date, no crystal structure has been reported where the SO_2 function is involved.

4.3 ESMS of the ligands

While the free CO ligand is not electron rich enough to associate with protons, isonitriles are known to be stronger Lewis bases. However, CNPh did not give any signals under standard conditions in the ESMS. The lone pair of electrons at the carbon atom did not seem to be sufficiently basic towards protons. In contrast, CNPh* provided the expected $[M + H]^+$ ion, most probably through protonation at the MeO group only.

The sulfone group in TosMIC can be considered a 'dioxide' and should therefore be basic enough to give an $[M + H]^+$ ion in the ESMS. Oxides of *e.g.* phosphines associate readily with available protons giving very intense $[M + H]^+$ signals. Surprisingly, TosMIC alone did not follow the same pattern, even when formic acid was added to enhance protonation. In order to investigate this phenomenon further, other sulfones were prepared and analysed under the same conditions. However, for both dimethyl and dibenzyl sulfone the same results were obtained. As far as three compounds allow general conclusions, it seems that this observation is common for sulfones. Hence, the SO_2 group cannot be used as a functional group for electrospray-friendly isonitrile ligands.

---

[10] M. J. Mays, D. W. Prest and P. R. Raithby, *J. Chem. Soc. Dalton Trans.*, 1981, 771; X.-H. Han and Y. Yamamoto, *J. Organomet. Chem.*, 1998, **561**, 157; M. Knorr and C. Strohmann, *Organometallics*, 1999, **18**, 248.

4.4 Some aspects of isonitrile complexes of $[Fe_3(CO)_{12}]$

4.4.1 $[Fe_3(CO)_{12}]$ and its isonitrile complexes

The advent of the first metal carbonyl cluster, $[Fe_3(CO)_{12}]$, is now almost 100 years old[11]. $[Fe_3(CO)_{12}]$ is often described as one of the most intriguing of triangular M_3 clusters. No other transition-metal complex has received as much attention in the elucidation of its solid state structure. In fact, it is said to be the archetypal carbonyl cluster showing metal atom disorder. In early 1964, after some thirty years and a large number of wrong propositions, the solid state structure of $[Fe_3(CO)_{12}]$ was eventually resolved. Desiderato and Dobson have summarised the long and exciting history of the structure determination[12]. X-ray crystallographic evidence for the structure was first given in 1966 by Wei and Dahl[13] and was refined by Cotton and Troup in 1974 [14]. The crystal structure is highly disordered and two bridging carbonyls span the same Fe–Fe bond. The structure of $[Fe_3(CO)_{12}]$ differs from its ruthenium (and osmium) analogue, which has only terminal CO ligands (shown in Figure 4.2).

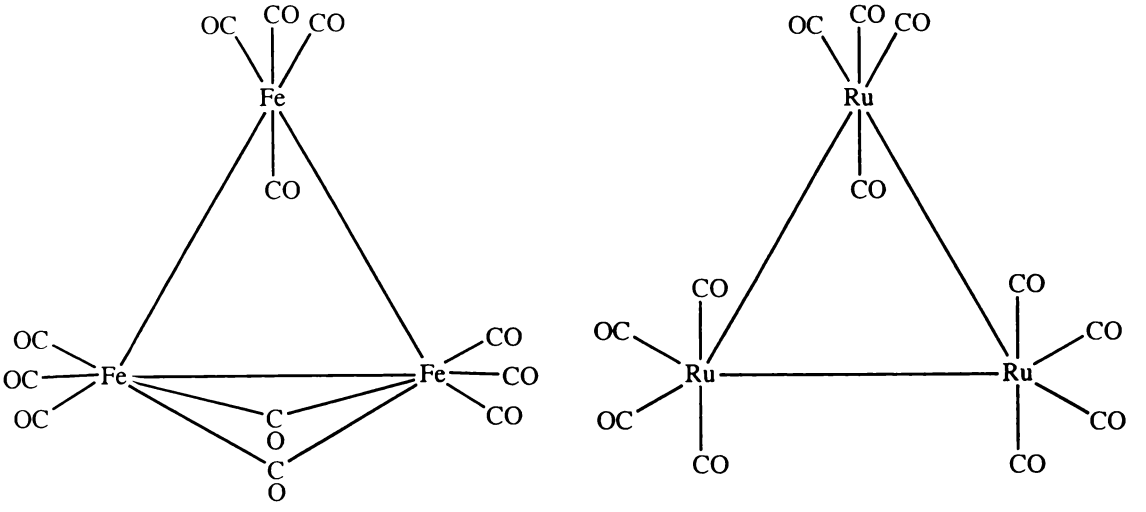

Fig. 4.2 The structures of $[Fe_3(CO)_{12}]$ and $[Ru_3(CO)_{12}]$.

---

[11] J. Dewar and H. O. Jones, *Proc. Roy. Soc. (London)*, 1905, **A76**, 558; J. Dewar and H. O. Jones, *Proc. Roy. Soc. (London)*, 1907, **A79**, 66.
[12] R. Desiderato and G. R. Dobson, *J. Chem. Ed.*, 1982, **59**, 752.
[13] C. H. Wei and L. F. Dahl, *J. Am. Chem. Soc.*, 1966, **88**, 1821; C. H. Wei and L. F. Dahl, *J. Am. Chem. Soc.*, 1969, **91**, 1351.
[14] F. A. Cotton and J. M. Troup, *J. Am. Chem. Soc.*, 1974, **96**, 3070.

There was (and still is) no general explanation for these structural differences and so studies regarding this phenomenon declined in numbers. When discovered that $[Fe_3(CO)_{12}]$ undergoes a dynamic process in the solid state[15], interest in this molecule was renewed. In solution, $[Fe_3(CO)_{12}]$ is highly fluxional, all CO ligands remaining equivalent down to a temperature of 123 K. There is an ongoing dispute about the exact mechanism of its solution and solid state fluxionality[16]. Among the techniques for examining the fluxional pathway there are a variety of dynamic NMR spectroscopy methods, variable-temperature X-ray crystallography, but also substitution of one or more CO ligands by phosphines or isonitriles, as they may not block certain mechanisms of CO migration.

All known isonitrile derivatives of $[Fe_3(CO)_{12}]$, together with the reported characterisation data are summarised in Table 4.1a (systems with ligands other than CO and RNC have been omitted). The known pyrolysis products are listed separately in Table 4.1b. Compared to phosphine derivatives of $[Fe_3(CO)_{12}]$, the number of compounds is amazingly small. It can also be seen how the numbers of studied ligands as well as the available characterisation data for the compounds shrink with the degree of substitution. $[Fe_3(CO)_{11}(CNBu^t)]$, $[Fe_3(CO)_{10}(CNBu^t)_2]$ and $[Fe_3(CO)_{11}(CNCF_3)]$ are the only derivatives whose structures have been determined. They are displayed in Figure 4.10 in section 4.4.3.

Table 4.1a The reported isonitrile derivatives of $[Fe_3(CO)_{12}]$.

Complex	R	X-ray struct.	other data available
$[Fe_3(CO)_{11}(CNR)]$	Bu^t	✓ [17,18]	mp, EA, MS, IR, ^1H NMR, ^{13}C NMR
	Xy	–	mp, EA, MS, IR, ^1H NMR, ^{13}C NMR[19]

[15] H. Dorn, B. E. Hanson and E. Motell, *Inorg. Chim. Acta*, 1981, **54**, L71; J. W. Gleeson and R. W. Vaughan, *J. Chem. Phys.*, 1983, **78**, 5384.
[16] B. F. G. Johnson and S. Tay, *Inorg. Chim. Acta*, 2002, **332**, 201; B. F. G. Johnson, *J. Chem. Soc. Dalton Trans.*, 1997, 1473; B. E. Mann, *J. Chem. Soc. Dalton Trans.*, 1997, 1457; L. J. Farrugia, *J. Chem. Soc. Dalton Trans.*, 1997, 1783; B. E. Hanson, E. C. Lisic, J. T. Petty and G. A. Iannaconne, *Inorg. Chem.*, 1986, **25**, 4062; D. Lentz and R. Marshall, *Organometallics*, 1991, **10**, 1487; D. Braga, F. Grepioni, L. J. Farrugia and B. F. G. Johnson, *J. Chem. Soc. Dalton Trans.*, 1994, 2911.
[17] M. I. Bruce, T. W. Hambley and B. K. Nicholson, *J. Chem. Soc., Chem. Commun.*, 1982, 353.
[18] M. I. Bruce, T. W. Hambley and B. K. Nicholson, *J. Chem. Soc. Dalton Trans.*, 1983, 2385.
[19] J. B. Murray, B. K. Nicholson and A. J. Whitton, *J. Organomet. Chem.*, 1990, **385**, 91.

	Me	–	–[20]
	CF_3	✓[21]	mp, MS, IR, ^{19}F NMR, ^{13}C NMR
$[Fe_3(CO)_{10}(CNR)_2]$:	Bu^t	✓[19]	mp, MS, IR, ^1H NMR, ^{13}C NMR
	Xy	–	IR, ^1H NMR[19]
	Me	–	–[20]
$[Fe_3(CO)_9(CNR)_3]$	Bu^t	–	mp, MS, IR, ^1H NMR, ^{13}C NMR[19]
	Xy	–	MS, IR[19]
$[Fe_3(CO)_8(CNR)_4]$	Bu^t	–	EA, MS, IR[22]

Table 4.1b The reported pyrolysis products of isonitrile derivatives of $[Fe_3(CO)_{12}]$.

Complex	R	X-ray struct.	other data available
$[Fe_3(CO)_9(\mu_3\text{-}\eta^2\text{-}CNR)]$	Bu^t	✓[18]	mp, EA, MS, IR, ^1H NMR, ^{13}C NMR
$[Fe_3(CO)_8(\mu_3\text{-}\eta^2\text{-}CNR)(CNR)]$	Bu^t	–	mp, EA, MS, IR[18]

While a fair amount of work has been carried out on $CNBu^t$ derivatives of $[Fe_3(CO)_{12}]$, there is still a number of unanswered questions. One of them is the possible extent of substitution by isonitrile ligands as well as the isolation and characterisation of the detected species. Substitution products of the type $[Fe_3(CO)_{12-n}(CNR)_n]$ are known for n = 1-4. The synthesis of complexes, where n is any higher than three, is known to be difficult[20]. $[Fe_3(CO)_8(CNBu^t)_4]$ is the only tetra-substituted isonitrile complex of $[Fe_3(CO)_{12}]$ to date. It was found that these types of complexes decompose readily in solution into monomeric species. Therefore, no ^{13}C NMR spectra could be recorded and attempts to obtain suitable crystals for X-ray analysis were unsuccessful. ESMS is an excellent tool for detecting higher-substituted products as compounds do not have to be crystalline or isolated, nor do they have to be stable for a long period of time.

---

[20] S. Grant, J. Newman and A. R. Manning, *J. Organomet. Chem.*, 1975, **96**, C11.
[21] I. Brüdgam, H. Hartl and D. Lentz, *Z. Naturforsch.*, 1984, **39b**, 721.
[22] X. Chen and B. E. Mann, *Chem. Commun.*, 1997, 2233.

$[Fe_3(CO)_9(\mu_3\text{-}\eta^2\text{-}CNBu^t)]$ is the best characterised pyrolysis product so far and is obtained by thermal rearrangement of $[Fe_3(CO)_{11}(CNBu^t)]$. In $[Fe_3(CO)_9(\mu_3\text{-}\eta^2\text{-}CNBu^t)]$, the triply-bridging isonitrile ligand lies across the face of the metal triangle and donates six electrons in a $\sigma + 2\pi$ fashion. The structure of this complex is given in Figure 4.3. Equivalent species for other isonitriles have never been reported. Other products are known to form as well, but have not been characterised (other than by IR). By means of ESMS, it should be possible to confirm the formation of the reported as well as detect any other species present in solution.

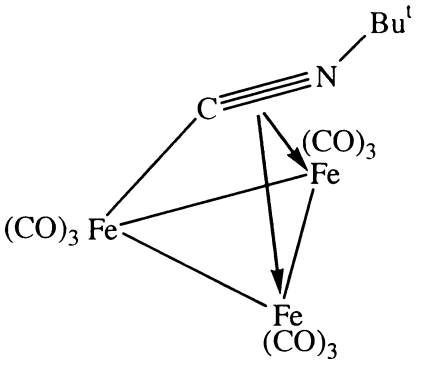

Fig. 4.3 The structure of $[Fe_3(CO)_9(\mu_3\text{-}\eta^2\text{-}CNBu^t)]$.

4.4.2 ESMS of isonitrile derivatives of $[Fe_3(CO)_{12}]$

4.4.2.1 Reactions of isonitriles with $[Fe_3(CO)_{12}]$ at room temperature

Stirring $[Fe_3(CO)_{12}]$ with four equivalents of isonitrile at room temperature yielded a number of substitution products according to tlc. The crude reaction products were analysed by ESMS. Figure 4.4 shows the spectrum for CNPh*. Although this spectrum looks like a 'forest of peaks' it was actually straightforward to assign. The trinuclear iron complex substituted its CO ligands consecutively and $[M + H]^+$ peaks according to the tri-, tetra-, and penta-substituted products were detected. Furthermore, there was a series of peaks attributable to the dinuclear iron complex $[Fe_2(CO)_9]$, which is a decomposition product of the parent complex $[Fe_3(CO)_{12}]$. This substituted as well yielding the corresponding tetra-, penta- and hexa-substituted products. Another by-product in this reaction was the mononuclear $[Fe(CO)_5]$, which substituted CO ligands to produce compounds ranging from di- to the fully-substituted $[Fe(CNPh^*)_5]$. The observed ions

are summarised in Table 4.2. The detection of this wide number of substitution products was very interesting as, according to tlc, only three major products seemed to have formed. Thus, ESMS is a simple and straightforward method to show how many simultaneous reactions are occurring, with detection of not only the major but also by-products.

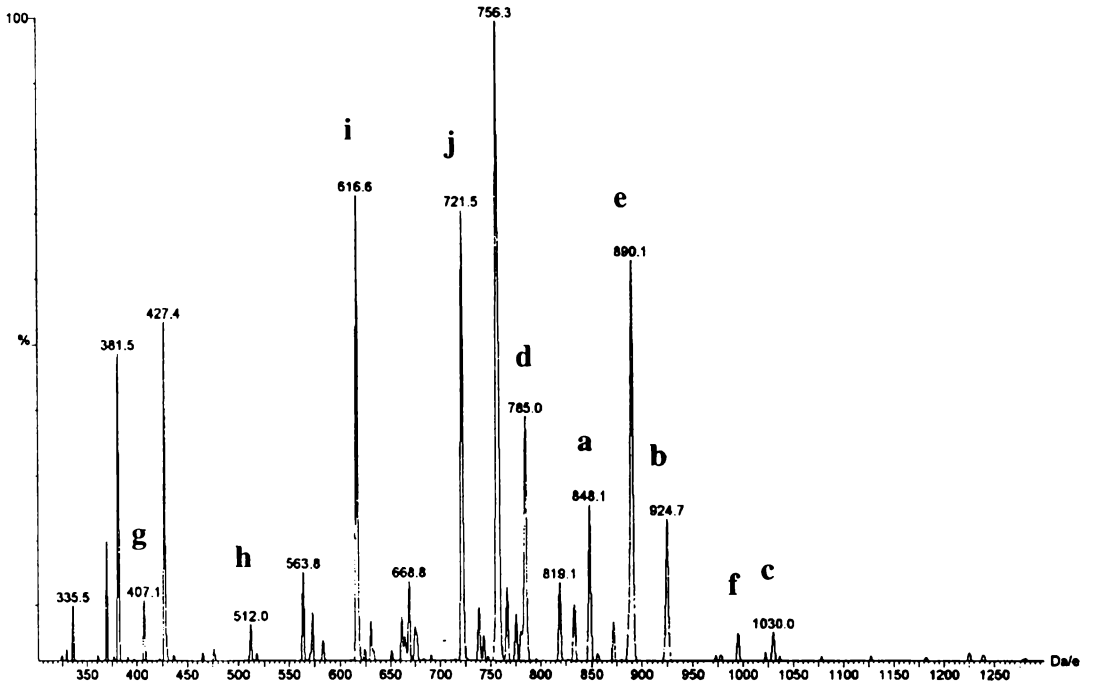

Fig. 4.4 The positive-ion ES mass spectrum of the crude reaction mixture of $[Fe_3(CO)_{12}]$ and CNPh*, recorded in MeOH at cV = 10 V.

Table 4.2 The detected substitution products in the reaction between $[Fe_3(CO)_{12}]$ and CNPh*.

Complex	Substitution products		*m/z* [23]
$[Fe_3(CO)_{12}]$	$[Fe_3(CO)_9(CNPh^*)_3]$	**a**	819
	$[Fe_3(CO)_8(CNPh^*)_4]$	**b**	925
	$[Fe_3(CO)_7(CNPh^*)_5]$	**c**	1030
$[Fe_2(CO)_9]$	$[Fe_2(CO)_5(CNPh^*)_4]$	**d**	785

[23] The *m/z* values correspond to the respective $[M + H]^+$ ions.

	$[Fe_2(CO)_4(CNPh^*)_5]$	**e**	890
	$[Fe_2(CO)_3(CNPh^*)_6]$	**f**	995
$[Fe(CO)_5]$	$[Fe(CO)_3(CNPh^*)_2]$	**g**	407
	$[Fe(CO)_2(CNPh^*)_3]$	**h**	512
	$[Fe(CO)(CNPh^*)_4]$	**i**	617
	$[Fe(CNPh^*)_5]$	**j**	722

In the reaction between CNPh and $[Fe_3(CO)_{12}]$, very similar results were obtained. The mono- and di-substituted products did not appear in the spectrum of the crude reaction solution. However, additionally, a peak at *m/z* 955 (though of low intensity) was observed and tentatively assigned to $[Fe_3(CO)_6(CNPh)_6]$. Unlike in the reaction with CNPh*, no breakdown of the original cluster was observed. The detected species are listed in Table 4.3.

Table 4.3 The detected substitution products in the reaction between $[Fe_3(CO)_{12}]$ and CNPh, recorded in MeOH at cV = 20 V.

Substitution products	*m/z* [23]	Intensity (%)
unassigned	646	100
$[Fe_3(CO)_9(CNPh)_3]$	730	77
$[Fe_3(CO)_8(CNPh)_4]$	805	8
$[Fe_3(CO)_7(CNPh)_5]$	880	6
$[Fe_3(CO)_6(CNPh)_6]$	955	4

These results were particularly interesting, as the ligand CNPh was not considered electrospray-friendly. However, its complexes yielded spectra of the same quality as were obtained for CNPh*. Ionisation by formation of radicals (instead of $[M + H]^+$ ions) attributable to redox processes in the instrument has been observed before for other neutral molecules that do not contain a basic group (this process has been discussed in detail in Chapter one). In this case, however, the signals corresponded to $[M + H]^+$ ions, which was confirmed by recording the high-resolution isotope patterns. This phenomenon has been observed before for the ruthenium complex $[Ru_3(CO)_9(PPh_3)_3]$, which also lacks a basic site for protonation (refer to Chapter two). It was speculated that the three phosphine ligands donate enough electron density into the ruthenium triangle to increase the basicity of the metal-metal bonds. Isonitrile ligands are, however, poorer electron-donors than phosphines. In the case of $[Fe_3(CO)_{12}]$ derivatives,

protonation might also occur on the bridging CO groups, since they are believed to be of more basic character than terminal CO ligands[24]. A further site for electrophilic attack is at the unsaturated bonds in the ligand itself. Addition of electrophilic reagents (E^+) to acetylide complexes according to Scheme 4.1 is known[25], and might occur in a similar manner for isonitriles.

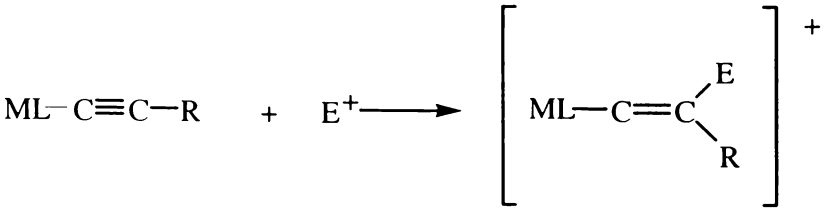

Scheme 4.1 The protonation mechanism proposed for acetylides.

In both reactions involving CNPh and CNPh*, the efficiency of ionisation appeared to increase with the degree of substitution. In fact, the mono- and di-substituted products of $[Fe_3(CO)_{12}]$ were not observed at all (although they had been formed as the major fractions according to tlc). Considering the fact that with a higher degree of substitution more electrospray-friendly ligands were present, this did initially not seem surprising. However, as the same results were obtained with the CNPh ligand, the higher ionisation efficiency appeared to depend on the degree of substitution, rather than on the number of methoxy groups. Isonitrile ligands are stronger σ-donors than CO and will therefore increase the electron-density in the metal cluster, supporting the theory that protonation occurs either at the metal-metal bonds or bridging CO ligands, as discussed earlier. Wherever the site for protonation, for the first time evidence for the formation of $[Fe_3(CO)_7(CNR)_5]$ (R = Ph, Ph*) and $[Fe_3(CO)_6(CNR)_6]$ (R = Ph) was detected. These highly-substituted species are probably extremely air-sensitive, but ESMS is an excellent tool for analysing air-sensitive compounds. Compounds can be injected directly from the reaction flask and therefore stay under a nitrogen atmosphere throughout.

Equivalent reactions using TosMIC provided similar results. The positive-ion ES mass spectrum of the crude product of the reaction between $[Fe_3(CO)_{12}]$ and TosMIC is displayed in Figure 4.5a and a list of observed ions is given in Table 4.4.

---

[24] C. P. Horwitz and D. F. Shriver, *Adv. Organomet. Chem.*, 1984, **23**, 219.

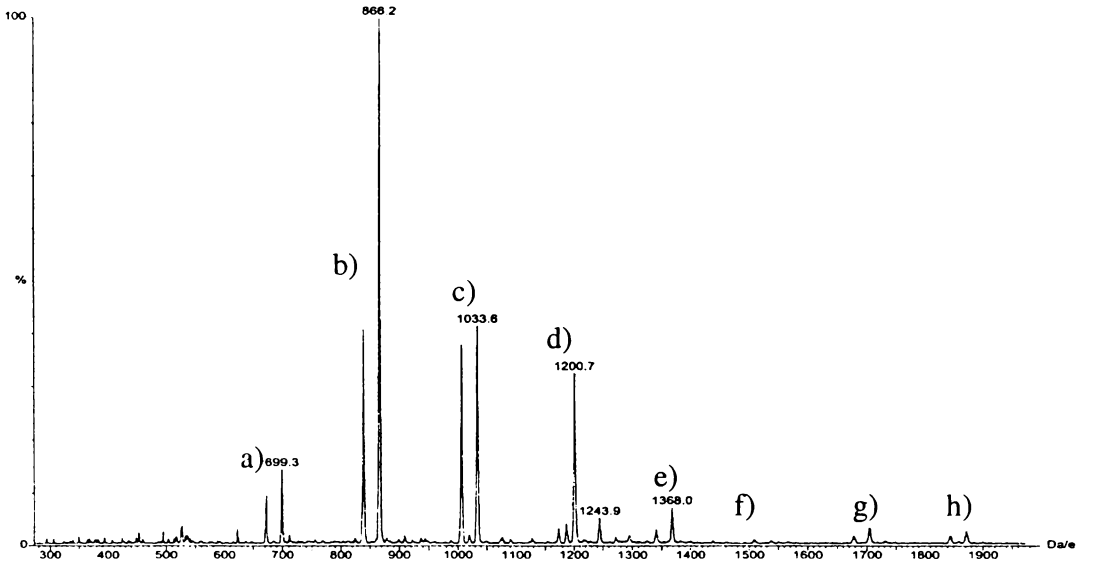

Fig. 4.5a The positive-ion ES mass spectrum of the crude reaction solution of $[Fe_3(CO)_{12}]$ and TosMIC, recorded in MeOH at cV = 20 V.

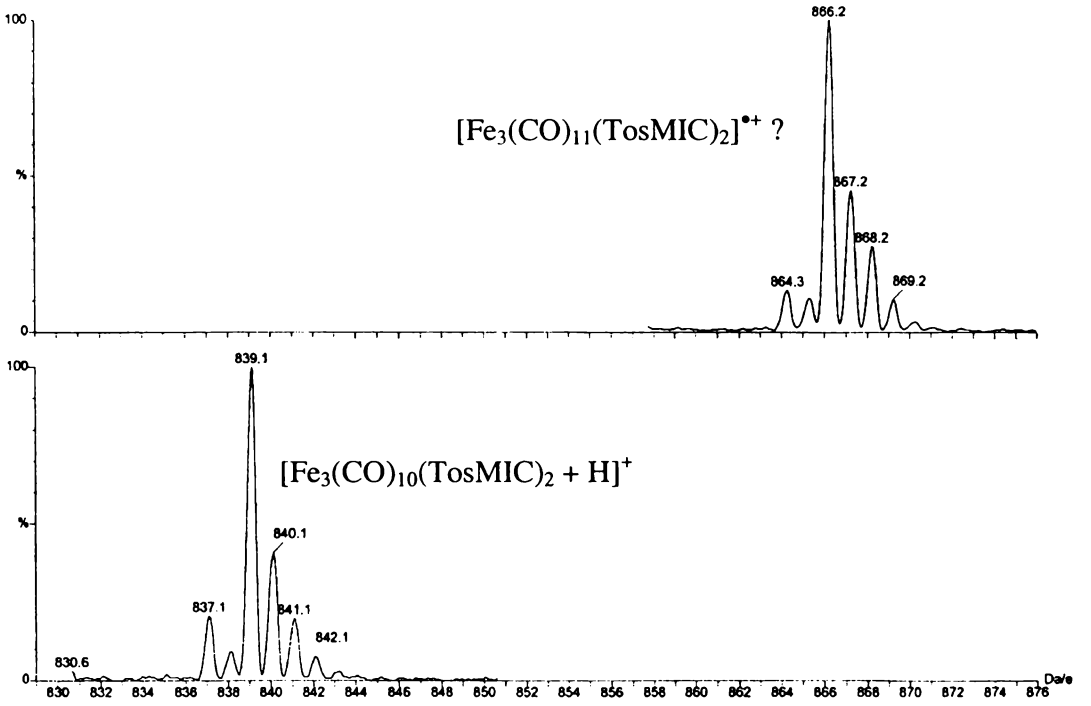

Fig. 4.5b The observed isotope patterns of the peaks at *m/z* 866 (top) and *m/z* 839 (bottom).

---

[25] M. I. Bruce and A. G. Swincer, *Adv. Organomet. Chem.*, 1983, **22**, 59; A. Davison and J. P. Selegue, *J. Am. Chem. Soc.*, 1978, **100**, 7763; M. I. Bruce and R. C. Wallis, *J. Organomet. Chem.*, 1978, **161**, C1.

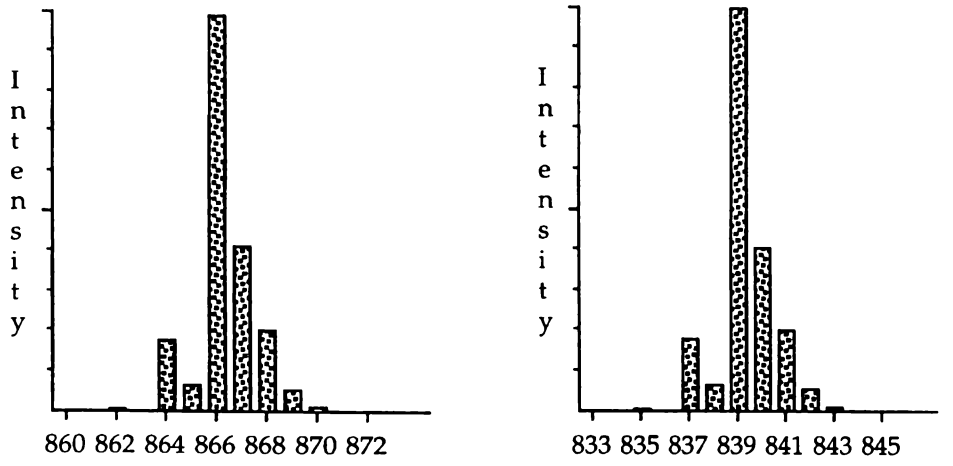

Fig. 4.5c The calculated isotope patterns of the peaks at *m/z* 866 (left) and *m/z* 839 (right).

Table 4.4 The detected products in the reaction between $[Fe_3(CO)_{12}]$ and TosMIC, recorded in MeOH at cV = 20 V.

	Products	*m/z*
a)	$[Fe_3(CO)_{11}(TosMIC) + H]^+$	672
	$[Fe_3(CO)_{12}(TosMIC)]^{\bullet+}$	699
b)	$[Fe_3(CO)_{10}(TosMIC)_2 + H]^+$	839
	$[Fe_3(CO)_{11}(TosMIC)_2]^{\bullet+}$	866
c)	$[Fe_3(CO)_9(TosMIC)_3 + H]^+$	1006
	$[Fe_3(CO)_{10}(TosMIC)_3]^{\bullet+}$	1033
d)	$[Fe_3(CO)_8(TosMIC)_4 + H]^+$	1173
	$[Fe_3(CO)_9(TosMIC)_4]^{\bullet+}$	1201
e)	$[Fe_3(CO)_7(TosMIC)_5 + H]^+$	1340
	$[Fe_3(CO)_8(TosMIC)_5]^{\bullet+}$	1368
f)	$[Fe_3(CO)_6(TosMIC)_6 + H]^+$	1507
	$[Fe_3(CO)_7(TosMIC)_6]^{\bullet+}$	1538
g)	$[2\{Fe_3(CO)_{10}(TosMIC)_2\} + H]^+$	1677
	$[2\{Fe_3(CO)_{11}(TosMIC)_2\}]^{\bullet+}$	1704
h)	$[2\{Fe_3(CO)_9(TosMIC)_3\} + H]^+$	1844
	$[2\{Fe_3(CO)_{10}(TosMIC)_3\}]^{\bullet+}$	1871

As before, substitution of the $[Fe_3(CO)_{12}]$ cluster by the isonitrile ligand was observed. In addition, all peaks arising from substitution of the metal carbonyl cluster were accompanied by a second signal with a mass difference of 27 amu with regard to a known species of the type $[Fe_3(CO)_{12-n}(TosMIC)_n]$. One possibility was the addition of cyanide (although this would effectively be a mass gain of only 26), which might be formed during the reaction (TosMIC is known to be a reagent for a convenient preparation of nitriles[26]). In an attempt to confirm this assignment, NaCN was added to samples of substituted $[Fe_3(CO)_{12}]$ derivatives. However, an increase in the +27 peaks was not observed. The only change in the spectrum was that some additional peaks according to $[M + Na]^+$ ions were observed. It has been observed[27] that TosMIC can, instead of substituting, add to a metal complex – a phenomenon that cannot yet be explained electronically. In that particular case, the addition products of TosMIC to a cobalt carbonyl cluster were detected in the ESMS as radical cations. In the reaction of $[Fe_3(CO)_{12}]$ and TosMIC, the recorded isotope patterns (shown in Figure 4.5b) show clearly, that the mass difference is exactly +27, so that addition of the ligand can only be considered if the resulting species ionise through formation of radical cations. Although a sudden change in the ionisation mechanism from $[M + H]^+$ to $[M]^{\bullet+}$ ions seems at first unlikely, it is possible and also reasonable from an electronic point of view. Addition of the ligand most likely results in scission of an Fe–Fe bond. This leads to an overall electron-rich species, which can undergo oxidation relatively easily to form radical cations. Attack on an intact cluster as a mechanism for substitution reactions is not new. The literature proposes a mechanism for ligand substitution that involves initial addition of L with concomitant scission of the M–M bond in the reaction between $[Co_4(CO)_{10}(PPh)_2]$ and $P(OMe)_3$ [28]. The additional peaks observed in the reaction between $[Fe_3(CO)_{12}]$ and TosMIC appeared to be similar intermediates, especially as these ions were no longer observed when analysing isolated fractions.

The major fractions for all three ligands were separated by chromatography and subsequently analysed by ESMS. This is a very straightforward way of determining which fraction corresponds to which compound, and requires only smallest amounts of

---

[26] Aldrich Catalogue. Handbook of fine Chemicals, 1996-1997, p.1438.
[27] C. Evans, personal communication.
[28] M. G. Richmond and J. K. Kochi, *Inorg. Chem.*, 1986, **25**, 1334.

sample[29]. As an example, the spectrum of the fifth fraction in the reaction with CNPh, $[Fe_3(CO)_8(CNPh)_4]$, is shown in Figure 4.6a. The recorded and calculated isotope patterns (Figure 4.6b) confirm the assignment.

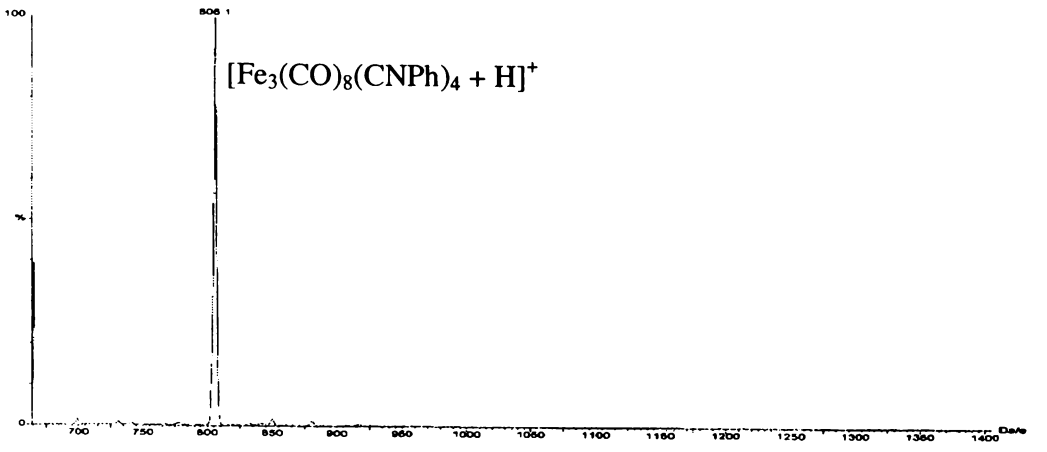

Fig 4.6a The positive-ion ES mass spectrum of $[Fe_3(CO)_8(CNPh)_4]$, recorded in MeOH at cV = 20 V.

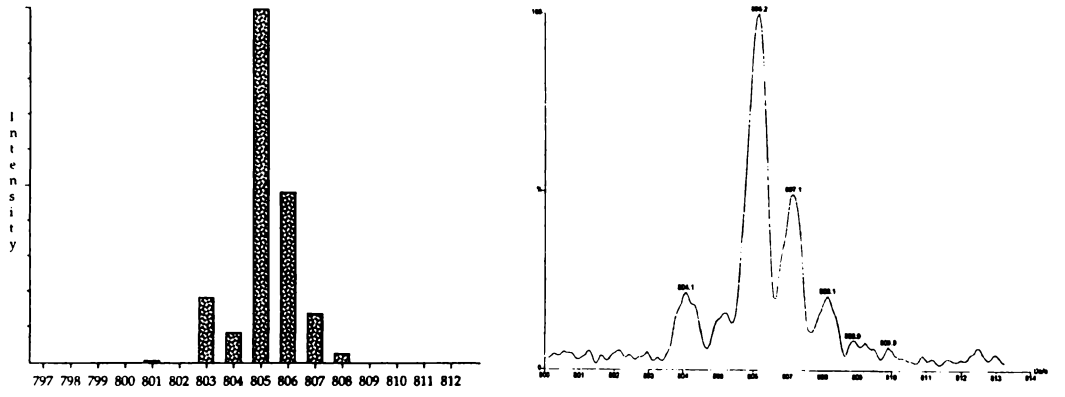

Fig 4.6b The calculated (left) and observed (right) isotope patterns of $[Fe_3(CO)_8(CNPh)_4 + H]^+$.

The first fraction, $[Fe_3(CO)_{12}]$, did not give a signal in the positive-ion mode of the ESMS. All substituted products $[Fe_3(CO)_{12-n}(CNR)_n]$ (n = 1 – 4) gave clean spectra with the $[M + H]^+$ peaks being the only major signal. ESMS signals of all mono-substituted $[Fe_3(CO)_{11}(CNR)]$ samples could only be obtained when injecting a very concentrated

[29] In fact, it was found that the fractions obtained from tlc plates of *ca.* 5 cm width were sufficient for an

solution of the sample. Whenever these compounds were not pure, only a weak signal appeared with an additional very intense peak for the following di-substituted complex. This confirms the assumption made earlier that the lower-substituted species are relatively electron-poor, and thus do not protonate very well. In the case of TosMIC-substituted products, the +27 peaks were no longer detected after isolation of each fraction. Instead, $[2M + H]^+$ peaks were observed for all TosMIC derivatives.

The most satisfactory yields for the synthesis of mono- to tetra-substituted products were obtained by using a ratio of 1:4 mole equivalents of metal cluster to ligand. Substitution occurred readily for up to four ligands, and these compounds separated well on chromatography plates. Attempts were made to isolate compounds for $n > 4$. However, the addition of an excess of ligand did not produce higher-substituted compounds in a better yield. Instead, it made it impossible to get a good separation by chromatography because the excess amount of ligand overloaded the lower region of the chromatography plates. The reaction solutions were typically stirred for two hours at room temperature. Heating the reaction resulted in the formation of other products (*vide infra*). Stirring the reaction mixture for longer than two hours resulted in breakdown of the cluster. In solution, the Fe_3-complexes were only stable for a longer period of time if stored at -20°C.

4.4.2.2 Negative-ion mode studies

When working with TosMIC derivatives of $[Fe_3(CO)_{12}]$, in particular when checking chromatography fractions, it was discovered that all of the samples also gave signals in the negative-ion mode. The first fraction, $[Fe_3(CO)_{12}]$, formed the radical anion $[Fe_3(CO)_{12}]^{\bullet-}$, and spectra at various cone voltages are shown in Figure 4.7. Although no external reducing agent was added, radical anions of metal carbonyls can be formed through a number of processes. Redox processes in the ESMS instrument have been extensively studied, and are summarised in Chapter one. The formation of $[Fe_3(CO)_{12}]^{\bullet-}$

ESMS analysis.

in THF followed by disproportionation has also been reported[30], as has the reaction with impurities[31], such as PPh_3O according to:

$$2\ [Fe_3(CO)_{12}] + PPh_3O \rightarrow [Fe_3(CO)_{12}]^{\bullet-} + [Fe_2(CO)_8]^{\bullet-} + [Fe(OPPh_3)_n]^{2+} + 4\ CO$$

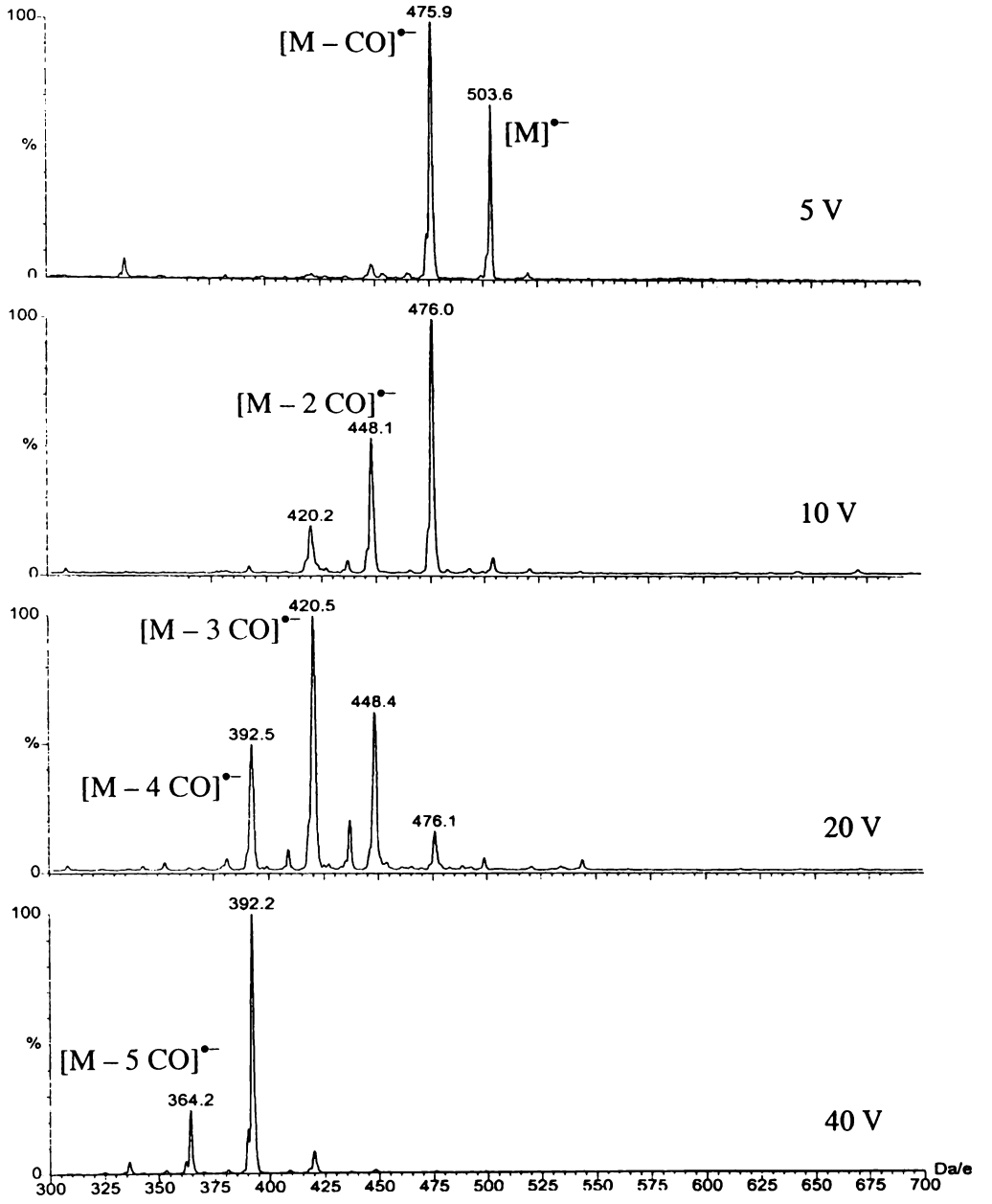

Fig. 4.7 The negative-ion ES mass spectra of $[Fe_3(CO)_{12}]$, recorded in MeOH at various cone voltages.

---

[30] P. A. Dawson, B. M. Peake, B. H. Robinson and J. Simpson, *Inorg. Chem.*, 1980, **19**, 465.
[31] F.-H. Luo, S.-R. Yang, C.-S. Li, J.-P. Duan and C.-H. Cheng, *J. Chem. Soc. Dalton Trans.*, 1991, 2435.

TosMIC-substituted derivatives of $[Fe_3(CO)_{12}]$ gave $[M - H]^-$ ions according to the proton abstraction mechanism. Spectra were of better quality for complexes with fewer isonitrile ligands. This agrees with the findings in positive-ion mode. For more electron-deficient clusters, the preferred ionisation method is proton abstraction, whereas for the higher-substituted clusters, protonation is preferred. Thus, depending on conditions and degree of substitution, isonitrile derivatives of $[Fe_3(CO)_{12}]$ can undergo either or both ionisation pathways.

It should be noted that, depending on the conditions, the $[M + MeO]^-$ ion could also be observed for $[Fe_3(CO)_{12}]$. MeO^- anions are present if MeOH is used as the mobile phase. However, when formic acid was added, the formation of the $[M + MeO]^-$ ion was subdued and the radical anion $[Fe_3(CO)_{12}]^{\bullet-}$ was the most intense peak. The $[M + MeO]^-$ ion was the only peak when NaOMe was added to the solution. Nucleophilic attack by MeO^- at the CO ligand of metal carbonyl clusters is known and has been studied by ESMS for a wide range of binary and substituted metal carbonyl clusters, including one isonitrile, $[Fe_3(CO)_{11}(CNBu^t)]$ [32].

4.4.2.3 Reactions with $[Fe_3(CO)_{12}]$ at elevated temperatures

Following the same procedure as previously reported for R = Bu^t [18], $[Fe_3(CO)_{11}(CNR)]$ and $[Fe_3(CO)_{10}(CNR)_2]$ (R = Ph, Ph*) were gently heated to 75°C, and the reactions followed by ESMS.

The positive-ion spectrum was overall relatively weak in intensity, but a few features should be noted. Starting from only one peak due to the $[M + H]^+$ ions of the parent compound, a rather large number of new peaks arose during the reaction. Heating the solution obviously resulted in the formation of higher-substituted products, such as $[Fe_3(CO)_{10}(CNPh)_2]$, $[Fe_3(CO)_9(CNPh)_3]$ and $[Fe_3(CO)_8(CNPh)_4]$ in the case of $[Fe_3(CO)_{11}(CNPh)]$. At the same time, breakdown of the Fe_3-triangle led to the formation of various decomposition products. The previously reported product of the type $[Fe_3(CO)_9(\mu_3\text{-}\eta^2\text{-}CNPh)]$ was, however, not detected.

---

[32] W. Henderson, J. S. McIndoe, B. K. Nicholson and P. J. Dyson, *J. Chem. Soc. Dalton Trans.*, 1998, 519.

When switching to negative-ion mode, different results were obtained, as can be seen in Figure 4.8, which shows the spectrum of the crude solution in the reaction of $[Fe_3(CO)_{11}(CNPh)]$.

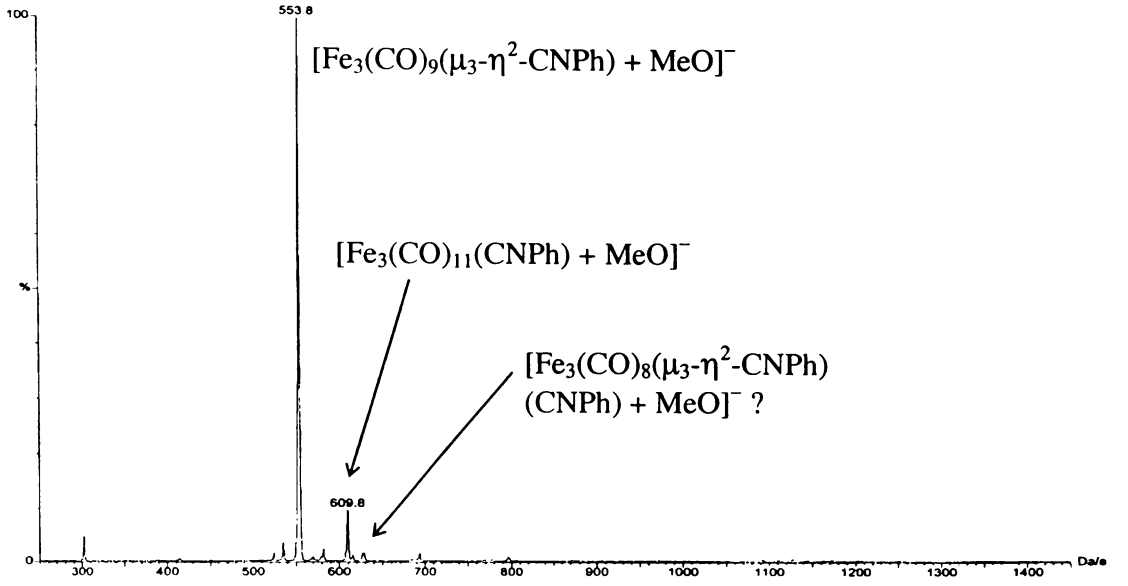

Fig. 4.8 The negative-ion ES mass spectrum of the crude solution of the pyrolysis reaction of $[Fe_3(CO)_{11}(CNPh)]$, recorded in MeOH at cV = 5 V.

The negative-ion spectrum clearly showed the previously reported species as its $[M + MeO]^-$ ion. Residual starting material as well as traces of $[Fe_3(CO)_8(\mu_3\text{-}\eta^2\text{-}(CNPh)(CNPh)]$ could also be detected. Although no ionisation aid had been added deliberately, $[M + MeO]^-$ ions were detected when using MeOH as the mobile phase, as observed previously for $[Fe_3(CO)_{12}]$. It should be mentioned that the addition of MeO^- is not entirely surprising, since $[Fe_3(CO)_9(\mu_3\text{-}\eta^2\text{-}CNBu^t)]$ was found to add H^- readily at the C atom of the triply-bridging isonitrile ligand[18].

Weak signals of $[Fe_3(CO)_9(\mu_3\text{-}CNR) + H]^+$ ions were also observed in positive-ion mode, but only after these species had been isolated and when analysing them as very concentrated solutions (similar to the lower-substituted species discussed in section 4.4.2.2).

Similar results were obtained with other substrates and ligands and the formed products are summarised in Table 4.5. It therefore seems that the thermal rearrangement of

$[Fe_3(CO)_{12-n}(CNR)_n]$ (n = 1, 2) is a general reaction, yielding complexes of the type $[Fe_3(CO)_{9-m}(\mu_3\text{-}\eta^2\text{-}CNR)(CNR)_m]$ (m = 0, 1) as the only major products.

Table 4.5 The major products detected in the pyrolysis reactions of $[Fe_3(CO)_{12-n}(CNR)_n]$ (n = 1, 2).

Substrate	Major product
$[Fe_3(CO)_{11}(CNPh)]$	$[Fe_3(CO)_9(\mu_3\text{-}\eta^2\text{-}CNPh)]$
$[Fe_3(CO)_{10}(CNPh)_2]$	$[Fe_3(CO)_8(\mu_3\text{-}\eta^2\text{-}CNPh)(CNPh)]$
$[Fe_3(CO)_{11}(CNPh^*)]$	$[Fe_3(CO)_9(\mu_3\text{-}\eta^2\text{-}CNPh^*)]$
$[Fe_3(CO)_{10}(CNPh^*)_2]$	$[Fe_3(CO)_8(\mu_3\text{-}\eta^2\text{-}CNPh^*)(CNPh^*)]$

4.4.3 X-ray crystal structure determinations of $[Fe_3(CO)_{10}(CNPh)_2]$

Crystal structures of the mono- and di-substituted $[Fe_3(CO)_{12}]$ with $CNBu^t$ have been available since 1982 and 1990, respectively. The only other crystal structure of the type $[Fe_3(CO)_{12-n}(CNR)_n]$ is for n = 1 and R = CF_3, where $CNCF_3$ occupies a bridging position. The structures of all three complexes are displayed in Figure 4.9 (for details refer to Table 4.1).

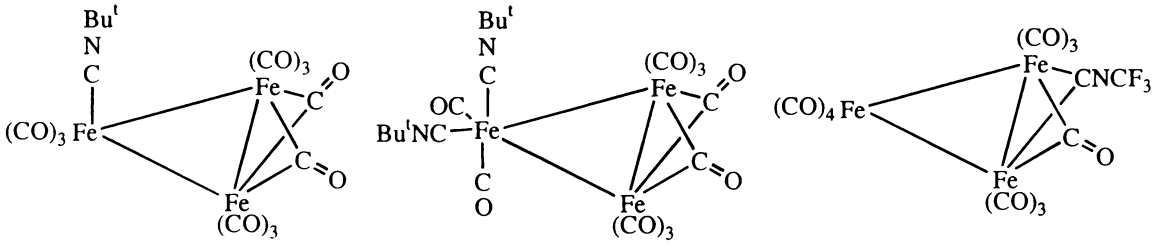

Fig. 4.9 The structures of the known isonitrile derivatives of $[Fe_3(CO)_{12}]$. From left to right: $[Fe_3(CO)_{11}(CNBu^t)]$, $[Fe_3(CO)_{10}(CNBu^t)_2]$ and $[Fe_3(CO)_{11}(CNCF_3)]$.

In $[Fe_3(CO)_{11}(CNBu^t)]$, the basic $[Fe_3(CO)_{12}]$ structure is preserved with the isonitrile ligand occupying an axial site on the non-bridged iron atom. Surprisingly, in $[Fe_3(CO)_{12}(CNBu^t)_2]$, both isonitrile ligands were found to be on the unique iron atom, one in an axial and the other in an equatorial site. $[Fe_3(CO)_{10}(\mu_2\text{-}CO)(\mu_2\text{-}CNCF_3)]$ differs from the two complexes discussed above, as the isonitrile occupies one of the two

bridging positions. There is no disorder for any derivative.

4.4.3.1 X-ray crystal structure determination of $[Fe_3(CO)_{10}(CNPh)_2]$ at low temperature (100 K)

Single crystals of $[Fe_3(CO)_{10}(CNPh)_2]$ were obtained from a concentrated CH_2Cl_2 solution that was slowly cooled to -20°C. The cluster crystallized unsolvated with four molecules in the unit cell, space group $P2_1/c$. The structure of $[Fe_3(CO)_{10}(CNPh)_2]$ is shown in Figure 4.10a (including full atom labelling) and from a different angle in Figure 4.10b. Selected bond parameters are provided in Table 4.6, while full lists of atomic coordinates, temperature factors, bond lengths, and bond angles are supplied in Appendix A. Data relating to the structure solution are listed in the Experimental section of this chapter.

Table 4.6 Selected bond lengths (Å) and bond angles (°) for $[Fe_3(CO)_{10}(CNPh)_2]$.

Fe(1)–Fe(2)	2.6921(11)	Fe(1)–C(1)	1.871(6)
Fe(1)–Fe(3)	2.6918(11)	Fe(1)–C(2)	1.853(6)
Fe(2)–Fe(3)	2.5594(11)		
Fe–C(equ.)	1.795(7) - 1.807(6)	C(1)–N(1)	1.143(6)
Fe–C(ax.)	1.807(6) - 1.818(6)	C(2)–N(2)	1.155(7)
C(1)–N(1)–C(11)	176.1(6)		
C(2)–N(2)–C(21)	176.3(6)		
C(1)–Fe(1)–C(2)	179.3(2)		

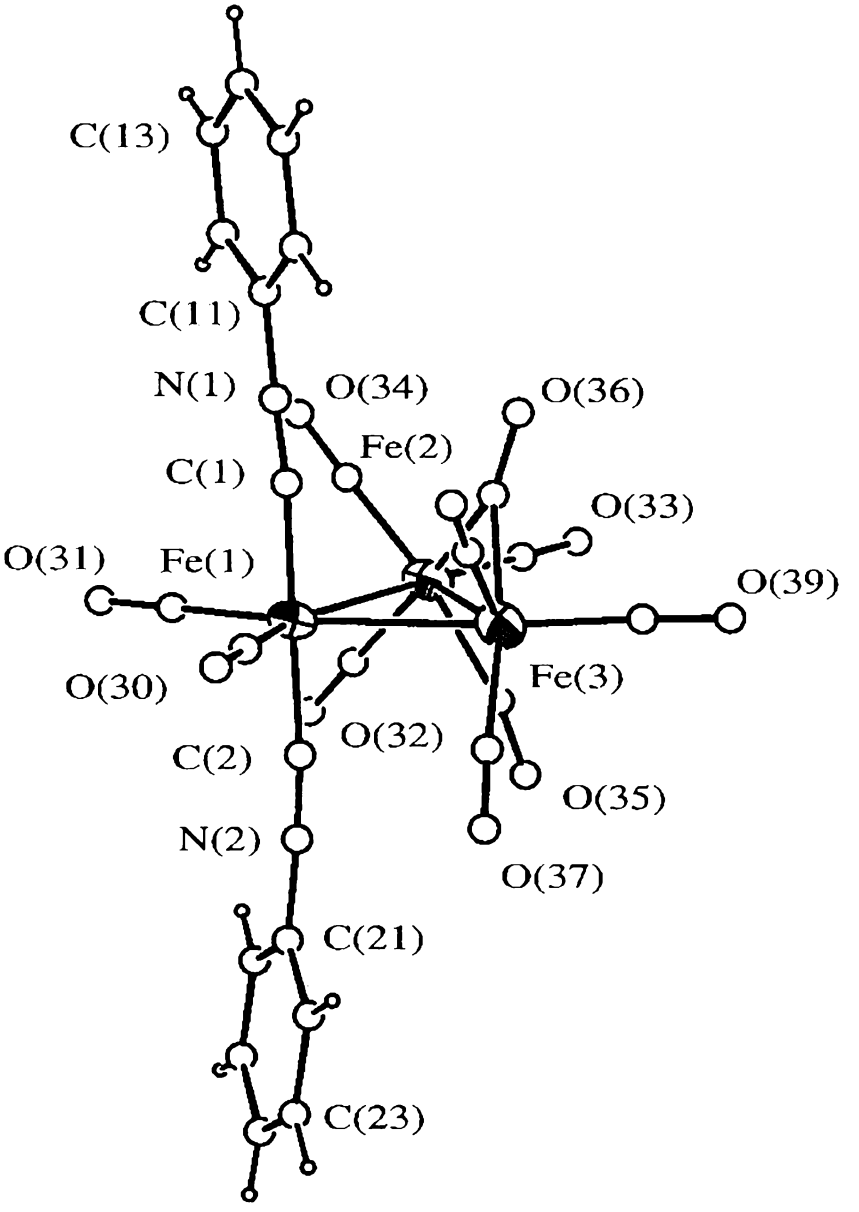

Fig. 4.10a The solid state structure of $[Fe_3(CO)_{10}(CNPh)_2]$ at low temperature, showing the atom-numbering scheme.

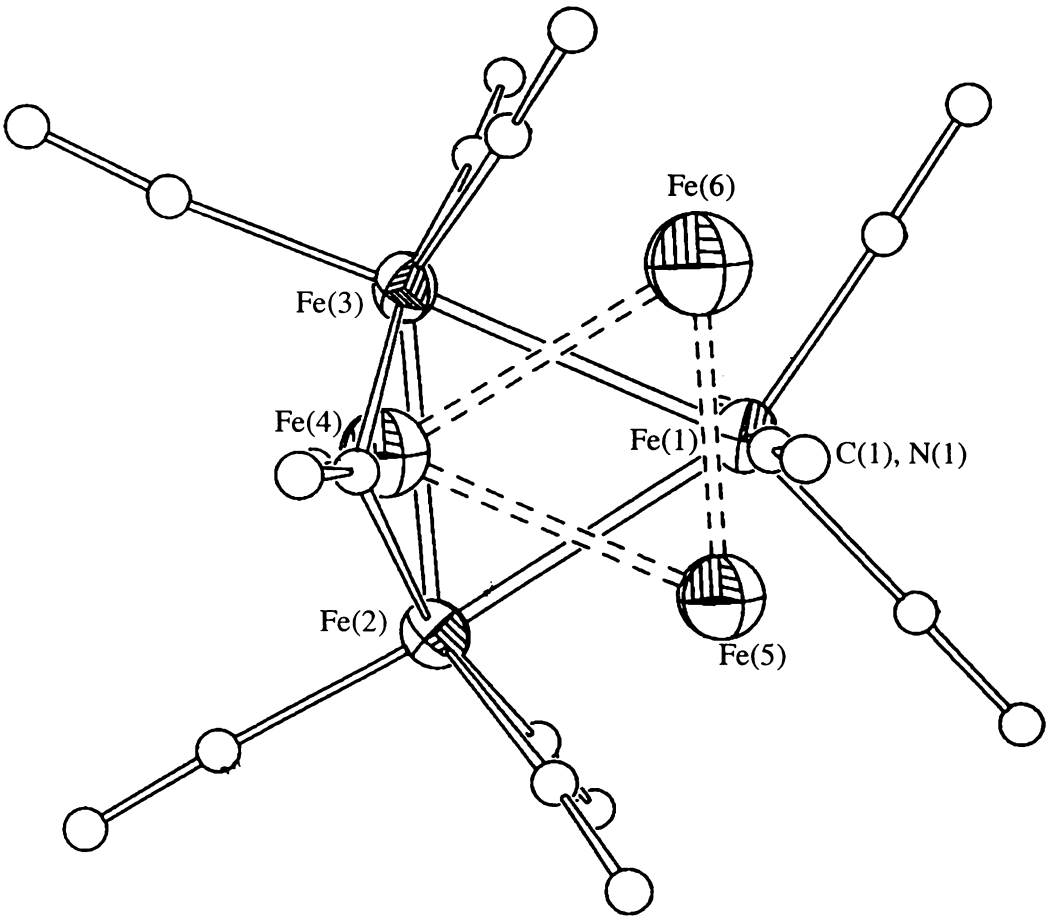

Fig. 4.10b The solid state structure of $[Fe_3(CO)_{10}(CNPh)_2]$ at low temperature (100 K). The phenyl rings have been removed to aid clarity. C, N and O atoms are presented as simple spheres while the Fe ellipsoids are drawn at the 50% probability level. The minor components of the disordered Fe atoms are shown with dashed bonds.

In the solid state, $[Fe_3(CO)_{10}(CNPh)_2]$ preserves the basic $[Fe_3(CO)_{12}]$ geometry. The two CNPh ligands replace the two axial CO ligands on the unique iron atom. This is different from the only other structurally characterised complex of this type, $[Fe_3(CO)_{10}(CNBu^t)_2]$, where the two isonitrile ligands (although both coordinated to the unique iron atom) occupy one axial and one equatorial position. The axial positions of both isonitrile ligands cannot be explained sterically, since the equatorial site is less

hindered (and hence preferred by bulky phosphine ligands[33]). In terms of electronic reasons, axial positions might be favoured by CNPh because the isonitrile is a weaker π-acceptor base than CO. In order to maximise π-bonding to the remaining CO ligands, the weaker π-acceptor ligand needs to be *trans* to CO, which is only accomplished if CNPh occupies an axial site. It has, however, also been suggested that because crystal packing forces are similar to the energy difference between axial and equatorial isomers, electronic and steric effects may be neglected altogether[18].

Generally, the effects of the isonitrile ligands on the rest of the molecule are small. The Fe–Fe bond lengths [2.5594(1) Å bridged, 2.6921(1) and 2.6918(1) Å unbridged] are not significantly different from those observed in $[Fe_3(CO)_{12}]$ [2.551(2) Å bridged, 2.677(2) and 2.684(2) Å unbridged, recorded at 160 K][34]. Because the CNPh ligands occupy both axial positions on Fe(1), the Fe(1)–Fe(2) and Fe(1)–Fe(3) bond lengths are equivalent. It is noteworthy that the same observation was made for $[Fe_3(CO)_{10}(CNBu^t)_2]$, although the Fe(1)–Fe(2) and Fe(1)–Fe(3) bonds are rendered inequivalent by the equatorial isonitrile ligand. This was considered to be a result of the close similarity in bonding interactions for CO and CNR.

The bond lengths associated with the isonitrile ligands [Fe(1)–C(1) and Fe(1)–C(2)], are equivalent [1.853(6) and 1.871(6) Å] and are longer than those observed for $Fe–C_{CO}$ (the $Fe–C_{CO}$ bonds range from 1.807 to 1.818 Å). This is expected, as CNPh is the weaker π-acceptor ligand. The axial and equatorial Fe–C bond lengths to CO ligands deviate only marginally in $[Fe_3(CO)_{10}(CNPh)_2]$. The same is true for all other reported isonitrile-substituted derivatives. The μ_2-CO ligands, unlike in $[Fe_3(CO)_{12}]$, are not significantly asymmetric and may be a result of introducing another ligand into the system (a similar observation was reported for all other derivatives).

The C≡N distances are equivalent for the two ligands [1.143(6) and 1.155(7) Å], as are the C–N–C angles [176.1(6)° and 176.3(1)°], which imply an almost linear arrangement. The angle involving both CNPh ligands and the unique iron atom is very close to 180°, as expected for two axial ligands.

---

[33] D. J. Dahm and R. A. Jacobson, *J. Am. Chem. Soc.*, 1968, **90**, 5106.

Towards the end of the refinement, three major residual peaks formed a triangle 60° from the major Fe_3-triangle. This was clearly a Star of David disorder in the location of the iron atoms, and refinement gave 5% for the second compound. This was very surprising since in all other reported isonitrile-substituted derivatives of $[Fe_3(CO)_{12}]$, the disorder is eliminated. Furthermore, for the Star of David disorder, a 60° rotation of the iron triangle is required. However, for axial ligands this leads to a structure with the isonitrile ligands in bridging positions, which is preferred by the CO rather than the isonitrile ligands[35] (an exception is $CNCF_3$). It should be noted that a small amount of metal site disorder has recently been observed for the mixed-metal species $[FeRu_2(CO)_{11}(CNBu^t)]$ and $[FeRu_2(CO)_{10}(CNBu^t)_2]$, but not for $[Fe_2Ru(CO)_{11}(CNBu^t)]$ and $[Fe_2Ru(CO)_{10}(CNBu^t)_2]$ [36].

4.4.3.2 X-ray crystal structure determination of $[Fe_3(CO)_{10}(CNPh)_2]$ at room temperature (293 K)

Having found partial disorder in the location of the iron atoms, a variable temperature X-ray structure analysis was considered appropriate in order to see the extent of disorder varied with temperature, since previous work showed dynamic disorder to be a larger component at higher temperatures. Full lists of atomic coordinates, temperature factors, bond lengths, and bond angles are supplied in Appendix B. Data relating to the structure solution are listed in the Experimental section of this chapter.

The structure analysis unexpectedly showed that there was no metal framework disorder at room temperature. There are a variety of possible explanations. Crystals of the first batch might have crystallised over a shorter period of time. Consequently, a structure with disorder might have been frozen out by crystal packing interactions, or twinning of the crystals might have occurred. Another explanation is that some $[Fe_3(CO)_{12}]$ had co-crystallised with $[Fe_3(CO)_{10}(CNPh)_2]$. Either explanation implies that the disorder is not dynamic in origin. Further investigations into this phenomenon were not pursued. The room temperature analysis had been carried out on a separate crystal from the previous one at low temperatures since the crystals from the low-temperature experiment were no

---

[34] D. Braga, L. Farrugia, F. Grepioni and B. F. G. Johnson, *J. Organomet. Chem.*, 1994, **464**, C39.
[35] R. D. Adams, F. A. Cotton and J. M. Troup, *Inorg. Chem.*, 1974, **13**, 257.
[36] L. J. Farrugia and P. Mertes, *J. Cluster Sci.*, 2002, **13**, 199.

longer available. Unfortunately, the cooling system of the machine broke down after acquisition of the room temperature data, and so no low-temperature data set could be collected on the same crystal, since it had decomposed. Examination of a series of $[Fe_3(CO)_{10}(CNPh)_2]$ crystals may provide a greater understanding of the disorder processes, but was also not undertaken because of financial restraints and the limitations of diffractometer time. The differences between the low- and high-temperature data are most likely a result of two different crystals. Hence, previous examples of temperature-dependent disorder may have been affected by similar variations from crystal to crystal.

The space group and unit cell were identical at 293 K to those found at low temperature. There were also no significant geometric differences in the structures between the two temperatures. A reported variable temperature X-ray structure analysis of $[Fe_2Ru(CO)_{10}(CNBu^t)_2]$ [36] indicated that the Fe–Fe bond was longer and the C–C bond distances in the Bu^t group were shorter at higher temperature, which was attributed to librational effects. An equivalent effect was not observed for $[Fe_3(CO)_{10}(CNPh)_2]$.

4.5 Some aspects of isonitrile complexes of $[Ru_3(CO)_{12}]$

4.5.1 $[Ru_3(CO)_{12}]$ and its isonitrile complexes

The structure of $[Ru_3(CO)_{12}]$ has been displayed earlier in Figure 4.2. It was first determined by Dahl in 1961 [37], who also determined the structure of $[Fe_3(CO)_{12}]$ some years later, together with the Os analogue. The structure has been redetermined several times since[38]. $[Ru_3(CO)_{12}]$ is not disordered, but many of its derivatives show disorder of the metal framework[39], *e.g.* $[Ru_3(CO)_{10}\{P(OMe)_3\}_2]$, $[Ru_3(CO)_{11}(CNBu^t)]$ and $[Ru_3(CO)_{10}(PMe_3)_2]$, but not $[Ru_3(CO)_{11}\{P(C_6H_{11})_3\}]$. This disorder has been rationalised in terms of a model in which the Ru_3-triangle occupies two symmetry-related positions while the peripheral atom polyhedron (*i.e.* the O of the CO ligand and the P of the phosphine or phosphite ligand) remains unchanged[40]. For

---

[37] E. R. Corey and L. F. Dahl, *J. Am. Chem. Soc.*, 1961, **83**, 2203.
[38] R. Mason and A. I. M. Rae, J. Chem. Soc. A, 1968, 778; M. R. Churchill, F. J. Hollander and J. P. Hutchinson, *Inorg. Chem.*, 1977, **16**, 2655; D. Braga, F. Grepioni, E. Tedesco, P. J. Dyson, C. M. Martin and B. F. G. Johnson, *Trans. Metal Chem.*, 1995, **20**, 615.
[39] L. J. Farrugia, C. Rosenhahn and S. Whitworth, *J. Cluster Sci.*, 1998, **9**, 505.
[40] M. I. Bruce, J. G. Matison, B. W. Skelton and A. H. White, *J. Chem. Soc. Dalton Trans.*, 1983, 2375.

$[Ru_3(CO)_{11}(CNBu^t)]$ and $[Ru_3(CO)_{11}(PMe_3)]$, it has also been shown that the disorder is dynamic in origin[39]. The work on the structures and fluxionality of all three $[M_3(CO)_{12}]$ members of the iron triad has been reviewed[16].

With 17 members, the number of known isonitrile-substituted derivatives of $[Ru_3(CO)_{12}]$ is as limited as for $[Fe_3(CO)_{12}]$ derivatives (if compared to the phosphine analogues). Table 4.7a summarises the complexes reported so far. The products obtained by pyrolysis of specific isonitrile derivatives of $[Ru_3(CO)_{12}]$ are listed separately in Table 4.7b.

Table 4.7a The reported isonitrile derivatives of $[Ru_3(CO)_{12}]$.

Complex	R	X-ray struct.	other data available
$[Ru_3(CO)_{11}(CNR)]$	Bu^t	✓[41,42]	mp, EA, MS, IR, ^{1}H NMR, ^{13}C NMR
	Me	–	mp, IR, ^{1}H NMR, ^{13}C NMR[43]
	Pr	–	EA, MS, IR, ^{1}H NMR[44]
	^{i}Pr	–	IR, ^{1}H NMR[44]
	Bz	–	MS, IR, ^{1}H NMR[44]
	C_3H_5	–	mp, IR[43]
	Ph	–	mp, IR, ^{1}H NMR, MS, EA[43]
	C_6H_4-2-Me	–	mp, IR, ^{1}H NMR, MS, EA[43]
	C_6H_{11}	–	mp, EA, MS, IR, ^{1}H NMR[41]
	$MeOC_6H_5$	–	mp, EA, IR, ^{1}H NMR[41]
	CHMePh	–	mp, EA, IR, ^{1}H NMR[45]

[41] M. I. Bruce, J. G. Matison, R. C. Wallis, J. M. Patrick, B. W. Skelton and A. H. White, *J. Chem. Soc. Dalton Trans.*, 1983, 2365.
[42] M. I. Bruce, G. N. Pain, C. A. Hughes, J. M. Patrick, B. K. Skelton and A. H. White, *J. Organomet. Chem.*, 1986, **307**, 343.
[43] C. J. Cardin, D. J. Cardin, N. B. Kelly, G. A. Lawless and M. B. Power, *J. Organomet. Chem.*, 1988, **341**, 447.
[44] K.-L. Lu, C.-C. Chen, Y.-W. Lin, F.-E. Hong., H.-M. Gau, L.-L. Gan and H.-D. Luoh, *J. Organomet. Chem.*, 1993, **453**, 263.
[45] M. I. Bruce, J. G. Matisons and B. K. Nicholson, *J. Organomet. Chem.*, 1983, **247**, 321.

	CF_3	✓[46]	mp, EA, MS, IR, ^{19}F NMR, ^{13}C NMR
$[Ru_3(CO)_{10}(CNR)_2]$	Bu^t	✓[41]	mp, EA, MS, IR, ^1H NMR, ^{13}C NMR
	TosMIC	–	mp, EA, IR[45]
	$MeOC_6H_5$	–	MS, EA, IR[41]
$[Ru_3(CO)_9(CNR)_3]$	Bu^t	–	IR, ^1H NMR, ^{13}C NMR[41]
	TosMIC	–	EA, IR[41]

Table 4.7b The reported pyrolysis products of isonitrile derivatives of $[Ru_3(CO)_{12}]$.

Complex	R	X-ray struct.	other data available
$[Ru_5(CO)_{14}(CNR)_2]$	Bu^t	✓[47]	MS, IR, ^1H NMR, ^{13}C NMR
$[Ru_6(C)(CO)_{15}(\mu\text{-}CO)(CNR)]$	Bu^t	✓[48]	MS

For $[Ru_3(CO)_{11}(CNBu^t)]$ and $[Ru_3(CO)_{10}(CNBu^t)_2]$, substitution was shown to occur progressively on different metal atoms on axial sites and as terminal ligands. This differs from phosphine derivatives of $[Ru_3(CO)_{12}]$, which were found to prefer equatorial sites[40]. As for the Fe analogue, the $CNCF_3$-substituted complex is an exception. $[Ru_3(CO)_{10}(\mu_2\text{-}CO)(\mu_2\text{-}CNCF_3)]$ has the unusual $[Fe_3(CO)_{12}]$ structure with two bridging ligands. The structures of all three complex types are displayed in Figure 4.11.

[46] D. Lentz, R. Marschall and E. Hahn, *Chem. Ber.*, 1991, **124**, 777.
[47] M. I. Bruce, J. G. Matisons, J. G. Rogers and R. C. Wallis, *J. Chem. Soc., Chem. Commun.*, 1981, 1070.
[48] R. D. Adams, P. Mathur and B. E. Segmüller, *Organometallics*, 1983, **2**, 1258.

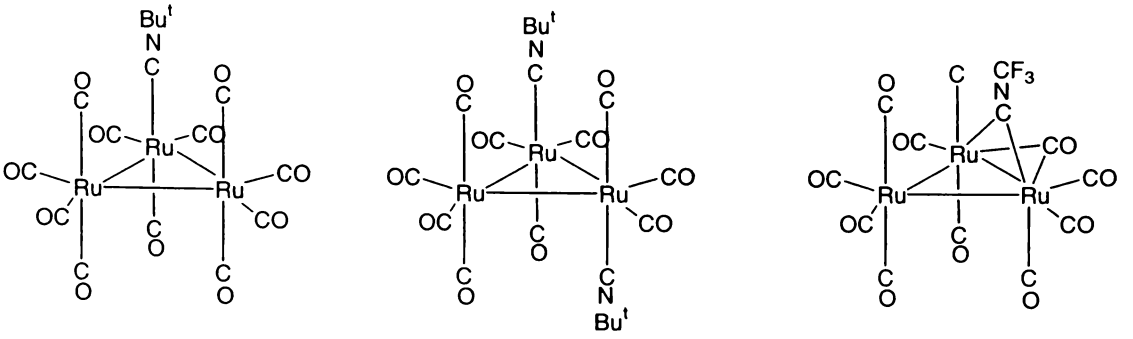

Fig. 4.11 The structures of the known isonitrile derivatives of $[Ru_3(CO)_{12}]$. From left to right: $[Ru_3(CO)_{11}(CNBu^t)]$, $[Ru_3(CO)_{10}(CNBu^t)_2]$ and $[Ru_3(CO)_{11}(CNCF_3)]$.

Evidence for substitution higher than two is still limited. One report briefly mentions the synthesis of the complexes $[Ru_3(CO)_{12-n}(CNBu^t)_n]$ (n = 1-4), but without characterisation data[49]. Upon closer investigation, the citation refers to unpublished work by Edwards and Knox, and no publication on this topic could be found since the initial report in 1979. Bruce and co-workers have isolated two tri-substituted complexes (refer to Table 4.5), but no satisfactory microanalytical data could be obtained, since this derivative was found to be very sensitive to oxidation. Unlike the phosphine and phosphite analogues[50], no tetra-substituted derivative is known. If tri- or even tetra-substitution is possible, ESMS is the tool of choice for their detection. Even if they are highly air-sensitive and difficult to isolate, they should still be detected in the ES mass spectrum of the crude reaction solution.

Pyrolysis of phosphine-ruthenium compounds generally leads to a number of high-nuclearity clusters and cyclometallation is common[51]. By heating isonitrile derivatives of $[Ru_3(CO)_{12}]$ (not including systems with ligands other than CO and RNC), only two higher-nuclearity clusters have been fully characterised and their structures are shown in Figure 4.12. By heating $[Ru_3(CO)_{11}(CNBu^t)]$, initial investigations by mass spectrometry[52] indicated the formation of two air-sensitive complexes, possibly Ru_5 and

---

[49] J.-M. Bassett, D. E. Berry, G. K. Barker, M. Green, J. A. K. Howard and F. G. A. Stone, *J. Chem. Soc. Dalton Trans.*, 1979, 1003.
[50] M. I. Bruce, M. J. Liddell, O. bin Shawkataly, I. Bytheway, B. W. Skelton and A. H. White, *J. Organomet. Chem.*, 1989, **369**, 217.
[51] M. I. Bruce, G. Shaw and F. G. Stone, *J. Chem. Soc. Dalton Trans.*, 1972, 2094.
[52] The paper is a communication and does not mention which ionisation method was used.

Ru_6 clusters[53]. Two years later, using the same method, the same group was able to obtain a crystal, and its structure revealed it to be $[Ru_5(CO)_{14}(CNBu^t)_2]$ with one terminal and the other a μ_5-isocyanide ligand acting as a 6e-donor. By heating this very compound, abstraction of the carbon atom of an isonitrile ligand yielded the carbido cluster $[Ru_6(C)(CO)_{16}(CNBu^t)]$.

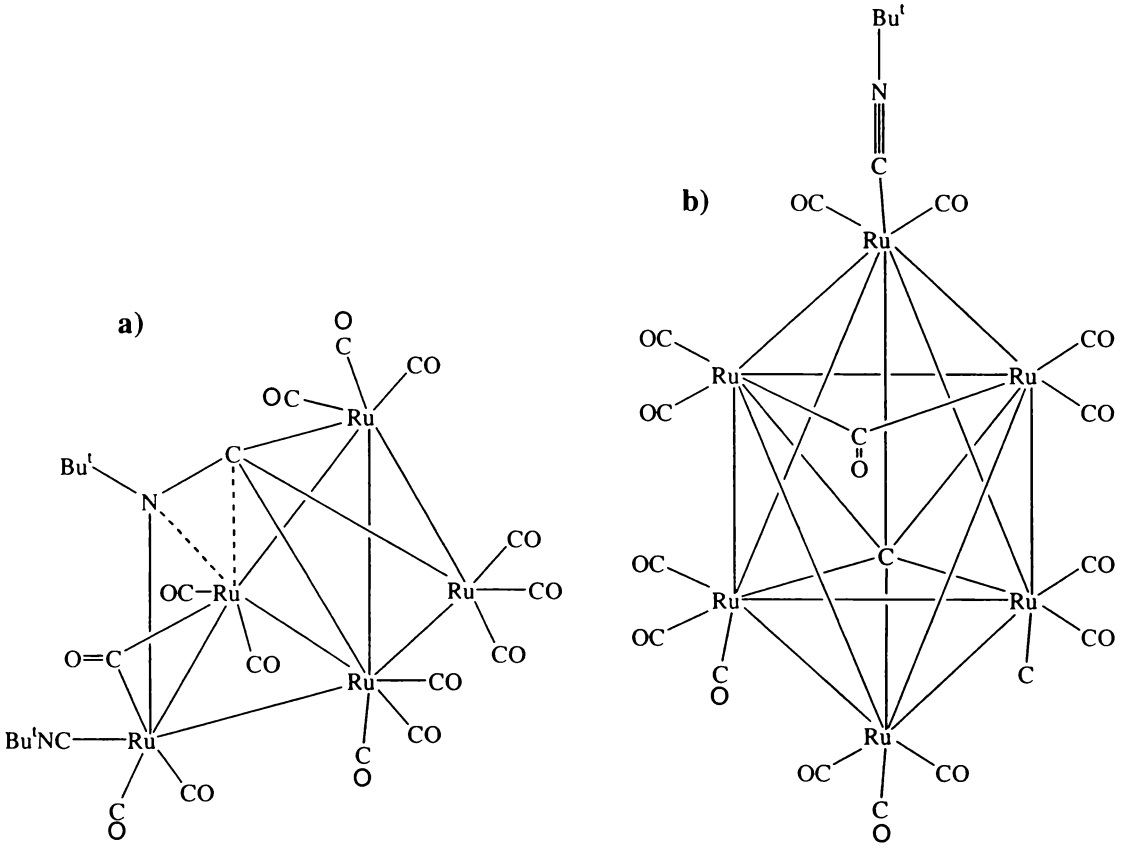

Fig. 4.12 The structures of $[Ru_5(CO)_{14}(CNBu^t)_2]$ (a) and $[Ru_6(C)(CO)_{16}(CNBu^t)]$ (b).

These two clusters were the only characterised species in the respective reactions, although, in the case of $[Ru_6(C)(CO)_{16}(CNBu^t)]$, other species were suggested to have formed, and this is also very likely in the case of $[Ru_5(CO)_{14}(CNBu^t)_2]$. Using the ESMS technique, all formed species should be able to be readily detected and possibly assigned.

[53] M. I. Bruce, D. Schultz and R. C. Wallis, *J. Organomet. Chem.*, 1979, **169**, C15.

4.5.2 ESMS of isonitrile derivatives of $[Ru_3(CO)_{12}]$

$[Ru_3(CO)_{12}]$ was gently heated in toluene for 30 minutes with four equivalents of the isonitrile ligand (CNPh or CNPh*) and the crude reaction mixtures were injected into the ESMS. Figure 4.13 shows both the positive- and negative-ion ES mass spectra for the reaction between $[Ru_3(CO)_{12}]$ and CNPh*.

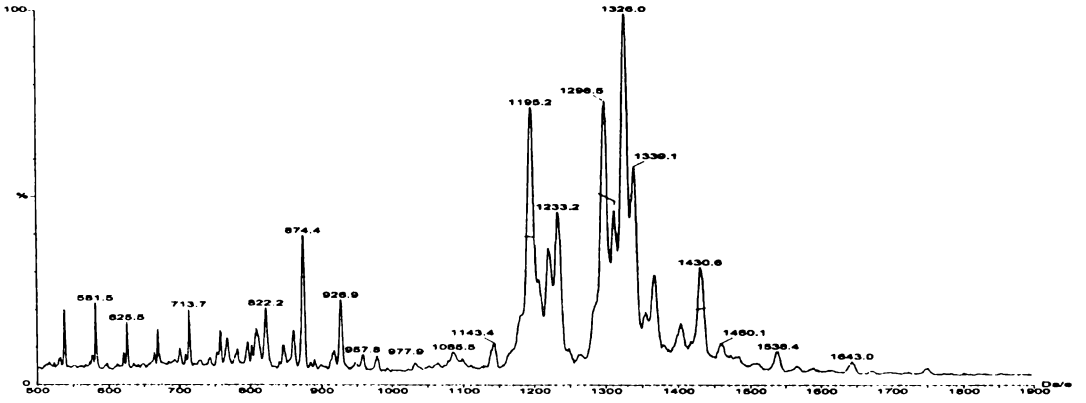

Fig. 4.13a The positive-ion ES mass spectrum of the crude reaction solution of $[Ru_3(CO)_{12}]$ with CNPh*, recorded in MeOH at cV = 20 V.

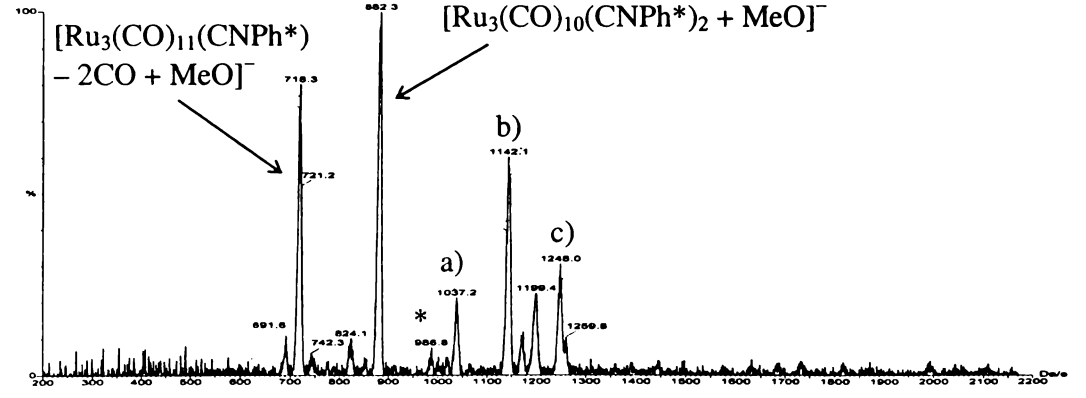

Fig. 4.13b The negative-ion ES mass spectrum of the crude reaction solution of $[Ru_3(CO)_{12}]$ with CNPh*, recorded in MeOH at cV = 5 V.

In positive-ion mode, none of the expected signals, such as $[M + H]^+$ ions of $[Ru_3(CO)_{11}(CNPh^*)]$ or $[Ru_3(CO)_{10}(CNPh^*)_2]$ were observed. However, these compounds gave strong signals in the negative-ion spectrum associated with their $[M + MeO]^-$ ions. This phenomenon is not unprecedented, as it has already been observed for

the Fe analogues discussed in section 4.4.2. $[Ru_3(CO)_{12}]$ itself has been found to ionise by alkoxide addition[32], yielding the ions $[M + EtO]^-$ and $[M + EtO - C_3O_2]^-$, but ruthenium isonitrile derivatives have not yet been shown to undergo the same mechanism. Unlike the Fe-isonitriles, the positive-ion spectrum did not show any of the higher-substituted products, such as $[Ru_3(CO)_9(CNR)_3 + H]^+$. The detected peaks could also not be assigned to any higher-nuclearity clusters of the type $[Ru_x(CO)_y(CNR)_z + H]^+$. Substitution seemed to occur, as mass differences of 105 amu (representing loss of CO and gain of CNPh*) could be detected between various signals, but the exact nature of these species remained unsolved. The rather large number of signals observed could be either a factor of a large number of products or only few products associating with a large number of other molecules (or both). The spectrum did not change significantly when adding various species such as HCOOH, NH_4^+ or Na^+ to the solution, which sometimes form adducts with the analyte.

With regard to the negative-ion spectrum of the crude reaction solution, the mono-substituted $[Ru_3(CO)_{11}(CNPh^*)]$ gave rise to $[M - 2CO + MeO]^-$ as the most intense ion, whereas for the di-substituted analogue, the parent ion $[M + MeO]^-$ dominated the spectrum. In addition, a weak signal for $[Ru_3(CO)_9(CNPh^*)_3 + MeO]^-$ at *m/z* 987 was observed, indicated by an asterisk. A number of signals associated with higher-nuclearity clusters were also detected. The most intense peaks [a), b) and c)] had a mass difference of 105 amu, reflecting substitution of CO for CNPh*. From the given information, a cluster series according to $[Ru_4(CO)_{14-n}(CNPh^*)_n]$ (n = 2-4) was tentatively proposed. The two less intense ions between b) and c) were not associated with loss of CO ligands of species c), as they lost mass units of (approximately) 49 and 75 respectively. They could represent one (with the loss of one CO ligand) or two other cluster types, but remained the only two unassigned ions in the spectrum.

Very similar results were obtained for the CNPh derivatives. The most intense ion for $[Ru_3(CO)_{11}(CNPh)]$ was $[M - 2CO + MeO]^-$ and $[M + MeO]^-$ for $[Ru_3(CO)_{10}(CNPh)_2]$. Likewise, an equivalent higher-nuclearity series according to $[Ru_4(CO)_{14-n}(CNPh)_n]$ (n = 2-4) was observed, which also had two weaker signals between $[Ru_4(CO)_{11}(CNPh)_3 + MeO]^-$ and $[Ru_4(CO)_{10}(CNPh)_4 + MeO]^-$ that could not be assigned. All ions observed in the crude reaction solutions are summarised in Table 4.8.

Table 4.8 The detected ions in the negative-ion ES mass spectrum of the reaction between $[Ru_3(CO)_{12}]$ and CNR (R = Ph, Ph*), recorded in MeOH at cV = 5 V.

R	Observed ions	*m/z*	Relative peak height (%)
Ph	$[Ru_3(CO)_{11}(CNPh) + MeO]^-$	747	12
	$[Ru_3(CO)_{11}(CNPh) - CO + MeO]^-$	717	18
	$[Ru_3(CO)_{11}(CNPh) - 2CO + MeO]^-$	687	100
	$[Ru_3(CO)_{10}(CNPh)_2 + MeO]^-$	822	18
	$[Ru_3(CO)_{11}(CNPh) - 2CO + MeO]^-$	765	10
	$[Ru_4(CO)_{12}(CNPh)_2 + MeO]^-$	977	12
	$[Ru_4(CO)_{11}(CNPh)_3 + MeO]^-$	1052	32
	$[Ru_4(CO)_{10}(CNPh)_4 + MeO]^-$	1129	22
	unassigned	1173	25
	unassigned	1199	15
Ph*	$[Ru_3(CO)_{11}(CNPh^*) - CO + MeO]^-$	742	6
	$[Ru_3(CO)_{11}(CNPh^*) - 2CO + MeO]^-$	718	80
	$[Ru_3(CO)_{11}(CNPh^*) - 3CO + MeO]^-$	692	11
	$[Ru_3(CO)_{10}(CNPh^*)_2 + MeO]^-$	882	100
	$[Ru_3(CO)_{11}(CNPh^*) - 2CO + MeO]^-$	824	11
	$[Ru_3(CO)_9(CNPh^*)_3 + MeO]^-$	987	9
	$[Ru_4(CO)_{12}(CNPh^*)_2 + MeO]^-$	1037	21
	$[Ru_4(CO)_{11}(CNPh^*)_3 + MeO]^-$	1142	60
	$[Ru_4(CO)_{10}(CNPh^*)_4 + MeO]^-$	1248	30
	unassigned	1080	12
	unassigned	1107	20

It should be noted that in the ruthenium systems under investigation, the exact *m/z* values in the spectra have to be carefully considered. The *m/z* values generally represent the peak of greatest intensity in the isotope distribution pattern, which normally matches exactly the calculated *m/z* value of a given species. In this case, however, mismatches were sometimes observed, especially when ions were of limited intensity. This is

because the isotope patterns of multinuclear ruthenium compounds are very broad, increasing in signal width with the number of metal atoms in the system. Figure 4.14 illustrates this by showing the isotope distribution patterns of a Ru_3 and a Ru_5 species.

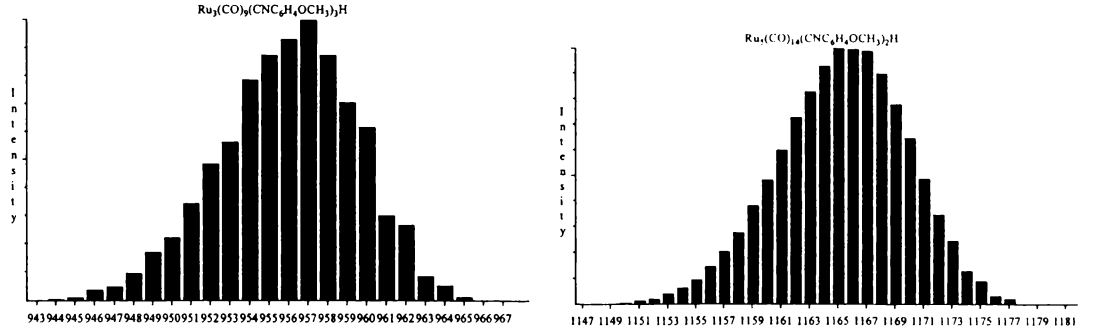

Fig. 4.14 The calculated isotope patterns of $[Ru_3(CO)_9(CNPh^*)_3 + H]^+$ and $[Ru_5(CO)_{14}(CNPh^*)_2 + H]^+$.

After separation by chromatography, the products were again analysed by ESMS. Both $[Ru_3(CO)_{11}(CNR)]$ and $[Ru_3(CO)_{10}(CNR)_2]$ ionised by methoxide addition as well as by protonation, even though $[M + H]^+$ ions had not been observed in the crude reaction solution (refer to Figure 4. 13a). As an example, the positive-ion spectrum of $[Ru_3(CO)_{10}(CNPh)_2]$ is shown in Figure 4.15.

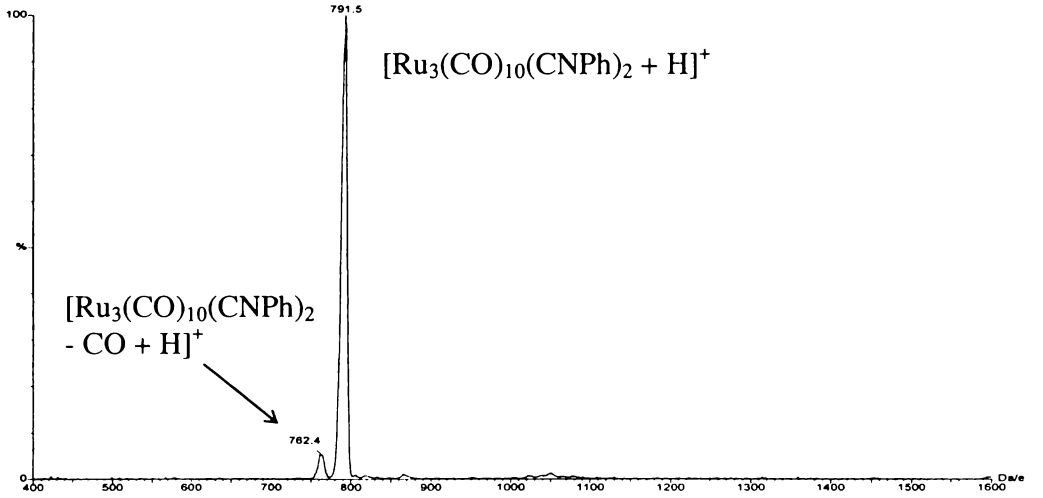

Fig 4.15 The positive-ion ES mass spectrum of $[Ru_3(CO)_{10}(CNPh)_2]$, recorded in MeOH at cV = 20 V.

The following bands were of more interest as they represented higher-substituted and/or higher-nuclearity products. In the case of CNPh*, they were however very close together and could not be separated satisfactorily. Together they gave a signal associated with $[Ru_3(CO)_9(CNPh^*)_3 + H]^+$ as well as one or more higher-nuclearity clusters, as shown in Figure 4.16. The ion at *m/z* 1113 could represent $[Ru_4(CO)_{11}(CNPh^*)_3 + H]^+$, followed by a number of other peaks, possibly associated with coordination with different species present in the system.

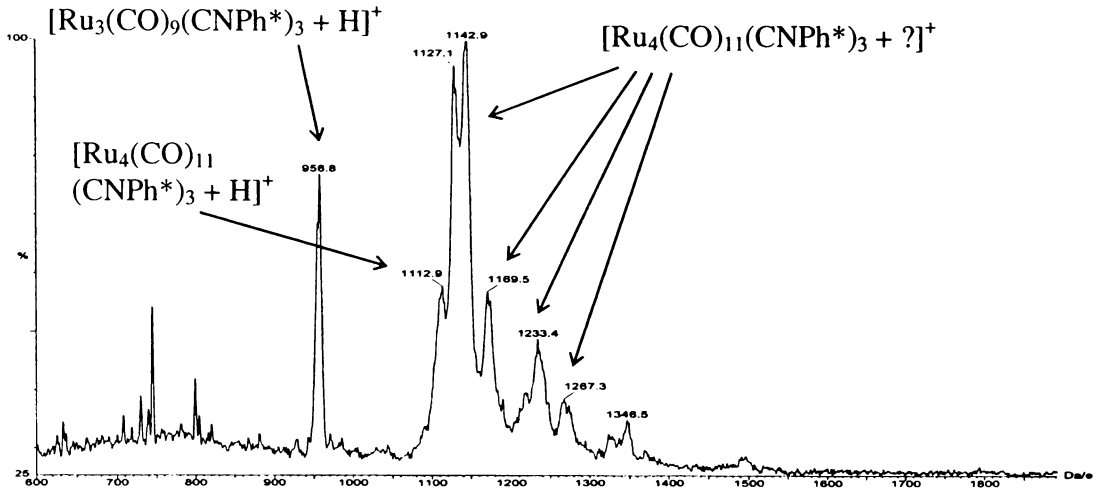

Fig. 4.16 The positive-ion ES mass spectrum of $[Ru_3(CO)_9(CNPh^*)_3]$ and one or more Ru_4-clusters, recorded in MeOH at cV = 5 V.

It should be noted that these results were only reproducible to a certain degree. This led to the conclusion that the observed species were either extremely air-sensitive (*i.e.* small differences in handling results in changes in the spectrum), and/or they were very sensitive with regard to the species available within the instrument, which very much depends on previous users as well as the solvent system used. Another example (recorded in $MeCN/H_2O$) is shown in Figure 4.17, where the ion of greatest intensity (*m/z* 1114) probably represents $[Ru_4(CO)_{11}(CNPh^*)_3 + H]^+$. The other ions present in the spectrum are most likely the same compound associating with various species present in solution, as the $[M + MeO]^-$ ion of $[Ru_4(CO)_{11}(CNPh^*)_3]$ was the only signal observed in negative-ion mode for the same sample. In the case shown in Figure 4.17, these peaks were tentatively assigned as coordination with MeCN solvent.

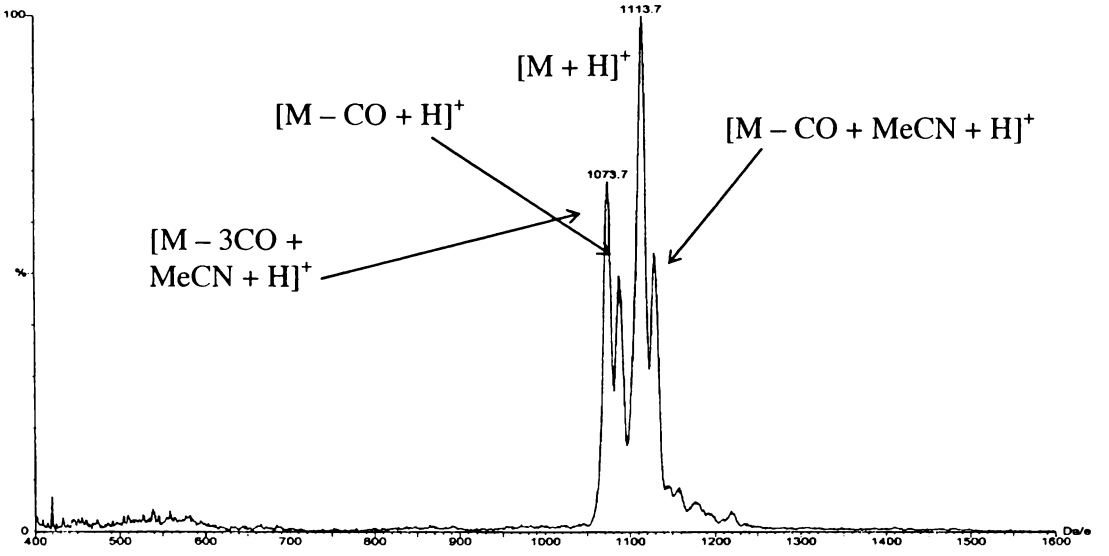

Fig. 4.17 The positive-ion mass spectrum of $[Ru_4(CO)_{11}(CNPh^*)_3]$, recorded in $MeCN/H_2O$, at cV = 20 V.

For the system involving CNPh, a better separation of the bands occurred. Thus, the bands following the di-substituted complex were isolated and injected in the mass spectrometer. An intense peak corresponding to $[Ru_3(CO)_9(CNPh)_3 + H]^+$ was observed in the positive-ion mode and is shown in Figure 4.18a, together with the observed and calculated isotope patterns in Figure 4.18b. This species was additionally confirmed by switching to the negative mode, which showed the corresponding $[Ru_3(CO)_9(CNPh)_3 + MeO]^-$ ion.

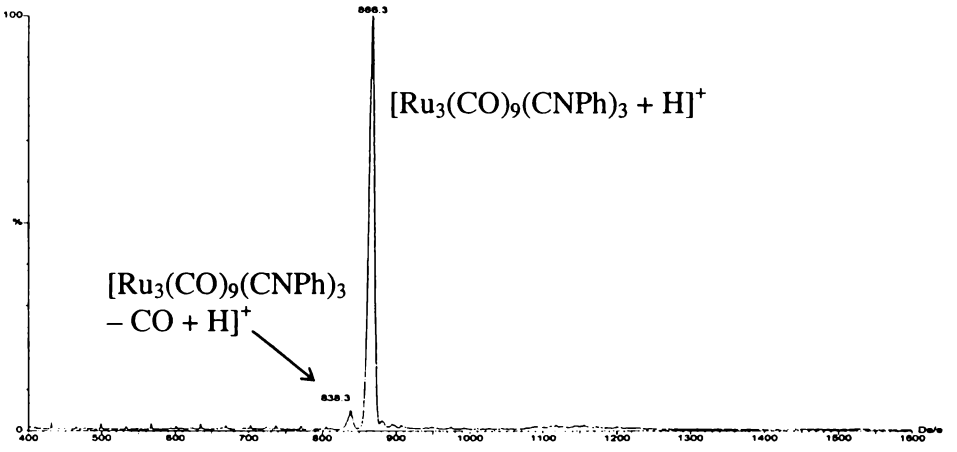

Fig. 4.18a The positive-ion ES mass spectrum of $[Ru_3(CO)_9(CNPh)_3]$, recorded in MeOH at cV = 20 V.

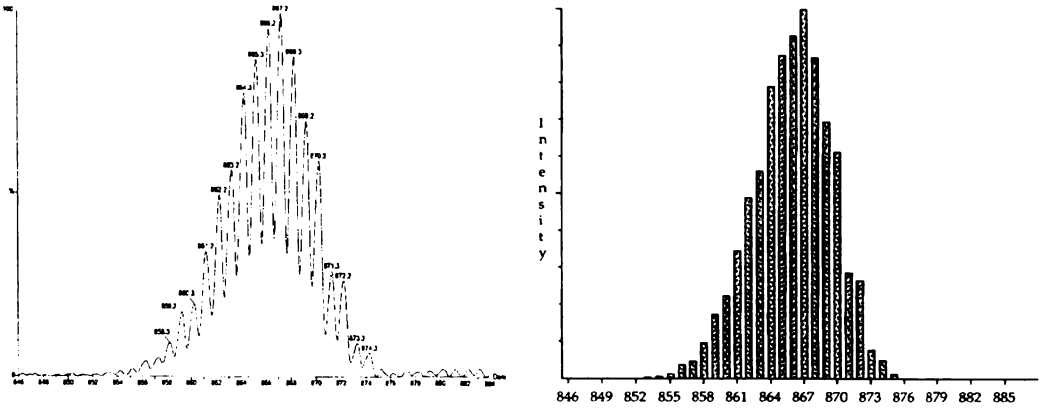

Fig. 4.18b The observed (left) and calculated (right) isotope patterns of $[Ru_3(CO)_9(CNPh)_3 + H]^+$.

Isolation of the following band in the $[Ru_3(CO)_{12}]$/CNPh system, gave a single signal at *m/z* 1024 in positive- and a number of ions with the most intense at *m/z* 1054 in negative-ion mode. Presuming the ions to be $[M + H]^+$ and $[M + MeO]^-$ respectively, the cluster of the formula $[Ru_4(CO)_{11}(CNPh)_3]$ was predicted. The negative-ion spectrum is shown in Figure 4.19. The cluster appeared to lose a phenyl ring readily giving a signal at *m/z* 977. A more likely explanation is, however, that the ion is $[Ru_4(CO)_{12}(CNPh)_2 + MeO]^-$. It is noteworthy that this fraction consisted of two bands, which were very close together, both of which gave the same IR and ES spectra. Upon crystallisation of a mixture of these, only $[Ru_4(CO)_{11}(CNPh)_3]$ yielded satisfactory crystals (its structure is discussed in section 4.5.3), so that the exact nature of the other species could not be confirmed.

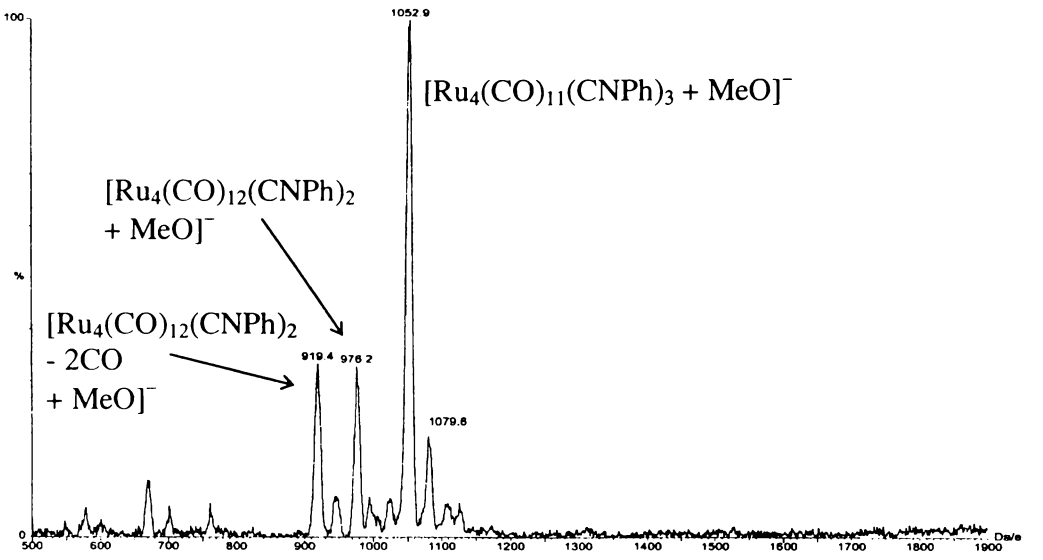

Fig. 4.19 The negative-ion ES mass spectrum of $[Ru_4(CO)_{11}(CNPh)_3]$ and $[Ru_4(CO)_{12}(CNPh)_2]$, recorded in MeOH/MeO^- at cV = 5 V.

Only one study could be found where a mass spectrometric analysis was carried out on isonitrile derivatives of $[Ru_3(CO)_{12}]$ [41] using EI ionisation. From the spectra it was concluded that the loss of CO and isonitrile ligands becomes competitive after cleavage of the first Ru–CO bond on each metal atom. It was of interest to compare these results with the ES ionisation method, where by slowly increasing the cone voltage, fragmentation can be induced to a desired degree. This experiment was carried out on $[Ru_3(CO)_9(CNPh)_3]$, and the observed ions are listed in Table 4.9. At 60 V, up to six CO ligands were lost progressively. The loss of the isonitrile ligand was not observed, in contrast to the previous EI results.

Table 4.9 The observed ions in the positive-ion ES mass spectrum of $[Ru_3(CO)_9(CNPh)_3]$, recorded in MeOH at various cone voltages.

cV (V)	Ions observed [*m/z*, relative peak height (%)]
20	$[M + H]^+$ (866, 100), $[M - CO + H]^+$ (838, 5)
40	$[M + H]^+$ (866, 85), $[M - CO + H]^+$ (838, 90), $[M - 2CO + H]^+$ (810, 100), $[M - 3CO + H]^+$ (782, 12)
60	$[M + H]^+$ (865, 22), $[M - CO + H]^+$ (838, 20), $[M - 2CO + H]^+$ (810, 50), $[M - 3CO + H]^+$ (782, 68), $[M - 4CO + H]^+$ (754, 100), $[M - 5CO + H]^+$ (726, 51), $[M - 6CO + H]^+$ (698, 13)

In a separate experiment, the free ligand CNPh was electrosprayed (not giving any signals), followed by the crude reaction solution with $[Ru_3(CO)_{12}]$. As can be seen in Figure 4.20, substitution occurred to a very high degree, with the penta-substituted species $[Ru_3(CO)_7(CNPh)_5 + H]^+$ still observed as an intense signal. Unlike in all other ESMS experiments, the species in this particular case must have been generated inside the spectrometer. The additionally observed peaks a) – d) were all 2+ ions with a mass separation of 37.5, indicating substitution of CO by CNPh, but the exact nature of these peaks remained unsolved. This experiment shows, however, that multiple-substitution of $[Ru_3(CO)_{12}]$ by isonitriles is possible under certain circumstances, and deserves further investigation.

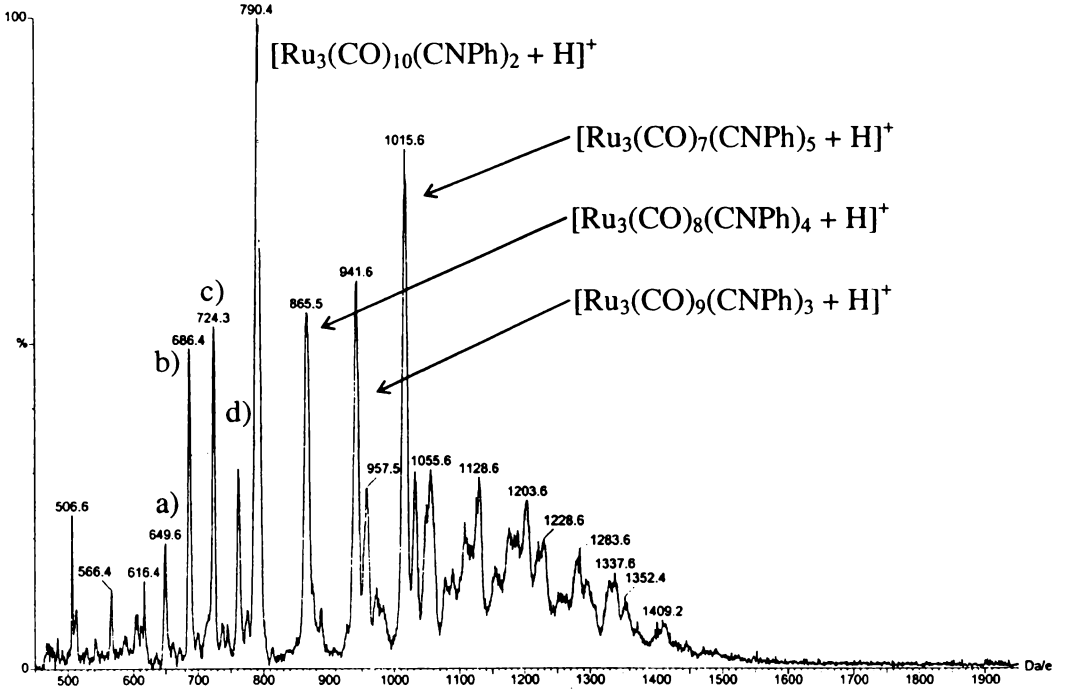

Fig. 4.20 The positive-ion ES mass spectrum of the free ligand CNPh and the crude reaction solution of $[Ru_3(CO)_{12}]$ and CNPh, recorded in MeOH at cV = 20 V.

4.5.3 X-ray crystal structure determination of $[Ru_4(CO)_{11}(CNPh)_3]$

Crystals of the cluster $[Ru_4(CO)_{11}(CNPh)_3]$ were obtained from a concentrated CH_2Cl_2/Et_2O solution by cooling to -20°C. $[Ru_4(CO)_{11}(CNPh)_3]$ crystallised without solvent and refined cleanly without disorder. The full structure is shown in Figure 4.21a and from a different angle in Figure 4.21b. A list of selected bond lengths and angles is displayed in Table 4.10, while full lists of atomic coordinates, temperature factors, bond lengths and bond angles are supplied in Appendix C. Data relating to the structure solution are listed in the Experimental part of this chapter.

Table 4.10 Selected bond lengths (Å) and bond angles (°) for $[Ru_4(CO)_{11}(CNPh)_3]$.

Ru(1)–Ru(2)	2.8341(3)	Ru(1)–C(61)	2.172(3)
Ru(1)–Ru(3)	2.8226(3)	Ru(2)–C(61)	1.962(3)
Ru(2)–Ru(3)	2.8895(3)	Ru(1)–C(71)	2.127(3)
Ru(1)–Ru(4)	2.8258(3)	Ru(3)–C(71)	1.966(3)
C(61)–N(61)	1.274(3)	C(1)–N(1)	1.143(6)
C(71)–N(71)	1.270(3)	C(2)–N(2)	1.155(7)
C(51)–N(51)	1.159(3)		
Ru(1)–Ru(2)–Ru(3)	59.088(7)	Ru(1)–C(61)–Ru(2)	86.40(11)
Ru(1)–Ru(3)–Ru(2)	59.479(8)	Ru(1)–C(71)–Ru(3)	87.12(10)
Ru(3)–Ru(1)–Ru(2)	61.434(8)		
Ru(3)–Ru(1)–Ru(4)	107.587(9)	C(61)–N(61)–C(62)	126.2(2)
Ru(2)–Ru(1)–Ru(4)	107.745(9)	C(71)–N(71)–C(72)	123.6(2)
		C(51)–N(51)–C(52)	177.5(3)

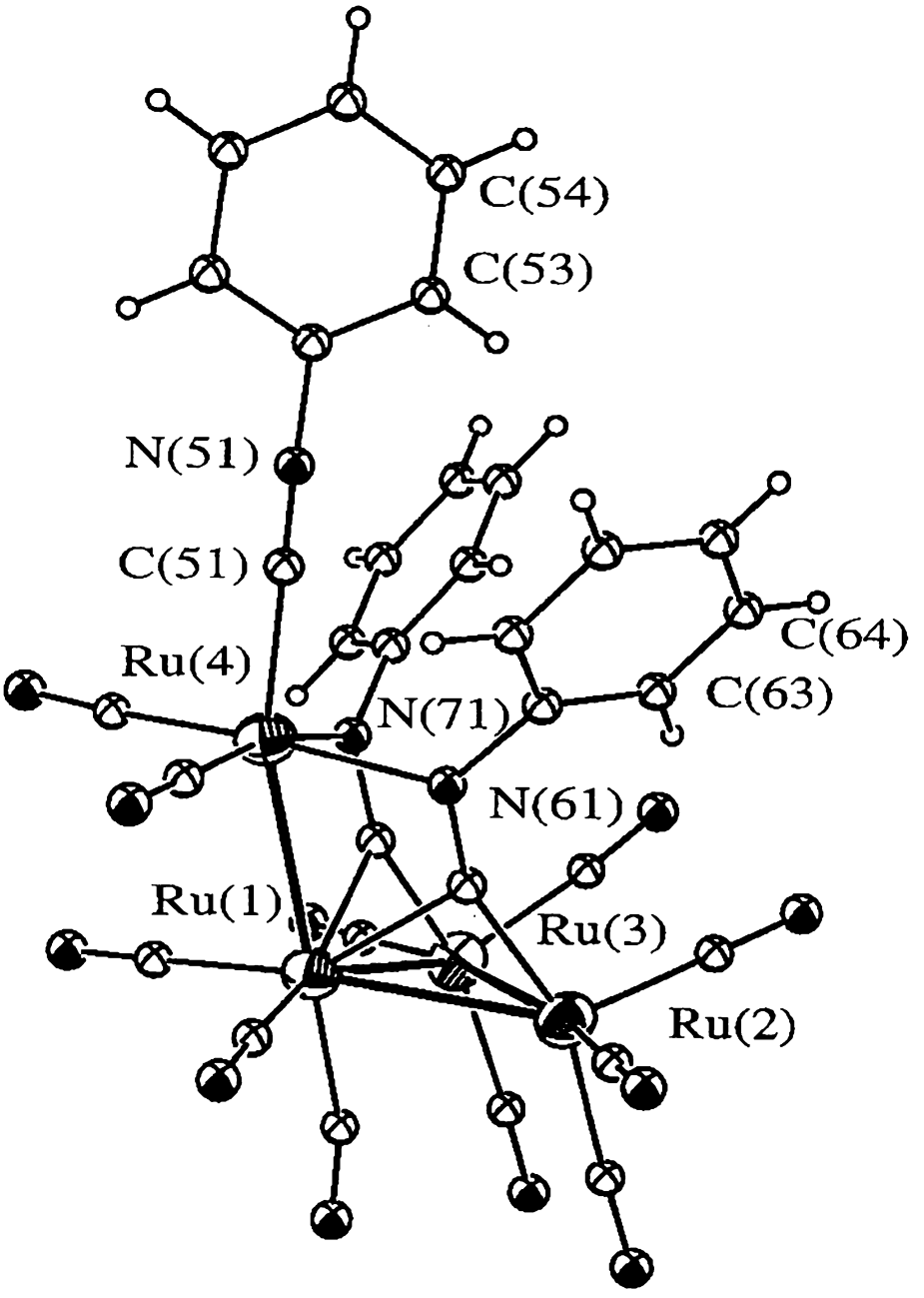

Fig. 4.21a The structure of $[Ru_4(CO)_{11}(CNPh)_3]$.

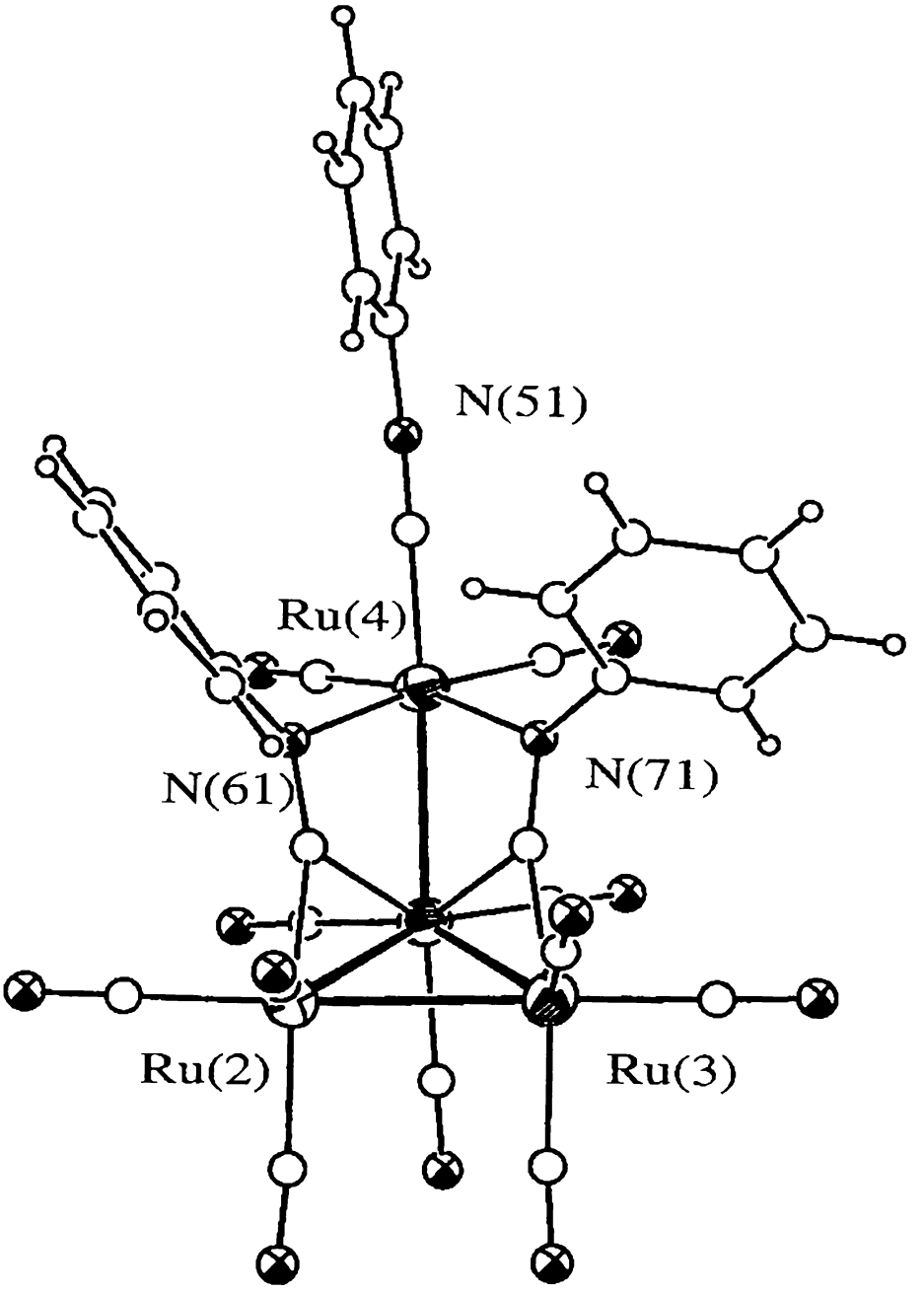

Fig. 4.21b The structure of $[Ru_4(CO)_{11}(CNPh)_3]$.

The core geometry of $[Ru_4(CO)_{11}(CNPh)_3]$ is that of a spiked triangle. Each metal atom is bonded to three terminal 2e-donor ligands. The metal atoms of the triangle each have three terminal CO ligands while the unique ruthenium atom [Ru(4)] is attached to two terminal CO groups and one terminal isonitrile ligand. The remaining two CNPh ligands each bridge a metal-metal bond of the triangle through the isonitrile carbon atom. They also bridge the spike in a μ_2-CN bond, as illustrated in Fig 4.23. Because of the nature of the bridging ligands, the Ru(1)–Ru(2) and Ru(1)–Ru(3) bond lengths [2.8341(3) Å and 2.8226(3) Å, respectively] are identical. An equivalent bond length was noted for Ru(1)–Ru(4) [2.8258(3) Å] and is marginally shorter than the unbridged Ru(2)–Ru(3) bond [2.8895(3) Å]. As a consequence, the bond angles within the Ru-triangle are not all 60°. While the angles involving the unbridged Ru(2)–Ru(3) bond are equivalent and fractionally short of 60° [59.088(7)° for Ru(1)–Ru(2)–Ru(3) and 59.479(8)° for Ru(1)–Ru(3)–Ru(2)], the Ru(3)–Ru(1)–Ru(2) angle is opened up by two degrees [61.434(8)°]. The spike is bonded to the triangle by an angle of approximately 107°.

When comparing the bridging isonitrile ligands, both Ru–C–Ru bond angles [86.40(11)° for Ru(1)–C(61)–Ru(2) and 87.12(10)° for Ru(1)–C(71)–Ru(3)] and the corresponding Ru–C bond lengths [2.172(3) for Ru(1)–C(61) compared to 2.127(3) Å for Ru(1)–C(71) and 1.962(3) Å for Ru(2)–C(61) compared to 1.966(3) Å for Ru(3)–C(71)] are very similar, indicating high symmetry. In fact, the cluster appears to be highly symmetrical about a mirror plane containing Ru(1) and bisecting the Ru(2)–Ru(3) bond. However, this symmetry is lost due to the orientation of the phenyl rings of the isonitrile ligands.

The bonding mode of the two bridging isonitrile ligands is of particular interest. The two carbon atoms [C(61) and C(71)] bridge two metal atoms while the nitrogen atoms [N(61) and N(71)] form a single bond to the unique ruthenium atom. This results in a double rather than triple bond between the C and N atoms. The C–N bond lengths [1.274(3) for C(61)–N(61) Å and 1.270(3) for C(71)–N(71) Å] are consistent with this, being longer than in the terminal isonitrile ligand [1.159(3) for C(51)–N(51) Å]. The bonding mode observed can be equated with an imine-type arrangement. The C(61)–N(61)–C(62) [126.2(2)°] and C(71)–N(71)–C(72) [123.6(2)°] bond angles of the bridging isonitrile ligands also reflect their similarity to imines (~ 120°) rather than that

of isonitriles (~ 180°). The terminal isonitrile ligand has an expected C–N–C angle of 177.5(3)°.

The overall electron count averages 18 for each metal atom, *i.e.* 19 for Ru(1) and Ru(4) and 17 for the identical Ru(2) and Ru(3) atoms. This is achieved when the bridging isonitrile ligands donate 1e to each metal through the carbon atoms and 2e to the unique Ru(4) through the nitrogen atoms. Thus, Ru(1) and Ru(4) are electron-rich (19e) whereas the two identical Ru(2) and Ru(3) atoms are electron-deficient (17e). This is reflected in the structure of the bridging ligands as they both are bent away from Ru(1) towards Ru(2) and Ru(3). The difference in bond lengths of the Ru–C–Ru bridges is a further consequence. Both Ru(1)–C(61) [2.172(3) Å] and Ru(1)–C(71) [2.127(3) Å] bonds are slightly longer than those observed for Ru(2)–C(61) [1.962(3) Å] and Ru(3)–C(71) [1.966(3) Å].

$[Ru_4(CO)_{11}(CNPh)_3]$ is the only reported Ru_4-isonitrile structure to date. The observed imine-type bonding mode within the bridging isonitrile ligands (as illustrated in Fig 4.22) has been reported before, but only for a small number of other systems. They include Rh_3 [54], Ru_3 [55], and Os_5 [56] clusters.

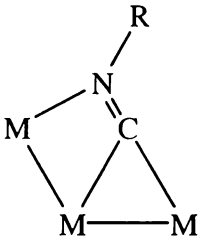

Fig. 4.22 The bonding mode of the bridging isonitrile ligands.

[54] A. L. Bach, L. A. Fossett and M. M. Olmstead, *Organometallics*, 1987, **6**, 1827.
[55] O. B. Shawkataly, S.-G. Teoh and H.-K. Fun, *J. Organomet. Chem.*, 1994, **464**, C29.
[56] A. V. Rivera, G. M. Sheldrick and M. B. Hursthouse, *Acta Crystallogr.*, Sect. B, 1978, **34**, 1985.

4.6 Summary and Conclusions

Electrospray-friendly ligands are not required for studying isonitrile derivatives of $[Fe_3(CO)_{12}]$ and $[Ru_3(CO)_{12}]$ by ESMS. Depending on the respective ligand and degree of substitution, they can be studied in positive-, negative- or both ion modes. Because of the fact that now any isonitrile will 'do the job', the number of possible candidates for the analysis by ESMS has risen dramatically. This is of particular interest, as by changing the R group, the properties of the complex may be fine-tuned and might lead to the solution of unanswered questions. For example, the structure of $[Fe_3(CO)_9(CNR)_3]$ is very interesting with regard to the site of the third isonitrile ligand, but remains unsolved because no suitable crystals have been obtained with the ligands used so far.

With the ligands available in this study, it has been shown that higher-substituted products do exist for both $[Fe_3(CO)_{12}]$ and $[Ru_3(CO)_{12}]$. Even though they are likely to become more air-sensitive with the degree of substitution, they can still be studied by ESMS as it is possible to work under a nitrogen atmosphere.

The structure of $[Fe_3(CO)_{10}(CNPh)_2]$ has been determined and differs from the only other structurally characterised di-substituted isonitrile derivative of $[Fe_3(CO)_{12}]$ with respect to the orientations of the isonitrile ligands. The metal framework disorder observed at low temperature is not dynamic in origin, because a separate structure determination at room temperature did not show any disorder.

Pyrolysis reactions of isonitrile derivatives of $[Fe_3(CO)_{12}]$ led to the previously observed species $[Fe_3(CO)_{9-m}(\mu_3\text{-}CNR)(CNR)_m]$ (m = 0, 1) as the only major products, extending R = Bu^t to R = aryl examples. They ionise by formation of $[M + MeO]^-$ ions and can be detected readily in the negative-ion mode. It would be interesting to see whether this series continues for m = 2 and 3. The analogous pyrolysis reaction of derivatives of $[Ru_3(CO)_{12}]$ led to a series of products according to $[Ru_4(CO)_{14-n}(CNR)_n]$ (n = 2-4) as the only major higher-nuclearity product, and is also best studied in the negative-ion mode. $[Ru_4(CO)_{11}(CNPh)_3]$ has been characterised structurally and represents the only fully characterised isonitrile-substituted derivative of $[Ru_3(CO)_{12}]$ incorporating four metal atoms.

4.7 Experimental

General experimental techniques as well as the atom labelling for the assignment of NMR signals are in keeping with those outlined in Chapter two. X-ray crystal data were recorded at the University of Auckland with a Siemens SMART CCD diffractometer. The structures were solved by direct methods and refined routinely using the SHELX-97 program[57].

$[Fe_3(CO)_{12}]$, $[Ru_3(CO)_{12}]$ (Strem) and TosMIC (Aldrich) were used as supplied. 4-Methoxyphenylisonitrile and phenylisonitrile were prepared by the published procedures[3].

4.7.1 Reactions of $[Fe_3(CO)_{12}]$ with isonitriles

The general reaction was carried out as follows: $[Fe_3(CO)_{12}]$ (0.5 g, 0.99 mmol) was dissolved in 10 mL of THF. The isonitrile (3.97 mmol) was added by syringe or as a solid and the reaction stirred at room temperature for *ca.* two hours. Aliquots were withdrawn at appropriate time intervals and the course of the reaction was monitored by tlc. The solvent was removed *in vacuo*, the reaction products redissolved in a minimum amount of CH_2Cl_2, and subsequently chromatographed on silica plates (Merck, Silica gel 60G) with a solvent mixture of pet. spirits (b.p. 60 - 80°C)/CH_2Cl_2 (CNPh derivatives 1:1, CNPh* derivatives 1:2, TosMIC derivatives 1:2). Yields of the isolated complexes were not determined because only parts of the crude reaction product were used at a time for chromatography. Satisfactory elemental analyses were obtained for CNPh and TosMIC derivatives, but not for any compounds involving the CNPh* ligand.

4.7.1.1 Synthesis of $[Fe_3(CO)_{11}(CNPh)]$

$R_f = 0.68$ (green).

Elemental analysis: C, 37.79; H, 1.31; N, 2.35%. $C_{18}H_5Fe_3NO_{11}$ requires C, 37.31; H, 0.86; N, 2.42%.

---

[57] G. M. Sheldrick, SHELX-97, *Program for solution and refinement of crystal structures*, University of Göttingen, Germany, 1997.

IR ($CHCl_3$): ν (CN) 2153 (m); ν (CO) 2080 (m), 2039 (sh), 2033 (s), 2014 (sh), 1998 (sh) cm^{-1}.

ESMS (MeOH, +ve ion, 20 V): $[M + H]^+$ *m/z* 580 (100%).

4.7.1.2 Synthesis of $[Fe_3(CO)_{10}(CNPh)_2]$

R_f = 0.49 (green).

Elemental analysis: C, 44.65; H, 1.52; N, 4.14%. $C_{24}H_{10}Fe_3N_2O_{10}$ requires C, 44.04; H, 1.53; N, 4.28%.

IR (pet. sprits): ν (CN) 2150 (w), 2118 (m); ν (CO) 2056 (s), 2030 (sh), 2019 (s), 1996 (sh), 1988 (sh), 1974 (sh) cm^{-1}.

ESMS (MeOH, +ve ion, 20 V): $[M + H]^+$ *m/z* 655 (100%).

X-ray crystal structure determination of $[Fe_3(CO)_{10}(CNPh)_2]$

Single crystals of $[Fe_3(CO)_{10}(CNPh)_2]$ were obtained as described in section 4.4.3. Crystallographic data are given in Table 4.11.

Table 4.11 Crystallographic data and structure refinement for $[Fe_3(CO)_{10}(CNPh)_2]$.

	100(2) K	293(2) K
Empirical formula	$C_{24}H_{10}Fe_3N_2O_{10}$	$C_{24}H_{10}Fe_3N_2O_{10}$
M_r	653.89	653.89
Crystal system	monoclinic	monoclinic
Space group	$P2_1/c$	$P2_1/c$
Unit cell dimension	a = 15.2294(2) Å b = 13.91250(10) Å c = 15.2294(2) Å ß = 99.8080(10)°	a = 15.5504(9) Å b = 14.0675(8) Å c = 11.9746(7) Å ß = 100.8130(10)°
Volume	2469.73(6) $Å^3$	2573.0(3) $Å^3$
Z	4	4

Density (calculated)	1.759 Mg/m^3	1.688 Mg/m^3
Absorption coefficient	1.800 mm^{-1}	1.728 mm^{-1}
F(000)	1304	1304
Crystal size	0.08 x 0.08 x 0.12	0.18 x 0.16 x 0.10
θ range for data collection	2.00 to 25.11°	1.33 to 25.04°
Reflections collected	12815	13634
Independent reflections	4376 (R_{int} = 0.0663)	4718 (R_{int} = 0.0357)
Goodness of fit on F^2	1.054	1.115
Final R indices [I>2σ(I)]	R_1 = 0.0673, wR_2 = 0.1481	R_1 = 0.0382, wR_2 = 0.0708
R indices (all data)	R_1 = 0.1092, wR_2 = 0.1704	R_1 = 0.0703, wR_2 = 0.0839
T_{max}/T_{min}	0.8943/0.7109	0.8754/0.6273

4.7.1.3 Synthesis of $[Fe_3(CO)_9(CNPh)_3]$

R_f = 0.24 (green).

Elemental analysis: acceptable values could not be obtained, *e.g.* C, 53.34; H, 3.98; N, 4.51%. $C_{30}H_{15}Fe_3N_3O_9$ requires C, 49.40; H, 2.08; N, 5.76%.

IR (pet. spirits): ν (CN) 2148 (w), 2113 (m); ν (CO) 2052 (m), 2038 (m), 2016 (sh), 2009 (s), 1990 (sh), 1978 (sh) cm^{-1}.

ESMS (MeOH, +ve ion, 20 V): $[M + H]^+$ *m/z* 730 (100%).

4.7.1.4 Synthesis of $[Fe_3(CO)_8(CNPh)_4]$

R_f = 0.09 (green).

IR ($CHCl_3$): ν (CN) 2148 (w), 2113 (m); ν (CO) 2000 (s), 1990 (sh), 1986 (sh), 1965 (sh) cm^{-1}.

ESMS (MeOH, +ve ion, 20 V): $[M + H]^+$ *m/z* 806 (100%).

4.7.1.5 Synthesis of $[Fe_3(CO)_9(\mu_3\text{-}\eta^2\text{-}CNPh)]$

$R_f = 0.83$ (brown).

IR ($CHCl_3$): ν (CO) 2087 (m), 2055 (sh), 2041 (s), 2033 (s), 2017 (sh), 1996 (sh), 1978 (sh) cm^{-1}.

ESMS (MeOH/MeO^-, -ve ion, 5 V): $[M + MeO]^-$ *m/z* 554 (100%).

4.7.1.6 Synthesis of $[Fe_3(CO)_8(\mu_3\text{-}\eta^2\text{-}CNPh)(CNPh)]$

$R_f = 0.43$ (red).

IR ($CHCl_3$): ν (CN) 2146 (m), 2107 (m); ν (CO) 2041 (s), 2023 (sh), 2015 (sh) cm^{-1}.

ESMS (MeOH/MeO^-, -ve ion, 5 V): $[M + MeO]^-$ *m/z* 629 (100%).

4.7.1.7 Synthesis of $[Fe_3(CO)_{11}(CNPh^*)]$

$R_f = 0.58$ (green).

IR ($CHCl_3$): ν (CN) 2157 (br); ν (CO) 2081 (s), 2057 (sh), 2034 (s), 2041 (sh), 1996 (sh), 1972 (sh) cm^{-1}.

^1H NMR ($CDCl_3$): δ 7.44 (2H, s, H2'), δ 6.95 (2H, s, H3'), δ 3.86 (3H, s, $OC\underline{H}_3$).

$^{13}C\text{-}\{^1H\}$ NMR ($CDCl_3$): δ 212.7 (s, $\underline{C}O$), δ 160.1 (s, C4'), δ 126.9 (s, C2'), δ 114.8 (s, C3'), δ 55.7 (s, $O\underline{C}H_3$).

ESMS (MeOH, +ve ion, 20 V): $[M + H]^+$ *m/z* 610 (100%).

4.7.1.8 Synthesis of $[Fe_3(CO)_{10}(CNPh^*)_2]$

$R_f = 0.21$ (green).

Elemental analysis: acceptable values could not be obtained, *e.g.* C, 47.28; H, 2.96; N 3.67%. $C_{26}H_{14}Fe_3N_2O_{12}$ requires C, 43.70; H, 0.16; N, 3.92%.

IR ($CHCl_3$): ν (CN) 2126 (br); ν (CO) 2059 (s), 2032 (s), 2014 (sh), 1994 (sh), 1989 (sh), 1964 (sh) cm^{-1}.

IR (pet. spirits): ν (CN) 2135 (sh) 2125 (m); ν (CO) 2057 (s), 2028 (s), 2024 (sh), 2018 (s), 2013 (sh), 1999 (m), 1987 (sh), 1972 (s) cm^{-1}.

^1H NMR ($CDCl_3$): δ 7.39 (4H, d, $^3J_{H2',H3'}$ = 2.5 Hz, H2'), δ 6.91 (4H, d, $^3J_{H3',H2'}$ = 5.8 Hz, H3'), δ 3.85 (3H, s, $OC\underline{H}_3$).

ESMS (MeOH, +ve ion, 20 V): $[M + H]^+$ *m/z* 715 (100%).

4.7.1.9 Synthesis of $[Fe_3(CO)_9(CNPh^*)_3]$

R_f = 0.06 (green).

IR (pet. sprits): ν (CN) 2120 (m); ν (CO) 2053 (sh), 2037 (m), 2021 (sh), 2016 (sh), 2006 (s), 2000 (sh), 1991 (sh), 1984 (sh), 1974 (m) cm^{-1}.

ESMS (MeOH, +ve ion, 20 V): $[M + H]^+$ *m/z* 820 (100%).

4.7.1.10 Synthesis of $[Fe_3(CO)_9(\mu_3\text{-}\eta^2\text{-}CNPh^*)]$

R_f = 0.73 (brown).

IR ($CHCl_3$): ν (CO) 2086 (m), 2059 (w), 2040 (vs), 2031 (vs), 2015 (s), 1995 (m), 1975 (w) cm^{-1}.

ESMS (MeOH/MeO^-, -ve ion, 5 V): $[M + MeO]^-$ *m/z* 584 (100%).

4.7.1.11 Synthesis of $[Fe_3(CO)_8(\mu_3\text{-}\eta^2\text{-}CNPh^*)(CNPh^*)]$

R_f = 0.4 (red-brown).

IR ($CHCl_3$): ν (CN) 2146 (m); ν (CO) 2064 (sh), 2058 (m), 2038 (w), 2019 (vs), 1980 (m) cm^{-1}.

ESMS (MeOH/MeO^-, -ve ion, 5 V): $[M + MeO]^-$ *m/z* 689 (100%).

4.7.1.12 Synthesis of $[Fe_3(CO)_{11}(TosMIC)]$

$R_f = 0.78$ (green).

Elemental analysis: C, 35.94; H, 1.35; N, 2.16%. $C_{20}H_9Fe_3NSO_{13}$ requires C, 35.77; H, 1.34; N, 2.10%.

IR ($CHCl_3$): ν (CN) 2173 (m, br); ν (CO) 2082 (sh), 2062 (s), 2047 (sh), 2003 (sh), 1974 (s) cm^{-1}.

ESMS (MeOH, +ve ion, 20 V): $[M + H]^+$ *m/z* 672 (100%), $[2M + H]^+$ *m/z* 1344 (10%).

ESMS (MeOH, -ve ion, 5 V): $[M - H]^-$ *m/z* 670 (20%), $[M - CO - H]^-$ *m/z* 642 (100%).

4.7.1.13 Synthesis of $[Fe_3(CO)_{10}(TosMIC)_2]$

$R_f = 0.63$ (green).

Elemental analysis: C, 39.97; H, 2.13; N, 3.35%. $C_{28}H_{18}Fe_3N_2S_2O_{14}$ requires C, 40.10; H, 2.15; N, 3.34%.

IR ($CHCl_3$): ν (CN) 2164 (m, br); ν (CO) 2098 (sh), 2080 (s), 2062 (sh), 2042 (s), 2033 (sh), 2020 (sh) cm^{-1}.

ESMS (MeOH, +ve ion, 20 V): $[M + H]^+$ *m/z* 839 (100%), $[2M + H]^+$ *m/z* 1677 (5%).

ESMS (MeOH, -ve ion, 5 V): $[M - H]^-$ *m/z* 837 (57%), $[M - CO - H]^-$ *m/z* 809 (100%).

4.7.1.14 Synthesis of $[Fe_3(CO)_9(TosMIC)_3]$

$R_f = 0.39$ (green).

Elemental analysis: C, 44.18; H, 4.28; N, 3.43%. $C_{36}H_{27}Fe_3N_3S_3O_{15}$ requires C, 42.99; H, 2.69; N, 4.18%.

IR ($CHCl_3$): ν (CN) 2168 (m, br), 2143 (w); ν (CO) 2083 (sh), 2074 (sh), 2061 (m), 2030 (s), 2015 (sh), 1991 (sh), 1965 (sh) cm^{-1}.

ESMS (MeOH, +ve ion, 20 V): $[M + H]^+$ *m/z* 1006 (100%).

ESMS (MeOH, -ve ion, 5 V): $[M - H]^-$ *m/z* 1004 (100%), $[M - CO - H]^-$ *m/z* 976 (20%).

4.7.2 Reactions of $[Ru_3(CO)_{12}]$ with isonitriles

The general reaction was carried out as follows: $[Ru_3(CO)_{12}]$ (0.5 g, 0.78 mmol) was dissolved in 10 mL of toluene. The isonitrile (3.13 mmol) was added by syringe or as a solid and the reaction was gently refluxed for *ca.* 30 minutes. Samples were withdrawn at appropriate time intervals and the course of the reaction monitored by tlc. The solvent was removed *in vacuo*, the reaction products redissolved in a minimum amount of CH_2Cl_2, and subsequently chromatographed on silica plates (Merck, Silica gel 60G) with a solvent mixture of pet. spirits (b.p. 60 - 80°C)/CH_2Cl_2 (CNPh derivatives 1:1, CNPh* derivatives 1:2). Yields of the isolated complexes were not determined because only parts of the crude reaction product were used at a time for chromatography. The identity of the complexes $[Ru_3(CO)_{10}(CNPh)_2]$ and $[Ru_3(CO)_9(CNPh)_3]$ were confirmed by comparison with the IR frequencies of previously reported analogues.

4.7.2.1 Synthesis of $[Ru_3(CO)_{11}(CNPh)]$

$R_f = 0.89$ (yellow).

IR ($CHCl_3$): ν (CN) 2158 (m); ν (CO) 2091 (m), 2049 (s), 2041 (s), 2021 (sh), 2010 (s), 1998 (sh) cm^{-1}. [Lit: ν (CO) 2080 (m), 2035 (sh), 2020 (s), 2005 (sh), 1992 (s), 1982 (s), 1975 (sh), 1958 (m), 1948 (m), 1843 (m), 1805 (m), 1790 (m) cm^{-1} [43]].

^1H NMR ($CDCl_3$): δ 7.39 – 7.28 (5H, m, H2-4).

ESMS (MeOH, +ve ion, 20 V): $[M + H]^+$ *m/z* 716 (100%).

ESMS (MeOH/MeO^-, -ve ion, 5 V): $[M - 2CO + MeO]^-$ *m/z* 690 (100%), $[M - 3CO + MeO]^-$ *m/z* 661 (31%).

4.7.2.2 Synthesis of $[Ru_3(CO)_{10}(CNPh)_2]$

$R_f = 0.79$ (orange).

IR ($CHCl_3$): ν (CN) 2157 (sh), 2137 (m); ν (CO) 2066 (m), 2030 (s), 2005 (sh), 1994 (s), 1986 (sh) cm^{-1}. [Lit. for R = Bu^t: ν (CO) 2065 (w), 2020 (s), 2057(m), 1996 (s), 1990 (m), 1986 (m) cm^{-1} [41]].

ESMS (MeOH, +ve ion, 20 V): $[M + H]^+$ *m/z* 791 (100%), $[M - CO + H]^+$ *m/z* 762 (7%).

ESMS (MeOH/MeO^-, -ve ion, 5 V): $[M + MeO]^-$ *m/z* 821 (50%), $[M - CO + MeO]^-$ *m/z* 792 (8%), $[M - 2CO + MeO]^-$ *m/z* 763 (100%), $[M - 3CO + MeO]^-$ *m/z* 734 (8%).

4.7.2.3 Synthesis of $[Ru_3(CO)_9(CNPh)_3]$

R_f = 0.73 (red).

IR ($CHCl_3$): ν (CN) 2162 (m), 2140 (m), 2123 (sh); ν (CO) 2062 (m), 2030 (s), 1997 (m), 1978 (sh) cm^{-1}. [Lit. for R = Bu^t: ν (CO) 2040 (m), 1998 (s), 1971 (s) cm^{-1} [41]].

ESMS (MeOH, +ve ion, 20 V): $[M + H]^+$ *m/z* 866 (100%), $[M - CO + H]^+$ *m/z* 838 (5%).

ESMS (MeOH/MeO^-, -ve ion, 5 V): $[M + MeO]^-$ *m/z* 896 (100%), $[M - 2CO + MeO]^-$ *m/z* 838 (20%).

4.7.2.4 Synthesis of $[Ru_4(CO)_{11}(CNPh)_3]$

R_f = 0.65 (red).

Elemental analysis: This fraction was of mixture of two compounds, which could not be separated by chromatography, and so no elemental analysis could be obtained.

IR ($CHCl_3$): ν (CN) 2166 (m); ν (CO) 2076 (m), 2050 (s), 2033 (s), 2006 (m), 1985 (sh) cm^{-1}.

ESMS (MeOH, +ve ion, 20 V): $[M + H]^+$ *m/z* 1024 (100%).

ESMS (MeOH/MeO^-, -ve ion, 5 V): $[M + MeO]^-$ *m/z* 1053 (100%) {also observed: $[Ru_4(CO)_{12}(CNPh)_2 + MeO]^-$ *m/z* 976 (33%), $[Ru_4(CO)_{12}(CNPh)_2 - CO + MeO]^-$ *m/z*

946 (8%), $[Ru_4(CO)_{12}(CNPh)_2 - 2CO + MeO]^-$ *m/z* 919 (35%)}.

X-ray crystal structure determination of $[Ru_4(CO)_{11}(CNPh)_3]$

Single crystals of $[Ru_4(CO)_{11}(CNPh)_3]$ were obtained as described in section 4.5.3. Crystallographic data are given in Table 4.12.

Table 4.12 Crystallographic data and structure refinement for $[Ru_4(CO)_{11}(CNPh)_3]$.

Empirical formula	$C_{32}H_{15}N_3O_{11}Ru_4$
M_r	1021.75
Temperature	100(2) K
Crystal system	monoclinic
Space group	$P2_1/c$
Unit cell dimension	a = 9.46990(10) Å b = 19.65330(10) Å c = 18.5984(2) Å ß = 102.6660(10)°
Volume	3377.20(5) $Å^3$
Z	4
Density (calculated)	2.010 Mg/m^3
Absorption coefficient	1.819 mm^{-1}
F(000)	1968
Crystal size	0.46 x 0.08 x 0.08
θ range for data collection	1.53 to 25.73°
Reflections collected	18284
Independent reflections	6392 (R_{int} = 0.0226)
Goodness of fit on F^2	1.086
Final R indices [I>2σ(I)]	R_1 = 0.0231, wR_2 = 0.0462
R indices (all data)	R_1 = 0.0305, wR_2 = 0.0487
T_{max}/T_{min}	0.897054/0.712398

4.7.2.5 Synthesis of $[Ru_3(CO)_{11}(CNPh^*)]$

$R_f = 0.95$ (yellow).

IR ($CHCl_3$): ν (CN) 2161 (m); ν (CO) 2092 (m), 2048 (s), 2041 (s), 2020 (sh), 2009 (s), 1996 (sh) cm^{-1}. [Lit: ν (CN) 2155 (w); ν (CO) 2092 (w), 2071 (vw), 2062 (w), 2049 (s), 2041 (vs), 2019 (w), 1999 (m), 1992 (m) cm^{-1} [41]].

ESMS (MeOH, +ve ion, 20 V): $[M + H]^+$ *m/z* 745 (100%), $[M - CO + H]^+$ *m/z* 719 (30%).

ESMS ($MeOH/MeO^-$, -ve ion, 5 V): $[M - 2CO + MeO]^-$ *m/z* 719 (100%), $[M - 3CO + MeO]^-$ *m/z* 690 (18%).

4.7.2.6 Synthesis of $[Ru_3(CO)_{10}(CNPh^*)_2]$

$R_f = 0.78$ (yellow).

IR ($CHCl_3$): ν (CN) 2159 (sh), 2142 (m); ν (CO) 2067 (m), 2029 (s), 2004 (sh), 1993 (s), 1980 (sh) cm^{-1}. [Lit: ν (CN) 2154 (w); ν (CO) 2093 (m), 2062 (m), 208 (s), 2040 (s), 2030 (vs), 2022 (s), 1996 (s), 19907 (s), 1990 (s) cm^{-1} [41]].

ESMS (MeOH, +ve ion, 20 V): $[M + H]^+$ *m/z* 851 (100%), $[M - CO + H]^+$ *m/z* 822 (5%).

ESMS ($MeOH/MeO^-$, -ve ion, 5 V): $[M + MeO]^-$ *m/z* 881 (28%), $[M - CO + MeO]^-$ *m/z* 853 (12%, $[M - 2CO + MeO]^-$ *m/z* 822 (100%).

4.7.2.7 Synthesis of $[Ru_4(CO)_{11}(CNPh^*)_3]$

$R_f = 0.53$ (red).

Elemental analysis: This fraction was of mixture of two compounds, which could not be separated by chromatography, and so no elemental analysis could be obtained.

IR ($CHCl_3$): ν (CN) 2165 (m); ν (CO) 2075 (m), 2062 (sh), 2058 (sh), 2049 (s), 2032 (vs), 2004 (m), 1981 (w) cm^{-1}.

ESMS ($MeCN/H_2O$, +ve ion, 20 V): $[M + H]^+$ *m/z* 1114, (100%), $[M - CO + H]^+$ *m/z* 1085, (17%), $[M - CO + MeCN + H]^+$ *m/z* 1128, (42%), $[M + MeCN + H]^+$ *m/z* 1155, (28%).

ESMS ($MeOH/MeO^-$, -ve ion, 5 V): $[M + MeO]^-$ *m/z* 1143, (100%).

Chapter 5

Electrospray-friendly sulfur-based complexes

The high reactivity of metal complexes with sulfur-containing ligands is clearly demonstrated by the wide scope of metal-sulfur coordination chemistry and has been reviewed[1,2]. An impetus into research is given by the importance of transition-metal sulfur complexes in biological[3] (proteins and metalloenzymes exhibit thiolate and sulfide coordination) and industrial processes[4]. The classical sulfur-containing ligands are thiolates RS^-, hydrosulfide HS^- and sulfide S^{2-}. Difunctional, sterically hindered and mixed sulfide-thiolate ligands are examples of various sub-areas. The chemistry of S-donor ligands is further complicated by the various potential bonding modes. Monofunctional ligands can bond in a terminal, μ_2- or μ_3-bridging manner, while the possibilities for difunctional ligands are even greater.

The sulfur-based compounds studied in this chapter consist of transition-metal thiolate complexes as well as compounds that contain sulfide bridges. Thiolate ligands incorporating a basic site were analysed with regard to their use as electrospray-friendly ligands, *i.e.* whether or not they are able to make the thiolate complexes visible in the ESMS. This is followed by the investigation of exchange processes in cadmium thiophenolate complexes. The last part of this chapter investigates the chemistry of the platinum sulfide complex $[Pt_2(\mu\text{-}S)_2(PPh_3)_4]$ and derivatives thereof.

5.1 Electrospray-friendly thiolate ligands

For the design of electrospray-friendly thiolate ligands, the same concepts apply as for the previously described electrospray-friendly ligands. Firstly, incorporation of a basic group should ensure that metal complexes of this ligand give $[M + H]^+$ signals in the

---

[1] P.J. Blower and J. R. Dilworth, *Coord. Chem. Rev.*, 1987, **76**, 121.
[2] J. R. Dilworth and J. Hu, *Adv. Inorg. Chem.*, 1993, **40**, 411.
[3] B. Krebs and G. Henkel, *Ang. Chem. Int. Ed. Engl.*, 1991, **30**, 769.
[4] C. J. Bowlas, A. E. Underhill and D. Thetford, *Phosphorus, Sulfur, Silicon Relat. Elem.*, 1992, **67**, 301; G. Matsubayashi, M. Hirao, T. Tanaka, *Inorg. Chim. Acta*, 1988, **144**, 217; N. Brugat, A. Polo, A. Alvarez-Larena, J. F. Piniella and J. Real, *Inorg. Chem.*, 1999, **38**, 4829; G. B. Karet and N. M. Kostik, *Inorg. Chem.*, 1998, **37**, 1021.

ESMS and can thus be easily studied by this method. Secondly, if the basic group is in *para*-position the derivatives will be relatively similar to the parent ligand with respect to its electronic and steric properties. In the coordination chemistry of aromatic thiolate ligands, substituents are often found in *ortho*-positions[1]. These sterically hindered ligands are commonly employed to prevent C–S bond cleavage and formation of thiolate-bridged polymers. For the purposes in this project, however, having the substituent in *para*-position is important for the reasons mentioned above.

An obvious analogue to thiophenol, PhSH, is *p*-methoxythiophenol, HS*. HS*, like PhSH, is a colourless volatile liquid with a distinctive thiol smell. A compound that makes use of a basic nitrogen function is the pyridine analogue 4-mercaptopyridine, HS$^{\bullet}$. HS$^{\bullet}$ is a crystalline solid and, like HS*, commercially available. Both HS* and HS$^{\bullet}$ are shown in Figure 5.1.

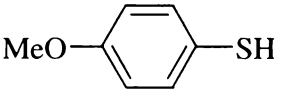

HS*

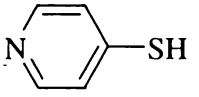

HS$^{\bullet}$

Fig. 5.1 The two electrospray-friendly thiols HS* and HS$^{\bullet}$.

With regard to protonation of the thiolate complexes in the ESMS, it was of interest to compare the basicities of both ligands. S$^{\bullet -}$ should be the more basic thiolate ligand, as it incorporates the strongly basic pyridine moiety as compared to anisole in S*$^{-}$. Amines, in general, are more basic than alcohols and ethers as their ions $[BH]^+$ (B = base) are more stable relative to the amine from which they are formed (N is less electronegative than O and can therefore better accommodate the positive charge on the ion). A number of scales have been introduced in order to determine the strengths of various bases. The β-scale of hydrogen-bond basicities by Kamlet and Taft is one of them[5]. It provides a database for the basicity of a large number of solvents. Other scales have been

introduced more recently[6]. The values for anisole and pyridine are listed in Table 5.1 (the larger β, the stronger the base). The strongly basic hexamethylphosphoramide is included as well for comparison.

Table 5.1 The basicity values for selected solvents, according to the β-scale of hydrogen-bond basicities by Kamlet and Taft.

Solvent	β
Anisole	0.247
Pyridine	0.661
$(Me_2N)_3PO$	0.990

In order to compare the basicity of the two electrospray-friendly thiols with HSPh, a β-value for benzene would be required. Since benzene belongs to the group of non-hydrogen-bonding solvents there are, however, no β-values for it, or any other inert solvents. Benzene is not classified as a compound with basic properties.

As 'modified thiophenols', both HS* and HS$^{\bullet}$ can offer advantages over the simple HSPh, as improvements might be achieved with regard to the properties under investigation. Thus, S*$^{-}$ has been commonly employed when a variety of *para*-substituted thiophenolate complexes were investigated, *e.g.* for their structural[7], kinetic[8], or photophysical[9] properties, or simply when substituent effects on classical physical properties were the primary concern[10]. S$^{\bullet-}$ can potentially act as a thiolate as well as pyridine ligand. However, while there are many examples for coordination through the S

---

[5] M. J. Kamlet and R. W. Taft, *J. Am. Chem. Soc.*, 1976, **98**, 377.
[6] J. Catalán, J. Gómez, A. Couto and J. Laynez, *J. Am. Chem. Soc.*, 1990, **112**, 1678 and refs. therein.
[7] X. Chen, F. J. Femia, J. W. Babich and J. Zubieta, *Inorg. Chim. Acta*, 2000, **307**, 88; B. Nock, H. J. Pietzsch, F. Tisato, T. Maina, P. Leibnitz, H. Spies and E. Chiotellis, *Inorg. Chim. Acta*, 2000, **304**, 26; N. Ueyama, K. Taniuchi, T. Okamura, A. Nakamura, E. Hironobu and S. Emura, *Inorg. Chem.*, 1996, **35**, 1945.
[8] M. T. Ashby, J. H. Enemark and D. L. Lichtenberger, *Inorg. Chem.*, 1988, **27**, 191.
[9] V. W.-W. Yam, C.-H. Lam, W. K.-M. Fung and K.-K. Cheung, *Inorg. Chem.*, 2001, **40**, 3435.
[10] A. G. Larsen, A. H. Holm, M. Robertson and K. Daasbjerg, *J. Am. Chem. Soc.*, 2001, **123**, 1723; T. Schaefer and W. Parr, *Can. J. Chem.*, 1977, **55**, 552; G. Chuchani and A. Frohlich, *J. Chem. Soc. B.*, 1971, 1417.

atom[11], a structure with coordination through N is rather rare and involves $S^{\bullet-}$ as a disulfide or other substructure[12]. The biochemical and biological applications of metal complexes of mercaptopyridine and its derivatives range from antimicrobial and antifungal, use in plant, animal and human diseases, use as deodorants, as preservatives *etc.*, and have been reviewed[13].

5.2 Electrospray friendly thiophenolate complexes

The electron-rich thiolate groups RS^- are typical soft ligands, as defined by Pearson[14]. As a general rule for their stabilities in metal complexes, soft ligands form stable complexes with soft metal ions. Thiolates therefore have a great affinity for soft metal centres such as the late transition metals. In this work, a series of transition-metal thiolates was prepared incorporating the metal centres Ni^{2+}, Pd^{2+}, Pt^{2+}, Au^+ and Hg^{2+}.

Among the many routes to transition-metal thiolates, the method of choice was using the corresponding metal halide $[L_nMX_n]$ and thiol in the presence of a base. Other methods include the use of lithium, sodium or potassium salts of thiols or, alternatively, more covalent thiolate sources such as $Pb(SR)_2$ or AgSR. Metal halides also react with Me_3SiSR with the formation of the volatile Me_3SiCl. These and other methods are described in more detail in the literature[1]. The complexes in this study were all prepared from the corresponding metal chloride with Et_3N as a base in MeOH solvent. In each case, the two thiols, HS* and $HS^{\bullet}$, were employed to produce potentially electrospray-friendly complexes. The parent SPh complexes were prepared as well for comparative purposes.

5.2.1 ESMS of the thiophenolate complexes

A list of the prepared thiophenolate complexes is given in Table 5.2, together with the observed ions in the ESMS.

---

[11] See for example: S. Brand and J. R. Shapley, *Inorg. Chem.*, 2000, **39**, 32; W. Gaete, J. Ros, R. Yanez, X. Solans and M. Font-Altaba, *J. Organomet. Chem.*, 1986, **316**, 169.
[12] M. Kondo, M. Shimamura, S. Noro, Y. Kimura, K. Uemura and S. Kitagawa, *J. Solid State Chem.*, 2000, **152**, 113; O.-S. Jung, S. H. Park, D. C. Kim and K. M. Kim, *Inorg. Chem.*, 1998, **37**, 610.
[13] T. S. Lobana and P. K. Bhatia, *J. Sci. Ind. Res.*, 1989, **48**, 394.
[14] D. F. Shriver, P. W. Atkins and C. H. Langford, *Inorganic Chemistry,* 2nd ed., University Press, Oxford, 1994, p.212.

Table 5.2 The positive-ion ESMS data for the prepared thiophenolate complexes, recorded in MeOH at 20 V.

Complex	Ions observed [*m/z*, relative peak height (%)][(a)]
[(dppe)Ni(SPh)$_2$]	–
[(dppe)NiS*$_2$]	–
[(dppe)NiS$^{\bullet}_2$]	$[M + H]^{2+}$ (340, 100), $[M - S^{\bullet}]^{+}$ (566, 32), $[M + H]^{+}$ (677, 65)
[(dppe)Pd(SPh)$_2$]	–
[(dppe)PdS*$_2$]	–
[(dppe)PdS$^{\bullet}_2$]	$[M + H]^{2+}$ (346, 34), $[M - S^{\bullet}]^{+}$ (614, 8), $[M + H]^{+}$ (724, 100), $[2M - S^{\bullet}]^{+}$ (1341, 5), $[2M + H]^{+}$ (1452, 10)
[(dppe)Pt(SPh)$_2$]	–
[(dppe)PtS*$_2$]	$[M + H]^{+}$ (873, 10)
[(dppe)PtS$^{\bullet}_2$]	$[M + H]^{2+}$ (408, 50), $[M - S^{\bullet}]^{+}$ (704, 4), $[2M - S^{\bullet}]^{2+}$ (759, 8), $[M + H]^{+}$ (814, 100), $[2M - S^{\bullet}]^{+}$ (1517, 15), $[2M + H]^{+}$ (1627, 5)
[(Ph$_3$P)Au(SPh)]	–
[(Ph$_3$P)AuS*]	–
[(Ph$_3$P)AuS$^{\bullet}$]	$[M + H]^{+}$ (570, 55), $[Au(PPh_3)_2]^{+}$ (721, 100)
[PhHg(SPh)]	–
[PhHgS$^{\bullet}$]	$[M + H]^{+}$ (387, 100)

[(a)] Ions resulting from ionic impurities are not listed.

As expected, none of the thiophenolate complexes incorporating the SPh ligand gave $[M + H]^{+}$ ions in the ESMS. However, a number of very intense signals appeared for all group VIII complexes of the general formula [(dppe)M(SPh)$_2$], [dppe = 1,2-bis(diphenylphosphino)ethane] resulting from ionic side products. At the cone voltage of 20 V, the most intense signal was the dimeric $[(dppe)M(\mu\text{-}SPh)]_2^{2+}$ ion, whose likely structure is shown in Figure 5.2. Other signals were associated with the coordination of various combinations of $[(dppe)M(\mu\text{-}SPh)]_2^{2+}$ with [(dppe)M(SPh)$_2$] or the $[M - SPh]^{+}$ fragment, and are listed in the Experimental part of this chapter.

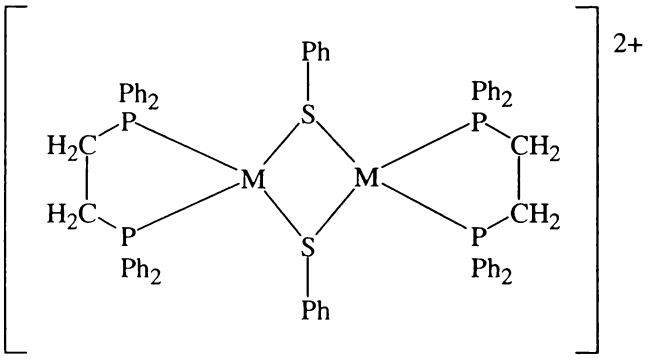

Fig. 5.2 The structure of $[(dppe)M(\mu\text{-}SPh)]_2^{2+}$ (M = Ni, Pd, Pt).

All ions were most probably due to impurities or aggregates with impurities, because the characterisation of the complexes (elemental analyses, integration of ^1H NMR spectrum) ruled out the possibility that dimeric products had been formed instead of the desired monomeric complexes. For species containing Pt, the formation of the monomeric complex was additionally confirmed by calculation of the $^1J_{Pt,P}$ coupling constants in the ^{31}P NMR spectrum. Not only would $[(dppe)Pt(\mu\text{-}SPh)]_2^{2+}$ have a different coupling constant, it would also show further coupling between phosphorus and the other platinum nucleus.

Similarly, the only observed ions for the gold complex $[(Ph_3P)Au(SPh)]$ originated from side products and were of the type $[(Ph_3P)_xAu_y(SPh)_z]^+$. They were assigned to $[(Ph_3P)_2Au_2(SPh)]^+$, $[(Ph_3P)_3Au_2(SPh)]^+$ and $[(Ph_3P)_3Au_3(SPh)_2]^+$ and their presumed structures are shown in Figure 5.3. Ligand scrambling in gold-phosphine complexes has been observed previously by other groups[15]. The structures of species A[16] and C[17] have been determined and the structure of D[18] has been proposed.

---

[15] S. Onaka, Y. Katsukawa, M. Shiotsuka, O. Kanegawa and M. Yamashita, *Inorg. Chim. Acta*, 2001, **312**, 100; R. Colton, K. L. Harrison, Y. A. Mah and J. C. Traeger, *Inorg. Chim. Acta*, 1995, **231**, 65; B. Assmann and H. Schmidbaur, *Chem. Ber.*, 1997, **130**, 217.

[16] N. C. Baenzinger, W. E. Bennett, D. M. Soboroff, P. S. O'Donnell and J. R. Doyle, *Polyhedron*, 1998, **17**, 2379.

[17] A. Sladek, W. Schneider, K. Angemaier, A. Bauer and H. Schmidbaur, *Z. Naturforsch.*, 1996, Teil B, **51**, 765.

[18] H. Schmidbaur, *Chem. Soc. Rev.*, 1995, 391.

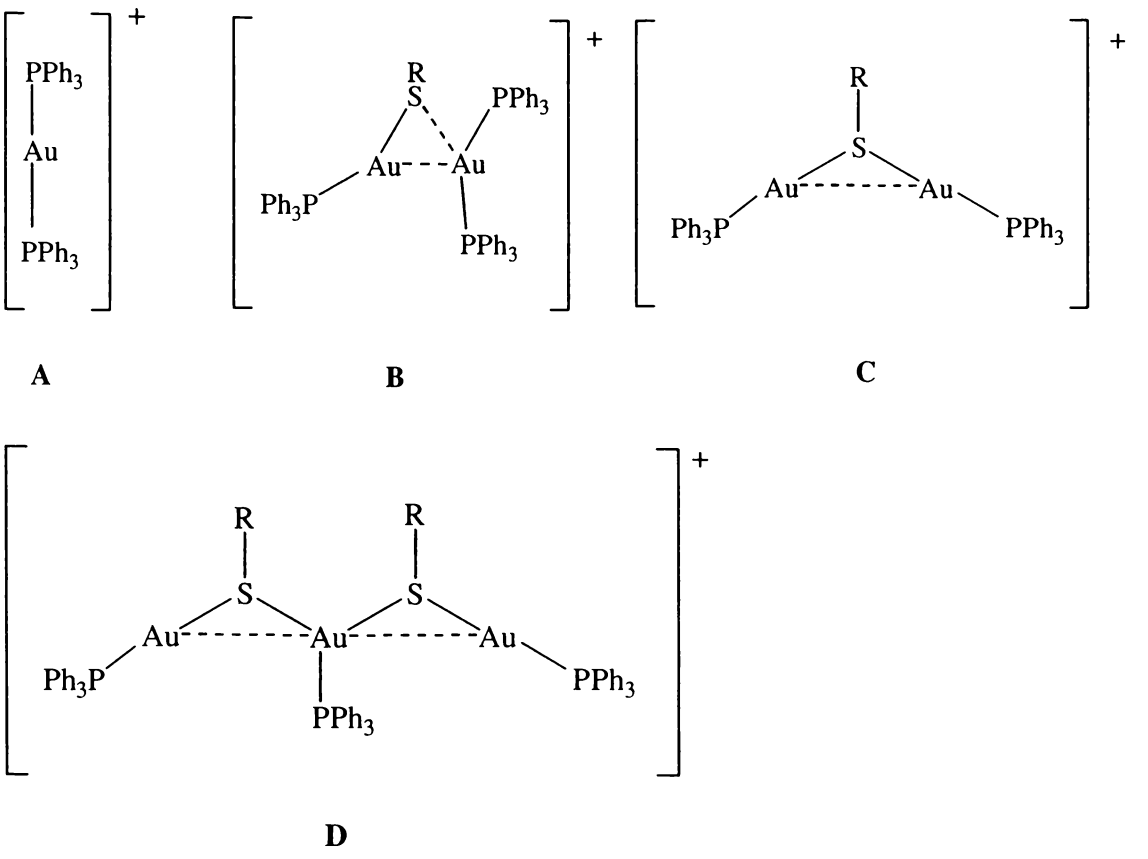

Fig. 5.3 The proposed and determined structures of $[Au(PPh_3)_2]^+$(A), $[(Ph_3P)_3Au_2(SR)]^+$ (B), $[(Ph_3P)_2Au_2(SR)]^+$(C), and $[(Ph_3P)_3Au_3(SR)_2]^+$(D).

Surprisingly, none of the S* complexes, although having a basic site for protonation, gave rise to an $[M + H]^+$ ion. They all behaved very much like non-electrospray-friendly complexes. The only exception was $[(dppe)PtS^*_2]$, for which an $[M + H]^+$ ion was detected. However, the intensity of this signal was relatively weak with a low signal to noise ratio, illustrated in Figure 5.4, which shows only a small region of the spectrum. Other signals were ionic species similar to those observed for all previous SPh complexes.

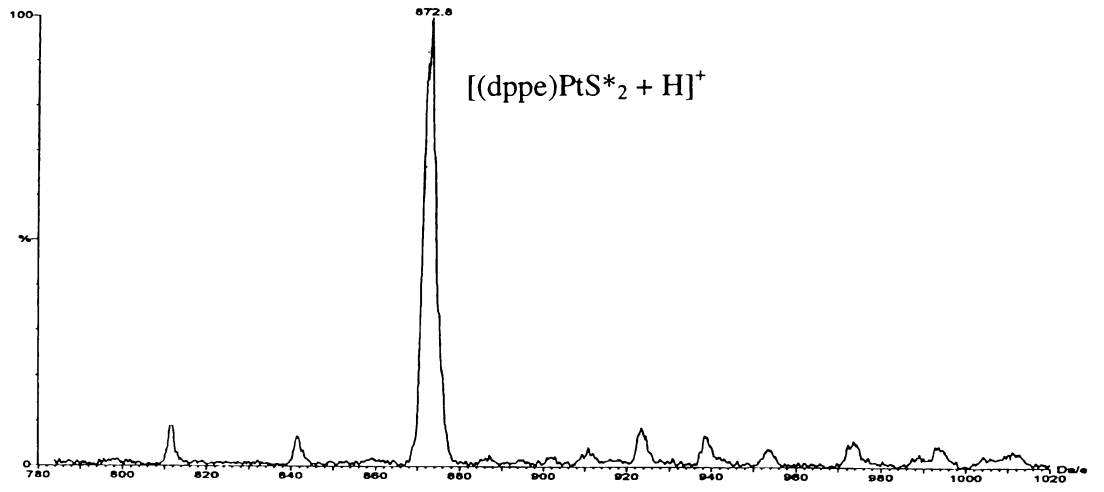

Fig. 5.4 The positive-ion ES mass spectrum of [(dppe)PtS*$_2$], recorded in MeCN/H_2O at cV = 20 V.

It should be noted that this phenomenon was reproducible on numerous occasions, ruling out the possibility that some sort of ionisation aid had been present in the system and the reason for the detection of the $[M + H]^+$ ion. Thus, the Pt complex was the only example where the desired monomeric species was observed as its $[M + H]^+$ ion. In fact, the formation of dimers and oligomers of Ni, Pd and Pt thiolate complexes has been studied extensively[19] and it was found that within the triad, platinum was the metal most likely to form monomers. Complexes of nickel and palladium appeared to have a stronger tendency to form dimers, oligomers, and eventually insoluble polymers through thiolate bridges, as illustrated in Scheme 5.1.

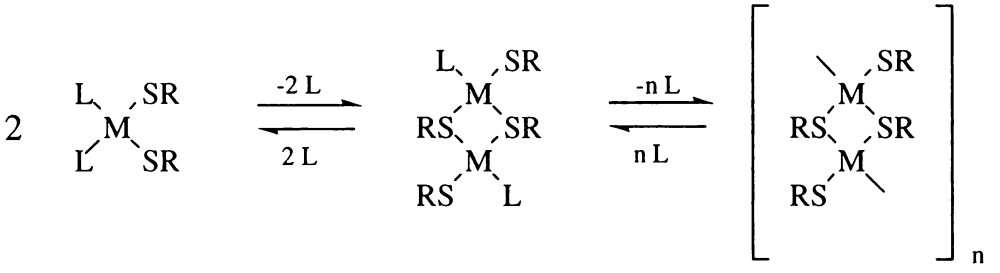

Scheme 5.1 The formation of thiolate bridges leading to long-chain oligomers.

[19] T. B. Rauchfuss, J. S. Shu and D. M. Roundhill, *Inorg. Chem.*, 1976, **15**, 2096.

All S$^{\bullet}$-complexes ionised as desired by protonation. In the case of the group VIII complexes with two thiolate ligands, both N atoms were protonated, yielding $[M + H]^+$ as well as $[M + 2H]^{2+}$ ions. Additionally, these complexes ionised by losing a thiolate ligand, thereby forming the $[M - S^{\bullet}]^+$ ion. This is the ionisation pathway commonly observed for metal halide complexes[20]. To some extent, the reactivity and electronic structure of thiolates are comparable to those of halide ligands (*e.g.* terminal RS^- ligands can replace halide ligands and *vice versa*[21]). The preferred pathway depended very much on the cone voltages used. Figure 5.5 illustrates how protonation dominated at low cone voltages, while signals associated with halide loss were more intense at higher cone voltages.

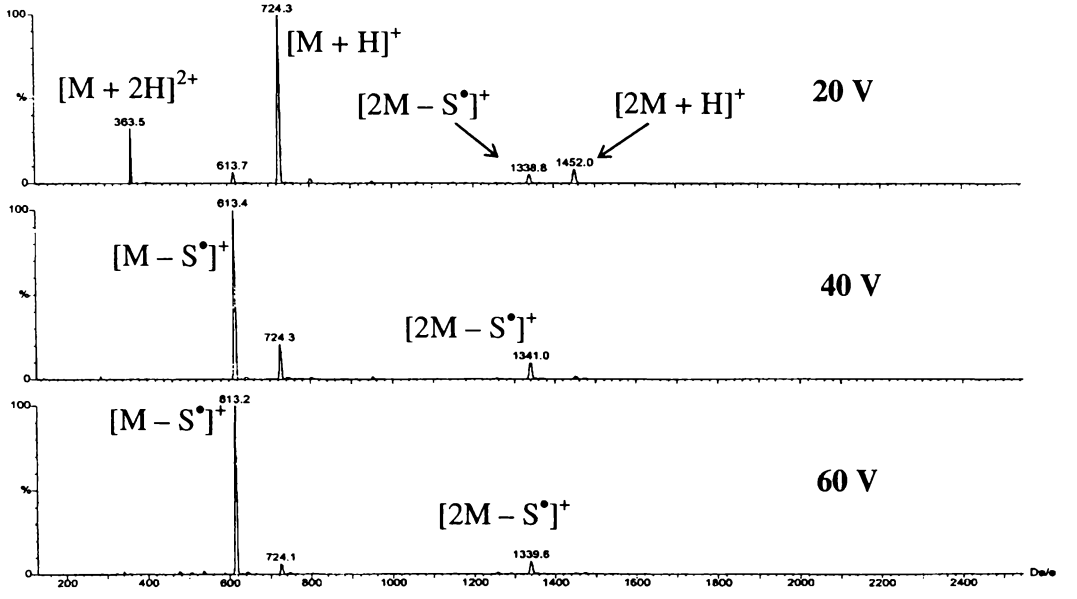

Fig. 5.5 The positive-ion ES mass spectrum of [(dppe)PdS$^{\bullet}_2$], recorded in MeOH at cV = 20, 40, and 60 V.

The mercaptopyridine complex of the platinum series behaved in a manner similar to the other two S$^{\bullet}$-complexes of the nickel triad. The ES mass spectrum of [(dppe)PtS$^{\bullet}_2$] at 20 V is shown in Figure 5.6a. Apart from the parent $[M + H]^+$ ion, the dicationic $[M + 2H]^{2+}$ was observed at half the *m/z* value. At the other end of the spectrum, the [2M +

[20] W. Henderson and C. Evans, *Inorg. Chim. Acta*, 1999, **294**, 183.
[21] R. Zanella R. Ros and M. Graziani, *Inorg. Chem.*, 1973, **12**, 2736.

$H]^+$ ion was observed as well. The isotope patterns for all three signals are shown in Figure 5.6b. They can easily be distinguished as the 2+ ion has *m/z* separations of 0.5, whereas the $[2M + H]^+$ ion exhibits more signals in its isotope pattern due to the two platinum atoms. The signal associated with the $[M - S^\bullet]^+$ ion was relatively low in intensity and is indicated by an asterisk. Greater in intensity was the second ion formed by ligand loss, $[2M - S^\bullet]^+$ at *m/z* 1517. At exactly half its *m/z* value, a 2+ ion was detected with an isotope pattern suggesting the presence of two platinum atoms. This indicated the formation of $[2M - S^\bullet]^{2+}$, but it could not be explained how the second positive charge was achieved.

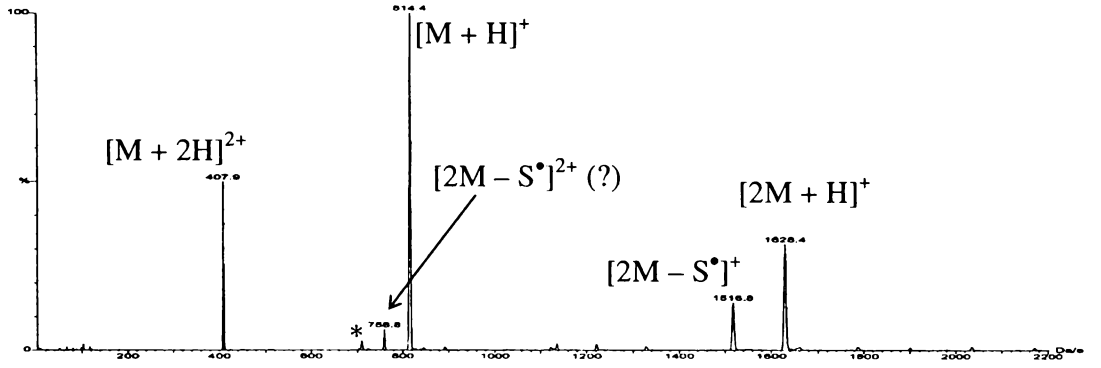

Fig. 5.6a The positive-ion ES mass spectrum of $[(dppe)PtS^\bullet_2]$, recorded in MeOH at cV = 20 V.

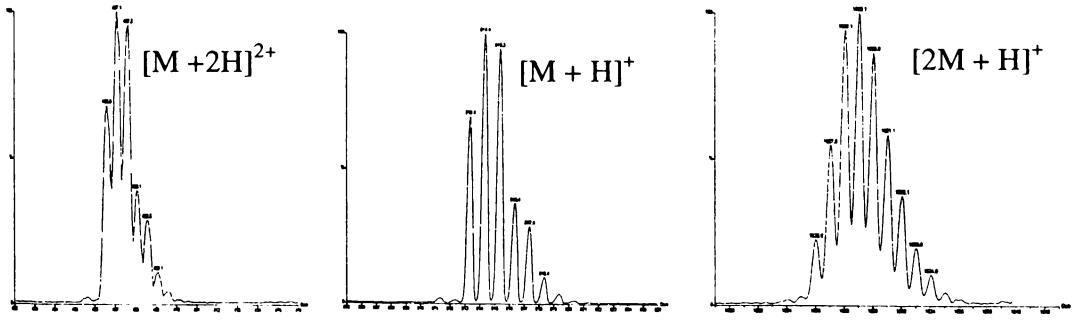

Fig. 5.6b The observed isotope patterns of the ions $[M +2H]^{2+}$, $[M + H]^+$ and $[2M + H]^+$ for M = $[(dppe)PtS^\bullet_2]$.

In an attempt to prepare [PhHgS*], an insoluble, possibly polymeric compound was isolated. NMR and elemental analysis suggested [HgS^*_2] (or [$HgS^*_2]_n$). For the purpose of this study, the fact that a different compound was obtained did not matter. In fact, chances for ionisation might even be increased with the presence of more methoxy-functionalised ligands. However, since the complex did not dissolve in solvents other than DMSO, it could not be analysed by ESMS. It is noteworthy that, before recrystallisation of [PhHgS*], its ESMS spectrum showed a weak signal at *m/z* 694 whose isotope pattern suggested the presence of two mercury atoms. In the reaction of [$(Ph_3P)AuS^\bullet$] with [PhHgCl], and also [PhHg(OAc)], (refer to section 5.2.4), an analogous ion was detected at *m/z* 665, which is exactly 29 mass units lower (= difference between S* and $S^\bullet$). This led to the conclusion that this particular ion had only one thiolate ligand, and was therefore assigned as $[Ph_2Hg_2(\mu\text{-}S^*)]^+$.

5.2.2 Reactivity of selected $S^\bullet$ complexes towards other metal centres

Pyridine and related pyridine-type ligands are widely known to coordinate to a number of transition metals[22]. Complexes of $S^\bullet$ can therefore be regarded as a pyridine-type metalloligand acting as a precursor for the synthesis of larger molecules. Any metal fragment that has a soft metal centre should react with the prepared $S^\bullet$-complexes. As examples, [$(Ph_3P)AuS^\bullet$], [$(dppe)PdS^\bullet_2$] and [$(dppe)PtS^\bullet_2$] were chosen to react with a number of transition-metal compounds and the products were identified by ESMS. The compounds used are listed in Table 5.3 together with a summary of the formed products detected by ESMS.

[22] F. A. Cotton, G. Wilkinson, C. A. Murillo and M. Bochmann, *Advanced Inorganic Chemistry*, 6th ed., Wiley, N.Y., 1999, p.350.

Table 5.3 The observed ions for the reactions between $[(Ph_3P)AuS^{\bullet}]$, $[(dppe)PdS^{\bullet}{}_2]$ or $[(dppe)PtS^{\bullet}{}_2]$ and various transition-metal complexes, recorded in MeOH at cV = 20 V.

	$[(Ph_3P)AuS^{\bullet}]$	$[(dppe)PdS^{\bullet}{}_2]$	$[(dppe)PtS^{\bullet}{}_2]$
$[Hg(OAc)_2]$	$[(Ph_3P)AuS^{\bullet}Hg(OAc)]^+$	–	–
[PhHg(OAc)]	$[(Ph_3P)AuS^{\bullet}HgPh]^+$ $[(Ph_3P)AuS^{\bullet}Hg_2Ph_2(OAc)]^+$ $[Ph_2Hg_2(\mu\text{-}SPh)]^+$	–	–
[PhHgCl]	$[(Ph_3P)AuS^{\bullet}HgPh]^+$ $[Ph_2Hg_2(\mu\text{-}SPh)]^+$ $[(Ph_3P)AuS^{\bullet}Hg_2Ph_2(OAc)]^+$	–	–
$Ag[BF_4]$	–	–	–
$ZnSO_4$	–	–	–
$[(dppe)PtCl_2]$	–	$[(dppe)PdS^{\bullet}{}_2Pt(dppe)]^{2+}$	$[(dppe)PtS^{\bullet}{}_2Pt(dppe)]^{2+}$
$[(dppe)PdCl_2]$	–	$[(dppe)PdS^{\bullet}{}_2Pd(dppe)]^{2+}$	$[(dppe)PtS^{\bullet}{}_2Pd(dppe)]^{2+}$
$[(Ph_3P)AuCl]$	$[(Ph_3P)AuS^{\bullet}Au(PPh_3)]^+$	–	–
$\{[(Ph_2PC_2H_4)_2CH]PdCl\}$	$\{(Ph_3P)AuS^{\bullet}[(Ph_2PC_2H_4)_2CH]Pd\}^+$	–	$[(dppe)PtS^{\bullet}{}_2[(Ph_2PC_2H_4)_2CH]Pd]^+$ $[(dppe)PtS^{\bullet}{}_2\{[(Ph_2PC_2H_4)_2CH]Pd\}_2]^{2+}$

The results in Table 5.2 show that there was no general rule as to which complexes underwent a reaction with the selected metal thiolates. In the reaction between [$(Ph_3P)AuS^{\bullet}$] and [$Hg(OAc)_2$], the cation $[(Ph_3P)AuS^{\bullet}Hg(OAc)]^+$ formed readily. Another ion at 14 amu lower was observed as well, but could not be reproduced on another day. Presumably, the formed complex lost the acetate anion and coordinated to formate, as formic acid is commonly used to flush the instrument. When using [PhHg(OAc)] as a source of mercury, the gold thiolate did not associate with the mercury acetate moiety, but the ion $[(Ph_3P)AuS^{\bullet}HgPh]^+$ was detected. [PhHgCl] used as a precursor gave rise to the same peak. This result can be expected, as the Hg–C bond is less labile than the Hg–Cl or the Hg–O bonds. Two additional ions of minor intensity were observed at *m/z* 665 and 1186, respectively. Their isotope patterns suggested that two mercury atoms were present, so that the latter one was assigned as $[(Ph_3P)AuS^{\bullet}Hg_2Ph_2(OAc)]^+$. An analogous ion for the signal at lower mass units had been observed before in the spectrum of [PhHgS*] (refer to section 5.2.3), so that this signal most likely corresponded to the dinuclear $[Ph_2Hg_2(\mu\text{-}SPh^*)]^+$. LHg^+ adducts have been observed before in the ESMS by other goups[23].

With regard to the three metal chlorides $[(dppe)PtCl_2]$, $[(dppe)PdCl_2]$ and $[(Ph_3P)AuCl]$, products were detected in the reactions of the Pt and Pd halides with the Pt and Pd thiolates, and the gold halide with the gold thiolate. The 2+ ions detected for the Pt and Pd halides indicated that they had been bridged by the $S^{\bullet}$-complexes with the formation of a metal–N coordination bond. $\{[(Ph_2PC_2H_4)_2CH]PdCl\}$ reacted with both Au and Pt thiolates, but not with Pd and was the only complex that gave rise to both one- and two-coordinated species. Some of the presumed structures for the observed reaction products are shown in Scheme 5.2.

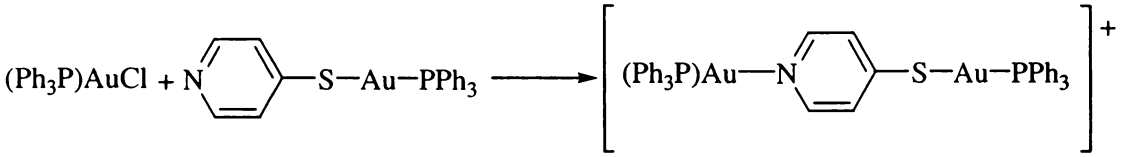

[23] A. J. Canty and R. Colton, *Inorg. Chim. Acta*, 1994, **215**, 179; M. I. Bruce, K. Costuas, J.-F. Halet, B. C. Hall, P. J. Low, B. K. Nicholson, B. W. Skelton and A. H. White, *J. Chem. Soc. Dalton Trans.*, 2002, 383.

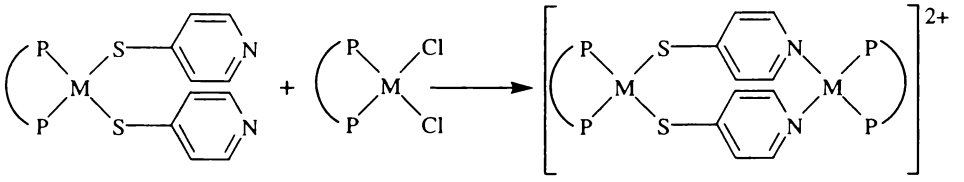

(M = Pt, Pd)

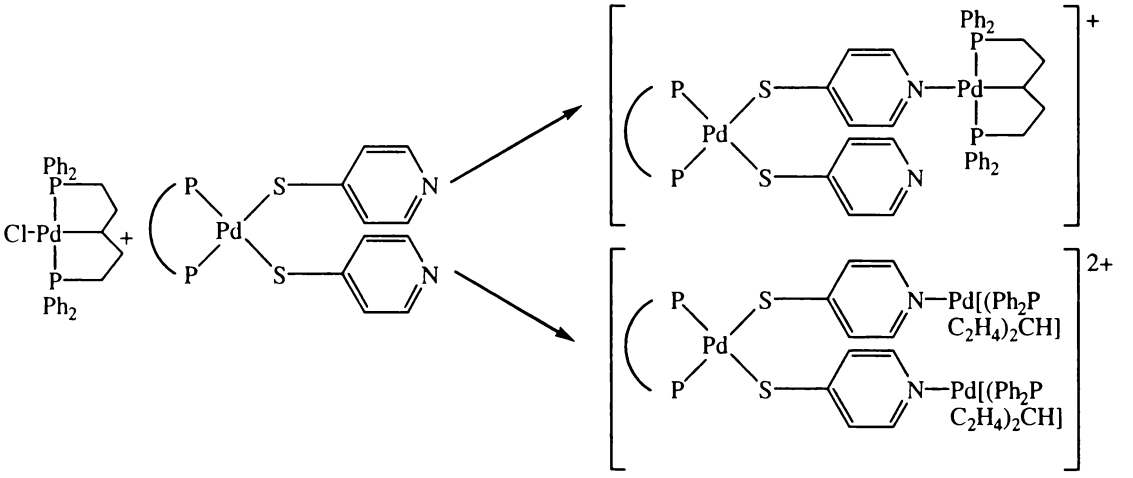

Scheme 5.2 The proposed reaction pathways in the reactions between selected $S^{\bullet}$-complexes and a number of other metal centres.

5.3 Exchange processes of thiophenolate and sulfide-thiophenolate complexes of cadmium

Exchange reactions of the thiolate ligands in the three complex anions $[Cd_4(SPh)_{10}]^{2-}$, $[S_4Cd_{10}(SPh)_{16}]^{4-}$ and $[S_4Cd_{17}(SPh)_{28}]^{2-}$ (as their $[Me_4N]^+$ salts) were studied by ESMS. HS* and $HS^{\bullet}$ were used to replace SPh in the parent complexes. The three complex anions all give signals in the negative-ion mode. ESMS has already been applied to the analysis of fragmentation patterns of these complexes, but investigations of exchange processes has been limited to the metal and the sulfide[24].

5.3.1 Background

The thiolate chemistry of the closed shell d^{10} elements Zn, Cd and Hg is very different from that of other transition-metal elements. Their characteristic property is the tendency

to form polynuclear aggregates of tetrahedral building blocks. Through condensation of the MS_4 tetrahedra, polynuclear complexes of Cd and Zn can form adamantane-like cage systems. Structures of the systems $[Cd_4(SPh)_{10}]^{2-}$, $[S_4Cd_{10}(SPh)_{16}]^{4-}$ and $[S_4Cd_{17}(SPh)_{28}]^{2-}$ are displayed in Figure 5.7. The thiophenolate ligands are either terminal or doubly-bridging while the non-thiolate sulfur atoms all have four bonds to the cadmium metals.

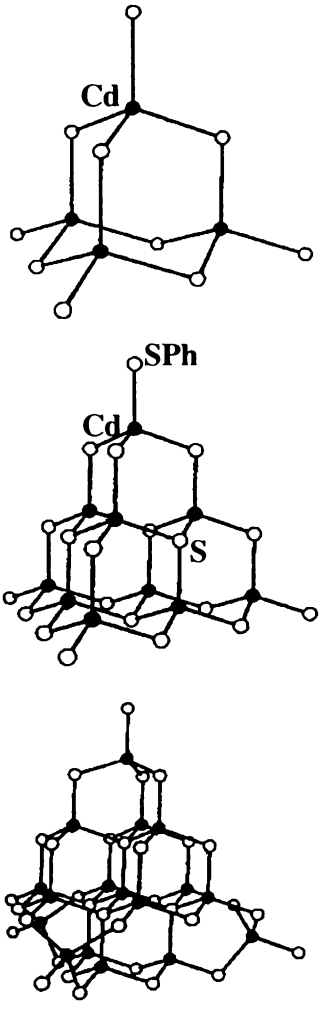

Fig 5.7 The structures of $[Cd_4(SPh)_{10}]^{2-}$ (top), $[S_4Cd_{10}(SPh)_{16}]^{4-}$ (middle) and $[S_4Cd_{17}(SPh)_{28}]^{2-}$ (bottom). Shaded atoms are Cd, unshaded atoms with one or two bonds are the S atoms of terminal or doubly-bridging thiolate, respectively; unshaded atoms with three or four bonds are non-thiolate S atoms[24].

[24] T. Løver, W. Henderson, G. A. Bowmaker, J. M. Seakins and R. P. Cooney, *Inorg. Chem.*, 1997, **36**, 3711.

The chemistry of sulfide thiolate clusters of the type $[S_xM_y(SPh)_z]^{n-}$ and metal thiophenolate complexes has been reviewed by Dance and Fisher[25]. Compounds of this type are particularly interesting as they are used as precursors for nanometre-sized semiconductor clusters[26]. The optical, electronic and catalytic properties of these materials are very much dependent on the nature of the surface and the size. Therefore, inhomogeneous distribution of the cluster size, shape and surface need to be kept at a minimum. The ideal case is a cluster of a definite size. Among other methods, monodispersity can be achieved by stabilising ligands, such as thiolates. The cluster can be precipitated in the presence of capping ligands or, alternatively, precursors are employed that already incorporate capping ligands. Exchange processes in these systems are of importance as they can lead to new precursors with different properties. Known single-sized, ligand-stabilised CdS clusters are $[S_4Cd_{10}(SPh)_{16}]^{4-}$ [27] and $[S_4Cd_{17}(SPh)_{28}]^{2-}$ [28] Larger homologues have been proposed to be $[S_4Cd_{17}(SCH_2CH_2OH)_{26}]$ [29], $[S_{13}Cd_{20}(SPh)_{22}]^{8-}$ [30] and $[S_{14}Cd_{32}(SPh)_{36} \cdot 4DMF]$ (DMF = dimethylformamide)[31]. They are, however, difficult to crystallise and there is evidence (from solution NMR[32]) that a far greater number of clusters exists.

ESMS is an excellent tool for the detection of species in solution, provided the analytes are ionic or ionise by other means. In the case of the thiophenolate clusters used in this study, simple exchange of the SPh ligands will give analogous complexes of the same charge and the reaction products should be readily detected in the negative-ion mode of the ESMS. A second aim was the detection of any neutral species in solution, observed as their $[M + H]^+$ ions, if the cluster ionises by protonation at the site of the electrospray-friendly ligand. Should multiple-protonation occur, anionic M^{n-} species might be detected in the positive-ion mode as their $[M + (n+1)H]^+$ ions.

---

[25] I. Dance and K. Fisher, *Prog. Inorg. Chem.*, 1994, **41**, 637.
[26] T. Løver, G. A. Bowmaker, J. M. Seakins, R. P. Cooney and W. Henderson, *J. Mater. Chem.*, 1997, **7**, 647; H. Weller, *Angew. Chem. Int. Ed. Engl.*, 1993, **32**, 41; Y. Wang and N. Herron, *J. Phys. Chem.*, 1991, **95**, 525; T. Vossmeyer, G. Reck, B. Shulz, L. Katsikas and H. Weller, *J. Am. Chem. Soc.*, 1995, **117**, 12881.
[27] I. G. Dance, A. Choy and M. L. Scudder, *J. Am. Soc.*, 1984, **106**, 6285.
[28] G. S. H. Lee, D. C. Craig, I. Ma, M. L. Scudder, T. D. Bailey and I. G. Dance, *J. Am. Chem. Soc.*, 1988, **110**, 4863.
[29] T. Vossmeyer, G. Reck, L. Katsikas, E. T. K. Haupt, B. Schulz and H. Weller, *Science*, 1995, **267**, 1476.
[30] N. Herron, A. Suna and Y. Wang, *J. Chem. Soc. Dalton Trans.*, 1992, 2329.
[31] N. Herron, J. C. Calabrese, W. E. Farneth and Y. Wang, *Science*, 1993, **259**, 1426.

5.3.2 ESMS of (sulfide) thiolate complexes of cadmium with HS*

For the study of possible exchange processes, the three complexes $[Me_4N]_2[Cd_4(SPh)_{10}]$, $[Me_4N]_4[S_4Cd_{10}(SPh)_{16}]$ and $[Me_4N]_2[S_4Cd_{17}(SPh)_{28}]$ were treated with various mole equivalents of HS* [33], and subsequently injected into the ESMS. In the negative-ion mode, ligand exchange processes were observed immediately. Figure 5.8 shows this with $[Cd_4(SPh)_{10}]^{2-}$ as an example.

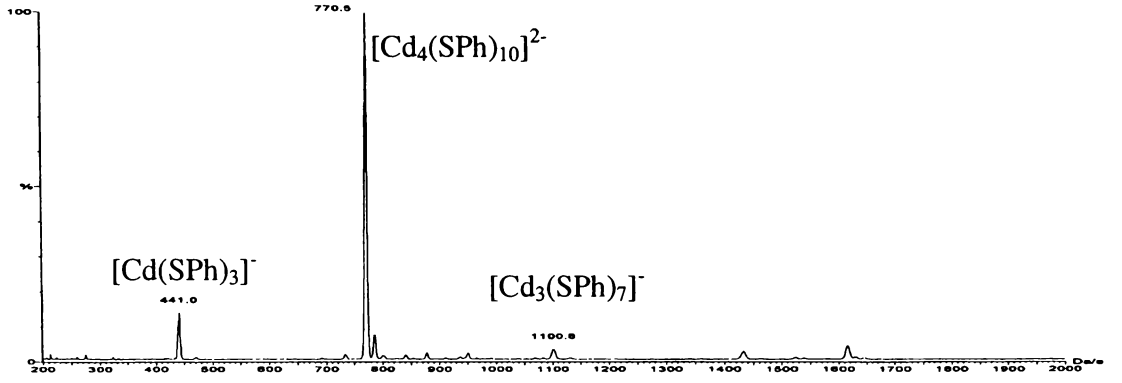

Fig. 5.8a The negative-ion ES mass spectrum of $[Cd_4(SPh)_{10}]^{2-}$, recorded in $MeCN/H_2O$ at cV = 5 V.

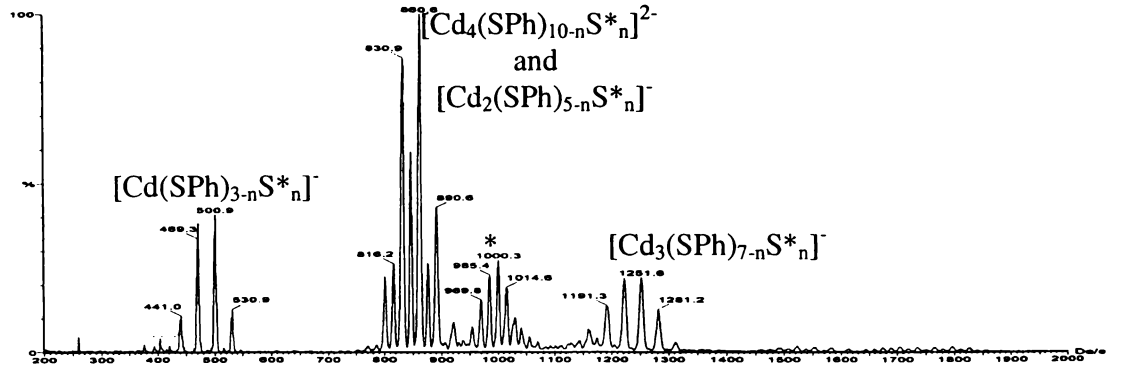

Fig. 5.8b The negative-ion ES mass spectrum of $[Cd_4(SPh)_{10}]^{2-}$ with the addition of HS* (1:10), recorded in $MeCN/H_2O$ at cV = 5 V.

The spectrum at the top represents the complex alone with the observed ions being the parent ion $[Cd_4(SPh)_{10}]^{2-}$ at 100% as well as the fragments $[Cd_3(SPh)_7]^-$ and

---

[32] Y. Nosaka, H. Shigeno and T. Ikeuchi, *J. Phys. Chem.*, 1995, **99**, 8317.
[33] In this chapter all mole equivalent ratios refer to metal complex : ligand.

$[Cd(SPh)_3]^-$. When adding HS* in a 1:10 ratio, several series of peaks appeared according to ligand exchange processes. The intensities normally followed the expected statistical distribution. An exception was the second set of peaks, which was not a smooth symmetric pattern. This series corresponded to both $[Cd_4(SPh)_{10-n}S^*_n]^{2-}$ and $[Cd_2(SPh)_{5-n}S^*_n]^-$, which were superimposed on each other. The reason for the irregular intensities of peaks is probably the different numbers of terminal *vs.* bridging SPh ligands present in both species, presuming that terminal ligands are more easily replaced than bridging ones. On increasing the cone voltage, the $[Cd_4(SPh)_{10-n}S^*_n]^{2-}$ ions disappeared and only the series consisting of the singly-charged ions $[Cd_2(SPh)_{5-n}S^*_n]^-$ remained. This observation has been reported before[24].

Obviously, the more ligand added the higher the number of exchanged SPh on the metal complex, and the further the signals shifted to the higher mass end of the spectrum. Thus, the reaction products could be easily controlled by the amount of ligand added. This can be seen beautifully in Figure 5.9, which shows $[S_4Cd_{17}(SPh)_{28}]^{2-}$ with HS* (1:2 and 1:28 ratios).

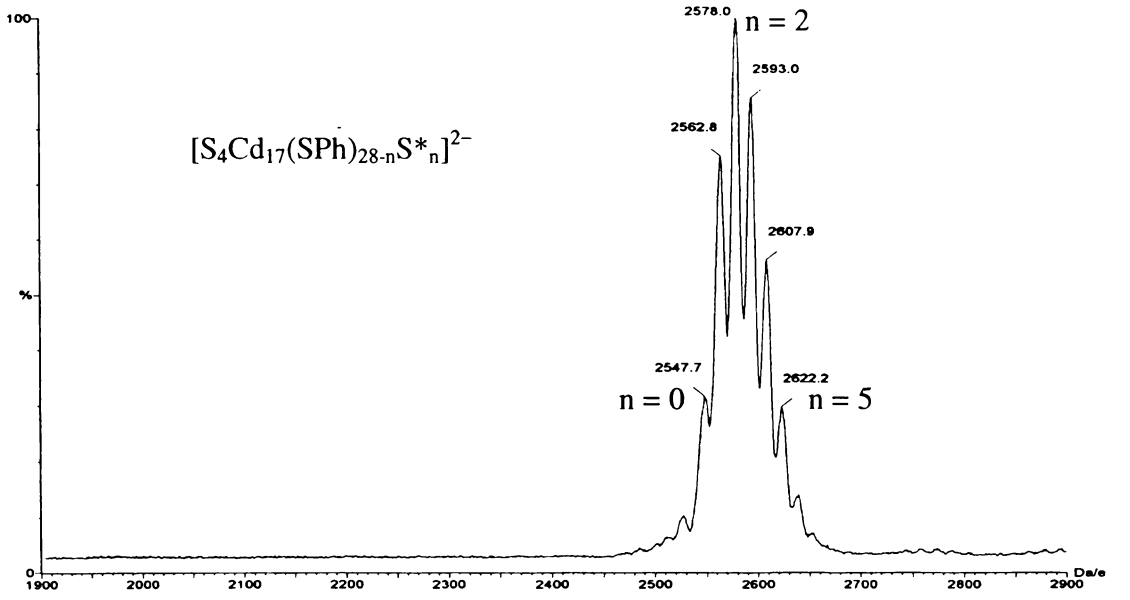

Fig. 5.9a The negative-ion ES mass spectrum of the reaction between $[Me_4N]_2[S_4Cd_{17}(SPh)_{28}]$ and HS* (1:2), recorded in $MeCH/H_2O$ at cV = 5 V.

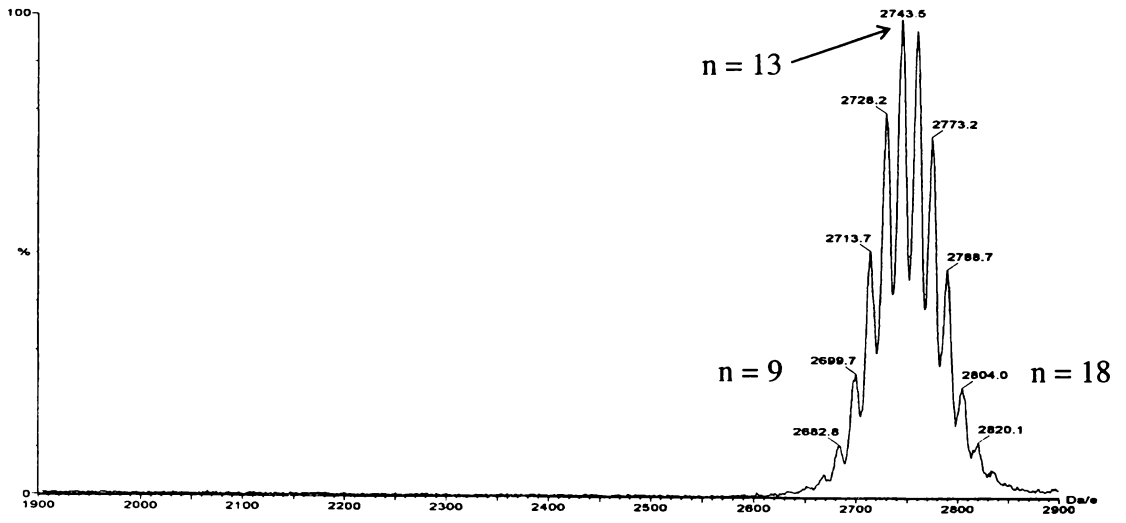

Fig. 5.9b The negative-ion ES mass spectrum of the reaction between $[Me_4N]_2[S_4Cd_{17}(SPh)_{28}]$ and HS* (1:28), recorded in MeCH/H_2O at cV = 5 V.

In the top spectrum, the most intense ion was the di-substituted $[S_4Cd_{17}(SPh)_{26}S^*_2]^{2-}$ ion at *m/z* 2578 with the observed ions ranging from the unsubstituted $[S_4Cd_{17}(SPh)_{28}]^{2-}$ ion to the penta-substituted $[S_4Cd_{17}(SPh)_{23}S^*_5]^{2-}$ ion. After addition of HS* (1:28) the most intense ion was $[S_4Cd_{17}(SPh)_{15}S^*_{13}]^{2-}$ at *m/z* 2744 with a total range from $[S_4Cd_{17}(SPh)_{19}S^*_9]^{2-}$ to $[S_4Cd_{17}(SPh)_{10}S^*_{18}]^{2-}$. The most abundant species in the envelopes of peaks for all three parent complexes with various equivalents of HS* are listed in Table 5.4.

Table 5.4 The most abundant ions observed in the negative-ion ES mass spectra of the reactions between $[Cd_4(SPh)_{10}]^{2-}$, $[S_4Cd_{10}(SPh)_{16}]^{4-}$ or $[S_4Cd_{17}(SPh)_{28}]^{2-}$ and HS*, recorded in MeCN/H_2O at cV = 5V.

Molar ratios	$[Cd_4(SPh)_{10}]^{2-}$	$[S_4Cd_{10}(SPh)_{16}]^{4-}$	$[S_4Cd_{17}(SPh)_{28}]^{2-}$
1:0	$[Cd_4(SPh)_{10}]^{2-}$	$[S_4Cd_{10}(SPh)_{16}]^{4-}$	$[S_4Cd_{17}(SPh)_{28}]^{2-}$
1:1	$[Cd_4(SPh)_{10}]^{2-}$	$[S_4Cd_{10}(SPh)_{12}S^*_4]^{4-}$	$[S_4Cd_{17}(SPh)_{28}]^{2-}$
1:2	$[Cd_4(SPh)_8S^*_2]^{2-}$	$[S_4Cd_{10}(SPh)_{10}S^*_6]^{4-}$	$[S_4Cd_{17}(SPh)_{26}S^*_2]^{2-}$
1:4	$[Cd_4(SPh)_7S^*_3]^{2-}$	$[S_4Cd_{10}(SPh)_{11}S^*_5]^{4-}$	$[S_4Cd_{17}(SPh)_{24}S^*_4]^{2-}$
1:8	$[Cd_4(SPh)_6S^*_4]^{2-}$	$[S_4Cd_{10}(SPh)_9S^*_7]^{4-}$	$[S_4Cd_{17}(SPh)_{21}S^*_7]^{2-}$

	$[Cd_4(SPh)_4S^*_6]^{2-}$ (1:10 ratio)	$[S_4Cd_{10}(SPh)_6S^*_{10}]^{4-}$ (1:16 ratio)	$[S_4Cd_{17}(SPh)_{15}S^*_{13}]^{2-}$ (1:28 ratio)
	$[Cd_4S^*_{10}]^{2-}$ (1:40 ratio)	$[S_4Cd_{10}(SPh)_1S^*_{15}]^{4-}$ (1:160 ratio)	$[S_4Cd_{17}(SPh)_1S^*_{27}]^{2-}$ (1:320 ratio)

It was interesting to see that when adding the maximum mole equivalent of HS* {1:10 in the case of $[Cd_4(SPh)_{10}]^{2-}$}, not all of the thiolate ligands were replaced readily. The observed peak pattern seemed to represent the equilibrium that had been reached after adding HS*, and obviously involved incomplete exchange. Hence, if complete ligand exchange is desired, an excess of HS* is required. For $[Cd_4(SPh)_{10}]^{2-}$, addition of HS* (1:100) gave the product $[Cd_4S^*_{10}]^{2-}$ with 100% intensity, but other, less-substituted products were still present. The reaction solutions were also analysed after 24 and 48 hours. However, the signal intensities did not change over the period of two days leading to the conclusion that the reaction equilibrium in these systems is reached within a few seconds.

Depending on the complex and amount of ligand added, in addition to the series of peaks arising from ligand exchange, a number of new peak envelopes were observed. In Figure 5.8b, one can see how the peaks arising from $[Cd_4(SPh)_{10-n}S^*_n]^{2-}$ were accompanied by a less intense group, indicated by an asterisk. This phenomenon was particularly distinct when a vast excess of ligand was added, which is illustrated in Figure 5.10 showing $[Cd_4(SPh)_{10}]^{2-}$ with S* (1:100).

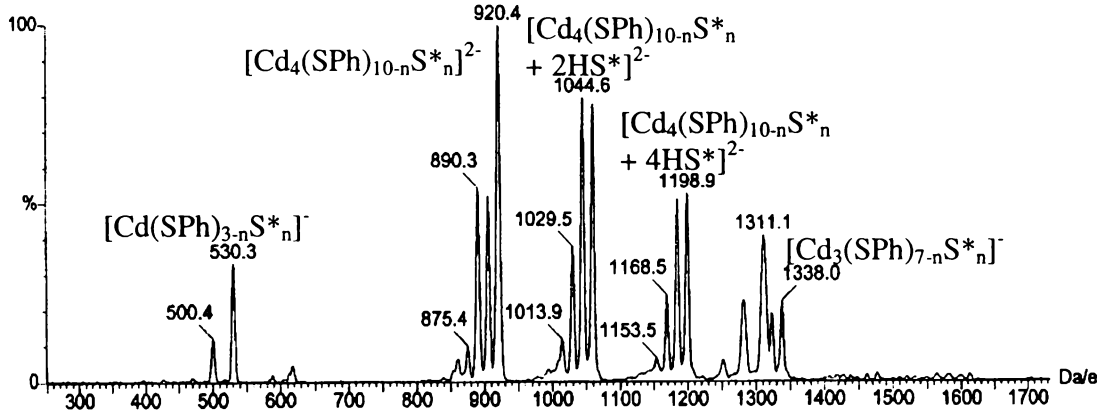

Fig 5.10 The negative-ion ES mass spectrum of $[Cd_4(SPh)_{10}]^{2-}$ with the addition of HS* (1:100), recorded in MeOH at cV = 5 V.

The *m/z* values indicated addition of thiolate ligands pairwise. However, the overall charge of 2- was maintained, which led to the speculation that association with protons had occurred. Otherwise, one would expect the charge to increase by two with every two ligands coordinated. The fact that the reaction of $[Cd_4(SPh)_{10}]^{2-}$ with HSPh (1:1, 1:10 or 1:100) did not give rise to additional signals of this type also speaks for protonation according to $[Cd_4(SPh)_{12-n}S^*_n + 2H]^{2-}$, $[Cd_4(SPh)_{14-n}S^*_n + 4H]^{2-}$ and $[Cd_4(SPh)_{12-n}S^*_n + 6H]^{2-}$, as only the S*-complexes have a basic site for protoantion. However, the most abundant peaks in the high-resolution isotope patterns matched exactly for non-protonated species according to $[Cd_4(SPh)_{12-n}S^*_n]^{2-}$, $[Cd_4(SPh)_{14-n}S^*_n]^{2-}$ *etc.* Furthermore, carrying out the experiment in deuterated solvent (CD_3OD) yielded the same peaks, while they should have had higher *m/z* values if D was present. The other question arose, why the signals only increased according to coordination of two ligands as ions of the type $[Cd_4(SPh)_{13-n}S^*_n + 3H]^{2-}$ or $[Cd_4(SPh)_{15-n}S^*_n + 5H]^{2-}$ were not observed. Addition of disulfides, RSSR, which are common decomposition products of thiols, was considered as another possibility. Thus, both disulfides PhSSPh and $MeOC_6H_4SSC6H_4OMe$ were prepared and solutions consisting of disulfide (1:1, 1:10 and 1:100) were added to $[Cd_4(SPh)_{10}]^{2-}$. In both cases, coordination of disulfides did not occur and the spectrum was identical to that of the cadmium complex only. Further investigations included analysing the complexes with the other thiol available, $HS^\bullet$. As the mass separation between $HS^\bullet$ and HS* differs by 29 amu, analogous signals should be observed at the corresponding lower *m/z* values. Addition of $HS^\bullet$ did, however, only lead to very insoluble products and no spectrum was obtained for any of the cadmium complexes. A highly insoluble compound was also obtained when attempting to prepare the complex $[Me_4N]_2[Cd_4S^\bullet_{10}]$ according to the synthetic procedure reported for $[Me_4N]_2[Cd_4(SPh)_{10}]$. Presumably, due to the high basicity of $HS^\bullet$, the ligand cannot only undergo simple exchange with SPh, but can also bond to further metal atoms, leading to the formation of other, probably polymeric products. It should be noted that addition of more S* ligands occurred for $[Cd_4(SPh)_{10}]^{2-}$ and $[S_4Cd_{10}(SPh)_{16}]^{4-}$, but not for $[S_4Cd_{17}(SPh)_{28}]^{2-}$.

So far, only the anionic species of the cadmium thiolate and thiolate-bridged CdS complexes have been analysed by ESMS. The presence of neutral compounds should in

theory also be detected if the ligand HS* is used. Furthermore, provided this ligand is powerful enough to associate with a number of protons, signals according to originally anionic species might be detected in the positive-ion mode of the instrument. In fact, a series of weak signals indicating exchange reactions was observed when an excess of HS* was added to the complexes. The ions observed are summarised in Table 5.5, but could not be assigned readily. For $[Cd_4(SPh)_{10}]^{2-}$, series d) might be ions corresponding to $[Cd_4(SPh)_{12-n}S^*_n + 3H]^+$ (n = 8-11), which correspond to the unclear species in the negative-ion mode. When increasing the cone voltage to 40-100 V, the only species still observed were series c) and d), which both lost up to three CdS^*_2 fragments. Although protonation could not be proven in the negative-ion mode, it is presumed to occur since the formation of positive ions could not be explained otherwise. It is noteworthy that the complex $[S_4Cd_{17}(SPh)_{28}]^{2-}$, which did not show any ions according to additional coordination of ligand in the negative-ion, also gave no signals in the positive-ion spectrum.

Table 5.5 The positive-ion ESMS data for the reactions between the Cd-complexes and HS*, recorded in $MeCN/H_2O$ at cV = 20 V.

Complex	HS*	*m/z* of unassigned ions
$[Cd_4(SPh)_{10}]^{2-}$	1:100	a) 1053, 1069, 1082, 1096, 1111, 1125 (2+ ions) b) 1367, 1381, 1396, 1409 (2+ ions) c) 1911, 1925, 1943, 1954 (2+ ions) d) 2002, 2031, 2061, 2090 (1+ ions)
$[S_4Cd_{10}(SPh)_{16}]^{4-}$	1:160	a) 1739 b) 1840, 1852, 1869 (2+ ions) c) 1946, 1958, 1975, 1990 (2+ ions) d) 2164
$[S_4Cd_{17}(SPh)_{28}]^{2-}$	1:280	no signals

5.4 Some aspects of the chemistry of the $\{Pt_2S_2\}$ system

The following section will describe the ESMS analysis of complexes based on the $\{Pt_2S_2\}$ butterfly core. The PPh_3 version, $\{Pt_2S_2\}$, is shown in Figure 5.11.

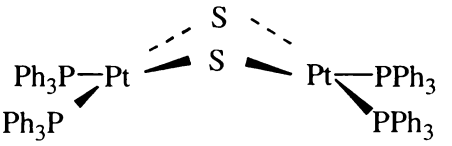

Fig. 5.11 The structure of $[Pt_2(\mu\text{-}S)_2(PPh_3)_4]$, $\{Pt_2S_2\}$.

5.4.1 Background

The development of the $\{Pt_2S_2\}$ system was one of the milestones in the general Pt-S chemistry, which dates back to the early 1900s when the first Pt-S complex, $[NH_4]_2[Pt(\eta^2\text{-}S_5)_3]$ was reported[34]. The first complex with a $\{Pt_2S_2\}$ core was reported by Chatt and Mingos[35], who synthesised $[Pt_2S_2(PMe_2Ph)_4]$ in 1970, closely followed by Ugo *et al.*[36], who prepared the PPh_3 analogue by a different route. The structure of these types of complexes can be described as butterfly structures with the platinum atoms at the wing tips or, alternatively, as hinged $\{Pt_2S_2\}$ cores with the Pt atoms located at the hinge. Their most outstanding property is the strong nucleophilicity of the sulfur bridges, resulting in many of the early studies involving reactions of a $\{Pt_2S_2\}$ system with alkyl halides. More recently, its nucleophilicity is utilised in reactions with metal complexes, where they act as metallo ligands. Mingos[37] introduced the term 'aggregates' (as opposed to 'clusters') for polynuclear structures without formal metal-metal bonds. Both the nuclearity and the coordination modes of these metal aggregates can vary to a large degree. Due to the flexibility of the hinge angle, aggregates with a variety of geometries have been isolated, ranging from square-planar[38], tetrahedral[39] to linear[40].

---

[34] K. A. Hofmann and F. Hoechlen, *Chem. Ber.*, 1903, **36**, 3090.
[35] J. Chatt and D. M. P. Mingos, *J. Chem. Soc. A*, 1970, 1243.
[36] R. Ugo, G. La Monica, S. Cenini, A. Segre and F. Conti, *J. Chem. Soc. A*, 1971, 522.
[37] C. E. Briant, T. S. A. Hor, N. D. Howels and D. M. P. Mingos, *J. Chem. Soc., Chem. Commun.*, 1983, 1118.
[38] C. E. Briant, D. I. Gilmour, M. A. Luke and D. M. P. Mingos, *J. Chem. Soc. Dalton Trans.*, 1985, 851.
[39] B. H. Aw, K. K. Looh, H. S. O. Chan, K. L. Tan and T. S. A. Hor, *J. Chem. Soc. Dalton Trans.*, 1994, 3177.

The chemistry of $\{Pt_2S_2\}$ complexes was reviewed by Hor *et al.* in 1996[41] and 1999[42]. It was also this group who undertook the first systematic ESMS study with regard to the reactivity of $\{Pt_2S_2\}$ towards a larger number of transition-metal fragments[43]. However, only ionic species were detected, because once bonded to a metal centre, neutral metal aggregates will be invisible (unless they can be ionised at another basic site). Electrospray-friendly derivatives of $\{Pt_2S_2\}$ should therefore lead to the detection of any neutral species formed in the reaction with neutral metal complex precursors.

5.4.2 ESMS of $\{Pt_2S_2\}$ and electrospray-friendly analogues

Analogues of $\{Pt_2S_2\}$ were obtained by the same method as $\{Pt_2S_2\}$, using some of the previously prepared electrospray-friendly phosphine ligands. The complexes were analysed by ESMS, all yielding clean ES mass spectra with the $[M + H]^+$ as the only ion in the spectrum. The complete range of prepared complexes together with their observed ions in the ESMS are summarised in Table 5.6.

Table 5.6 The positive-ion ESMS data for $[Pt_2(\mu\text{-}S)_2L_4]$.

L	Complex	Ions observed [*m/z*, relative peak height (%)]
PPh_3	$\{Pt_2S_2\}$	$[M + H]^+$ (1504, 100)
P*	$\{Pt_2S_2\}$*	$[M + H]^+$ (1624, 100)
P**	$\{Pt_2S_2\}$**	$[M + H]^+$ (1744, 100)
P***	$\{Pt_2S_2\}$***	$[M + H]^+$ (1864, 100)
P$^\bullet$	$\{Pt_2S_2\}^\bullet$	$[M + H]^+$ (1677, 100)
As***	$\{Pt_2S_2\}^{As***}$	$[M + H]^+$ (2041, 100)

[40] W. Bos, J. J. Bour, P. P. J. Schlebos, P. Hageman, P. Bosman, J. M. M. Smits, J. A. C. van Wietmarschen and T. Beurskens, *Inorg. Chim. Acta*, 1986, **119**, 141.
[41] T. S. A. Hor, *J. Cluster Sci.*, 1996, **7**, 263.
[42] S. W. A. Fong and T. S. A. Hor, *J. Chem. Soc. Dalton Trans.*, 1999, 639.
[43] S. W. A. Fong, Y. Teck, V. Woon, J. Jagadese, T. S. A. Hor, W. Henderson, A. G. Oliver and C. E. F. Rickard, *J. Chem. Soc. Dalton Trans.*, 2001, 1986.

No complexes incorporating the heavier homologue As have been reported. The As*** analogue was prepared in the same manner as all other complexes and its ES mass spectrum is shown in Figure 5.12.

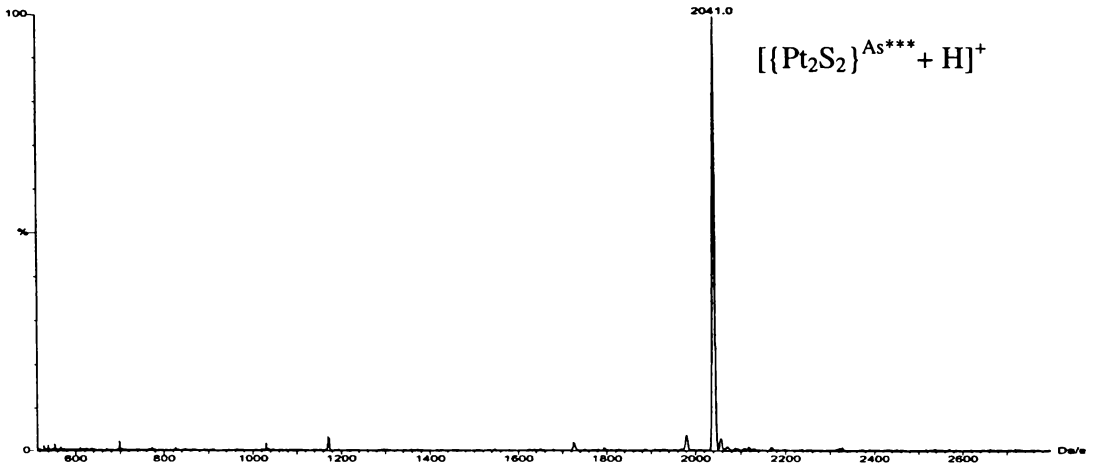

Fig. 5.12a The positive-ion ES mass spectrum of $\{Pt_2S_2\}^{As***}$, recorded in MeOH at cV = 20 V.

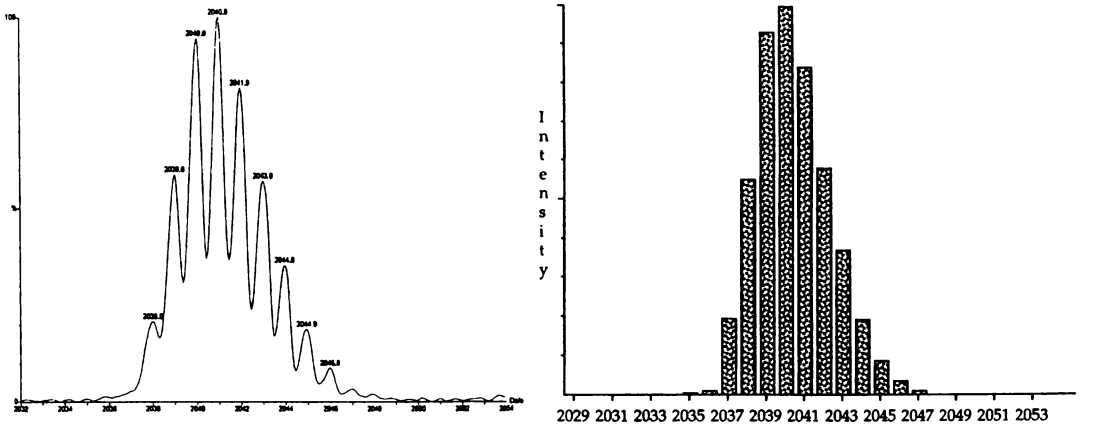

Fig. 5.12b The observed (left) and calculated (right) isotope patterns of $\{Pt_2S_2\}^{As***}$.

In general, analogues of $\{Pt_2S_2\}$ are more soluble than the parent PPh_3 complex. This is of particular advantage, as it facilitates access to chracterisational data. No ^{31}P NMR data, satisfactory elemental analyses or crystal structure of $\{Pt_2S_2\}$ is available due to the very poor solubility of this complex. The range of polar solvents is further limited as $\{Pt_2S_2\}$ decomposes readily in halogenated solvents. Unlike $\{Pt_2S_2\}$, the methoxy

derivatives are soluble in MeCN, THF, toluene and DMSO. Thus, NMR data could be recorded readily and are listed in the Experimental part of this chapter. Crystals of $\{Pt_2S_2\}$* also formed from a DMSO solution, but did not diffract well enough to obtain a data set by X-ray crystal analysis.

In order to investigate the effect of the methoxy groups on the ionisation efficiency, an equimolar mixture of $\{Pt_2S_2\}$ and $\{Pt_2S_2\}$* was analysed by ESMS. Because $\{Pt_2S_2\}$ is extremely insoluble, a relatively large amount of solvent was required[44] to ensure that the complex was fully dissolved. As can be seen in Figure 5.13, the signal for $\{Pt_2S_2\}$* is almost double in intensity compared to that of $\{Pt_2S_2\}$. One would expect signals of equal intensities if only the S atoms of $\{Pt_2S_2\}$* were involved in protonation. Hence, protonation takes place on both the S as well as the O atoms of the methoxy-derivatised complexes.

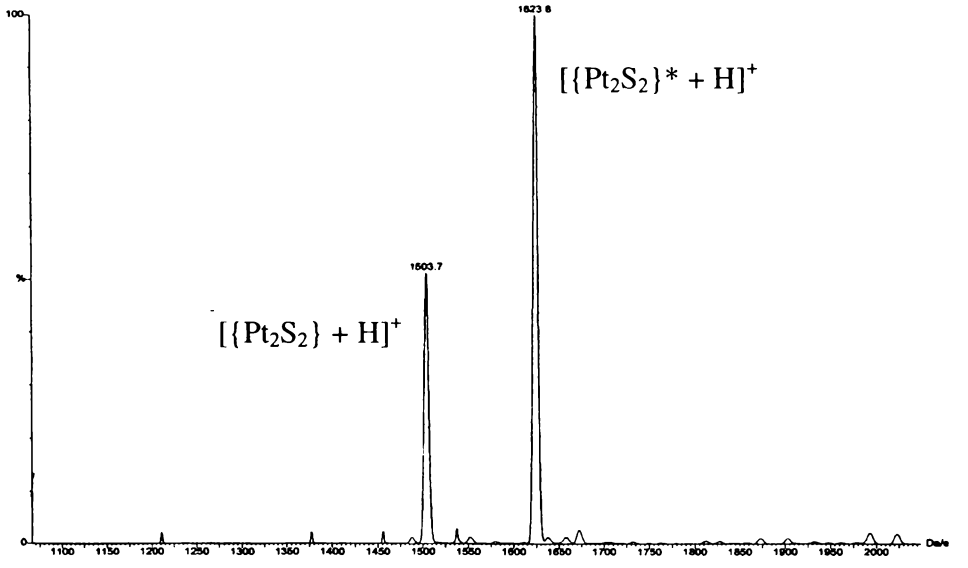

Fig. 5.13 The positive-ion ES mass spectrum of an equimolar mixture of $\{Pt_2S_2\}$ and $\{Pt_2S_2\}$*, recorded in MeOH at cV = 20 V.

[44] 1.5 mg $\{Pt_2S_2\}$ required 10 mL of MeCN, followed by 15 minutes in an ultrasound bath.

5.4.3 Exchange reactions of $\{Pt_2S_2\}$ with P**

For the investigation of possible exchange processes of PPh_3 ligands of the parent $\{Pt_2S_2\}$ complex, four mole equivalents of P** were added to a toluene/MeOH suspension of $\{Pt_2S_2\}$ and subsequently analysed by ESMS. Exchange processes did not seem to occur as no further peaks apart from $[\{Pt_2S_2\} + H]^+$ were detected. When adding an excess of P**, signals of very low intensity appeared indicating that exchange processes might take place under more vigorous conditions. Thus, a mixture of $\{Pt_2S_2\}$ with P** (1:8) in toluene/MeOH (1:1) was refluxed for one hour yielding an envelope of peaks in the ES mass spectrum (shown in Figure 5.14). The accurate ratios of the observed species listed in the inset should however be read with care since the ionisation efficiency depends on the number of MeO groups present. Although an excess of P** had been used, not all of the PPh_3 ligands were replaced. Either an equilibrium state was reached or the reaction had not come to completion.

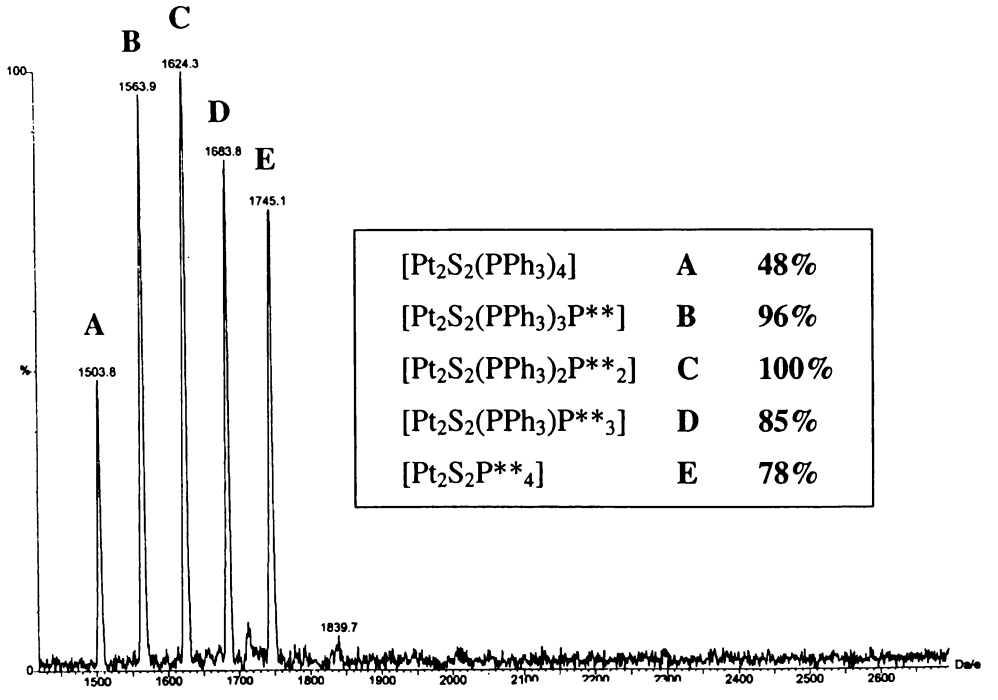

Fig. 5.14 The positive-ion ES mass spectrum of the exchange reaction of $\{Pt_2S_2\}$ with excess P**, recorded in MeOH at cV = 20 V.

5.4.4 Metal complexes of $\{Pt_2S_2\}$*

$\{Pt_2S_2\}$ systems have the potential to form heterometallic materials in the presence of virtually any metal complex provided they have some Lewis acid character or easy leaving group. In order to detect neutral metal complexes in the ESMS, an electrospray-friendly analogue of $\{Pt_2S_2\}$ is required as both S atoms might be involved in bonding and hence not be available for protonation. Before attempting to prepare a range of low-valent neutral metal complexes incorporating electrospray-friendly analogues of $\{Pt_2S_2\}$ as metalloligands, a number of metal complexes were used for which it was known that ionic heterometallic complexes are formed[42]. The electrospray-friendly derivative $\{Pt_2S_2\}$* behaved in the same manner as $\{Pt_2S_2\}$ and the results are listed in Table 5.7.

Table 5.7 The observed ions in the ES mass spectra of the reactions between $\{Pt_2S_2\}$ or $\{Pt_2S_2\}$* and various metal complexes, recorded in MeOH at cV = 20 V.

Metal complex	Ions observed[45]
$[Et_2SnCl_2]$	$[\{Pt_2S_2\}*SnEt_2]^{2+}$, $[\{Pt_2S_2\}*SnEt_2Cl]^+$
$[VO(acac)_2]$	$[PtP*_2(acac)]^+$, $[\{Pt_2S_2\}*VO(OMe)_2]^+$
$[Fe(acac)_3]$	$[\{Pt_2S_2\}*Fe(acac)(OMe)]^+$
$[AuCl(PPh_3)]$	$[\{Pt_2S_2\}*\{Au(PPh_3)\}_2]^{2+}$

Systems such as $[Pd_2(dba)_3]$ (dba = *trans, trans*-dibenzylidene acetone), $[Fe_2(CO)_9]$, $[(Ph_3P)_2Pt(trans\text{-}PhCH{=}CHPh)]$ or $[Mo(CO)_4(pip)_2]$ (pip = piperidine) exhibit easily displaced ligands. They should be able to form neutral complexes according to the structure illustrated in Figure 5.15.

[45] The observed ions are listed for $\{Pt_2S_2\}$*, but analogous ions were also observed for $\{Pt_2S_2\}$.

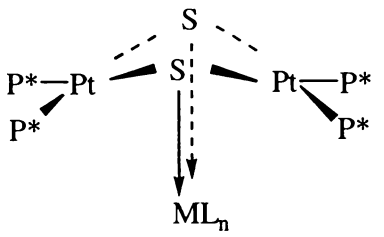

Fig. 5.15 The structure of the likely product in reactions between neutral metal complexes ML_nX_m (X = easy leaving group) and $\{Pt_2S_2\}$*.

Unlike the ionic metal complexes, where clean reactions had been obtained, most of the neutral compounds did not seem to react at all. The only exception was the reaction of $[Mo(CO)_4(pip)_2]$ and $\{Pt_2S_2\}$*. The most intense peak in the isotope pattern at *m/z* 1784 was 49 mass units too low for the product to be $[Pt_2Mo(\mu_3\text{-}S)_2P^*_4(CO)_4 + H]^+$. The isotope pattern further suggested the presence of one molybdenum and two platinum atoms. More evidence for these components was given by the reaction of analogous systems. Thus, $\{Pt_2S_2\}$** and $[Mo(CO)_4(pip)_2]$ gave rise to the corresponding peak at *m/z* 1904, which is 120 amu higher (= four MeO groups) than the signal obtained using $\{Pt_2S_2\}$*. The ES mass spectrum of the reaction between $[Mo(CO)_4(pip)_2]$ and $\{Pt_2S_2\}$** is shown in Figure 5.16a and the observed isotope pattern for the peak at *m/z* 1904 in Figure 5.16b. The calculated pattern for the expected product $[Pt_2Mo(\mu_3\text{-}S)_2P^{**}_4(CO)_4 + H]^+$ is also displayed in Figure 5.16b.

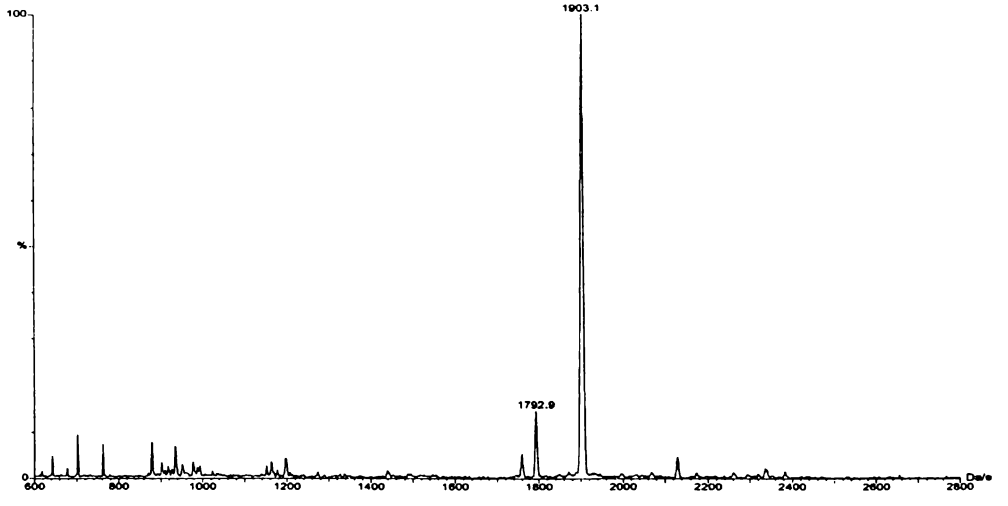

Fig. 5.16a The positive-ion ES spectrum of the reaction between $[Mo(CO)_4(pip)_2]$ and $\{Pt_2S_2\}$**, recorded in MeOH at cV = 20 V.

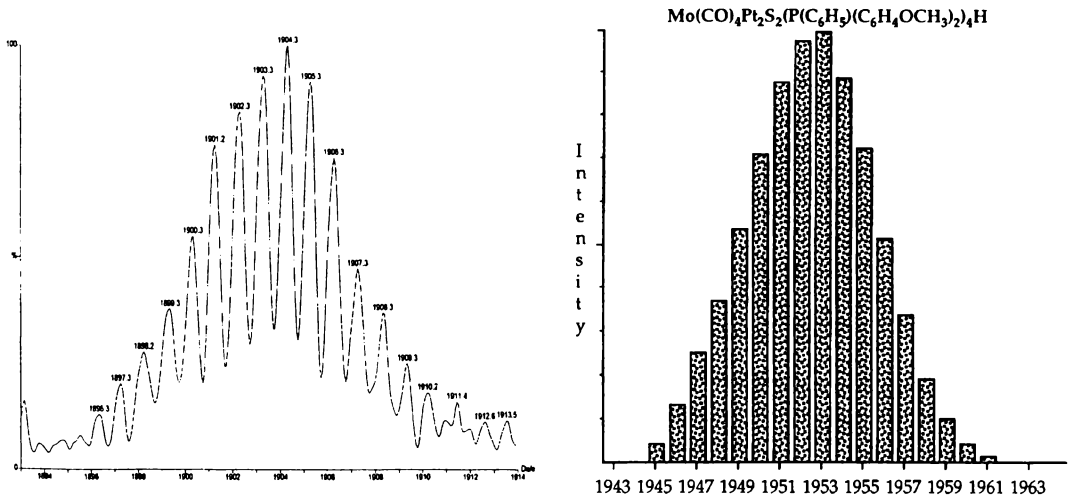

Fig. 5.16b The observed isotope pattern for the peak at *m/z* 1904 (left) and the recorded isotope pattern for the expected product $[Mo(CO)_4\{Pt_2S_2\}^{**} + H]^+$ (right).

The investigation of other systems further included the reaction between $[W(CO)_4(MeCN)_2]$ and $\{Pt_2S_2\}^*$, which led to a signal at *m/z* 1872 (48 amu lower than the expected $[W(CO)_4\{Pt_2S_2\}^* + H]^+$). Identical ions were observed when using $[Mo(CO)_4(MeCN)_2]$ (in MeCN solvent) or $[Mo(CO)_6]$ and Me_3NO (in MeOH/toluene solvent). Hence, the reaction did not seem to be solvent dependent. The use of different solvents further ruled out the coordination of solvent molecules as other ligands. The reaction of the underivatised $\{Pt_2S_2\}$ with $[Mo(CO)_4(pip)_2]$ gave rise to a corresponding signal at *m/z* 1663. The appearance of this signal led to the conclusion that all previous observed ions were cationic in nature, rather than $[M + H]^+$ ions of the reaction product.

When increasing the cone voltage, the observed ion in the reaction between $[Mo(CO)_4(pip)_2]$ and $\{Pt_2S_2\}^*$ did not show any fragmentation due to CO loss, indicating that no CO ligands were present in the system. This was confirmed by the solution IR spectrum, which did not have any bands in the CO region. No fragmentation occurred below the cone voltage of 100 V, where a peak at 323 amu lower than the reaction product was observed. This could be due to the loss of a P*S fragment, although the formation of a P*–S bond seemed unlikely. The ESMS analysis of the reaction product further included the addition of CH_2Cl_2 to the solution to see whether one or more sulfide bridges of the $\{Pt_2S_2\}$ moiety could be alkylated. However, the signal persisted in the spectrum indicating no free S-bridges. ^{31}P NMR of the sample did not

lead to more answers, as it showed numerous peaks with the most abundant ones being the phosphine sulfide at 42 ppm and the phosphine oxide at 29 ppm.

The reaction between $[Mo(CO)_4(MeCN)_2]$ and $\{Pt_2S_2\}$ in MeCN solvent has been reported before[46]. No molybdenum-containing species were detected. Instead, the product isolated was identified as $[Pt_2(\mu\text{-}S)(PPh_3)_3(CO)]$, which was formed from $\{Pt_2S_2\}$ by reductive carbonylation and desulfurisation, as shown in Figure 5.17. It is noteworthy that this neutral complex was not detected in the ESMS, although it should be visible when using any of the electrospray-friendly $\{Pt_2S_2\}$ analogues.

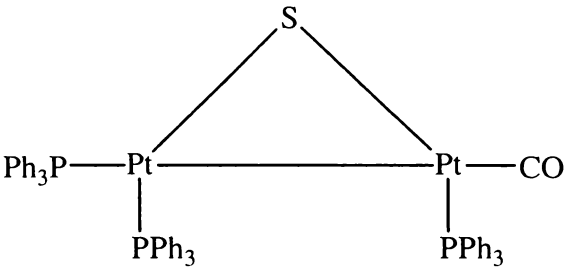

Fig. 5.17 The product isolated in the reaction between $[Mo(CO)_4(MeCN)_2]$ and $\{Pt_2S_2\}$ by Hor's group[46].

5.5 Summary and conclusions

Out of the three thiolate ligands used in this study, only $S^{\bullet}$-complexes reliably underwent the desired protonation-type mechanism in the ESMS. Complexes of S* did not seem to be basic enough to associate with H^+. Only in the case of $[(dppe)PtS^*_2]$ could a weak $[M + H]^+$ signal be observed. All other complexes of S* did not ionise at all at low cone voltages, and only signals due to impurities were observed. These results were also obtained for the complexes without electrospray-friendly ligands. Thus, out of the ligands used in this study, $S^{\bullet-}$ is the ligand of choice for ESMS analyses of thiolate complexes.

$S^{\bullet}$-complexes were reactive towards a number of other metal centres. They can be considered as metalloligands coordinating through the pyridine nitrogen atom. The ionic reaction products could be detected and assigned readily by ESMS.

Anionic cadmium thiolate and cadmium sulfur thiolate clusters undergo rapid exchange processes and can be studied in the negative-ion mode. Peaks in addition to simple ligand exchange were observed in the negative-ion spectra, which were tentatively assigned to addition of further ligands. Protonation of these species, which is necessary to maintain the overall charge, could not be proven. Similar species were observed in the positive-ion mode, assignment was however not possible for most ions. S^{*-} seems to be the ideal ligand for the ESMS analysis of the discussed Cd thiolate systems. Although its basicity was not sufficient to yield strong signals in positive-ion mode, the more basic $S^{\bullet-}$ ligand appeared to be too reactive, resulting in insoluble products that could not be analysed.

The complex $\{Pt_2S_2\}$ and its electrospray-friendly analogues can be analysed routinely by ESMS due to the formation of very intense $[M + H]^+$ ions. In the case of the methoxy-derivatised complexes, protonation takes place on both S and O atoms. They are not only the better option due to their higher ionisation efficiencies, but also because of their solubility in solvents common for ESMS analysis. While the preparation of the derivatives in a manner similar to that of $\{Pt_2S_2\}$ gives products with four equal phosphine ligands, compounds of the type $[Pt_2(\mu\text{-}S)_2(PPh_3)_{4-m}P^n{}^*{}_m]$ may be obtained by ligand exchange reactions. The reaction with neutral metal complexes appears to be not as straightforward as with ionic species. In the reaction with $[Mo(CO)_4(pip)_2]$, a cationic product was obtained, whose exact nature remained, however, unsolved.

---

[46] H. Liu, C. Jiang, J. S. L. Yeo, K. F. Mok, L. K. Liu, T. S. A. Hor and Y. K. Yan, *J. Organomet. Chem.*, 2000, **595**, 276.

5.6 Experimental

General experimental techniques as well as the atom labelling for the assignment of NMR signals are in keeping with those outlined in Chapter two.

5.6.1 Syntheses of the thiolate complexes

The ligands thiophenol (Riedel-de Haën), *p*-methoxybenzenethiol (Aldrich) and 4-mercaptopyridine (Aldrich) were used as supplied. The precursors [PhHgCl] (BDH), [$Hg(OAc)_2$] (BDH), [PhHg(OAc)] (BDH), $Ag[BF_4]$ (Aldrich) and $ZnSO_4 \cdot 7H_2O$ (Unilab) were used as supplied. The precursors [(dppe)$PdCl_2$], [(dppe)$PtCl_2$] and [$(Ph_3P)AuCl$] were prepared as described in Chapter two. The ligand dppe[47] [1,2-bis(diphenylphosphino)ethane] and [(dppe)$NiCl_2$][48] were prepared according to the literature. [{$(Ph_2PC_2H_4)_2CH$}PdCl] was kindly supplied by K. E. Neo, University of Singapore.

Electrospray mass spectra were obtained by dissolving the complexes in a few drops of CH_2Cl_2 before adding approximately 1 mL of the mobile phase (either MeOH or $MeCN/H_2O$). All spectra were run at 20 V, unless otherwise stated.

All complexes were prepared by the following method: Et_3N and the thiol were added to a suspension of the metal halide in MeOH. After refluxing for 30 minutes, the solution was cooled to room temperature. If necessary, water was added to induce precipitation. After leaving at -20°C overnight, the product was collected by filtration, washed with cold MeOH, and dried under vacuum.

5.6.1.1 Synthesis of [(dppe)$Ni(SPh)_2$]

[(dppe)$NiCl_2$] (0.05 g, 0.09 mmol), Et_3N (0.014 mL, 0.19 mmol) and HSPh (0.02 mL, 0.19 mmol) in MeOH (10 mL) gave [(dppe)$Ni(SPh)_2$] as a red powder. Yield: 0.048 g (79%). The preparation of this complex has been reported before[49].

---

[47] Y. Ruina, L. Kunhua, H. Yimin, W. Dongmei and J. Douman, *Polyhedron*, 1997, **16**, 4033.
[48] G. Booth and J. Chatt, *J. Chem. Soc.*, 1965, 3238.
[49] R. G. Hayter and F. S. Humiec, *J. Inorg. Nucl. Chem.*, 1964, **26**, 807.

m.p. 250 - 254°C. [Lit. 250 - 260°C [49]].

^{31}P NMR ($CDCl_3$): δ 55.9 (s).

^{1}H NMR ($CDCl_3$): δ 7.84 - 6.64 (30H, m, aromatic H of dppe and SPh), δ 2.12 (4H, m, $C_2\underline{H}_4$ of dppe).

^{13} C-{^{1}H} NMR ($CDCl_3$): δ 143.9 (s), δ 133.6 (m), δ 133.1 (s), δ 130.9 (m), δ 128.9 (m), δ 126.2 (m), δ 27.8 (m, $\underline{C}_2H_4$ of dppe).

ESMS (MeOH, +ve ion, 20 V): $[(dppe)_2Ni_2(\mu\text{-}SPh)_2]^{2+}$ *m/z* 565 (100%), unassigned *m/z* 902 (1+ ion, 22%), unassigned *m/z* 1176 (1+ ion, 15%), $[(dppe)_2Ni_2(\mu\text{-}SPh)_2$ + 2 $(dppe)Ni(SPh)_2]^{2+}$ and $[(dppe)Ni(SPh)$ + $(dppe)Ni(SPh)_2]^{+}$ *m/z* 1239 (8%).

5.6.1.2 Synthesis of $[(dppe)Ni(SC_6H_4OCH_3)_2]$, $[(dppe)NiS^*_2]$

$[(dppe)NiCl_2]$ (0.06 g, 0.114 mmol), Et_3N (0.017 mL, 0.23 mmol) and HS* (0.03 mL, 0.23 mmol) in MeOH (10 mL) gave $[(dppe)NiS^*_2]$ as a brown powder. Yield: 0.065 g (77%).

m.p. 166 - 168°C.

Elemental analysis: C, 64.66; H, 5.11%. $C_{40}H_{38}O_2P_2NiS_2$ requires C, 65.26; H, 5.17%.

^{31}P NMR ($CDCl_3$): δ 56.06 (s).

^{1}H NMR ($CDCl_3$): δ 7.86 - 7.38 (20H, m, H2-4 of dppe), δ 7.01 (4H, d, $^{3}J_{H3',H2'}$ = 8.60 Hz, H2' of S*) 6.25 (4H, d, $^{3}J_{H2',H3'}$ = 8.59 Hz, H3' of S*), δ 3.65 (6H, s, $OC\underline{H}_3$), δ 2.06 (4H, m, $C_2\underline{H}_4$ of dppe).

^{13} C-{^{1}H} NMR ($CDCl_3$): δ 157.9 (s, C4'), δ 135.4 (m), δ 133.7 (m,), δ 130.9 (m), δ 128.9 (m), δ 114.4 (m), δ 54.8 (s, $O\underline{C}H_3$), δ 21.8 (m, $\underline{C}_2H_4$).

ESMS (MeOH, +ve ion, 20 V): $[(dppe)_2Ni_2(\mu\text{-}S^*)_2]^{2+}$ *m/z* 595 (100%), unassigned *m/z* 764 (2+ ion, 5%), unassigned *m/z* 932 (2+ ion, 15%), unassigned *m/z* 1236 (1+ ion, 7%).

5.6.1.3 Synthesis of [(dppe)Ni($SC_5H_4N)_2$], [(dppe)$NiS^{\bullet}_2$]

[(dppe)$NiCl_2$] (0.05 g, 0.086 mmol), Et_3N (0.01 mL, 0.17 mmol) and $HS^{\bullet}$ (0.019 g, 0.17 mmol) in MeOH (10 mL) gave [(dppe)$NiS^{\bullet}_2$] as dark red crystals. Yield: 0.018 g (31%).

m.p. 174 - 176°C.

Elemental analysis: C, 63.32; H, 4.71; N, 4.30%. $C_{36}H_{32}N_2P_2NiS_2$ requires C, 63.81; H, 4.73; N, 4.14%.

^{31}P NMR ($CDCl_3$): δ 57.4 (s).

^{1}H NMR ($CDCl_3$): δ 7.83 - 7.47 (24H, m, H2-4 of dppe and H2' of $S^{\bullet}$), δ 7.05 (4H, m, H3' of $S^{\bullet}$), δ 2.27 (4H, m, $C_2\underline{H}_4$ of dppe).

^{13} C-{^{1}H} NMR ($CDCl_3$): δ 156.8 (s), δ 146.6 (m), δ 133.5 (m), δ 131.7 (s), δ 129.0 (m), δ 128.5 (m), δ 128.1 (m), δ 27.5 (m, $\underline{C}_2H_4$ of dppe).

ESMS (MeOH, +ve ion, 20 V): $[M + H]^{2+}$ *m/z* 340 (100%), $[M - S^{\bullet}]^{+}$ *m/z* 566 (32%), $[M + H]^{+}$ *m/z* 677 (65%).

ESMS (MeOH, +ve ion, 40 V): $[M - S^{\bullet}]^{+}$ *m/z* 566 (100%).

ESMS (MeOH, +ve ion, 60 V): $[M - S^{\bullet}]^{+}$ *m/z* 566 (100%).

5.6.1.4 Synthesis of [(dppe)$Pd(SPh)_2$]

[(dppe)$PdCl_2$] (0.25 g, 0.43 mmol), Et_3N (0.072 mL, 1 mmol) and HSPh (0.1 mL, 1 mmol) in MeOH (20 mL) gave [(dppe)$Pd(SPh)_2$] orange crystals. Yield: 0.23 g (75%). The preparation of this complex has been reported before[50].

m.p. 208 - 212°C. [Lit. 210 - 215°C [50]].

^{31}P NMR ($CDCl_3$): δ 55.3 (s).

---

[50] P. S. Bratermann, V. A Wilson and K. K. Joshi, *J. Organometal. Chem.*, 1971, **31**, 123.

^{1}H NMR ($CDCl_3$): δ 7.74 - 6.67 (30H, m, aromatic H of dppe and SPh), δ 2.28 (4H, m, $C_2\underline{H}_4$ of dppe).

^{13}C-{^{1}H} NMR ($CDCl_3$): δ 144.1 (s), δ 134.6 (m), δ 134.2 (m), δ 131.3 (s), δ 129.1 (m), δ 126.3 (s), δ 28.9 (m, $\underline{C}_2H_4$ of dppe).

ESMS (MeOH, +ve ion, 20 V): $[(dppe)_2Pd_2(\mu\text{-}SPh)_2]^{2+}$ *m/z* 613 (100%) $[(dppe)_2Pd_2(\mu\text{-}SPh)_2 + (dppe)Pd(SPh)_2]^{2+}$ *m/z* 975 (10%), $[(dppe)_2Pd_2(\mu\text{-}SPh)_2 + 2\ (dppe)Pd(SPh)_2]^{2+}$ *m/z* 1273 (3%), unassigned *m/z* 1336 (1+ ion, 8%).

5.6.1.5 Synthesis of [(dppe)Pd($SC_6H_4OCH_3$)$_2$], [(dppe)PdS*$_2$]

[(dppe)$PdCl_2$] (0.25 g, 0.43 mmol), Et_3N (0.072 mL, 1 mmol) and HS* (0.15 mL, 1 mmol) in MeOH (20 mL) gave [(dppe)PdS*$_2$] as red crystals. Yield: 0.18 g (54%).

m.p. 156 - 159°C.

Elemental analysis: C, 61.09; H, 4.81%. $C_{40}H_{38}O_2P_2PdS_2$ requires C, 61.35; H, 4.86%.

^{31}P NMR ($CDCl_3$): δ 54.9 (s).

^{1}H NMR ($CDCl_3$): δ 7.73 - 7.37 (20H, m, aromatic H of dppe), δ 7.05 (4H, d, $^3J_{H3',H2'}$ = 8.5 Hz, H2' of S*) δ 6.25 (4H, d, $^3J_{H2',H3'}$ = 9.0 Hz, H3' of S*), δ 3.65 (6H, s, $OC\underline{H}_3$), δ 2.21 (4H, m, $C_2\underline{H}_4$ of dppe).

^{13}C-{^{1}H} NMR ($CDCl_3$): δ 156.2 (s, C4'), δ 135.5 (m), δ 133.6 (m), δ 131.2 (s), δ 128.8 (m), δ 112.8 (m), δ 54.8 (s, $O\underline{C}H_3$), δ 29.4 (m, $\underline{C}_2H_4$).

ESMS (MeOH, +ve ion, 20 V): $[(dppe)_2Pd_2(\mu\text{-}S^*)_2]^{2+}$ *m/z* 643 (100%), $[(dppe)_2Pd_2(\mu\text{-}S^*)_2 + (dppe)PdS^*_2]^{2+}$ *m/z* 1035 (8%), unassigned *m/z* 1332 (1+ ion, 4%), $[(dppe)PdS^* + (dppe)PdS^*_2]^+$ *m/z* 1428 (12%).

5.6.1.6 Synthesis of [(dppe)Pd(SC_5H_4N)$_2$], [(dppe)PdS$^\bullet_2$]

[(dppe)$PdCl_2$] (0.165 g, 0.28 mmol), Et_3N (0.043 mL, 0.6 mmol) and HS$^\bullet$ (0.065 g, 0.58 mmol) in MeOH (20 mL) gave [(dppe)PdS$^\bullet_2$] as orange crystals. Yield: 0.23 g (25%).

m.p. 192 - 194°C.

Elemental analysis: C, 59.64; H, 4.54; N, 4.04%. $C_{36}H_{32}N_2P_2PtS_2$ requires C, 59.64; H, 4.42; N, 3.87%.

^{31}P NMR ($CDCl_3$): δ 57.2 (s).

^{1}H NMR ($CDCl_3$): δ 7.79 - 7.43 (24H, m, aromatic H of dppe and H2' of $S^{\bullet}$), δ 7.03 (4H, d, $^{3}J_{H2',H3'}$ = 5.2 Hz, H3' of $S^{\bullet}$), δ 2.43 (4H, m, $C_2\underline{H}_4$ of dppe).

^{13} C-{^{1}H} NMR ($CDCl_3$): δ 156.8 (s), δ 147.0 (s), δ 133.4 (m), δ 133.0 (m), δ 132.0 (s), δ 129.2 (m), δ 128.6 (m), δ 128.0 (m), δ 29.8 (m, $\underline{C}_2H_4$ of dppe).

ESMS (MeOH, +ve ion, 20 V): $[M + H]^{2+}$ *m/z* 364 (34%), $[M - S^{\bullet}]^{+}$ *m/z* 614 (8%), $[M + H]^{+}$ *m/z* 724 (100%), $[2M - S^{\bullet}]^{+}$ *m/z* 1341 (5%), $[2M + H]^{+}$ *m/z* 1452 (10%).

ESMS (MeOH, +ve ion, 40 V): $[M - S^{\bullet}]^{+}$ *m/z* 613 (100%), $[M + H]^{+}$ *m/z* 724 (22%), $[2M - S^{\bullet}]^{+}$ *m/z* 1341 (10%).

ESMS (MeOH, +ve ion, 60 V): $[M - S^{\bullet}]^{+}$ *m/z* 613 (100%), $[M + H]^{+}$ *m/z* 724 (5%), $[2M - S^{\bullet}]^{+}$ *m/z* 1340 (8%).

5.6.1.7 Synthesis of [(dppe)Pt(SPh)$_2$]

This complex was kindly supplied by W. Henderson. The preparation of this complex has been reported before[51].

m.p. 228 - 229°C. [Lit. 225 - 226°C [51]].

^{31}P NMR ($CDCl_3$): δ 46.4 (s, $^{1}J_{Pt,P}$ = 2884 Hz). [Lit. δ 45.6 (s, $^{1}J_{Pt,P}$ = 2885 Hz)[51]].

^{1}H NMR ($CDCl_3$): δ 7.79 - 6.68 (30H, m, aromatic Hs of dppe and SPh), δ 2.19 (4H, m, $C_2\underline{H}_4$ of dppe).

---

[51] V. K. Jain, Sh. Kannan, R. J. Butcher and J. P. Jasinski, *J. Chem. Soc. Dalton Trans.*, 1993, 1509.

^{13}C-{^{1}H} NMR ($CDCl_3$): δ 134.0 (s), δ 133.7 (m), δ 131.3 (s), δ 128.7 (m), δ 128.1 (s), δ 126.6 (s), δ 122.6 (s), δ 28.1 (m, $\underline{C}_2H_4$ of dppe).

ESMS (MeOH, +ve ion, 20 V): $[(dppe)_2Pt_2(\mu\text{-}SPh)_2]^{2+}$ *m/z* 701 (100%), $[(dppe)_2Pt_2(\mu\text{-}SPh)_2 + (dppe)Pt(SPh)_2]^{2+}$ *m/z* 1106 (50%), $[(dppe)_2Pt_2(\mu\text{-}SPh)_2 + 2\ (dppe)Pt(SPh)_2]^{2+}$ *m/z* 1513 (8%), unassigned *m/z* 1732 (2+ ion, 50%), $[(dppe)_2Pt_2(\mu\text{-}SPh)_2 + 3\ (dppe)Pt(SPh)_2]^{2+}$ *m/z* 1920 (5%).

5.6.1.8 Synthesis of [(dppe)Pt($SC_6H_4OCH_3$)$_2$, [(dppe)PtS*$_2$]

[(dppe)$PtCl_2$] (0.153 g, 0.23 mmol), Et_3N (0.46 mmol, 0.06 mL) and HS* (0.033 mL, 0.46 mmol) in MeOH (20 mL) gave [(dppe)PtS*$_2$] as yellow crystals. Yield: 0.195 g (98%).

m.p. 196 - 197°C.

Elemental analysis: C, 54.96; H, 4.54%. $C_{40}H_{38}O_2P_2PtS_2$ requires C, 55.11; H, 4.36%.

^{31}P NMR ($CDCl_3$): δ 46.5 (s, $^{1}J_{Pt,\,P}$ = 2892 Hz).

^{1}H NMR ($CDCl_3$): δ 7.77 - 7.39 (20H, m, H2-4 of dppe), δ 6.99 (4H, d, $^{3}J_{H3',\,H2'}$ = 8.3 Hz, H2' of S*) 6.25 (4H, d, $^{3}J_{H2',\,H3'}$ = 8.1 Hz, H3' of S*), δ 3.64 (6H, s, $OC\underline{H}_3$), δ 2.18 (4H, m, $C_2\underline{H}_4$ of dppe).

^{13}C-{^{1}H} NMR ($CDCl_3$): δ 156.3 (s, C4'), δ 135.2 (s, C2'), δ 133.5 (m, C2), δ 131.2 (s, C4), δ 128.6 (m, C3), δ 112.5 (s, C3'), δ 55.2 (s, $O\underline{C}H_3$), δ 23.4 (m, $\underline{C}_2H_4$).

ESMS ($MeCN/H_2O$, +ve ion, 20 V): $[(dppe)_2Pt_2(\mu\text{-}S^*)_2]^{2+}$ *m/z* 732 (100%), $[M + H]^+$ *m/z* 873 (10%), $[(dppe)_2Pt_2(\mu\text{-}S^*)_2 + (dppe)PtS^*_2]^{2+}$ *m/z* 1168 (15%), unassigned *m/z* 1411 (2+ ion, 5%), unassigned *m/z* 1500 (1+ ion, 5%), $[(dppe)_2Pt_2(\mu\text{-}S^*)_2 + 2\ (dppe)PtS^*_2]^{2+}$ *m/z* 1603 (3%), unassigned *m/z* 1848 (2+ ion, 5%).

5.6.1.9 Synthesis of [(dppe)Pt(SC_5H_4N)$_2$], [(dppe)PtS$^{\bullet}_2$]

This complex was kindly supplied by W. Henderson.

m.p. 218 - 220°C.

Elemental analysis: C, 52.3; H, 3.76; N, 3.36%. $C_{36}H_{32}N_2P_2PtS_2$ requires C, 53.1; H, 3.94; N, 3.44%.

^{31}P NMR ($CDCl_3$): δ 46.8 (s, $^1J_{Pt,P}$ = 2890 Hz).

^1H NMR ($CDCl_3$): δ 7.83 - 7.23 (24H, m, H2-4 of dppe and H2' of S$^\bullet$), δ 7.05 (4H, m, H3' of S$^\bullet$), δ 2.19 (4H, m, $C_2\underline{H}_4$ of dppe).

^{13} C-{^{1}H} NMR ($CDCl_3$): δ 146.6 (s), δ 133.5 (m), δ 132.0 (s), δ 129.0 (m), δ 128.1 (m), δ 126.8 (m), δ 29.1 (m, $\underline{C}_2H_4$ of dppe).

ESMS (MeOH, +ve ion, 20 V): $[M + H]^{2+}$ *m/z* 408 (50%), $[M - S^\bullet]^+$ *m/z* 704 (4%), $[2M - S^\bullet]^{2+}$ *m/z* 759 (8%), $[M + H]^+$ *m/z* 814 (100%), $[2M - S^\bullet]^+$ *m/z* 1517 (15%), $[2M + H]^+$ *m/z* 1627 (5%).

5.6.1.10 Synthesis of [(Ph$_3$P)Au(SPh)]

[(Ph_3P)AuCl] (0.248 g, 0.5 mmol), Et_3N (0.035 mL, 0.5 mmol) and HSPh (0.055 mL, 0.5 mmol) in MeOH (20 mL) gave [(Ph_3P)Au(SPh)] as a grey powder. Yield: 0.215 g (76%). The preparation of this complex has been reported before[52].

m.p. 155 - 160°C.

Elemental analysis: C, 50.50; H, 3.52%. $C_{24}H_{20}AuPS$ requires C, 50.70; H, 3.52%.

^{31}P NMR ($CDCl_3$): δ 39.5 (s). [Lit. 38.6 [52]].

^1H NMR ($CDCl_3$): δ 7.58 - 6.97 (24H, m, aromatic H of PPh_3 and SPh).

^{13} C-{^{1}H} NMR ($CDCl_3$): δ 141.6 (s, C1'), δ 134.3 (m, C2), δ 132.7 (s, C2'), δ 131.8 (s, C4), δ 130.0 (s, C3'), δ 129.3 (m, C3), δ 128.1 (m, C1), δ 128.0 (s, C4'). [Lit. δ 141.4 (s, C1'), δ 134.2 (m, C2), δ 132.5 (s, C4'), δ 131.8 (m, C4), δ 128.4 (s, C3'), δ 128.0 (s, C2'), δ 129.2 (m, C3), δ 128.0 (m, C1)[52]].

---

[52] J. M. Forward, D. Bohmann, J. P. Fackler, Jr. and R. J. Staples, *Inorg. Chem.*, 1995, **34**, 6330; E. Delgado and E. Hernandez, *Polyhedron*, 1992, **11**, 3135.

ESMS (MeOH, +ve ion, 20 V): $[Au(PPh_3)_2]^+$ *m/z* 721 (29%), $[(Ph_3P)_2Au_2(SPh)]^+$ *m/z* 1027 (100%), $[(Ph_3P)_3Au_2(SPh)]^+$ *m/z* 1289 (30%), $[(Ph_3P)_3Au_3(SPh)_2]^+$ *m/z* 1595 (50%).

5.6.1.11 Synthesis of $[(Ph_3P)Au(SC_6H_4OCH_3)]$, $[(Ph_3P)AuS^*]$

$[(Ph_3P)AuCl]$ (0.2 g, 0.4 mmol), Et_3N (0.05 mL, 0.4 mmol) and HS* (0.03 mL, 0.4 mmol) in MeOH (20 mL) gave $[(Ph_3P)AuS^*]$ as yellow crystals. Yield: 0.24 g (62%).

m.p. 62 - 64°C.

Elemental analysis: C, 50.33; H, 3.70%. $C_{40}H_{38}O_2P_2PtS_2$ requires C, 50.17; H, 3.68%.

^{31}P NMR ($CDCl_3$): δ 39.2.

^1H NMR ($CDCl_3$): δ 7.59 - 7.28 (17H, m, aromatic H of PPh_3 and H2' of S*), δ 6.71 (2H, d, $^3J_{H2',H3'}$ = 8.59 Hz, H3' of S*) δ 3.76 (3H, s, $OC\underline{H}_3$).

^{13} C-{^1H} NMR ($CDCl_3$): δ 156.9 (s, C4'), δ 134.5 (d, $^2J_{C2,P}$ = 10.4 Hz, C2), δ 134.0 (s, C2'), δ 132.0 (d, $^4J_{C4,P}$ = 1.5 Hz, C4), δ 131.5 (s, C1'), δ 129.9 (d, $^1J_{C1,P}$ = 42.3 Hz, C1), δ 129.5 (d, $^3J_{C3,P}$ = 8.6 Hz C3), δ 55.72 (s, $O\underline{C}H_3$).

ESMS (MeOH, +ve ion, 20 V): $[Au(PPh_3)_2]^+$ *m/z* 721 (42%), $[(Ph_3P)_2Au_2S^*]^+$ *m/z* 1057 (100%), $[(Ph_3P)_3Au_2S^*]^+$ *m/z* 1319 (43%), $[(Ph_3P)_3Au_3S^*_2]^+$ *m/z* 1655 (40%).

5.6.1.12 Synthesis of $[(Ph_3P)Au(SC_5H_4N)]$, $[(Ph_3P)AuS^\bullet]$

$[(Ph_3P)AuCl]$ (0.495 g, 1 mmol), Et_3N (0.08 mL, 1 mmol) and $HS^\bullet$ (0.11 g, 1 mmol) in MeOH (20 mL) gave $[(Ph_3P)AuS^\bullet]$ as yellow crystals. Yield: 0.445 g (62%). The preparation of this complex has been reported before[53].

m.p. 174 - 176°C.

Elemental analysis: C, 48.59; H, 3.67; N, 2.16%. $C_{23}H_{19}AuNPS$ requires C, 48.51; H, 3.34; N, 2.46%.

---

[53] K. Nunokawa, S. Onaka, T. Tatematsu, M. Ito and J. Sakai, *Inorg. Chim. Acta*, 2001, **322**, 56.

^{31}P NMR ($CDCl_3$): δ 39.6 (s). [Lit: 39.76 [53]].

^{1}H NMR ($CDCl_3$): δ 8.18 (2H, m, $^{3}J_{H2',H3'}$ = 3.26 Hz, H3' of S$^{\bullet}$), δ 7.60 - 7.42 (7H, m, aromatic H of PPh_3 and H2' of S$^{\bullet}$).

^{13}C-{^{1}H} NMR ($CDCl_3$): δ 155.5 (s, C1'), δ 148.3 (s, C2'), δ 134.2 (d, $^{2}J_{C2,P}$ = 11.3 Hz, C2), δ 132.0 (d, $^{4}J_{C4,P}$ = 1.5 Hz C4), δ 129.4 (d, $^{3}J_{C3,P}$ = 10.4 Hz, C3), δ 129.2 (d, $^{2}J_{C1,P}$ = 37.7 Hz, C1), δ 127.4 (s, C3').

ESMS (MeOH, +ve ion, 20 V): $[M + H]^+$ *m/z* 570 (55%), $[Au(PPh_3)_2]^+$ *m/z* 721 (100%).

5.6.1.13 Synthesis of [PhHg(SPh)]

[PhHgCl] (0.1 g, 0.32 mmol), Et_3N (0.03 mL, 0.33 mmol) and HSPh (0.04 mL, 0.33 mmol) in MeOH (20 mL) gave [PhHg(SPh)] as an off-white powder. Yield: 0.09 g (73%). The preparation of this complex has been reported before[54].

m.p. 92 - 95°C. [Lit. 105°C [54]].

^{1}H NMR ($CDCl_3$): δ 7.51 - 7.17 (10H, m, aromatic H of Ph and SPh). [Lit. δ 7.5 - 7.05 (m, Ph), δ 7.12 (m, SPh)].

^{13}C-{^{1}H} NMR ($CDCl_3$): δ 160.4 (s), δ 136.5 (s), δ 134.5 (s), δ 133.3 (s), δ 129.1 (m), δ 125.8 (m).

5.6.1.14 Synthesis of [Hg($SC_6H_4OCH_3$)$_2$], [HgS*$_2$]

In an attempt to prepare [PhHg($SC_6H_4OCH_3$)], [PhHgS*], [PhHgCl] (0.1 g, 0.32 mmol), Et_3N (0.03 mL, 0.33 mmol) and HS* (0.05 mL, 0.33 mmol) in MeOH (20 mL) gave an off-white powder. Upon recrystallisation [HgS*$_2$] was obtained as a silvery powder, which was soluble only in DMSO. Yield: 0.037 g (30%).

m.p. 192 - 195°C.

Elemental analysis: C, 35.06; H, 2.79%. $C_{14}H_{14}HgO_2S_2$ requires C, 35.10; H, 2.79%.

^{1}H NMR (DMSO): δ 7.28 (2H, d, $^3J_{H3',H2'}$ = (8.5 Hz, H2'), δ 6.76 (2H, d, $^3J_{H2',H3'}$ = 8.5 Hz, H3'), δ 3.69 (3H, s, $OC\underline{H}_3$).

^{13} C-{^{1}H} NMR (DMSO): δ 157.9 (s, C4'), δ 134.0 (s, C2'), δ 127.0 (s, C1'), δ 114.8 (s, C3').

5.6.1.15 Synthesis of [PhHg(SC_5H_4N)], [PhHgS$^\bullet$]

[PhHgCl] (0.1 g, 0.32 mmol), Et_3N (0.03 mL, 0.33 mmol) and HS$^\bullet$ (0.0366 g, 0.33 mmol) in MeOH (20 mL) gave [PhHgS$^\bullet$] as an off-white powder. Yield: 0.065 g (53%).

m.p. 166 - 169°C.

A satisfactory elemental analysis was not obtained, *e.g.* C, 31.35; H, 1.93; N, 3.53%. $C_{11}H_9HgNS$ requires C, 34.06; H, 2.32; N, 3.61%.

^{1}H NMR ($CDCl_3$): δ 8.36 (2H, d, $^3J_{H2',H3'}$ = 3.6 Hz, H2' of S$^\bullet$), δ 7.87 (2H, d, $^3J_{H3',H2'}$ = 7.5 Hz, H3' of S$^\bullet$), δ 7.45 - 7.27 (5H, m, aromatic H of Ph).

ESMS (MeOH, +ve ion, 20 V): $[M + H]^+$ *m/z* 387 (100%).

5.6.2 ESMS of exchange processes of (sulfide) thiolate complexes of cadmium

The complex $[Me_4N]_2[Cd_4(SPh)_{10}]$ was prepared according to the literature[27]. $[Me_4N]_4[S_4Cd_{10}(SPh)_{16}]$ and $[Me_4N]_2[S_4Cd_{17}(SPh)_{28}]$ were kindly provided by W. Henderson, but can be prepared by previously described methods[24]. Stock solutions (500 ppm w/v) of each metal complex were prepared by dissolving 0.01 g of the complex in 20 mL of MeCN. The preparation of the corresponding stock solutions of the ligand HS* are listed below. Mixtures of the metal complexes and HS* were prepared by adding 0.05 mL of the metal complex solution to 0.05 mL of the corresponding HS* solutions, which were prepared by serial dilution. All solutions were made fresh and were subsequently injected into the ESMS. The spectra were obtained using a mobile phase of

---

[54] C. Dell'Erba, G. Guanti, M. Novi and G. Leandri, *J. Chem. Soc. Perkin II*, 1973, 1879; A. J. Canty and R. Kishimoto, *Inorg. Chim. Acta*, 1977, **24**, 109.

MeCN/H_2O. The observed ions for all three complexes are summarised in Table 5.8. Data are listed for the addition of 0, 1 and full mole equivalents of HS*.

Table 5.8 The negative-ion ESMS data for the reactions between $[Cd_4(SPh)_{10}]^{2-}$ (**1**), $[S_4Cd_{10}(SPh)_{16}]^{4-}$ (**2**) or $[S_4Cd_{17}(SPh)_{28}]^{2-}$ (**3**) and HS*, recorded in MeCN/H_2O at cV = 5 V. Ions with additional ligands are presented in italics and were assigned by adding the appropriate amount of protons in order to maintain the observed charge.

	Ratio[(a)]	Ions observed [*m/z*, relative peak height (%)]
1	1:0	$[Cd_4(SPh)_{10}]^{2-}$ (771, 100) $[Cd_3(SPh)_7]^-$ (1101, 14) $[Cd(SPh)_3]^-$ (441, 4)
	1:1	$[Cd_4(SPh)_{10}]^{2-}$ (771, 100), $[Cd_4(SPh)_9S^*]^{2-}$ (786, 97), $[Cd_4(SPh)_8S^*_2]^{2-}$ (801, 72), $[Cd_4(SPh)_7S^*_3]^{2-}$ (816, 17), $[Cd_4(SPh)_6S^*_4]^{2-}$ (831,8), *$[Cd_4(SPh)_{10}S^*_2 + 2H]^{2-}$ (908, 2), $[Cd_4(SPh)_9S^*_3 + 2H]^{2-}$ (925, 2), $[Cd_4(SPh)_8S^*_4 + 2H]^{2-}$ (938, 2), unidentified: (951, 5), (965, 6), (983, 4), (995, 2)* $[Cd_3(SPh)_7]^-$ (1101, 5), $[Cd_3(SPh)_6S^*]^-$ (1132, 6), $[Cd_3(SPh)_5S^*_2]^-$ (1161, 3), $[Cd_3(SPh)_4S^*_3]^-$ (1191, 1), $[Cd_3(SPh)_3S^*_4]^-$ (1221, 1) $[Cd(SPh)_3]^-$ (441, 13), $[Cd(SPh)_2S^*]^-$ (471, 4), $[Cd(SPh)S^*_2]^-$ (499, 1)
	1:10	$[Cd_4(SPh)_8S^*_2]^{2-}$ (801, 22), $[Cd_4(SPh)_7S^*_3]^{2-}$ (816, 27), $[Cd_4(SPh)_6S^*_4]^{2-}$ (831,87), $[Cd_4(SPh)_5S^*_5]^{2-}$ (846,60), $[Cd_4(SPh)_4S^*_6]^{2-}$ (861,100), $[Cd_4(SPh)_3S^*_7]^{2-}$ (876,27), $[Cd_4(SPh)_2S^*_8]^{2-}$ (891,43) *$[Cd_4(SPh)_7S^*_5 + 2H]^{2-}$ (954, 8), $[Cd_4(SPh)_6S^*_6 + 2H]^{2-}$ (970, 15), $[Cd_4(SPh)_5S^*_7 + 2H]^{2-}$ (985, 23), $[Cd_4(SPh)_4S^*_8 + 2H]^{2-}$ (1000, 27), $[Cd_4(SPh)_3S^*_9 + 2H]^{2-}$ (1015, 18), $[Cd_4(SPh)_2S^*_{10} + 2H]^{2-}$ (1030, 10), unidentified: (1040, 7), (1054, 5)* $[Cd_3(SPh)_5S^*_2]^-$ (1159, 7), $[Cd_3(SPh)_4S^*_3]^-$ (1191, 14), $[Cd_3(SPh)_3S^*_4]^-$ (1222, 22), $[Cd_3(SPh)_2S^*_5]^-$ (1252, 22), $[Cd_3(SPh)S^*_6]^-$ (1281, 13), $[Cd_3S^*_7]^-$ (1312, 3) $[Cd(SPh)_3]^-$ (441, 11), $[Cd(SPh)_2S^*]^-$ (471, 38), $[Cd(SPh)S^*_2]^-$ (501, 40), $[CdS^*_3]^-$ (531, 13)
2	1:0	$[S_4Cd_{10}(SPh)_{16}]^{4-}$ (750, 100) $[S_4Cd_{10}(SPh)_{15}]^{3-}$ (964, 49)

	$[Me_4N][S_4Cd_{10}(SPh)_{16}]^{3-}$ (1025,33) $[Me_4N][S_4Cd_{10}(SPh)_{15}]^{2-}$ (1482,13) $[Cd(SPh)_3]^-$ (441, 5)
1:1	$[S_4Cd_{10}(SPh)_{15}S^*]^{4-}$ (757, 100), $[S_4Cd_{10}(SPh)_{14}S^*_2]^{4-}$ (765, 53), $[S_4Cd_{10}(SPh)_{13}S^*_3]^{4-}$ (772, 88), $[S_4Cd_{10}(SPh)_{12}S^*_4]^{4-}$ (779, 100), $[S_4Cd_{10}(SPh)_{11}S^*_5]^{4-}$ (787, 82), $[S_4Cd_{10}(SPh)_{10}S^*_6]^{4-}$ (795, 53), $[S_4Cd_{10}(SPh)_9S^*_7]^{4-}$ (802, 30), $[S_4Cd_{10}(SPh)_8S^*_8]^{4-}$ (810, 15) *$[S_4Cd_{10}(SPh)_{16}S^*_2 + 2H]^{4-}$ (818, 12), $[S_4Cd_{10}(SPh)_{15}S^*_3 + 2H]^{4-}$ (826, 15),* *$[S_4Cd_{10}(SPh)_{14}S^*_4 + 2H]^{4-}$ (833, 21), $[S_4Cd_{10}(SPh)_{13}S^*_5 + 2H]^{4-}$ (842, 26),* *$[S_4Cd_{10}(SPh)_{12}S^*_6 + 2H]^{4-}$ (849, 29), $[S_4Cd_{10}(SPh)_{11}S^*_7 + 2H]^{4-}$ (857, 25),* *$[S_4Cd_{10}(SPh)_{10}S^*_8 + 2H]^{4-}$ (863, 18), $[S_4Cd_{10}(SPh)_9S^*_9 + 2H]^{4-}$ (871, 12)* $[S_4Cd_{10}(SPh)_{14}S^*]^{3-}$ (974, 12), $[S_4Cd_{10}(SPh)_{13}S^*_2]^{3-}$ (983, 28), $[S_4Cd_{10}(SPh)_{12}S^*_3]^{3-}$ (993, 46), $[S_4Cd_{10}(SPh)_{11}S^*_4]^{3-}$ (1003, 47), $[S_4Cd_{10}(SPh)_{10}S^*_5]^{3-}$ (1013, 42), $[S_4Cd_{10}(SPh)_9S^*_6]^{3-}$ (1023, 28), $[S_4Cd_{10}(SPh)_8S^*_7]^{3-}$ (1032, 16) *$[S_4Cd_{10}(SPh)_{15}S^*_2 + 2H]^{3-}$ (1054, 19), $[S_4Cd_{10}(SPh)_{14}S^*_3 + 2H]^{3-}$ (1064,23),* *$[S_4Cd_{10}(SPh)_{13}S^*_4 + 2H]^{3-}$ (1076, 24), $[S_4Cd_{10}(SPh)_{12}S^*_5 + 2H]^{3-}$ (1085, 20),* *$[S_4Cd_{10}(SPh)_{11}S^*_6 + 2H]^{3-}$ (1095, 16), $[S_4Cd_{10}(SPh)_{10}S^*_7 + 2H]^{3-}$ (1106, 12),* *$[S_4Cd_{10}(SPh)_9S^*_8 + 2H]^{3-}$ (1115, 8), $[S_4Cd_{10}(SPh)_8S^*_9 + 2H]^{3-}$ (1125, 6)* $[Cd(SPh)_3]^-$ (441, 27), $[Cd(SPh)_2S^*]^-$ (471, 20), $[Cd(SPh)S^*_2]^-$ (501, 9), $[CdS^*_3]^-$ (531, 5)
1:16	$[S_4Cd_{10}(SPh)_{11}S^*_5]^{4-}$ (787, 7), $[S_4Cd_{10}(SPh)_{10}S^*_6]^{4-}$ (795, 19), $[S_4Cd_{10}(SPh)_9S^*_7]^{4-}$ (802, 41), $[S_4Cd_{10}(SPh)_8S^*_8]^{4-}$ (810, 71), $[S_4Cd_{10}(SPh)_7S^*_9]^{4-}$ (817, 97), $[S_4Cd_{10}(SPh)_6S^*_{10}]^{4-}$ (824, 100), $[S_4Cd_{10}(SPh)_5S^*_{11}]^{4-}$ (833, 88), $[S_4Cd_{10}(SPh)_4S^*_{12}]^{4-}$ (840, 56), $[S_4Cd_{10}(SPh)_3S^*_{13}]^{4-}$ (846, 35) *$[S_4Cd_{10}(SPh)_{11}S^*_7 + 2H]^{4-}$ (855, 16), $[S_4Cd_{10}(SPh)_{10}S^*_8 + 2H]^{4-}$ (863, 19),* *$[S_4Cd_{10}(SPh)_9S^*_9 + 2H]^{4-}$ (873, 32), $[S_4Cd_{10}(SPh)_8S^*_{10} + 2H]^{4-}$ (879, 41),* *$[S_4Cd_{10}(SPh)_7S^*_{11} + 2H]^{4-}$ (886, 53), $[S_4Cd_{10}(SPh)_6S^*_{12} + 2H]^{4-}$ (894, 56),* *$[S_4Cd_{10}(SPh)_5S^*_{13} + 2H]^{4-}$ (902, 44), $[S_4Cd_{10}(SPh)_4S^*_{14} + 2H]^{4-}$ (909, 29),* *$[S_4Cd_{10}(SPh)_3S^*_{15} + 2H]^{4-}$ (917, 16)* *$[S_4Cd_{10}(SPh)_{10}S^*_{10} + 4H]^{4-}$ (932, 8), $[S_4Cd_{10}(SPh)_9S^*_{11} + 4H]^{4-}$ (941, 11),* *$[S_4Cd_{10}(SPh)_8S^*_{12} + 4H]^{4-}$ (949, 14), $[S_4Cd_{10}(SPh)_7S^*_{13} + 4H]^{4-}$ (956, 17),* *$[S_4Cd_{10}(SPh)_6S^*_{14} + 4H]^{4-}$ (963, 14), $[S_4Cd_{10}(SPh)_5S^*_{15} + 4H]^{4-}$ (971, 13),* *$[S_4Cd_{10}(SPh)_4S^*_{16} + 4H]^{4-}$ (978, 11), $[S_4Cd_{10}(SPh)_3S^*_{17} + 4H]^{4-}$ (986, 6),* *$[S_4Cd_{10}(SPh)_2S^*_{18} + 4H]^{4-}$ (991, 5)*

		$[S_4Cd_{10}(SPh)_{10}S^*_5]^{3-}$ (1012, 5), $[S_4Cd_{10}(SPh)_9S^*_6]^{3-}$ (1024, 9), $[S_4Cd_{10}(SPh)_8S^*_7]^{3-}$ (1033, 19), $[S_4Cd_{10}(SPh)_7S^*_8]^{3-}$ (1043, 25), $[S_4Cd_{10}(SPh)_6S^*_9]^{3-}$ (1053, 32), $[S_4Cd_{10}(SPh)_5S^*_{10}]^{3-}$ (1063, 29), $[S_4Cd_{10}(SPh)_4S^*_{11}]^{3-}$ (1073, 22), $[S_4Cd_{10}(SPh)_3S^*_{12}]^{3-}$ (1083, 13), $[S_4Cd_{10}(SPh)_2S^*_{13}]^{3-}$ (1095, 10) *$[S_4Cd_{10}(SPh)_{11}S^*_6 + 2H]^{3-}$ (1095, 10), $[S_4Cd_{10}(SPh)_{10}S^*_7 + 2H]^{3-}$ (1104, 12), $[S_4Cd_{10}(SPh)_9S^*_8 + 2H]^{3-}$ (1114, 19), $[S_4Cd_{10}(SPh)_8S^*_9 + 2H]^{3-}$ (1125, 22), $[S_4Cd_{10}(SPh)_7S^*_{10} + 2H]^{3-}$ (1136, 26), $[S_4Cd_{10}(SPh)_6S^*_{11} + 2H]^{3-}$ (1145, 24), $[S_4Cd_{10}(SPh)_5S^*_{12} + 2H]^{3-}$ (1155, 20), $[S_4Cd_{10}(SPh)_4S^*_{13} + 2H]^{3-}$ (1165, 14), $[S_4Cd_{10}(SPh)_3S^*_{14} + 2H]^{3-}$ (1176, 9), $[S_4Cd_{10}(SPh)_2S^*_{15} + 2H]^{3-}$ (1187, 8)* *$[S_4Cd_{10}(SPh)_{11}S^*_8 + 4H]^{3-}$ (1187, 8), $[S_4Cd_{10}(SPh)_{10}S^*_9 + 4H]^{3-}$ (1197, 10), $[S_4Cd_{10}(SPh)_9S^*_{10} + 4H]^{3-}$ (1207, 13), $[S_4Cd_{10}(SPh)_8S^*_{11} + 4H]^{3-}$ (1217, 15), $[S_4Cd_{10}(SPh)_7S^*_{12} + 4H]^{3-}$ (1227, 17), $[S_4Cd_{10}(SPh)_6S^*_{13} + 4H]^{3-}$ (1238, 15), $[S_4Cd_{10}(SPh)_5S^*_{14} + 4H]^{3-}$ (1247, 12), $[S_4Cd_{10}(SPh)_4S^*_{15} + 4H]^{3-}$ (1257, 8), $[S_4Cd_{10}(SPh)_3S^*_{16} + 4H]^{3-}$ (1268, 5)* *$[S_4Cd_{10}(SPh)_{11}S^*_{10} + 6H]^{3-}$ (1279, 4), $[S_4Cd_{10}(SPh)_{10}S^*_{11} + 6H]^{3-}$ (1290, 5), $[S_4Cd_{10}(SPh)_9S^*_{12} + 6H]^{3-}$ (1299, 7), $[S_4Cd_{10}(SPh)_8S^*_{13} + 6H]^{3-}$ (1310, 8), $[S_4Cd_{10}(SPh)_7S^*_{14} + 6H]^{3-}$ (1320, 7), $[S_4Cd_{10}(SPh)_6S^*_{15} + 6H]^{3-}$ (1331, 6), $[S_4Cd_{10}(SPh)_5S^*_{16} + 6H]^{3-}$ (1339, 5), $[S_4Cd_{10}(SPh)_4S^*_{17} + 6H]^{3-}$ (1350, 4)* unidentified: (1393, 3), (1405, 5), (1422, 5), (1436, 6), (1452, 5), (1466, 5) unidentified: (1587, 1), (1602, 2), (1617, 3), (1632, 3), (1645, 2), (1661, 1), (1675, 1) $[Cd(SPh)_3]^-$ (439, 8), $[Cd(SPh)_2S^*]^-$ (471, 24), $[Cd(SPh)S^*_2]^-$ (501,35), $[CdS^*_3]^-$ (531, 22)
3	1:0	$[S_4Cd_{17}(SPh)_{28}]^{2-}$ (2548, 100) $[S_4Cd_{17}Cl(SPh)_{27}]^{2-}$ (2511, 50) $[S_4Cd_{17}Cl_2(SPh)_{26}]^{2-}$ (2474, 13)
	1:1	$[S_4Cd_{17}(SPh)_{28}]^{2-}$ (2548, 100), $[S_4Cd_{17}(SPh)_{27}S^*]^{2-}$ (2563, 94), $[S_4Cd_{17}(SPh)_{26}S^*_2]^{2-}$ (2578, 44) $[S_4Cd_{17}Cl(SPh)_{27}]^{2-}$ (2511, 26), $[S_4Cd_{17}Cl(SPh)_{26}S^*]^{2-}$ (2526, 24)
	1:28	$[S_4Cd_{17}(SPh)_{19}S^*_9]^{2-}$ (2683, 12), $[S_4Cd_{17}(SPh)_{18}S^*_{10}]^{2-}$ (2700, 27), $[S_4Cd_{17}(SPh)_{17}S^*_{11}]^{2-}$ (2714, 50), $[S_4Cd_{17}(SPh)_{16}S^*_{12}]^{2-}$ (2728, 81), $[S_4Cd_{17}(SPh)_{15}S^*_{13}]^{2-}$ (2744, 100), $[S_4Cd_{17}(SPh)_{14}S^*_{14}]^{2-}$ (2759, 96), $[S_4Cd_{17}(SPh)_{13}S^*_{15}]^{2-}$ (2773, 73), $[S_4Cd_{17}(SPh)_{12}S^*_{16}]^{2-}$ (2789, 46), $[S_4Cd_{17}(SPh)_{11}S^*_{17}]^{2-}$ (2804, 23), $[S_4Cd_{17}(SPh)_{10}S^*_{18}]^{2-}$ (2820, 12)

[(a)] complex : HS*

5.6.2.1 Stock solutions of $[Me_4N]_2[Cd_4(SPh)_{10}]$ and HS*

A solution of 500 ppm (w/v) of $[Me_4N]_2[Cd_4(SPh)_{10}]$ (0.29656 mmol L^{-1}) required a stock solution of 100n HS*. The stock solution consisted of 0.4152 g or 0.55 mL S* in 100 mL MeCN (29.656 mmol L^{-1}).

5.6.2.2 Stock solutions of $[Me_4N]_4[S_4Cd_{10}(SPh)_{16}]$ and HS*

A solution of 500 ppm (w/v) of $[Me_4N]_4[S_4Cd_{10}(SPh)_{16}]$ (0.15207 mmol L^{-1}) required a stock solution of 160n HS*. The stock solution consisted of 0.3406 g or 0.45 mL S* in 100 mL MeCN (24.3312 mmol L^{-1}).

5.6.2.3 Stock solutions of $[Me_4N]_2[S_4Cd_{17}(SPh)_{28}]$ and HS*

A solution of 500 ppm (w/v) of $[Me_4N]_2[S_4Cd_{17}(SPh)_{28}]$ (0.09557 mmol L^{-1}) required a stock solution of 280n HS*. The stock solution consisted of 0.3746 g or 0.49 mL S* in 100 mL MeCN (26.7584 mmol L^{-1}).

5.6.2.4 Synthesis of PhSSPh

HSPh (0.5 mL, 5 mmol) was dissolved in MeOH (5 mL) and a 27% solution of H_2O_2 (1 mL, 10 mmol) was added. The solution was stirred for one hour whereupon white crystals formed. They were collected by filtration, washed with MeOH (2x10 mL) and dried under vacuum. Yield: 0.54 g (99%). This compound is also commercially available[55].

m.p. 58 - 59°C. [Lit. 58 - 60°C [55]].

Elemental analysis: C, 65.62; H, 4.60%. $C_{12}H_{10}S_2$ requires C, 66.06; H, 4.59%.

^1H NMR ($CDCl_3$): δ 7.56 - 7.23 (10H, m, Ph).

$^{13}C-\{^1H\}$ NMR ($CDCl_3$): δ 137.1 (s, C1), δ 129.2 (s, C2), δ 127.6 (s, C3), δ 127.2 (s, C4).

---

[55] Aldrich Catalogue. Handbook of Fine Chemicals, 1996-97.

5.6.2.5 Synthesis of $(MeOC_6H_4S)_2$

$(MeOC_6H_4S)_2$ was prepared in the same manner as PhSSPh with the modification that the solution was left to stand overnight whereupon the product precipitated. Thus, HS* (0.12 mL, 1 mmol) and 27% H_2O_2 (0.2 mL, 2 mmol) in MeOH (5 mL) gave $(MeOC_6H_4S)_2$ as yellow crystals. Yield: 0.08 g (58%).

m.p. 32 - 35°C.

Elemental analysis: C, 60.53; H, 5.14%. $C_{14}H_{14}O_2S_2$ requires C, 60.43; H, 5.04%.

^{1}H NMR ($CDCl_3$): δ 7.42 (4H, d, H3), δ 6.85 (4H, d, H2), δ 3.82 (6H, d, OC$\underline{H}_3$).

^{13} C-{^{1}H} NMR ($CDCl_3$): δ 160.0 (s, C4), δ 132.7 (s, C2), δ 128.5 (s, C1), δ 114.7 (s, C3).

5.6.3 Synthesis and reactivity of complexes of the type $[Pt_2(\mu\text{-}S)_2L_4]$, $\{Pt_2S_2\}$

Sodium sulfide, $Na_2S{\bullet}9H_2O$, (Carlo Erba) was used as supplied. The reactions of $[Mo(CO)_4(MeCN)_2]$ and $\{Pt_2S_2\}$ as well as $[Mo(CO)_6]$ with Me_3NO and $\{Pt_2S_2\}$ were carried out as described in the literature[46]. The preparations of the precursors *cis*-$[PtCl_2L_2]$ (L = PPh_3, P*, P**, P***) are described in Chapter two. *cis*-$[PtCl_2As^{***}_2]$ [As*** = $As(C_6H_4OMe)_3$] and *cis*-$[PtCl_2P^{\bullet}_2]$ [P$^{\bullet}$ = $P(C_6H_5)_2(C_6H_4NMe_2)$] were prepared in the same manner and are described in the next sections. All complexes of the type $[Pt_2(\mu\text{-}S)_2L_4]$ were prepared as described for L = PPh_3 in section 5.6.3.3.

5.6.3.1 Synthesis of the precursor *cis*-$[PtCl_2As(C_6H_4OCH_3)_2]$, *cis*-$[PtCl_2As^{***}_2]$

$[(COD)PtCl_2]$ (0.3 g, 0.8 mmol) and As*** (0.65 g, 1.62 mmol) in CH_2Cl_2 (20 mL) gave *cis*-$[PtCl_2As^{***}_2]$ as a white powder. Yield: 0.7 g (83%).

^{1}H NMR ($CDCl_3$): δ 7.33 (12H, d, $^3J_{H3',H2'}$ = 8.5 Hz, H2'), δ 6.69 (12H, d, $^3J_{H2',H3'}$ = 8.5 Hz, H3'), δ 3.78 (18H, s, OC$\underline{H}_3$).

^{13} C-{^{1}H} NMR ($CDCl_3$): δ 161.1 (s, C4'), δ 135.1 (s, C2'), δ 122.6 (s, C1'), δ 113.9 (s,

C3'), δ 55.3 (s, O<u>C</u>H$_3$).

ESMS (MeCN/H_2O, +ve ion, 20 V): $[M - Cl]^+$ *m/z* 1022 (8%), $[M - Cl + MeCN]^+$ *m/z* 1063.5 (100%).

5.6.3.2 Synthesis of the precursor *cis*-[$PtCl_2\{P(C_6H_5)_2(C_6H_4NMe_2)\}_2$], *cis*-[$PtCl_2P^\bullet_2$]

[(COD)$PtCl_2$] (0.15 g, 0.4 mmol) and P$^\bullet$ (0.122 g, 0.8 mmol) in CH_2Cl_2 (20 mL) gave *cis*-[$PtCl_2P^\bullet_2$] as a white powder. Yield: 0.25 g (71%).

^{31}P NMR ($CDCl_3$): δ 13.1 (s, $^1J_{Pt,P}$ = 3696 Hz).

^{1}H NMR ($CDCl_3$): δ 7.48 - 7.08 (36H, m, H1-4, H2'), δ 6.45 (4H, d, $^3J_{H2',H3'}$ = 8.3 Hz, H3'), δ 2.97 (12H, s, N(C<u>H</u>$_3$)$_2$).

ESMS (MeCN/H_2O, +ve ion, 20 V): $[M - Cl]^+$ *m/z* 841 (100%), $[M - Cl + MeCN]^+$ *m/z* 882 (12%).

5.6.3.3 Synthesis of [$Pt_2(\mu\text{-}S)_2(PPh_3)_4$], {$Pt_2S_2$}

cis-[$PtCl_2(PPh_3)_2$] (0.5 g, 0.63 mmol) was suspended in benzene (20 mL). $Na_2S{\bullet}9H_2O$ (0.75 g, 3.1 mmol) was added, and the reaction mixture was stirred overnight at room temperature. The orange precipitate was filtered and washed with cold benzene. Yield: 0.937 g (99%).

^{31}P NMR (DMSO): δ 27.9 (s).

ESMS (MeOH, +ve ion, 20 V): $[M + H]^+$ *m/z* 1504 (100%).

5.6.3.4 Synthesis of [$Pt_2(\mu\text{-}S)_2P^*_4$], {$Pt_2S_2$}*

cis-[$PtCl_2P^*_2$] (0.45 g, 0.53 mmol) and $Na_2S{\bullet}9H_2O$ (0.62 g, 2.6 mmol) gave {Pt_2S_2}* as an orange powder. Yield: 0.42 g (52%).

m.p. 211 - 212°C.

Elemental analysis: C, 55.96; H, 4.28%. $C_{76}H_{68}O_4P_4Pt_2S_2$ requires C, 56.23; H, 4.19%.

^{31}P NMR (DMSO): δ 26.2 (s, $^{1}J_{Pt,P}$ = 2794 Hz).

ESMS (MeOH, +ve ion, 20 V): $[M + H]^+$ *m/z* 1624 (100%).

5.6.3.5 Synthesis of $[Pt_2(\mu\text{-}S)_2P^{**}_4]$, $\{Pt_2S_2\}^{**}$

cis-$[PtCl_2P^{**}_2]$ (0.675 g, 0.74 mmol) and $Na_2S{\bullet}9H_2O$ (0.87 g, 3.6 mmol) gave $\{Pt_2S_2\}^{**}$ as an orange powder. Yield: 0.61 g (47%).

m.p. 170 - 171°C.

Elemental analysis: C, 53.61; H, 4.47%. $C_{80}H_{76}O_8P_4Pt_2S_2$ requires C, 55.11; H, 4.36%.

^{31}P NMR (DMSO): δ 25.2 (s, $^{1}J_{Pt,P}$ = 2892 Hz).

ESMS (MeOH, +ve ion, 20 V): $[M + H]^+$ *m/z* 1744 (100%).

5.6.3.6 Synthesis of $[Pt_2(\mu\text{-}S)_2P^{***}_4]$, $\{Pt_2S_2\}^{***}$

cis-$[PtCl_2P^{***}_2]$ (0.25 g, 0.26 mmol) and $Na_2S{\bullet}9H_2O$ (0.3 g, 1.25 mmol) gave $\{Pt_2S_2\}^{***}$ as an orange powder. Yield: 0.168 g (35%).

m.p. 194 - 196°C.

Elemental analysis: C, 50.77; H, 4.35%. $C_{84}H_{84}O_{12}P_4Pt_2S_2$ requires C, 54.14; H, 4.51%.

^{31}P NMR (DMSO): δ 24.0 (s, $^{1}J_{Pt,P}$ = 2817 Hz).

^{1}H NMR (DMSO): δ 7.34 (24H, m, H2'), δ 6.60 (24H, d, $^{3}J_{H2',H3'}$ = 8.5 Hz, H3'), δ 3.39 (36H, s, $OC\underline{H}_3$).

ESMS (MeOH, +ve ion, 20 V): $[M + H]^+$ *m/z* 1864 (100%).

5.6.3.7 Synthesis of $[Pt_2(\mu\text{-}S)_2P^{\bullet}_4]$, $\{Pt_2S_2\}^{\bullet}$

cis-$[PtCl_2P^{\bullet}_2]$ (0.35 g, 0.4 mmol) and $Na_2S{\bullet}9H_2O$ (0.47 g, 1.96 mmol) gave $\{Pt_2S_2\}^{\bullet}$ as an orange powder. Yield: 0.246 g (37%).

m.p. 215 - 216°C.

^{31}P NMR (DMSO): δ 30.1 (s, $^{1}J_{Pt,P}$ = 2794 Hz).

^{1}H NMR (DMSO): δ 7.34 (24H, m, H2'), δ 6.60 (24H, d, $^{3}J_{H2',H3'}$ = 8.5 Hz, H3'), δ 3.39 (36H, s, OC$\underline{H}_3$).

ESMS (MeOH, +ve ion, 20 V): $[M + H]^+$ *m/z* 1677 (100%).

5.6.3.8 Synthesis of $[Pt_2(\mu\text{-}S)_2As^{***}{}_4]$, $\{Pt_2S_2\}^{As^{***}}$

cis-$[PtCl_2As^{***}{}_2]$ (0.25 g, 0.24 mmol) and $Na_2S{\bullet}9H_2O$ (0.275 g, 1.15 mmol) gave $\{Pt_2S_2\}^{As^{***}}$ as an orange powder. Yield: 0.127 g (26%).

ESMS (MeOH, +ve ion, 20 V): $[M + H]^+$ *m/z* 2041 (100%).

5.6.3.9 Reaction of $[Mo(CO)_4(pip)_2]$ and $\{Pt_2S_2\}$*

$[Mo(CO)_4(pip)_2]$ (0.0235 g, 0.06 mmol) and $\{Pt_2S_2\}$* (0.1 g, 0.06 mmol) were refluxed in toluene (15 mL) for 30 minutes. The solvent was reduced to *ca.* 5 mL, cooled to -20°C overnight, whereupon an orange powder precipitated. The product was collected by filtration, washed with MeOH and dried under vacuum. Yield: 0.08 g.

ESMS (MeOH, +ve ion, 20 V): unidentified *m/z* 1784 (100%).

Appendix A

Crystallographic Data for $[Fe_3(CO)_{10}(CNPh)_2]$ at 100 K

Table A.1 Atomic coordinates ($x10^4$) and equivalent isotropic displacement parameters ($Å^2 \times 10^3$) for $[Fe_3(CO)_{10}(CNPh)_2]$ at 100 K. U(eq) is defined as one third of the trace of the orthogonalized U_{ij} tensor.

	x	y	z	U(eq)
Fe(4)	1759(11)	10032(12)	419(14)	43(7)
Fe(5)	3070(12)	10898(13)	-400(15)	41(8)
Fe(6)	3062(15)	9125(15)	-377(17)	59(9)
Fe(3)	2005(1)	9186(1)	599(1)	25(1)
Fe(2)	1936(1)	11015(1)	369(1)	24(1)
Fe(1)	3270(1)	10061(1)	-367(1)	23(1)
C(1)	2566(3)	9984(4)	-1823(5)	25(1)
C(2)	3955(4)	10134(4)	1084(5)	25(1)
C(11)	1693(3)	9930(4)	-3870(5)	26(1)
C(12)	1503(4)	10782(4)	-4448(5)	32(1)
C(13)	1020(4)	10768(5)	-5535(5)	39(2)
C(14)	738(4)	9912(5)	-6049(5)	39(2)
C(15)	937(4)	9064(5)	-5472(5)	38(2)
C(16)	1418(4)	9067(4)	-4369(5)	35(2)
C(21)	5060(3)	10270(4)	2978(4)	25(1)
C(22)	5429(4)	9459(5)	3538(5)	34(1)
C(23)	6068(4)	9567(5)	4521(5)	40(2)
C(24)	6317(4)	10487(5)	4914(5)	45(2)
C(25)	5935(4)	11280(5)	4353(5)	43(2)
C(26)	5301(4)	11186(5)	3377(4)	34(1)
C(30)	3892(4)	9035(4)	-705(5)	28(1)
C(31)	3872(4)	11051(4)	-862(4)	29(1)
C(32)	2808(4)	11801(4)	1062(5)	27(1)
C(33)	1018(4)	11566(4)	896(4)	25(1)
C(34)	1820(4)	11650(4)	-992(5)	31(1)
C(35)	2255(3)	10208(4)	1764(5)	25(1)
C(36)	1181(4)	10017(4)	-479(5)	27(1)
C(37)	2882(4)	8547(4)	1528(5)	32(1)
C(38)	1983(4)	8385(4)	-615(5)	34(2)
C(39)	1096(4)	8652(4)	1176(5)	29(1)
N(1)	2194(3)	9940(3)	-2747(4)	27(1)
N(2)	4439(3)	10173(3)	1948(4)	27(1)
O(30)	4272(3)	8374(3)	-915(3)	37(1)
O(31)	4246(3)	11684(3)	-1157(3)	41(1)
O(32)	3327(3)	12315(3)	1506(4)	45(1)
O(33)	452(3)	11934(3)	1213(4)	41(1)
O(34)	1729(3)	12087(3)	-1811(3)	44(1)
O(35)	2463(3)	10319(3)	2745(3)	37(1)
O(36)	572(3)	9928(3)	-1205(3)	35(1)
O(37)	3398(3)	8125(3)	2136(4)	45(1)
O(38)	1943(3)	7862(3)	-1362(4)	46(1)
O(39)	562(3)	8259(3)	1534(3)	39(1)

Table A.2 Bond lengths (Å) and angles (°) for $[Fe_3(CO)_{10}(CNPh)_2]$ at 100 K.

Fe(4)-Fe(3)	1.242(16)	Fe(4)-C(36)	1.259(18)
Fe(4)-Fe(2)	1.397(16)	Fe(4)-C(35)	1.659(17)
Fe(4)-C(39)	2.411(17)	Fe(4)-Fe(1)	2.624(16)
Fe(4)-Fe(5)	2.65(2)	Fe(4)-Fe(6)	2.66(3)
Fe(5)-Fe(1)	1.203(18)	Fe(5)-C(31)	1.437(19)
Fe(5)-Fe(2)	2.091(18)	Fe(5)-C(1)	2.145(18)
Fe(5)-C(34)	2.181(19)	Fe(5)-C(32)	2.228(18)
Fe(5)-C(2)	2.285(19)	Fe(5)-O(31)	2.397(18)
Fe(5)-Fe(6)	2.47(3)	Fe(6)-Fe(1)	1.34(2)
Fe(6)-C(30)	1.39(2)	Fe(6)-C(38)	1.92(2)
Fe(6)-C(1)	2.12(2)	Fe(6)-Fe(3)	2.14(2)
Fe(6)-O(30)	2.30(2)	Fe(6)-C(2)	2.45(2)
Fe(6)-C(37)	2.45(2)	Fe(3)-C(39)	1.804(6)
Fe(3)-C(37)	1.811(6)	Fe(3)-C(38)	1.813(7)
Fe(3)-C(35)	1.972(6)	Fe(3)-C(36)	1.998(5)
Fe(3)-Fe(2)	2.5594(11)	Fe(3)-Fe(1)	2.6918(11)
Fe(2)-C(33)	1.797(6)	Fe(2)-C(32)	1.807(6)
Fe(2)-C(34)	1.818(6)	Fe(2)-C(36)	1.965(6)
Fe(2)-C(35)	1.987(5)	Fe(2)-Fe(1)	2.6921(11)
Fe(1)-C(30)	1.795(7)	Fe(1)-C(31)	1.807(6)
Fe(1)-C(2)	1.853(6)	Fe(1)-C(1)	1.871(6)
C(1)-N(1)	1.143(6)	C(2)-N(2)	1.155(7)
C(11)-C(16)	1.370(7)	C(11)-C(12)	1.375(7)
C(11)-N(1)	1.415(7)	C(12)-C(13)	1.369(8)
C(13)-C(14)	1.373(8)	C(14)-C(15)	1.371(8)
C(15)-C(16)	1.383(8)	C(21)-C(22)	1.379(8)
C(21)-C(26)	1.386(8)	C(21)-N(2)	1.416(7)
C(22)-C(23)	1.391(8)	C(23)-C(24)	1.392(9)
C(24)-C(25)	1.366(9)	C(25)-C(26)	1.380(8)
C(30)-O(30)	1.137(7)	C(31)-O(31)	1.135(6)
C(32)-O(32)	1.127(6)	C(33)-O(33)	1.121(6)
C(34)-O(34)	1.132(6)	C(35)-O(35)	1.160(6)
C(36)-O(36)	1.158(6)	C(37)-O(37)	1.135(7)
C(38)-O(38)	1.139(7)	C(39)-O(39)	1.121(6)

Fe(3)-Fe(4)-Fe(2)	151.7(14)	Fe(3)-Fe(4)-C(36)	106.0(12)
Fe(3)-Fe(4)-C(35)	84.3(10)	C(36)-Fe(4)-Fe(2)	95.3(11)
Fe(2)-Fe(4)-C(35)	80.6(8)	C(36)-Fe(4)-C(35)	161.8(13)
C(36)-Fe(4)-C(39)	91.3(9)	Fe(3)-Fe(4)-C(39)	46.8(6)
C(35)-Fe(4)-C(39)	85.0(7)	Fe(2)-Fe(4)-C(39)	153.0(10)
C(36)-Fe(4)-Fe(1)	103.3(9)	Fe(3)-Fe(4)-Fe(1)	79.5(8)
C(35)-Fe(4)-Fe(1)	93.1(7)	Fe(2)-Fe(4)-Fe(1)	77.5(7)
Fe(3)-Fe(4)-Fe(5)	105.6(10)	C(39)-Fe(4)-Fe(1)	126.3(7)
Fe(2)-Fe(4)-Fe(5)	51.5(7)	C(36)-Fe(4)-Fe(5)	99.3(10)
C(39)-Fe(4)-Fe(5)	152.4(9)	C(35)-Fe(4)-Fe(5)	92.0(8)
Fe(3)-Fe(4)-Fe(6)	52.3(8)	Fe(1)-Fe(4)-Fe(5)	26.4(4)
Fe(2)-Fe(4)-Fe(6)	106.8(10)	C(36)-Fe(4)-Fe(6)	98.7(10)
C(39)-Fe(4)-Fe(6)	98.0(8)	C(35)-Fe(4)-Fe(6)	99.5(9)
Fe(5)-Fe(4)-Fe(6)	55.4(7)	Fe(1)-Fe(4)-Fe(6)	29.4(5)
Fe(1)-Fe(5)-Fe(2)	106.5(11)	Fe(1)-Fe(5)-C(31)	85.9(11)
Fe(1)-Fe(5)-C(1)	60.4(7)	C(31)-Fe(5)-Fe(2)	166.7(12)
Fe(2)-Fe(5)-C(1)	100.1(8)	C(31)-Fe(5)-C(1)	90.2(9)
C(31)-Fe(5)-C(34)	124.0(11)	Fe(1)-Fe(5)-C(34)	132.6(12)
C(1)-Fe(5)-C(34)	81.7(6)	Fe(2)-Fe(5)-C(34)	50.3(5)
C(31)-Fe(5)-C(32)	119.2(10)	Fe(1)-Fe(5)-C(32)	126.8(12)
C(1)-Fe(5)-C(32)	148.9(10)	Fe(2)-Fe(5)-C(32)	49.3(4)
Fe(1)-Fe(5)-C(2)	54.0(7)	C(34)-Fe(5)-C(32)	73.6(6)
Fe(2)-Fe(5)-C(2)	97.2(7)	C(31)-Fe(5)-C(2)	86.1(9)
C(34)-Fe(5)-C(2)	146.9(9)	C(1)-Fe(5)-C(2)	114.4(8)

Fe(1)-Fe(5)-O(31)	104.7(11)	C(32)-Fe(5)-C(2)	80.0(6)
Fe(2)-Fe(5)-O(31)	148.4(9)	C(31)-Fe(5)-O(31)	18.8(4)
C(34)-Fe(5)-O(31)	109.2(7)	C(1)-Fe(5)-O(31)	99.7(7)
C(2)-Fe(5)-O(31)	96.8(7)	C(32)-Fe(5)-O(31)	106.1(7)
C(31)-Fe(5)-Fe(6)	99.1(11)	Fe(1)-Fe(5)-Fe(6)	14.8(7)
C(1)-Fe(5)-Fe(6)	54.1(6)	Fe(2)-Fe(5)-Fe(6)	93.8(8)
C(32)-Fe(5)-Fe(6)	123.6(9)	C(34)-Fe(5)-Fe(6)	118.5(9)
O(31)-Fe(5)-Fe(6)	117.7(9)	C(2)-Fe(5)-Fe(6)	61.9(7)
C(31)-Fe(5)-Fe(4)	161.4(12)	Fe(1)-Fe(5)-Fe(4)	75.5(9)
C(1)-Fe(5)-Fe(4)	80.0(7)	Fe(2)-Fe(5)-Fe(4)	31.5(4)
C(32)-Fe(5)-Fe(4)	74.2(7)	C(34)-Fe(5)-Fe(4)	70.4(7)
O(31)-Fe(5)-Fe(4)	179.5(9)	C(2)-Fe(5)-Fe(4)	83.7(7)
Fe(1)-Fe(6)-C(30)	82.2(12)	Fe(6)-Fe(5)-Fe(4)	62.3(8)
C(30)-Fe(6)-C(38)	135.1(14)	Fe(1)-Fe(6)-C(38)	135.9(14)
C(30)-Fe(6)-C(1)	92.4(11)	Fe(1)-Fe(6)-C(1)	60.6(8)
Fe(1)-Fe(6)-Fe(3)	98.9(11)	C(38)-Fe(6)-C(1)	90.3(9)
C(38)-Fe(6)-Fe(3)	52.8(6)	C(30)-Fe(6)-Fe(3)	163.6(14)
Fe(1)-Fe(6)-O(30)	104.2(12)	C(1)-Fe(6)-Fe(3)	102.5(9)
C(38)-Fe(6)-O(30)	115.0(10)	C(30)-Fe(6)-O(30)	21.9(5)
Fe(3)-Fe(6)-O(30)	151.7(10)	C(1)-Fe(6)-O(30)	103.0(9)
C(30)-Fe(6)-C(2)	80.0(10)	Fe(1)-Fe(6)-C(2)	48.3(7)
C(1)-Fe(6)-C(2)	109.0(9)	C(38)-Fe(6)-C(2)	140.3(11)
O(30)-Fe(6)-C(2)	94.7(8)	Fe(3)-Fe(6)-C(2)	88.6(7)
C(30)-Fe(6)-C(37)	118.5(12)	Fe(1)-Fe(6)-C(37)	112.0(12)
C(1)-Fe(6)-C(37)	147.9(11)	C(38)-Fe(6)-C(37)	74.4(7)
O(30)-Fe(6)-C(37)	109.0(8)	Fe(3)-Fe(6)-C(37)	45.9(4)
Fe(1)-Fe(6)-Fe(5)	13.2(6)	C(2)-Fe(6)-C(37)	71.1(6)
C(38)-Fe(6)-Fe(5)	122.7(11)	C(30)-Fe(6)-Fe(5)	94.6(11)
Fe(3)-Fe(6)-Fe(5)	88.4(8)	C(1)-Fe(6)-Fe(5)	55.1(6)
C(2)-Fe(6)-Fe(5)	55.4(6)	O(30)-Fe(6)-Fe(5)	116.4(10)
Fe(1)-Fe(6)-Fe(4)	74.0(10)	C(37)-Fe(6)-Fe(5)	109.9(9)
C(38)-Fe(6)-Fe(4)	68.5(8)	C(30)-Fe(6)-Fe(4)	155.8(14)
Fe(3)-Fe(6)-Fe(4)	27.4(4)	C(1)-Fe(6)-Fe(4)	80.4(8)
C(2)-Fe(6)-Fe(4)	80.6(7)	O(30)-Fe(6)-Fe(4)	174.9(10)
Fe(5)-Fe(6)-Fe(4)	62.2(7)	C(37)-Fe(6)-Fe(4)	67.8(7)
Fe(4)-Fe(3)-C(37)	137.6(8)	Fe(4)-Fe(3)-C(39)	103.1(8)
Fe(4)-Fe(3)-C(38)	118.8(8)	C(39)-Fe(3)-C(37)	95.9(3)
C(37)-Fe(3)-C(38)	95.2(3)	C(39)-Fe(3)-C(38)	97.7(3)
C(39)-Fe(3)-C(35)	95.8(2)	Fe(4)-Fe(3)-C(35)	56.8(8)
C(38)-Fe(3)-C(35)	166.4(2)	C(37)-Fe(3)-C(35)	84.0(2)
C(39)-Fe(3)-C(36)	92.3(2)	Fe(4)-Fe(3)-C(36)	37.3(8)
C(38)-Fe(3)-C(36)	85.7(2)	C(37)-Fe(3)-C(36)	171.5(2)
Fe(4)-Fe(3)-Fe(6)	100.2(9)	C(35)-Fe(3)-C(36)	93.1(2)
C(37)-Fe(3)-Fe(6)	76.3(6)	C(39)-Fe(3)-Fe(6)	152.3(6)
C(35)-Fe(3)-Fe(6)	109.4(6)	C(38)-Fe(3)-Fe(6)	57.4(6)
Fe(4)-Fe(3)-Fe(2)	15.0(8)	C(36)-Fe(3)-Fe(6)	97.3(6)
C(37)-Fe(3)-Fe(2)	124.42(18)	C(39)-Fe(3)-Fe(2)	115.41(18)
C(35)-Fe(3)-Fe(2)	49.98(16)	C(38)-Fe(3)-Fe(2)	122.10(18)
Fe(6)-Fe(3)-Fe(2)	90.2(5)	C(36)-Fe(3)-Fe(2)	49.21(16)
C(39)-Fe(3)-Fe(1)	175.69(18)	Fe(4)-Fe(3)-Fe(1)	73.5(8)
C(38)-Fe(3)-Fe(1)	81.93(18)	C(37)-Fe(3)-Fe(1)	88.43(18)
C(36)-Fe(3)-Fe(1)	83.37(16)	C(35)-Fe(3)-Fe(1)	84.48(15)
Fe(2)-Fe(3)-Fe(1)	61.62(3)	Fe(6)-Fe(3)-Fe(1)	29.4(5)
Fe(4)-Fe(2)-C(32)	134.8(7)	Fe(4)-Fe(2)-C(33)	103.7(7)
Fe(4)-Fe(2)-C(34)	121.6(7)	C(33)-Fe(2)-C(32)	98.0(2)
C(32)-Fe(2)-C(34)	93.5(2)	C(33)-Fe(2)-C(34)	97.8(2)
C(33)-Fe(2)-C(36)	93.3(2)	Fe(4)-Fe(2)-C(36)	39.7(7)
C(34)-Fe(2)-C(36)	86.1(2)	C(32)-Fe(2)-C(36)	168.7(2)
C(33)-Fe(2)-C(35)	92.7(2)	Fe(4)-Fe(2)-C(35)	55.5(7)
C(34)-Fe(2)-C(35)	169.5(2)	C(32)-Fe(2)-C(35)	84.7(2)
Fe(4)-Fe(2)-Fe(5)	97.0(8)	C(36)-Fe(2)-C(35)	93.6(2)

C(32)-Fe(2)-Fe(5)	69.3(5)	C(33)-Fe(2)-Fe(5)	158.9(5)
C(36)-Fe(2)-Fe(5)	100.3(5)	C(34)-Fe(2)-Fe(5)	67.4(5)
Fe(4)-Fe(2)-Fe(3)	13.3(7)	C(35)-Fe(2)-Fe(5)	02.4(5)
C(32)-Fe(2)-Fe(3)	122.67(17)	C(33)-Fe(2)-Fe(3)	114.08(18)
C(36)-Fe(2)-Fe(3)	50.34(16)	C(34)-Fe(2)-Fe(3)	125.01(18)
Fe(5)-Fe(2)-Fe(3)	87.0(5)	C(35)-Fe(2)-Fe(3)	49.46(16)
C(33)-Fe(2)-Fe(1)	175.68(18)	Fe(4)-Fe(2)-Fe(1)	72.1(7)
C(34)-Fe(2)-Fe(1)	85.33(18)	C(32)-Fe(2)-Fe(1)	84.73(18)
C(35)-Fe(2)-Fe(1)	84.18(15)	C(36)-Fe(2)-Fe(1)	83.96(16)
Fe(3)-Fe(2)-Fe(1)	61.61(3)	Fe(5)-Fe(2)-Fe(1)	25.4(5)
Fe(5)-Fe(1)-C(30)	154.5(9)	Fe(5)-Fe(1)-Fe(6)	152.0(13)
Fe(5)-Fe(1)-C(31)	52.5(9)	Fe(6)-Fe(1)-C(30)	50.1(9)
C(30)-Fe(1)-C(31)	102.5(3)	Fe(6)-Fe(1)-C(31)	150.5(9)
Fe(6)-Fe(1)-C(2)	99.0(9)	Fe(5)-Fe(1)-C(2)	94.4(9)
C(31)-Fe(1)-C(2)	91.2(2)	C(30)-Fe(1)-C(2)	90.8(2)
Fe(6)-Fe(1)-C(1)	0.8(9)	Fe(5)-Fe(1)-C(1)	85.6(9)
C(31)-Fe(1)-C(1)	89.3(2)	C(30)-Fe(1)-C(1)	89.5(2)
Fe(5)-Fe(1)-Fe(4)	78.1(9)	C(2)-Fe(1)-C(1)	179.3(2)
C(30)-Fe(1)-Fe(4)	126.5(4)	Fe(6)-Fe(1)-Fe(4)	76.6(10)
C(2)-Fe(1)-Fe(4)	93.5(4)	C(31)-Fe(1)-Fe(4)	130.6(4)
Fe(5)-Fe(1)-Fe(3)	104.9(9)	C(1)-Fe(1)-Fe(4)	85.8(4)
C(30)-Fe(1)-Fe(3)	100.27(18)	Fe(6)-Fe(1)-Fe(3)	51.6(9)
C(2)-Fe(1)-Fe(3)	87.84(16)	C(31)-Fe(1)-Fe(3)	157.20(19)
Fe(4)-Fe(1)-Fe(3)	27.0(4)	C(1)-Fe(1)-Fe(3)	91.48(16)
Fe(6)-Fe(1)-Fe(2)	107.0(9)	Fe(5)-Fe(1)-Fe(2)	48.1(9)
C(31)-Fe(1)-Fe(2)	100.48(19)	C(30)-Fe(1)-Fe(2)	156.91(18)
C(1)-Fe(1)-Fe(2)	88.84(16)	C(2)-Fe(1)-Fe(2)	90.59(17)
Fe(3)-Fe(1)-Fe(2)	56.77(3)	Fe(4)-Fe(1)-Fe(2)	30.4(4)
N(1)-C(1)-Fe(6)	142.3(7)	N(1)-C(1)-Fe(1)	174.8(5)
N(1)-C(1)-Fe(5)	146.6(7)	Fe(1)-C(1)-Fe(6)	38.6(6)
Fe(6)-C(1)-Fe(5)	70.7(8)	Fe(1)-C(1)-Fe(5)	34.0(5)
N(2)-C(2)-Fe(5)	149.5(6)	N(2)-C(2)-Fe(1)	174.7(5)
N(2)-C(2)-Fe(6)	147.6(6)	Fe(1)-C(2)-Fe(5)	31.7(5)
Fe(5)-C(2)-Fe(6)	62.7(7)	Fe(1)-C(2)-Fe(6)	32.7(5)
C(16)-C(11)-N(1)	119.3(5)	C(16)-C(11)-C(12)	121.2(5)
C(13)-C(12)-C(11)	119.2(5)	C(12)-C(11)-N(1)	119.5(5)
C(15)-C(14)-C(13)	120.0(5)	C(12)-C(13)-C(14)	120.4(6)
C(11)-C(16)-C(15)	118.9(6)	C(14)-C(15)-C(16)	120.2(6)
C(22)-C(21)-N(2)	119.5(5)	C(22)-C(21)-C(26)	121.7(5)
C(21)-C(22)-C(23)	118.9(6)	C(26)-C(21)-N(2)	118.7(5)
C(25)-C(24)-C(23)	120.7(6)	C(22)-C(23)-C(24)	119.3(6)
C(25)-C(26)-C(21)	118.6(6)	C(24)-C(25)-C(26)	120.7(6)
O(30)-C(30)-Fe(1)	178.6(5)	O(30)-C(30)-Fe(6)	130.9(10)
O(31)-C(31)-Fe(5)	137.2(9)	Fe(6)-C(30)-Fe(1)	47.7(9)
Fe(5)-C(31)-Fe(1)	41.6(7)	O(31)-C(31)-Fe(1)	178.6(5)
O(32)-C(32)-Fe(5)	121.0(7)	O(32)-C(32)-Fe(2)	177.3(5)
O(33)-C(33)-Fe(2)	178.1(5)	Fe(2)-C(32)-Fe(5)	61.4(5)
O(34)-C(34)-Fe(5)	120.3(6)	O(34)-C(34)-Fe(2)	176.3(5)
O(35)-C(35)-Fe(4)	168.8(7)	Fe(2)-C(34)-Fe(5)	62.3(5)
Fe(4)-C(35)-Fe(3)	38.8(6)	O(35)-C(35)-Fe(3)	141.5(5)
Fe(4)-C(35)-Fe(2)	43.9(6)	O(35)-C(35)-Fe(2)	137.9(5)
O(36)-C(36)-Fe(4)	169.7(9)	Fe(3)-C(35)-Fe(2)	80.6(2)
Fe(4)-C(36)-Fe(2)	45.1(8)	O(36)-C(36)-Fe(2)	141.1(5)
Fe(4)-C(36)-Fe(3)	36.7(8)	O(36)-C(36)-Fe(3)	138.4(5)
O(37)-C(37)-Fe(3)	176.4(5)	Fe(2)-C(36)-Fe(3)	80.5(2)
Fe(3)-C(37)-Fe(6)	57.8(5)	O(37)-C(37)-Fe(6)	125.4(7)
O(38)-C(38)-Fe(6)	112.9(8)	O(38)-C(38)-Fe(3)	177.2(5)
O(39)-C(39)-Fe(3)	175.0(5)	Fe(3)-C(38)-Fe(6)	69.8(7)
Fe(3)-C(39)-Fe(4)	30.1(4)	O(39)-C(39)-Fe(4)	154.8(6)
C(2)-N(2)-C(21)	176.3(6)	C(1)-N(1)-C(11)	176.1(6)
C(31)-O(31)-Fe(5)	24.0(5)	C(30)-O(30)-Fe(6)	27.2(6)

Table A.3 Anisotropic displacement parameters ($Å^2 \times 10^3$) for $[Fe_3(CO)_{10}(CNPh)_2]$ at 100 K. The anisotropic displacement factor exponent takes the form: $-2\pi^2(h^2a^{*2}U^{11} + ... + 2hka^*b^*U^{12})$.

	U^{11}	U^{22}	U^{33}	U^{23}	U^{13}	U^{12}
Fe(3)	19(1)	29(1)	26(1)	3(1)	2(1)	1(1)
Fe(2)	19(1)	28(1)	23(1)	0(1)	-2(1)	1(1)
Fe(1)	17(1)	31(1)	19(1)	2(1)	-2(1)	-1(1)
C(1)	15(3)	31(3)	28(3)	4(3)	5(2)	3(2)
C(2)	18(3)	34(3)	24(3)	5(3)	5(2)	1(2)
C(11)	17(3)	38(3)	22(3)	-3(3)	-1(2)	-3(2)
C(12)	32(3)	32(3)	27(3)	-4(3)	-3(3)	-6(3)
C(13)	36(4)	50(4)	29(3)	15(3)	4(3)	4(3)
C(14)	25(3)	71(5)	19(3)	-8(3)	2(2)	-1(3)
C(15)	17(3)	53(4)	38(3)	-17(3)	-7(3)	0(3)
C(16)	34(4)	33(4)	36(3)	-3(3)	1(3)	3(3)
C(21)	15(3)	42(4)	17(3)	-3(3)	-3(2)	3(2)
C(22)	29(3)	45(4)	31(3)	1(3)	7(3)	9(3)
C(23)	28(3)	67(5)	25(3)	14(3)	3(3)	15(3)
C(24)	25(3)	77(5)	31(4)	-1(4)	2(3)	-5(3)
C(25)	42(4)	58(4)	27(3)	-3(3)	-1(3)	-13(3)
C(26)	37(4)	46(4)	18(3)	-1(3)	0(3)	1(3)
C(30)	21(3)	39(4)	20(3)	5(3)	-4(2)	-6(3)
C(31)	24(3)	44(4)	16(3)	5(3)	-5(2)	1(3)
C(32)	25(3)	24(3)	29(3)	3(3)	-4(3)	5(3)
C(33)	18(3)	38(3)	16(3)	-1(3)	-7(2)	-4(3)
C(34)	28(3)	29(3)	33(3)	-3(3)	0(3)	-1(3)
C(35)	13(3)	38(3)	24(3)	3(3)	4(2)	4(2)
C(36)	21(3)	28(3)	29(3)	2(3)	2(3)	1(2)
C(37)	28(3)	25(3)	43(4)	6(3)	10(3)	2(3)
C(38)	31(4)	27(3)	43(4)	7(3)	5(3)	-7(3)
C(39)	29(3)	31(3)	26(3)	4(3)	4(3)	6(3)
N(1)	28(3)	36(3)	17(2)	0(2)	0(2)	-6(2)
N(2)	19(2)	35(3)	26(3)	4(2)	2(2)	1(2)
O(30)	33(2)	41(3)	36(2)	0(2)	0(2)	3(2)
O(31)	42(3)	42(3)	35(2)	8(2)	-2(2)	-10(2)
O(32)	34(3)	44(3)	52(3)	-6(2)	-10(2)	-4(2)
O(33)	28(3)	45(3)	51(3)	-6(2)	7(2)	-1(2)
O(34)	60(3)	46(3)	25(2)	13(2)	6(2)	17(2)
O(35)	33(2)	55(3)	21(2)	4(2)	0(2)	-1(2)
O(36)	25(2)	40(3)	34(2)	0(2)	-12(2)	-3(2)
O(37)	33(3)	43(3)	56(3)	21(2)	1(2)	12(2)
O(38)	56(3)	40(3)	46(3)	-13(2)	19(2)	-7(2)
O(39)	32(3)	44(3)	41(3)	9(2)	6(2)	0(2)

TableA.4 Hydrogen coordinates ($x10^4$) and isotropic displacement parameters ($Å^2 \times 10^3$) for $[Fe_3(CO)_{10}(CNPh)_2]$ at 100 K.

	x	y	z	U(eq)
H(12)	1702	11362	-4104	38
H(13)	881	11342	-5927	46
H(14)	413	9907	-6789	46
H(15)	748	8484	-5823	45
H(16)	1553	8494	-3972	42
H(22)	5254	8850	3263	41
H(23)	6327	9030	4911	48
H(24)	6749	10562	5565	54

H(25)	6103	11889	4633	51
H(26)	5040	11726	2994	41

Appendix B

Crystallographic Data for $[Fe_3(CO)_{10}(CNPh)_2]$ at 293 K

Table B.1 Atomic coordinates ($x10^4$) and equivalent isotropic displacement parameters ($Å^2 \times 10^3$) for $[Fe_3(CO)_{10}(CNPh)_2]$ at 293 K. U(eq) is defined as one third of the trace of the orthogonalized U_{ij} tensor.

	x	y	z	U(eq)
Fe(1)	6749(1)	71(1)	10365(1)	46(1)
Fe(2)	7984(1)	-815(1)	9432(1)	50(1)
Fe(3)	8055(1)	1004(1)	9626(1)	49(1)
N(1)	5570(2)	181(2)	8057(2)	54(1)
N(2)	7827(2)	-41(2)	12742(2)	57(1)
C(1)	6061(2)	140(2)	8915(3)	48(1)
C(2)	7454(2)	1(2)	11812(3)	50(1)
C(11)	4952(2)	266(3)	7042(3)	52(1)
C(12)	4567(3)	-525(3)	6509(3)	70(1)
C(13)	3939(3)	-407(4)	5520(3)	85(1)
C(14)	3726(3)	480(4)	5111(3)	91(1)
C(15)	4121(3)	1256(4)	5634(3)	96(2)
C(16)	4743(3)	1158(3)	6615(3)	72(1)
C(21)	8310(2)	-66(2)	13854(2)	48(1)
C(22)	8495(3)	759(3)	14437(3)	69(1)
C(23)	8976(3)	733(3)	15532(3)	84(1)
C(24)	9242(3)	-116(4)	16017(3)	80(1)
C(25)	9051(3)	-937(3)	15435(4)	84(1)
C(26)	8576(3)	-917(3)	14333(3)	70(1)
C(30)	6160(2)	1050(3)	10822(3)	57(1)
C(31)	6133(2)	-937(3)	10696(3)	53(1)
C(32)	8028(3)	-1602(3)	10635(3)	65(1)
C(33)	8855(3)	-1341(2)	8860(3)	57(1)
C(34)	7117(2)	-1456(2)	8517(3)	61(1)
C(35)	8810(2)	14(2)	10487(3)	53(1)
C(36)	7732(2)	191(2)	8244(3)	54(1)
C(37)	7206(3)	1785(3)	8921(3)	62(1)
C(38)	8187(3)	1644(2)	10953(3)	64(1)
C(39)	8951(3)	1540(2)	9104(3)	57(1)
O(30)	5794(2)	1675(2)	11111(2)	87(1)
O(31)	5756(2)	-1583(2)	10911(2)	76(1)
O(32)	8071(2)	-2122(2)	11371(3)	97(1)
O(33)	9394(2)	-1721(2)	8507(2)	76(1)
O(34)	6604(2)	-1878(2)	7926(3)	97(1)
O(35)	9419(2)	-62(2)	11205(2)	71(1)
O(36)	7526(2)	285(2)	7272(2)	75(1)
O(37)	6694(2)	2309(2)	8480(3)	95(1)
O(38)	8290(2)	2084(2)	11763(2)	99(1)
O(39)	9509(2)	1896(2)	8778(2)	83(1)

Table B.2 Bond lengths (Å) and angles (°) for $[Fe_3(CO)_{10}(CNPh)_2]$ at 293 K.

Fe(1)-C(30)	1.796(4)	C(11)-C(16)	1.371(5)
Fe(1)-C(31)	1.797(4)	C(12)-C(13)	1.396(5)
Fe(1)-C(1)	1.863(3)	C(13)-C(14)	1.359(6)
Fe(1)-C(2)	1.871(3)	C(14)-C(15)	1.348(6)

Fe(1)-Fe(2)	2.7008(7)	C(15)-C(16)	1.380(5)
Fe(1)-Fe(3)	2.7019(7)	C(21)-C(22)	1.357(4)
Fe(2)-C(33)	1.788(4)	C(21)-C(26)	1.358(4)
Fe(2)-C(32)	1.808(4)	C(22)-C(23)	1.383(5)
Fe(2)-C(34)	1.811(4)	C(23)-C(24)	1.358(5)
Fe(2)-C(36)	1.992(4)	C(24)-C(25)	1.353(5)
Fe(2)-C(35)	1.999(3)	C(25)-C(26)	1.387(5)
Fe(2)-Fe(3)	2.5685(6)	C(30)-O(30)	1.135(4)
Fe(3)-C(39)	1.797(4)	C(31)-O(31)	1.137(4)
Fe(3)-C(37)	1.802(4)	C(32)-O(32)	1.137(4)
Fe(3)-C(38)	1.805(4)	C(33)-O(33)	1.140(4)
Fe(3)-C(35)	1.981(3)	C(34)-O(34)	1.131(4)
Fe(3)-C(36)	1.997(3)	C(35)-O(35)	1.158(4)
N(1)-C(1)	1.161(4)	C(36)-O(36)	1.155(4)
N(1)-C(11)	1.406(4)	C(37)-O(37)	1.140(4)
N(2)-C(2)	1.157(4)	C(38)-O(38)	1.135(4)
N(2)-C(21)	1.400(4)	C(39)-O(39)	1.132(4)
C(11)-C(12)	1.364(5)		

C(30)-Fe(1)-C(31)	02.38(16)	C(39)-Fe(3)-Fe(2)	114.15(11)
C(30)-Fe(1)-C(1)	90.41(14)	C(37)-Fe(3)-Fe(2)	123.35(11)
C(31)-Fe(1)-C(1)	90.55(14)	C(38)-Fe(3)-Fe(2)	124.93(11)
C(30)-Fe(1)-C(2)	90.14(14)	C(35)-Fe(3)-Fe(2)	50.11(10)
C(31)-Fe(1)-C(2)	89.91(14)	C(36)-Fe(3)-Fe(2)	49.84(10)
C(1)-Fe(1)-C(2)	179.19(15)	C(39)-Fe(3)-Fe(1)	175.74(11)
C(30)-Fe(1)-Fe(2)	157.39(12)	C(37)-Fe(3)-Fe(1)	85.41(12)
C(31)-Fe(1)-Fe(2)	100.19(11)	C(38)-Fe(3)-Fe(1)	85.56(12)
C(1)-Fe(1)-Fe(2)	88.14(10)	C(35)-Fe(3)-Fe(1)	84.10(10)
C(2)-Fe(1)-Fe(2)	91.13(10)	C(36)-Fe(3)-Fe(1)	84.61(10)
C(30)-Fe(1)-Fe(3)	100.69(12)	Fe(2)-Fe(3)-Fe(1)	61.592(18)
C(31)-Fe(1)-Fe(3)	156.91(11)	C(1)-N(1)-C(11)	177.1(3)
C(1)-Fe(1)-Fe(3)	90.30(10)	C(2)-N(2)-C(21)	177.3(3)
C(2)-Fe(1)-Fe(3)	89.02(10)	N(1)-C(1)-Fe(1)	174.1(3)
Fe(2)-Fe(1)-Fe(3)	56.772(17)	N(2)-C(2)-Fe(1)	174.3(3)
C(33)-Fe(2)-C(32)	97.67(16)	C(12)-C(11)-C(16)	121.3(3)
C(33)-Fe(2)-C(34)	95.35(16)	C(12)-C(11)-N(1)	120.2(3)
C(32)-Fe(2)-C(34)	95.12(17)	C(16)-C(11)-N(1)	118.5(3)
C(33)-Fe(2)-C(36)	94.67(15)	C(11)-C(12)-C(13)	118.4(4)
C(32)-Fe(2)-C(36)	167.65(15)	C(14)-C(13)-C(12)	119.9(4)
C(34)-Fe(2)-C(36)	84.08(15)	C(15)-C(14)-C(13)	121.2(4)
C(33)-Fe(2)-C(35)	92.34(15)	C(14)-C(15)-C(16)	120.0(4)
C(32)-Fe(2)-C(35)	86.01(15)	C(11)-C(16)-C(15)	119.2(4)
C(34)-Fe(2)-C(35)	172.00(15)	C(22)-C(21)-C(26)	121.2(3)
C(36)-Fe(2)-C(35)	93.13(14)	C(22)-C(21)-N(2)	119.4(3)
C(33)-Fe(2)-Fe(3)	115.09(11)	C(26)-C(21)-N(2)	119.4(3)
C(32)-Fe(2)-Fe(3)	122.93(11)	C(21)-C(22)-C(23)	119.3(4)
C(34)-Fe(2)-Fe(3)	124.41(11)	C(24)-C(23)-C(22)	119.8(4)
C(36)-Fe(2)-Fe(3)	50.01(10)	C(25)-C(24)-C(23)	120.7(4)
C(35)-Fe(2)-Fe(3)	49.50(10)	C(24)-C(25)-C(26)	120.0(4)
C(33)-Fe(2)-Fe(1)	176.05(11)	C(21)-C(26)-C(25)	119.1(4)
C(32)-Fe(2)-Fe(1)	82.93(12)	O(30)-C(30)-Fe(1)	179.3(4)
C(34)-Fe(2)-Fe(1)	88.47(12)	O(31)-C(31)-Fe(1)	178.9(3)
C(36)-Fe(2)-Fe(1)	84.73(10)	O(32)-C(32)-Fe(2)	177.5(3)
C(35)-Fe(2)-Fe(1)	83.80(10)	O(33)-C(33)-Fe(2)	176.5(3)
Fe(3)-Fe(2)-Fe(1)	61.635(18)	O(34)-C(34)-Fe(2)	176.8(3)
C(39)-Fe(3)-C(37)	97.40(16)	O(35)-C(35)-Fe(3)	140.6(3)
C(39)-Fe(3)-C(38)	97.42(16)	O(35)-C(35)-Fe(2)	138.9(3)
C(37)-Fe(3)-C(38)	93.49(16)	Fe(3)-C(35)-Fe(2)	80.39(13)
C(39)-Fe(3)-C(35)	93.05(15)	O(36)-C(36)-Fe(2)	141.4(3)
C(37)-Fe(3)-C(35)	169.49(15)	O(36)-C(36)-Fe(3)	138.4(3)
C(38)-Fe(3)-C(35)	86.22(15)	Fe(2)-C(36)-Fe(3)	80.15(13)

C(39)-Fe(3)-C(36)	92.44(15)	O(37)-C(37)-Fe(3)	177.2(3)
C(37)-Fe(3)-C(36)	84.97(15)	O(38)-C(38)-Fe(3)	176.5(3)
C(38)-Fe(3)-C(36)	170.14(16)	O(39)-C(39)-Fe(3)	178.5(3)
C(35)-Fe(3)-C(36)	93.52(14)		

Table B.3 Anisotropic displacement parameters ($Å^2 \times 10^3$) for $[Fe_3(CO)_{10}(CNPh)_2]$ at 293 K. The anisotropic displacement factor exponent takes the form: $-2\pi^2(h^2a^{*2}U^{11} + ... + 2hka^*b^*U^{12})$.

	U11	U22	U33	U23	U13	U12
Fe(1)	45(1)	53(1)	38(1)	-3(1)	0(1)	2(1)
Fe(2)	50(1)	45(1)	54(1)	-6(1)	9(1)	-2(1)
Fe(3)	51(1)	44(1)	48(1)	0(1)	0(1)	-2(1)
N(1)	46(2)	69(2)	45(2)	-3(1)	2(1)	1(1)
N(2)	59(2)	66(2)	40(2)	0(1)	-4(1)	2(2)
C(1)	46(2)	53(2)	44(2)	-4(2)	7(2)	1(2)
C(2)	49(2)	50(2)	50(2)	-2(2)	5(2)	0(2)
C(11)	44(2)	73(2)	38(2)	-4(2)	3(2)	-6(2)
C(12)	71(3)	80(3)	56(2)	-7(2)	3(2)	-16(2)
C(13)	73(3)	119(4)	59(3)	-21(3)	3(2)	-35(3)
C(14)	70(3)	146(5)	51(3)	-2(3)	-7(2)	2(3)
C(15)	113(4)	107(4)	60(3)	8(3)	-9(3)	26(3)
C(16)	85(3)	73(3)	52(2)	-5(2)	-2(2)	3(2)
C(21)	45(2)	62(2)	37(2)	5(2)	3(2)	1(2)
C(22)	82(3)	63(2)	55(2)	-6(2)	-4(2)	15(2)
C(23)	91(3)	97(3)	57(2)	-25(2)	-4(2)	5(3)
C(24)	64(3)	128(4)	44(2)	13(2)	0(2)	-5(3)
C(25)	77(3)	90(3)	77(3)	37(3)	-8(2)	-2(2)
C(26)	71(3)	60(2)	70(2)	9(2)	-7(2)	-9(2)
C(30)	58(2)	64(2)	45(2)	-4(2)	-2(2)	6(2)
C(31)	51(2)	64(2)	43(2)	-5(2)	4(2)	7(2)
C(32)	72(3)	52(2)	72(3)	-9(2)	17(2)	4(2)
C(33)	60(3)	49(2)	58(2)	-4(2)	5(2)	-8(2)
C(34)	58(2)	52(2)	72(2)	-8(2)	7(2)	-4(2)
C(35)	50(2)	57(2)	48(2)	-2(2)	2(2)	-1(2)
C(36)	49(2)	60(2)	51(2)	-6(2)	6(2)	-3(2)
C(37)	64(3)	53(2)	64(2)	-3(2)	3(2)	-3(2)
C(38)	78(3)	52(2)	59(2)	1(2)	3(2)	-7(2)
C(39)	54(2)	52(2)	59(2)	6(2)	-6(2)	2(2)
O(30)	96(2)	82(2)	78(2)	-21(2)	4(2)	29(2)
O(31)	81(2)	69(2)	79(2)	0(1)	19(2)	-13(2)
O(32)	138(3)	68(2)	92(2)	27(2)	41(2)	23(2)
O(33)	68(2)	77(2)	87(2)	-14(2)	22(2)	6(2)
O(34)	82(2)	85(2)	115(2)	-35(2)	-2(2)	-23(2)
O(35)	65(2)	72(2)	64(2)	2(1)	-18(1)	3(1)
O(36)	84(2)	96(2)	41(1)	-3(1)	1(1)	-6(2)
O(37)	84(2)	73(2)	116(2)	19(2)	-15(2)	19(2)
O(38)	150(3)	79(2)	66(2)	-26(2)	14(2)	-28(2)
O(39)	65(2)	84(2)	99(2)	25(2)	14(2)	-8(2)

Appendix C

Crystallographic Data for $[Ru_4(CO)_{11}(CNPh)_3]$

Table C.1 Atomic coordinates ($x10^4$) and equivalent isotropic displacement parameters ($Å^2 \times 10^3$) for $[Ru_4(CO)_{11}(CNPh)_3]$. U(eq) is defined as one third of the trace of the orthogonalized U_{ij} tensor.

	x	y	z	U(eq)
Ru(1)	332(1)	4296(1)	2231(1)	19(1)
Ru(2)	-1956(1)	4436(1)	972(1)	21(1)
Ru(3)	-2022(1)	3384(1)	2050(1)	21(1)
Ru(4)	-52(1)	5296(1)	3263(1)	20(1)
N(51)	-1389(3)	6386(1)	4165(1)	27(1)
N(61)	-1453(2)	5543(1)	2242(1)	21(1)
N(71)	-1602(2)	4518(1)	3273(1)	22(1)
O(11)	1024(2)	3174(1)	1227(1)	39(1)
O(12)	2320(3)	3612(1)	3554(1)	45(1)
O(13)	2582(3)	5178(1)	1710(2)	64(1)
O(21)	-5228(2)	4494(1)	591(1)	43(1)
O(22)	-1712(3)	3404(1)	-258(1)	49(1)
O(23)	-1368(3)	5599(1)	-10(1)	43(1)
O(31)	-1420(3)	2305(1)	3257(1)	44(1)
O(32)	-1963(3)	2290(1)	854(1)	48(1)
O(33)	-5222(2)	3560(1)	2014(1)	44(1)
O(41)	2405(2)	6200(1)	3038(1)	42(1)
O(42)	1754(2)	4726(1)	4684(1)	38(1)
C(11)	560(3)	3575(2)	1561(2)	29(1)
C(12)	1623(3)	3884(2)	3062(2)	28(1)
C(13)	1759(3)	4855(2)	1917(2)	35(1)
C(21)	-3997(3)	4470(2)	736(2)	29(1)
C(22)	-1797(3)	3759(2)	213(2)	32(1)
C(23)	-1572(3)	5161(2)	357(2)	27(1)
C(31)	-1614(3)	2710(2)	2803(2)	27(1)
C(32)	-2010(3)	2706(2)	1275(2)	31(1)
C(33)	-4030(3)	3488(2)	1999(2)	30(1)
C(41)	1466(3)	5868(1)	3115(2)	26(1)
C(42)	1110(3)	4939(1)	4140(2)	26(1)
C(51)	-905(3)	5982(2)	3835(2)	25(1)
C(52)	-2011(3)	6889(1)	4535(2)	23(1)
C(53)	-3460(3)	7038(2)	4298(2)	37(1)
C(54)	-4029(4)	7551(2)	4663(2)	42(1)
C(55)	-3172(4)	7900(2)	5232(2)	39(1)
C(56)	-1742(4)	7746(2)	5457(2)	37(1)
C(57)	-1137(3)	7235(2)	5109(2)	30(1)
C(61)	-1382(3)	5027(1)	1836(2)	22(1)
C(62)	-2570(3)	6056(1)	2115(2)	22(1)
C(63)	-4004(3)	5892(1)	1836(2)	28(1)
C(64)	-5048(3)	6401(2)	1746(2)	33(1)
C(65)	-4662(3)	7060(2)	1951(2)	34(1)
C(66)	-3236(3)	7216(2)	2246(2)	33(1)
C(67)	-2185(3)	6719(1)	2330(2)	27(1)
C(71)	-1414(3)	4126(1)	2759(2)	21(1)
C(72)	-2745(3)	4435(1)	3659(2)	23(1)
C(73)	-3808(3)	4927(2)	3608(2)	30(1)
C(74)	-4886(3)	4834(2)	3993(2)	38(1)
C(75)	-4909(3)	4265(2)	4423(2)	38(1)

C(76)	-3853(4)	3780(2)	4471(2)	42(1)
C(77)	-2760(3)	3861(2)	4090(2)	34(1)

Table C.2 Bond lengths (Å) and angles (°) for $[Ru_4(CO)_{11}(CNPh)_3]$.

Ru(1)-C(12)	1.926(3)	Ru(1)-C(13)	1.929(3)
Ru(1)-C(11)	1.930(3)	Ru(1)-C(71)	2.127(3)
Ru(1)-C(61)	2.172(3)	Ru(1)-Ru(3)	2.8226(3)
Ru(1)-Ru(4)	2.8258(3)	Ru(1)-Ru(2)	2.8341(3)
Ru(2)-C(21)	1.887(3)	Ru(2)-C(23)	1.913(3)
Ru(2)-C(61)	1.962(3)	Ru(2)-C(22)	1.969(3)
Ru(2)-Ru(3)	2.8895(3)	Ru(3)-C(33)	1.894(3)
Ru(3)-C(31)	1.904(3)	Ru(3)-C(32)	1.965(3)
Ru(3)-C(71)	1.966(3)	Ru(4)-C(42)	1.890(3)
Ru(4)-C(41)	1.893(3)	Ru(4)-C(51)	1.994(3)
Ru(4)-N(61)	2.121(2)	Ru(4)-N(71)	2.122(2)
N(51)-C(51)	1.159(3)	N(51)-C(52)	1.406(3)
N(61)-C(61)	1.274(3)	N(61)-C(62)	1.443(3)
N(71)-C(71)	1.270(3)	N(71)-C(72)	1.433(3)
O(11)-C(11)	1.149(3)	O(12)-C(12)	1.137(4)
O(13)-C(13)	1.136(4)	O(21)-C(21)	1.138(4)
O(22)-C(22)	1.137(3)	O(23)-C(23)	1.141(3)
O(31)-C(31)	1.146(3)	O(32)-C(32)	1.140(3)
O(33)-C(33)	1.144(4)	O(41)-C(41)	1.137(3)
O(42)-C(42)	1.140(4)	C(52)-C(53)	1.377(4)
C(52)-C(57)	1.378(4)	C(53)-C(54)	1.388(4)
C(54)-C(55)	1.367(5)	C(55)-C(56)	1.361(5)
C(56)-C(57)	1.386(4)	C(62)-C(63)	1.381(4)
C(62)-C(67)	1.389(4)	C(63)-C(64)	1.391(4)
C(64)-C(65)	1.376(4)	C(65)-C(66)	1.376(4)
C(66)-C(67)	1.377(4)	C(72)-C(73)	1.384(4)
C(72)-C(77)	1.385(4)	C(73)-C(74)	1.381(4)
C(74)-C(75)	1.377(4)	C(75)-C(76)	1.370(5)
C(76)-C(77)	1.386(4)		

C(12)-Ru(1)-C(13)	96.84(14)	C(12)-Ru(1)-C(11)	93.93(12)
C(13)-Ru(1)-C(11)	92.14(13)	C(12)-Ru(1)-C(71)	89.11(11)
C(13)-Ru(1)-C(71)	153.73(11)	C(11)-Ru(1)-C(71)	113.03(11)
C(12)-Ru(1)-C(61)	147.73(11)	C(13)-Ru(1)-C(61)	92.41(12)
C(11)-Ru(1)-C(61)	116.61(11)	C(71)-Ru(1)-C(61)	70.18(10)
C(12)-Ru(1)-Ru(3)	100.05(9)	C(13)-Ru(1)-Ru(3)	155.91(10)
C(11)-Ru(1)-Ru(3)	69.76(9)	C(71)-Ru(1)-Ru(3)	44.07(7)
C(61)-Ru(1)-Ru(3)	82.38(7)	C(12)-Ru(1)-Ru(4)	84.35(8)
C(13)-Ru(1)-Ru(4)	90.74(9)	C(11)-Ru(1)-Ru(4)	176.81(9)
C(71)-Ru(1)-Ru(4)	64.32(7)	C(61)-Ru(1)-Ru(4)	64.63(7)
Ru(3)-Ru(1)-Ru(4)	107.857(9)	C(12)-Ru(1)-Ru(2)	159.96(9)
C(13)-Ru(1)-Ru(2)	98.86(10)	C(11)-Ru(1)-Ru(2)	73.17(9)
C(71)-Ru(1)-Ru(2)	82.28(7)	C(61)-Ru(1)-Ru(2)	43.69(7)
Ru(3)-Ru(1)-Ru(2)	61.434(8)	Ru(4)-Ru(1)-Ru(2)	107.745(9)
C(21)-Ru(2)-C(23)	98.87(12)	C(21)-Ru(2)-C(61)	104.80(12)
C(23)-Ru(2)-C(61)	89.62(12)	C(21)-Ru(2)-C(22)	95.29(13)
C(23)-Ru(2)-C(22)	91.17(12)	C(61)-Ru(2)-C(22)	159.52(12)
C(21)-Ru(2)-Ru(1)	138.98(9)	C(23)-Ru(2)-Ru(1)	110.81(9)
C(61)-Ru(2)-Ru(1)	49.91(8)	C(22)-Ru(2)-Ru(1)	111.23(9)
C(21)-Ru(2)-Ru(3)	90.57(9)	C(23)-Ru(2)-Ru(3)	169.82(9)
C(61)-Ru(2)-Ru(3)	84.25(8)	C(22)-Ru(2)-Ru(3)	91.75(9)
Ru(1)-Ru(2)-Ru(3)	59.088(7)	C(33)-Ru(3)-C(31)	98.68(12)
C(33)-Ru(3)-C(32)	01.73(13)	C(31)-Ru(3)-C(32)	92.01(12)
C(33)-Ru(3)-C(71)	95.57(12)	C(31)-Ru(3)-C(71)	92.29(11)
C(32)-Ru(3)-C(71)	61.32(12)	C(33)-Ru(3)-Ru(1)	34.10(9)

C(31)-Ru(3)-Ru(1)	09.03(9)	C(32)-Ru(3)-Ru(1)	12.76(9)
C(71)-Ru(3)-Ru(1)	48.81(8)	C(33)-Ru(3)-Ru(2)	93.60(8)
C(31)-Ru(3)-Ru(2)	67.37(9)	C(32)-Ru(3)-Ru(2)	88.36(8)
C(71)-Ru(3)-Ru(2)	83.54(7)	Ru(1)-Ru(3)-Ru(2)	59.479(8)
C(42)-Ru(4)-C(41)	91.64(12)	C(42)-Ru(4)-C(51)	91.03(12)
C(41)-Ru(4)-C(51)	94.91(11)	C(42)-Ru(4)-N(61)	71.41(10)
C(41)-Ru(4)-N(61)	94.55(11)	C(51)-Ru(4)-N(61)	94.37(10)
C(42)-Ru(4)-N(71)	89.94(11)	C(41)-Ru(4)-N(71)	68.01(10)
C(51)-Ru(4)-N(71)	96.95(10)	N(61)-Ru(4)-N(71)	82.79(9)
C(42)-Ru(4)-Ru(1)	100.97(8)	C(41)-Ru(4)-Ru(1)	95.67(8)
C(51)-Ru(4)-Ru(1)	163.74(8)	N(61)-Ru(4)-Ru(1)	72.51(6)
N(71)-Ru(4)-Ru(1)	72.36(6)	C(51)-N(51)-C(52)	177.5(3)
C(61)-N(61)-C(62)	126.2(2)	C(61)-N(61)-Ru(4)	104.16(17)
C(62)-N(61)-Ru(4)	126.81(17)	C(71)-N(71)-C(72)	123.6(2)
C(71)-N(71)-Ru(4)	102.70(17)	C(72)-N(71)-Ru(4)	133.27(18)
O(11)-C(11)-Ru(1)	164.3(3)	O(12)-C(12)-Ru(1)	175.8(3)
O(13)-C(13)-Ru(1)	177.9(3)	O(21)-C(21)-Ru(2)	179.5(3)
O(22)-C(22)-Ru(2)	175.3(3)	O(23)-C(23)-Ru(2)	178.7(3)
O(31)-C(31)-Ru(3)	177.5(3)	O(32)-C(32)-Ru(3)	176.2(3)
O(33)-C(33)-Ru(3)	175.8(3)	O(41)-C(41)-Ru(4)	178.1(3)
O(42)-C(42)-Ru(4)	176.7(3)	N(51)-C(51)-Ru(4)	179.1(2)
C(53)-C(52)-C(57)	122.1(3)	C(53)-C(52)-N(51)	119.2(3)
C(57)-C(52)-N(51)	118.7(3)	C(52)-C(53)-C(54)	117.6(3)
C(55)-C(54)-C(53)	120.9(3)	C(56)-C(55)-C(54)	120.6(3)
C(55)-C(56)-C(57)	120.2(3)	C(52)-C(57)-C(56)	118.6(3)
N(61)-C(61)-Ru(2)	156.3(2)	N(61)-C(61)-Ru(1)	117.3(2)
Ru(2)-C(61)-Ru(1)	86.40(11)	C(63)-C(62)-C(67)	120.1(3)
C(63)-C(62)-N(61)	121.6(2)	C(67)-C(62)-N(61)	118.2(3)
C(62)-C(63)-C(64)	119.5(3)	C(65)-C(64)-C(63)	120.3(3)
C(64)-C(65)-C(66)	119.8(3)	C(65)-C(66)-C(67)	120.6(3)
C(66)-C(67)-C(62)	119.7(3)	N(71)-C(71)-Ru(3)	152.4(2)
N(71)-C(71)-Ru(1)	120.22(19)	Ru(3)-C(71)-Ru(1)	87.12(10)
C(73)-C(72)-C(77)	120.6(3)	C(73)-C(72)-N(71)	120.3(2)
C(77)-C(72)-N(71)	119.1(2)	C(74)-C(73)-C(72)	118.7(3)
C(75)-C(74)-C(73)	121.1(3)	C(76)-C(75)-C(74)	119.9(3)
C(75)-C(76)-C(77)	120.2(3)	C(72)-C(77)-C(76)	119.5(3)

Table C.3 Anisotropic displacement parameters ($Å^2 \times 10^3$) for $[Ru_4(CO)_{11}(CNPh)_3]$. The anisotropic displacement factor exponent takes the form: $-2\pi^2(h^2a^{*2}U^{11} + ... + 2hka^*b^*U^{12})$.

	U11	U22	U33	U23	U13	U12
Ru(1)	20(1)	17(1)	20(1)	-1(1)	6(1)	1(1)
Ru(2)	25(1)	20(1)	18(1)	1(1)	4(1)	2(1)
Ru(3)	25(1)	17(1)	21(1)	0(1)	4(1)	-2(1)
Ru(4)	22(1)	17(1)	20(1)	-2(1)	6(1)	-1(1)
N(51)	35(1)	24(1)	25(1)	-2(1)	12(1)	0(1)
N(61)	25(1)	18(1)	23(1)	1(1)	8(1)	3(1)
N(71)	22(1)	21(1)	24(1)	1(1)	8(1)	0(1)
O(11)	38(1)	42(1)	36(1)	-16(1)	5(1)	11(1)
O(12)	52(2)	38(1)	36(1)	-3(1)	-8(1)	13(1)
O(13)	67(2)	53(2)	88(2)	-13(2)	51(2)	-28(1)
O(21)	29(1)	50(2)	47(1)	12(1)	1(1)	-1(1)
O(22)	71(2)	45(2)	28(1)	-12(1)	3(1)	13(1)
O(23)	50(2)	38(1)	44(1)	16(1)	20(1)	4(1)
O(31)	52(2)	37(1)	40(1)	15(1)	2(1)	1(1)
O(32)	72(2)	32(1)	40(1)	-12(1)	11(1)	-3(1)
O(33)	27(1)	51(2)	55(2)	11(1)	11(1)	-3(1)
O(41)	41(1)	30(1)	59(2)	-2(1)	19(1)	-10(1)

O(42)	40(1)	46(1)	26(1)	2(1)	2(1)	4(1)
C(11)	27(2)	30(2)	27(2)	-3(1)	3(1)	4(1)
C(12)	29(2)	25(2)	30(2)	-7(1)	5(1)	2(1)
C(13)	36(2)	31(2)	42(2)	-8(1)	16(2)	-3(1)
C(21)	32(2)	28(2)	26(2)	6(1)	5(1)	1(1)
C(22)	39(2)	31(2)	24(2)	2(1)	2(1)	6(1)
C(23)	29(2)	29(2)	26(2)	-1(1)	8(1)	5(1)
C(31)	28(2)	24(2)	27(2)	-2(1)	1(1)	-4(1)
C(32)	37(2)	23(2)	31(2)	1(1)	4(1)	-5(1)
C(33)	37(2)	24(2)	26(2)	5(1)	5(1)	-6(1)
C(41)	32(2)	20(2)	28(2)	-3(1)	7(1)	0(1)
C(42)	28(2)	24(2)	27(2)	-5(1)	9(1)	-2(1)
C(51)	27(2)	24(2)	24(2)	3(1)	5(1)	-4(1)
C(52)	33(2)	17(1)	24(1)	1(1)	14(1)	3(1)
C(53)	33(2)	39(2)	38(2)	-3(2)	8(1)	-2(1)
C(54)	33(2)	43(2)	55(2)	7(2)	18(2)	12(2)
C(55)	53(2)	32(2)	38(2)	-2(2)	25(2)	12(2)
C(56)	56(2)	31(2)	25(2)	-6(1)	12(2)	6(2)
C(57)	37(2)	30(2)	24(2)	0(1)	7(1)	7(1)
C(61)	24(1)	23(2)	21(1)	7(1)	7(1)	-2(1)
C(62)	28(2)	18(1)	22(1)	3(1)	10(1)	3(1)
C(63)	30(2)	21(2)	35(2)	-1(1)	10(1)	0(1)
C(64)	24(2)	33(2)	42(2)	3(1)	9(1)	5(1)
C(65)	34(2)	24(2)	46(2)	2(1)	14(2)	11(1)
C(66)	41(2)	19(2)	42(2)	2(1)	16(2)	2(1)
C(67)	30(2)	20(1)	31(2)	0(1)	9(1)	-1(1)
C(71)	23(1)	17(1)	22(1)	4(1)	5(1)	-1(1)
C(72)	24(1)	27(2)	20(1)	-1(1)	7(1)	-2(1)
C(73)	30(2)	32(2)	29(2)	3(1)	8(1)	4(1)
C(74)	27(2)	49(2)	38(2)	1(2)	10(1)	11(1)
C(75)	28(2)	55(2)	35(2)	4(2)	15(1)	0(2)
C(76)	41(2)	48(2)	40(2)	13(2)	18(2)	-1(2)
C(77)	34(2)	35(2)	37(2)	9(1)	15(1)	8(1)